Department of Aeronautics and Astronautics
Stanford University
Stanford, California

# ANALYSIS OF BOUNDARY LAYER STRUCTURE IN A SHOCK-GENERATED PLASMA FLOW, PART 1 EQUILIBRIUM IONIZATION

by

Stellan Knöös



SUDAAR 277
May 1966



Submitted by D. Bershader

Jointly supported by the
National Aeronautics and Space Administration,
Grant NGR 05-020-091 and by a
Ford Foundation Plasma Grant



This Report was also Issued as Report No. 80 of
the Institute for Plasma Research, Stanford University

## ABSTRACT

The structure of some convective, laminar boundary layers in a high density shock-heated 1 eV argon plasma is investigated theoretically. A general three-fluid continuum formulation of the problem is presented, and the equations solved for the case of thermo-chemical equilibrium with no applied electromagnetic fields. Solutions for boundary layer profiles and other quantities are presented for plasma boundary layers forming over a cold, infinite flat plate with an impulsively started motion in its own plane (Rayleigh's boundary layer), and the boundary layer behind a plane, ionizing shock wave moving over an infinite plane wall (shock tube side-wall boundary layer). Accurate transport data for partially ionized argon are calculated and used in the analysis. The induced electric field is shown to be of fundamental importance to these properties. Associated with the ambipolar diffusion is an electric potential difference of the order 10 Volts, which is much larger than the potential difference across the sheath. The assumptions of chemical and temperature equilibrium are checked in a rigorous way. It is found that equilibrium ionization will not exist close to the wall below typically 10,000°K, and that the electron temperature, which was calculated in a linearized model, is larger than the ion-atom temperature in the same region.

## ACKNOWLEDGEMENTS

The author expresses his gratitude to his advisor Professor D. Bershader for the guidance and encouragement received during the course of this study.

Thanks are also due to Professors I-Dee Chang and M. Mitchner for helpful discussions and Mrs. Jerri Rudnick, who carefully typed the manuscript.

This work was supported by NASA through contract NGR-05-020-091 and by the Ford Foundation through a Plasma Fellowship. Computer time was in part made available by a grant from the Computation Center of Stanford University.

TABLE OF CONTENTS

## NOMENCLATURE

$A^*$ Constant of integration

$B^*$ Constant of integration

$C$ Side-wall boundary layer parameter, $U_2/(U_w-U_2)$

$C_i$ Functions defined by equations (7.19)

$c_p$ Specific heat at constant pressure

$\vec{d}_s$ Driving force for diffusion

$D_{ij}$ Multicomponent diffusion coefficient

$\mathcal{D}_{ij}$ Binary diffusion coefficient

$D_{amb}$ Ambipolar diffusion coefficient

$e$ Internal energy per unit mass

$\vec{E}$ Electric field strength

$f$ Velocity distribution function

$F$ Function defined by equation (6.2)

$G$ Function defined by equation (6.2)

$h$ Enthalpy per unit mass

$H$ Function defined by equation (6.7)

$h^*$ Dimensionless enthalpy, $(h-h_w)/(h_\infty-h_w)$

$I_1$ Ionization potential of first argon ion

$\vec{j}$ Electric current vector

$k$ Boltzmann's constant

$K$ Function defined by equation (6.7)

$\ell$ Mean free path

$\ell_D$ Debye length

$m$ Particle mass

$n$ Number density

$p$ Pressure

$\underline{P}$ Kinetic stress tensor

$Pr$ Prandtl number, $Pr = \frac{c_p^{Eq.}\mu}{\lambda_{tot}}$

$q_e$ Electron charge

$q_i$ Ion charge

$\vec{q}$ Energy flux vector

$\vec{r}$ Space vector

$Q^{conv}$ Function defined by equations (6.45, 6.46)

$Q^{diff}$ Function defined by equations (6.45, 6.46)

$Q_{ij}$ Effective hard sphere cross-section

$S$ Normalized available kinetic energy transfer rate defined by equation (7.14)

$\tilde{S}$ Non-dimensional energy transfer rate defined by equation (7.2)

$t$ Time

$T$ Temperature

$u^*$ Dimensionless mean mass velocity, $u^* = u/U_w$ or $u^* = (u-U_2)/(U_w-U_2)$

$U_2$ Velocity behind shock wave in shock-fixed reference system

$U_s$ Mean thermal speed of component "s"

$\vec{U}_s$ Peculiar velocity vector of component "s", $\vec{U}_s = \vec{w}_s - \vec{v}_o$

$U_w$ Wall velocity

$\vec{v}_o$ Mean mass velocity vector, $\vec{v}_o = (u,v)$

$\vec{v}_s$ Mass velocity vector for component "s"

$\vec{V}_s$ Diffusion velocity vector of component "s"

$\vec{w}$ Particle velocity vector

$x$ Coordinate measured from shock wave

$y$ Coordinate measured from wall

$y^*$ Transformed similarity variable defined by equation (6.14)

$Y$ Transformed distance from wall defined by equation (2.18)

$Z$ Partition function

$\alpha$ Degree of ionization

$\delta$ Boundary layer thickness

$\epsilon_{ij}$ Collisional energy transfer rate

$\epsilon_o$ Permittivity of vacuum

$\eta$ Similarity variable defined by equations (2.22) and (2.36)

$\lambda$ Thermal conductivity

$\lambda_{tot}$ Total thermal conductivity (including "reactive" thermal conductivity)

$\mu$ Viscosity

$\rho$ Mass density

$\tau$ Viscous stress tensor

$\varphi$ Electron temperature parameter defined by equation (7.16)

$\psi$ Stream function defined by equation (2.33)

$\omega$ Space charge density

Subscripts:

$( )_o$ Value for gas mixture

$( )_1$ Value in front of shock wave

$( )_2$ Value behind shock wave

$( )_\infty$ Value at free stream

$( )_a$ Value for atoms

$( )_e$ Value for electrons

$( )_i$ Value for ions

$( )_s$ Value for arbitrary component "s"

$( )_w$ Value at wall

MKSA - (meter-kilogram-second-ampere) units are used throughout when not otherwise stated.

LIST OF ILLUSTRATIONS

# 1. INTRODUCTION

With the advent of high speed flight through planetary atmospheres laminar boundary layers in ionized gases have become increasingly important. More generally, the interaction between a moving plasma and a cold wall is of basic physical interest. The associated phenomena are considerably different in nature from those involving non-ionized gases and are presently far from being completely understood. The presence of free electrons and ions, for example, gives rise to induced electromagnetic fields partly due to the vast difference in relative diffusional behavior of the electrons and the heavy gas components. Such fields may couple the motion of the charged particles to the extent that the plasma transport properties are affected. In addition, finite gas phase reaction rates and energy transfer rates, in particular those between the electrons and the heavy particles, raise the question of deviation from thermochemical equilibrium. The local composition of the gas may deviate substantially from its equilibrium value, and the electron temperature may assume a different value from that of the ions and atoms. The present report is part of a combined theoretical and experimental program aimed at studying transport phenomena like the above mentioned in moving high density plasmas.

Available information on the structure of laminar ionized boundary layers and interactions between high density plasmas and solid walls is scarce. Most of the reported work is theoretical. Since the full problem is so extensive, it is natural that early investigators treated these problems only in some simple limits. Thus, Fay and Kemp [1]

studied the stagnation point boundary layer in air, assuming frozen or equilibrium flow in a simple "binary diffusion" model. Rose and Stankevics [2] measured heat transfer rates from such a boundary layer using a shock tube. Their results agreed well with the theory. Camac, Fay, Feinberg, and Kemp [3] studied the shock tube end wall boundary layer in argon theoretically and experimentally. For atomic argon they found good agreement between measured and predicted wall heat transfer rates. In strongly ionized argon the agreement was fair.

A great number of investigators have treated weakly ionized boundary layers with emphasis on the electrical characteristics. Principally, these papers have been aimed toward a better understanding of Langmuir probes. Confining ourselves to the case of collision-dominated interactions, with the possible exception of the charge separation sheath close to the solid surface, a few relevant papers can be mentioned. Pollin [4] made a theoretical and experimental investigation of a stagnation point Langmuir probe in a shock tube with weakly ionized air. In the experiment he applied a very strong negative voltage on the probe in order to repel all electrons and collect only an ion current. The measured current-voltage profiles were in part predicted by the theory, which neglected ion-electron recombinations in the boundary layer and the sheath. In the sheath the motion of the ions was considered to be collision-dominated. Turcotte and Gillespie [5] made a preliminary study with a shock tube side-wall probe, also in weakly ionized air. They measured the total resistance and the potential difference across the shock tube side-wall boundary layer. This potential difference was all attributed to the collision-dominated thin sheath of charge separation

over the cold wall. They were not able to explain why the measured total potential difference was 5-10 times larger than the theoretically calculated potential difference across the sheath. An explanation is clearly given by the present investigation. We will find that typically under collision-dominated conditions the potential difference across the ambipolar region outside of the sheath is not negligible, but often as large as one order of magnitude larger than the sheath voltage. Su and Lam [6] have given theoretical solutions for spherical electrostatic probes in a weakly ionized gas and a collision-dominated sheath. Lam [7] has since presented a general theory for the incompressible flow of a weakly ionized gas over biased absorbing surfaces. Mathematically, the sheath and ambipolar regions were treated separately. The concept of an electrical Reynolds number was introduced, and the extent of the electric boundary layer in general discussed in terms thereof. In particular, he points out the possibility of an electrical boundary layer extending further out than the viscous boundary layer, when the wall does not have a "floating potential", i.e., the current at the wall is not zero. Su [8] later studied a few theoretical aspects of the electrical characteristics of compressible gas flows.

In the limit of weak ionization and a collision-dominated motion of the charged particles in the sheath, Chung [9] solved the Couette flow problem. He used ideal gas thermodynamic and transport data, and also assumed no ion-electron recombinations, but a wall catalytic to such reactions. Later, Chung [10] included a few non-equilibrium effects in viscous air shock layers and calculated some electrostatic probe characteristics.

Regarding temperature non-equilibrium effects, or the question of energy non-equipartition in general, theoretical and some experimental work has been done mainly in the field of gas discharges. Here the average energy of the electrons is in general far higher than that of interest to us. Landau [11] first obtained expressions for the energy transfer rate between electrons and ions for Maxwellian distributions and inverse square law interaction. In an application of thermal and flow excitation of a gas by a shock wave, Petschek and Byron [12] used Landau's results and extended them to calculate electron-atom energy transfer rates in shock-heated argon. Morse [13] has given an extensive theoretical treatment of both energy and momentum exchange processes among species in non-equipartition gases, using various interaction laws. In general, for our purposes, the momentum exchange rate between electrons and the heavy particles is very rapid. Dix [14] made a theoretical study of energy transfer between parallel plates in partially ionized, non-radiating, non-reacting hydrogen. He included magnetic fields and also different electron and heavy particle temperatures. Among interesting results, he found that the associated electric field, even in the ambipolar region, was coupled to the electron motion. Camac and Kemp [15] have reported an attempt to determine the heat transfer to a shock-tube end-wall from a multi-temperature boundary layer. Assuming no electron-ion recombinations, they presented briefly a solution in which the electron temperature was much larger than the temperature of the atoms and ions outside the sheath. They did not mention the fact specifically, but their results show the possibility that the electron

temperature close to the unperturbed plasma is slightly less than the heavy particle temperature. In a later section of the present analysis similar features are shown to be also present for the present type of argon boundary layers.

Jaffrin [16] recently theoretically studied the structure of shock waves in partially ionized argon. He used a three-fluid continuum model and assumed frozen ionization. The results indicate a broad thermal layer of elevated electron temperature ahead of the shock and a precursor.

The scope of the present paper is to determine theoretically the structure of some simple boundary layers in partially ionized argon in thermochemical equilibrium. Hence, we assume the electron-ion recombination rate to be fast, at least in the region where the electrons and ions much determine the boundary layer structure.

For simplicity, we choose to study the simplest boundary layers such as the ionized convective Rayleigh boundary layer, the shock tube end-wall boundary layer (which is a special case of the Rayleigh boundary layer), and the shock-tube side-wall boundary layer. The latter boundary layer is a boundary layer forming over an infinite, flat wall behind a plane shock wave, which moves with uniform velocity along the wall. In the case of the Rayleigh boundary layer, we will determine the structure of the interaction, when the directed kinetic energy of the gas is at most of the same order of magnitude or smaller than the enthalpy of the gas. For the side-wall boundary layer we are only interested in experimentally obtainable cases in which, for a shock wave penetrating into gas at rest over the wall, the kinetic energy of the shock-heated

plasma is of the same order of magnitude as the gas enthalpy. These treatments will be restricted to the case of no applied electric or magnetic fields. The magnetic Reynolds number will be assumed to be small as well. Therefore, only the induced electric field is taken into account. In fact, this field is of extreme importance to the boundary layer problem, primarily because it couples the diffusive motion of the electrons and the ions and thereby affects strongly the transport properties of the gas.

Somewhat superficially, we will neglect radiation in the present treatment of the plasma boundary layer. However, it is clear that energy will be transferred in the radiative mode, at least when the temperatures are above 10,000°K. There may then be present a more or less strong coupling between the radiation field and the plasma flow. We shall, implicitly, assume this coupling to be weak and neglect radiative losses of energy. The radiation problem can then be treated separately from the convective problem, and could be added to the treatment in a future study.

Next, it is assumed that the mean free paths of the species are small everywhere in the interaction region compared to the size of this region. We are then justified in using a continuum approach in the mathematical description of the laminar boundary layer. In particular, we may use equations of the Navier-Stokes type for the electron, ion and atom fluids. Simple kinetic theory will, in part, be used for the calculations of the transport properties.

The considerations just discussed, together with some others, are

summarized in the following assumptions, which provide the framework of the physical model:

1. The boundary layer flow is laminar and steady.
2. The gas is an argon plasma in thermochemical equilibrium, i.e., the composition is given by a Saha type equation. This condition does not have to be satisfied in the weakly ionized region and in particular in the sheath, where the gas is essentially frozen, i.e., slow electron-ion reactions.
3. In any part of the boundary layer, the electron temperature may deviate only slightly from the temperature of the ions and atoms.
4. The Reynolds number is large. The mean free paths of the gas components are small compared to the boundary layer thickness.
5. The wall temperature is so low, that the gas is weakly ionized at the interface.
6. The wall has a "floating" potential with respect to the plasma. Hence there is no current to the wall.
7. There are no applied electromagnetic fields. The induced magnetic field is neglected (the magnetic Reynolds number is small).
8. The Debye length of the unperturbed plasma is small compared to the boundary layer thickness. The boundary layer is then mostly quasi-neutral, i.e., $n_i/n_e \simeq 1$.
9. The thermal speed of the electrons is large compared

to the mean mass velocities (small "electron Mach number").

10. The thermal diffusion is neglected.

11. Radiation is neglected. There is no radiation cooling of the free stream plasma.

The sequence of the treatment is as follows. The mathematical formulation of the boundary layer flows is given in Section 2. The governing equations are derived as moments of the Boltzmann equations for the electron, ion, and atom fluids. The electrical characteristics of the plasma boundary layer flow are discussed in the following section. Most attention is here given to the ambipolar diffusion region. The sheath is discussed briefly and the governing flow equations for the charged particles presented. In Section 4 the thermogasdynamic properties of shock heated, partially ionized argon are reviewed. Selected results of computer calculations of the shock heated plasma properties are presented. In the following section, the transport properties of such a plasma are calculated. For that purpose a simple, but powerful, mean free path approach is used. The results are presented in some detail, since they are very interesting in nature and evidently not widely reported in the literature. The boundary layer equations are solved numerically in Section 6. The results are presented and discussed. In Section 7, a two-temperature boundary layer is analyzed with a linearized analytical model. The governing equations are solved, and the results discussed. The report is concluded with a summary and discussion of results.

## 2. FORMULATION OF THE BOUNDARY LAYER EQUATIONS

### a. Moments of the Boltzmann Equation

The present plasma boundary layer problem is complex in nature due to the different, but coupled, behavior of the electron, ion, and atom fluids. For purposes of clarity and well defined mathematical formulation, we shall start from first principles. The formulation presented herein is well suited only for collision-dominated plasma boundary layers, where each fluid has a velocity distribution function which is close to Maxwellian. In parallel to simpler cases, the continuum, three-fluid conservation equations will be derived as moments of the Boltzmann equation. The overall conservation equations are then the usual Navier-Stokes equations. In part, this section will therefore be a review of known material [17].

We begin by presenting the Boltzmann equation for the distribution function $f_s(w_s,r,t)$ for any component "s" in the plasma

$$\frac{\partial f_s}{\partial t} + \vec{w}_s \cdot \nabla_{\vec{r}} f_s + \frac{q_s}{m_s} \vec{E} \cdot \nabla_{\vec{w}_s} f_s = \left[\frac{\partial f_s}{\partial t}\right]_{coll} \tag{2.1}$$

Here $\vec{w}_s$ is the particle velocity, $\vec{r}$ the space vector, $q_s$ the electric charge of the particle, $m_s$ the mass, $\vec{E}$ the electric field strength, and $[\partial f/\partial t]_{coll}$ the collisional rate of change of the distribution function in phase space and time (neglecting radiation).

Moments of this equation can be found by multiplying it by a function $\varphi_s = \varphi_s(\vec{w}_s, I_s)$, which may depend only upon the particle

velocity $\vec{w}_s$ and the excited energy $I_s$ of the particle. After integration over the entire velocity-space, we obtain the following well known Boltzmann moment equation (Chapman and Cowling [18]).

$$\frac{\partial}{\partial t}(n_s\langle\varphi_s\rangle) + \nabla_{\vec{r}}\cdot(n_s\langle\vec{w}_s\varphi_s\rangle) - \\ - \frac{q_s}{m_s} n_s\vec{E}\cdot\langle\nabla_{\vec{w}_s}\varphi_s\rangle = \frac{\partial}{\partial t}\left[\int\varphi_s f_s d\vec{w}_s\right]_{coll} \tag{2.2}$$

Here $n_s$ is the particle number density, the bracket $\langle\ \rangle$ indicates a value average in velocity space. The equations describing conservation of mass, momentum, and energy for the plasma components are obtained by letting $\varphi_s = m_s$, $\varphi_s = m_s\vec{w}_s$, and $\varphi_s = \frac{1}{2}m_s w_s^2 + I_s$ respectively. After some rearrangements of terms they yield:

$$\text{(mass)} \qquad \frac{\partial\rho_s}{\partial t} + \nabla_{\vec{r}}\cdot(\rho_s\vec{v}_s) = \left[\frac{\partial\rho_s}{\partial t}\right]_{coll} \tag{2.3}$$

$$\text{(momentum)} \qquad \frac{\partial}{\partial t}(\rho_s\vec{v}_s) + \nabla_{\vec{r}}(\rho_s\,\underline{\vec{v}_o\vec{v}_o}) + \nabla_{\vec{r}}[\rho_s(\underline{\vec{v}_o\vec{V}_s} + \underline{\vec{V}_s\vec{v}_o})] + \\ + \nabla_{\vec{r}}\underline{P_s} - \omega_s\vec{E} = \frac{\partial}{\partial t}[\rho_s\vec{v}_s]_{coll} \tag{2.4}$$

$$\text{(energy)} \qquad \frac{\partial}{\partial t}(\rho_s e_s) + \nabla_{\vec{r}}\cdot(\vec{v}_o\rho_s e_s) = -\rho_s\vec{V}_s\cdot\frac{\partial\vec{v}_o}{\partial t} - \\ - \nabla_{\vec{r}}\cdot\vec{q}_s - [\underline{P_s} + \rho_s\,\underline{\vec{V}_s\vec{v}_o}] : \underline{\nabla_{\vec{r}}\vec{v}_o} + \\ + \vec{j}_s\cdot\vec{E} + \frac{\partial}{\partial t}[\rho_s e_s]_{coll} \tag{2.5}$$

Here $(\underline{\quad})$ indicates a tensor quantity, and $(\underline{\quad}) : (\underline{\quad})$ a tensor multiplication. The mass density of specie "s" is $\rho_s = n_s m_s$, the mean value of the particle velocity of specie "s" $\vec{v}_s = \langle \vec{w}_s \rangle$, the mean mass velocity $\vec{v}_o$, the diffusion velocity $\vec{V}_s = \vec{v}_s - \vec{v}_o$, and the peculiar velocity $\vec{U}_s = \vec{w}_s - \vec{v}_o$. The kinetic stress tensor is $\underline{P}_s = \rho_s \langle U_s U_s \rangle$, the charge density of the component $\omega_s = q_s n_s$ (note $\omega_a = 0$; $\omega_e = -q_i n_e$; $\omega_i = q_i n_i$), and the component current density $\vec{j}_s = n_s q_s \vec{V}_s$. The convective energy flux vector $\vec{q}_s$, the kinetic temperature $T_s$, and the internal energy per unit mass $e_s$ for the component "s" are defined as follows:

$$\vec{q}_s = n_s \left[ \frac{1}{2} m_s \langle \vec{U}_s U_s^2 \rangle + \vec{V}_s \langle I_s \rangle \right] \tag{2.6}$$

$$T_s = \frac{1}{3} \frac{m_s}{k} \langle U_s^2 \rangle \tag{2.7}$$

$$e_s = \frac{3}{2} \frac{kT_s}{m_s} + \frac{\langle I_s \rangle}{m_s} \tag{2.8}$$

In obtaining these expressions for the energy flux, we have made the reasonable assumption that the particle velocity is not statistically correlated with the excitation energy of the particle.

The momentum and energy equations for the electron fluid may be simplified by the fact that the electron inertia and shear stresses are small compared to corresponding quantities in the ion and atom fluids. If the assumption is made, that everywhere the average mass velocity $\vec{v}_o$ is much smaller than the average thermal speed of the electrons, the convective terms can be neglected in the momentum equation. The equation then becomes

$$\nabla_{\vec{r}} p_e - \omega_e \vec{E} \doteq \frac{\partial}{\partial t} [\rho_e \vec{v}_e]_{coll} \tag{2.9}$$

Here, $p_e$ is the pressure of the electron gas. In the subsequent analysis we shall not be much concerned with this equation. For an equilibrium plasma flow, i.e., when the composition follows a Saha relation, the electron momentum equation is superfluous. However, it may be used to determine the flux of momentum to the electrons due to collisions with atoms and ions. The electron energy equation does not change as drastically in this limit of small "electron Mach number". It can be written

$$\frac{\partial}{\partial t} (\rho_e e_e) + \nabla_{\vec{r}} \cdot (\rho_e e_e \vec{v}_o) \doteq -\nabla_{\vec{r}} \cdot \vec{q}_e -$$

$$- p_e \nabla_{\vec{r}} \cdot \vec{v}_o + \vec{j}_e \cdot \vec{E} + \frac{\partial}{\partial t} [\rho_e e_e]_{coll} \tag{2.10}$$

The convective terms in the electron energy equation cannot in general be neglected. In some situations, e.g., for steady viscous flow adjacent to the a plane wall, the flow in the direction perpendicular to the wall is diffusive in character, and the convective terms small. The electron energy equation then degenerates into a form similar to Equation (2.9), and describes the balance between the heat transfer in the electron fluid itself, the Joule heating, and the collisional energy transfer to the fluid. For the case of a plasma in thermochemical equilibrium, the energy equation is superfluous. However, when the assumption of thermochemical equilibrium is in doubt, the electron energy equation should be considered. If kinetic theory data are available for the collisional energy transfer

rate between the fluids, the species energy equations, and in particular the electron energy equation, provide us with knowledge of the magnitude of the temperature difference between the electron fluid and the atom and ion fluids. In Section 7, a calculation of this kind is presented.

By summing the individual species equations and making use of the usual collisional invariants, we obtain the conservation equations for the whole plasma as follows:

$$\text{(mass)} \qquad \frac{\partial \rho}{\partial t} + \nabla_{\vec{r}} \cdot (\rho \vec{v}_o) = 0 \tag{2.11}$$

$$\text{(momentum)} \qquad \frac{\partial}{\partial t}(\rho \vec{v}_o) + \nabla_{\vec{r}} (\rho \underline{\vec{v}_o \vec{v}_o}) = -\nabla_{\vec{r}} \underline{P} + \omega \vec{E} \tag{2.12}$$

$$\text{(energy)} \qquad \frac{\partial}{\partial t}(\rho e) + \nabla_{\vec{r}} \cdot (\rho e \vec{v}_o) = -\nabla_{\vec{r}} \cdot \vec{q} - \underline{P} : \underline{\nabla_{\vec{r}} \vec{v}_o} + \vec{j} \cdot \vec{E} \tag{2.13}$$

Here $\rho$ is the total mass density, $\underline{P}$ the kinetic stress tensor, $\omega$ the total charge density, and $\vec{j}$ the total current density. The kinetic stress tensor $\underline{P}$ includes the viscous stress tensor $\underline{\tau}$. By making use of Poisson's equation, the momentum equation (2.12) could be written more conveniently as

$$\frac{\partial}{\partial t}(\rho \vec{v}_o) + \nabla_{\vec{r}} (\rho \underline{\vec{v}_o \vec{v}_o}) = -\nabla_{\vec{r}} \left(\underline{P} - \frac{\epsilon_o}{2} \underline{\vec{E}\vec{E}}\right) \tag{2.12}$$

Here $\epsilon_o$ is the permittivity of vacuum. In the present analysis, the electromagnetic stress tensor $\frac{\epsilon_o}{2} \underline{\vec{E}\vec{E}}$ will be attributed to the induced

electric field. It is easy to show, that if the Debye length is much smaller than a plasma boundary layer thickness, the electromagnetic stress stensor could be neglected in comparison to the kinetic stress tensor. For the high density plasmas considered here, the Debye length is in general smaller than $10^{-6}$ meters. We therefore, with confidence, neglect the electromagnetic stress in the description of the overall plasma flow. In the energy equation (2.13) the Joule heating term can be neglected for similar reasons. Also in our particular plasma boundary layer we will consider mainly the case when the current $\vec{j}$ is zero at the wall.

Thus far, we have included no expressions for the diffusion velocities, the kinetic stress tensors, and the energy fluxes in the above equations. In Section 5, we will relate these to properties of the thermogasdynamic flow field, as is usually done when the velocity distributions are close to Maxwellian. As mentioned earlier, we will primarily be treating the case where the composition of the plasma is close to that for equilibrium, i.e., the electron-ion reactions are considered to be fast. Initially, the temperatures of the fluids are assumed to be equal. Therefore, it is sufficient to solve only the conservation equations (2.11-2.13) for the whole plasma, together with the equations of state and equilibrium composition, i.e., a Saha equation. In addition, Poisson's equation has to be considered. The electron continuity equation will be used only in order to determine where in the plasma boundary layer the assumptions of quasi-equilibrium are valid. Similarly, the electron energy equation will be used to determine the region of the boundary layer in which the electron temperature and heavy particle temperatures are almost equal.

In practice, we will not have to study in detail the species momentum equations since in our collision-dominated, high Reynolds number boundary layer, the momentum exchange rate among the species is rapid enough to cause small "slip".

At first sight, it might appear as if the electric field has been eliminated in the hydrodynamic description. This is not correct. The induced electric field will strongly determine the plasma boundary layer structure. The mechanism is through the transport properties. In particular the thermal conductivity of the plasma is strongly dependent upon the electric field strength. Also the diffusional properties are affected. In addition, the question of thermochemical equilibrium is intimately coupled to the appearance of an induced electric field. The field provides, e.g., an additional mechanism besides the collisional, by which thermal energy can be transferred between the electron and the heavy particle fluids.

### b. The Rayleigh Boundary Layer Problem

The boundary layer equations for the Rayleigh boundary layer problem are given next. Classically, this boundary layer problem is the incompressible, viscous flow over an infinite flat plate, initially at rest, but given an impulsively started motion in its own plane. It was first discussed by Rayleigh [18]. The problem was studied subsequently by several authors for the case of compressible, heat conducting flow. Various degrees of approximations were employed. Howarth [19] calculated the pressure on the wall due to the viscous dissipation, which in turn induced velocities perpendicular to the wall, and also a shock wave.

Van Dyke [20] improved the compressible solution by iterating upon the boundary layer solution and the acoustic solution in the outer flow field. He considered a thermally insulated plate and simple gas properties. In the present analysis we shall study the boundary layer solution in the first approximation only, but allow for a realistic variation in the properties of the plasma.

Suppose that an infinite plate, as in Figure 1, is initially at rest in the plane $y = 0$, but insulated from a uniform plasma at rest which occupies the upper half plane $y > 0$. At time $t = 0$, the plate is given an impulsive motion with the velocity $U_w$ in its own plane. Simultaneously the plasma is allowed to come into thermal contact with the plate. The plate is kept at a constant temperature $T_w$, which we assume is much lower than the temperature of the undisturbed plasma. In addition, we assume no exchange of mass or electric charge between the wall and the gas. As mentioned previously, the unperturbed plasma is assumed not to change its properties with time, i.e., radiation cooling is neglected. In this case, Equations (2.11-2.13) simplify to the following well known boundary layer equations, which are valid at times $t$, when $|v/u| \ll 1$ (i.e., $tU_w \rho/\mu \gg 1$)

$$\frac{\partial \rho}{\partial t} + \frac{\partial}{\partial y}(\rho v) = 0 \tag{2.14}$$

$$\frac{\partial u}{\partial t} + v \frac{\partial u}{\partial y} = \frac{1}{\rho} \frac{\partial}{\partial y} \tau_{xy} \tag{2.15}$$

$$\frac{\partial h}{\partial t} + v \frac{\partial h}{\partial y} = - \frac{1}{\rho} \frac{\partial}{\partial y} q_y + \frac{1}{\rho} \tau_{xy} \frac{\partial u}{\partial y} \tag{2.16}$$

Here, $u$ and $v$ are the velocity components in the x- and y-directions, $h$ the gas enthalpy per unit mass, $q_y$ the total energy flux in the y-direction, and $\tau_{xy}$ the shear stress. The pressure of the plasma is constant. Notice that conditions are independent of the x-coordinate.

The appropriate boundary conditions are

$$
\begin{array}{ll}
t \leq 0: & t > 0: \\
u(y,0) = 0 & u(0,t) = U_w \\
v(y,0) = 0 & v(0,t) = 0 \\
h(y,0) = h_\infty & h(0,t) = h_w
\end{array}
\tag{2.17}
$$

By making a restricted Howarth's transformation (see e.g., [21])

$$
Y = \int_0^y \frac{\rho}{\rho_\infty}\, dy \; ; \quad \tau = t \tag{2.18}
$$

the equation for conservation of mass is automatically satisfied. The transformed momentum and energy equations become

$$
\left(\frac{\partial u}{\partial \tau}\right)_Y = \frac{1}{\rho_\infty} \frac{\partial}{\partial Y} \left(\mu \frac{\rho}{\rho_\infty} \frac{\partial u}{\partial Y}\right) \tag{2.19}
$$

$$
\left(\frac{\partial h}{\partial \tau}\right)_Y = \frac{1}{\rho_\infty} \frac{\partial}{\partial Y} \left(\lambda \frac{\rho}{\rho_\infty} \frac{\partial T}{\partial Y}\right) + \frac{\mu}{\rho_\infty} \frac{\rho}{\rho_\infty} \left(\frac{\partial u}{\partial Y}\right)^2 \tag{2.20}
$$

Here we have introduced the relations $\tau_{xy} = \mu\left(\frac{\partial u}{\partial y}\right)_x$ and $q = -\lambda\left(\frac{\partial T}{\partial y}\right)_x$, where $\mu$ is the viscosity and $\lambda$ the total thermal conductivity.

Since the plasma flow is considered to be in equilibrium and the

boundary conditions sufficiently clean, the boundary layer can be shown to be of a self-similar nature. An appropriate nondimensional similarity parameter is

$$\eta = \frac{Y}{2\sqrt{\frac{\lambda_\infty}{c_{p_\infty}} \frac{\tau}{\rho_\infty}}} \tag{2.21}$$

where $c_{p_\infty}$ is the equilibrium specific heat of the unperturbed plasma. It should be noted that we normalize with the total thermal conductivity $\lambda_\infty$, and not with the viscosity. The reason therefore is, in part, that the case of zero or small wall velocity is to be treated by these equations as well, and that the viscosity of the gas is then really not important. Also, it is not convenient to normalize the similarity parameter with viscosity because of the irregular behavior of the viscosity with temperature in the region of partial ionization. With the above transformation (2.21), the momentum and energy equations reduce to*

$$2\eta \frac{1}{Pr_\infty} \frac{du}{d\eta} + \frac{d}{d\eta} \left(\frac{\rho\mu}{\rho_\infty \mu_\infty} \frac{du}{d\eta}\right) = 0 \tag{2.22}$$

$$2\eta \frac{dh}{d\eta} + \frac{d}{d\eta} \left(\frac{\rho\mu}{\rho_\infty \mu_\infty} \frac{Pr_\infty}{Pr} \frac{dh}{d\eta}\right) + Pr_\infty \frac{\rho\mu}{\rho_\infty \mu_\infty} \left(\frac{du}{d\eta}\right)^2 = 0 \tag{2.23}$$

---

* Note that

$$\left(\frac{\partial}{\partial T}\right)_Y = -\frac{1}{2} \frac{\eta}{\tau} \frac{d}{d\eta} = \left(\frac{\partial}{\partial t}\right)_y + v\left(\frac{\partial}{\partial y}\right)_t ; \quad \left(\frac{\partial}{\partial Y}\right)_\tau = \frac{\eta}{Y} \frac{d}{d\eta}$$

For convenience, we have introduced the local Prandtl number $Pr = \frac{c_p \mu}{\lambda}$ and the "free stream" Prandtl number $Pr_\infty$. It is important to note that these quantities are based upon the equilibrium value of the specific heat. In addition, we have made use of the relation (valid at constant pressure only) $dh/d\eta = c_p \, dT/d\eta$. Equations (2.22, 2.23) are non-dimensionalized further by introducing the following quantities for the velocity and the enthalpy

$$u^* = \frac{u}{U_w} \qquad h^* = \frac{h-h_w}{h_\infty - h_w} \tag{2.24}$$

To summarize, the boundary layer equations and the boundary conditions are then

$$2\eta \frac{1}{Pr_\infty} \frac{du^*}{d\eta} + \frac{d}{d\eta} \left( \frac{\rho\mu}{\rho_\infty \mu_\infty} \frac{du^*}{d\eta} \right) = 0 \tag{2.25}$$

$$2\eta \frac{1}{Pr_\infty} \frac{dh^*}{d\eta} + \frac{d}{d\eta} \left( \frac{\rho\mu}{\rho_\infty \mu_\infty} \frac{1}{Pr} \frac{dh^*}{d\eta} \right) + \frac{U_w^2}{h_\infty (1 - \frac{h_w}{h_\infty})} \frac{\rho\mu}{\rho_\infty \mu_\infty} \left( \frac{du^*}{d\eta} \right)^2 = 0 \tag{2.26}$$

$t > 0$:

$$u^*(0,t) = 1 \qquad h^*(0,t) = 0$$

$$u^*(\infty,t) = 0 \qquad h^*(\infty,t) = 1 \tag{2.27}$$

In order to solve the above coupled system of ordinary non-linear parabolic differential equations, we must have at our disposal detailed information about the Prandtl number $Pr(h,p)$ and the density-viscosity factor $\rho\mu(h,p)$ in the enthalpy region of interest. The constant parameters of the problem are the Prandtl number at undisturbed conditions, $Pr_\infty$, and

$U_w^2/(h_\infty(1-h_w/h_\infty))$, which appears as a factor in the viscous dissipation term. The last parameter, in order to be more familiar, could be expressed in terms of a Mach number, which can be formed by the velocity of the wall $U_w$ and a speed of sound in the unperturbed plasma.

Finally, the equation governing the end-wall boundary layer will be given. This is obtained from the equations for the Rayleigh problem by simply putting $u^* \equiv 0$ and $U_w \equiv 0$. The momentum equation (2.25) is therefore superfluous. There is, on our approximation level, no viscous dissipation present. After some rearrangement, the energy equation (2.26) takes the simpler, parabolic form

$$2\eta \frac{dh^*}{d\eta} + \frac{d}{d\eta}\left(\frac{\rho}{\rho_\infty}\frac{\lambda}{\lambda_\infty}\frac{c_{p_\infty}}{c_p}\frac{dh^*}{d\eta}\right) = 0 \qquad (2.28)$$

As in the general Rayleigh problem, the boundary conditions for the non-dimensional enthalpy are

$$t > 0: \qquad h^*(0,t) = 0 \; ; \qquad h^*(\infty,t) = 1 \qquad (2.29)$$

The energy equation (2.28) for the end-wall boundary layer has been extensively studied in the literature, e.g., in connection with ordinary diffusion problems.

The shock-tube end wall boundary layer is possibly the simplest type of boundary layer which can be generated experimentally, and also one of the simplest to study theoretically for ionized gases. The boundary layer forms over the end wall of a shock tube in the reflected region. Hence, in the experimental situation, the gas in the boundary layer has been shock heated by passage through two shock waves. There

will naturally be an induced flow field in the y-direction perpendicular to the wall, due to the change in density of the gas in the boundary layer. This is taken into account in what follows.

As for the Rayleigh case, in general we shall consider only the boundary layer solution and neglect the outer, acoustic solution, which here does not carry a shock wave.

### c. The Shock Tube Side-Wall Problem

The equations governing the laminar boundary layer flow behind a plane shock wave propagating into a stationary gas over an infinite wall is studied next. We will refer to this boundary layer as the shock tube side-wall boundary layer, since it can be generated in the shock tube along its side-walls. The problem is theoretically more complicated to solve than the Rayleigh boundary layer. The reason for this is extra non-linear terms appearing in the governing boundary layer equations. Aspects of such flows have previously been studied by several authors, mainly for the simpler case of ideal gases.

Hollyer [22] formulated the simple problem and gave a solution. Further solutions have been given by, e.g., Mirels [23] and Bershader and Allport [24], who also carried out some experiments. Becker [25] has since given an extensive review of the shock tube boundary layer problem for low temperature gases.

We conveniently study the side-wall boundary layer in a coordinate system, which moves with the shock wave, as is shown in Fig. 2. The shock wave is assumed to be not attenuating. Therefore, in this reference system, the flow is time independent. Cold, non-ionized gas

of homogeneous conditions enters the plane shock wave with a velocity $U_s$, which equals the wall velocity $U_w$ in our reference system. Behind the shock wave the gas velocity is $U_2$ in the undisturbed region. In practice, for ionizing shock waves, there will be a finite region of relaxation to equilibrium conditions behind the shock wave. We shall neglect this, and assume the conditions of the plasma to be uniform behind the shock wave. The only possible exception is a variation in a small induced velocity perpendicular to the wall, due to the boundary layer displacement thickness.

In the shock-fixed coordinate system the time-independent boundary layer equations are (with symbols analagous to those used previously)

$$\text{(mass)} \qquad \frac{\partial}{\partial x}(\rho u) + \frac{\partial}{\partial y}(\rho v) = 0 \tag{2.30}$$

$$\text{(momentum)} \qquad u\frac{\partial u}{\partial x} + v\frac{\partial u}{\partial y} = \frac{1}{\rho}\frac{\partial}{\partial y}\tau_{xy} \tag{2.31}$$

$$\text{(energy)} \qquad u\frac{\partial h}{\partial x} + v\frac{\partial h}{\partial y} = -\frac{1}{\rho}\frac{\partial q_y}{\partial y} + \frac{\tau_{xy}}{\rho}\frac{\partial u}{\partial y} \tag{2.32}$$

with the boundary conditions

$x > 0$:

$u(x,0) = U_w$; $v(x,0) = 0$ $\qquad u(x,\infty) = U_2$

$h(x,0) = h_w \qquad\qquad h(x,\infty) = h_\infty$

A great number of similarities could be drawn to the classical compressible semi-infinite "flat plate" problem. The only difference is in fact the boundary condition at the wall, $u(x,0) = U_w$, which for the "flat plate" problem becomes $u(x,0) = 0$. Earlier, it was pointed out,

e.g., in the work by Bershader and Allport [24], that the shock tube side-wall boundary layer problem is more general than the "flat plate", i.e., the Blasius problem. The reason is the additional degree of freedom given by the possible variation in wall velocity $U_w$ (in the shock-fixed reference system).

The equation for conservation of mass (2.30) may be eliminated by introducing, instead of $y$, a stream-function $\psi$, defined as

$$\psi = \int_0^y \frac{\rho}{\rho_\infty} u \, dy \tag{2.33}$$

The velocity components are then

$$u = \frac{\rho_\infty}{\rho} \frac{\partial \psi}{\partial y} ; \qquad v = - \frac{\rho_\infty}{\rho} \frac{\partial \psi}{\partial x} \tag{2.34}$$

The substantial derivative along a streamline becomes

$$\frac{D}{Dt} \equiv u \frac{\partial}{\partial x} + v \frac{\partial}{\partial y} = u \left( \frac{\partial}{\partial x} \right)_\psi \tag{2.35}$$

With the present boundary conditions, the equations for conservation of momentum and energy (2.31, 2.32) can be brought into a self-similar form. The similarity variable may be conveniently defined for this case as

$$\eta = \frac{\psi}{2 \sqrt{\frac{\lambda_\infty}{c_{p_\infty} \rho_\infty} U_2 x}} \tag{2.36}$$

where the distance $x$ is measured from the shock wave. It should be noted, that we have normalized with the velocity $U_2$, and not with the

velocity difference $(U_w - U_2)$. The reason for this is not obvious at this point, but the equations with this choice of reference velocity take a more convenient form.

If, in addition, we introduce the following dimensionless quantities

$$u^* = \frac{u-U_2}{U_w-U_2} \; ; \qquad h^* = \frac{h-h_w}{h_\infty - h_w} \tag{2.37}$$

$$C = \frac{U_2}{U_w-U_2} \tag{2.38}$$

where $C$ is a constant parameter, less than unity, the boundary layer momentum and energy equations become

$$2\eta \frac{1}{Pr_\infty} \frac{du^*}{d\eta} + \frac{d}{d\eta} \left( \frac{\rho\mu}{\rho_\infty \mu_\infty} \left( \frac{u^*+C}{C} \right) \frac{du^*}{d\eta} \right) = 0 \tag{2.39}$$

$$2\eta \frac{1}{Pr_\infty} \frac{dh^*}{d\eta} + \frac{d}{d\eta} \left( \frac{\rho\mu}{\rho_\infty \mu_\infty} \frac{1}{Pr} \left( \frac{u^*+C}{C} \right) \frac{dh^*}{d\eta} \right) + $$

$$+ \frac{\rho\mu}{\rho_\infty \mu_\infty} \left( \frac{u^*+C}{C} \right) \frac{(U_w-U_2)^2}{h_\infty \left(1 - \frac{h_w}{h_\infty}\right)} \left( \frac{du^*}{d\eta} \right)^2 = 0 \tag{2.40}$$

The boundary conditions are

$x > 0$:

$$\begin{aligned} u^*(x,0) &= 1 \qquad & h^*(x,0) &= 0 \\ u^*(x,\infty) &= 0 \qquad & h^*(x,\infty) &= 1 \end{aligned} \tag{2.41}$$

These equations are quite general. In fact, they also govern the Rayleigh (and end-wall) boundary layer flow, as well as the compressible "flat plate" boundary layer flow, as was pointed out previously. By

giving the parameter $C$ the value $C = -1$, i.e., $U_w = 0$, we obtain the "flat plate" boundary layer equations. The dimensionless velocity parameter then degenerates to $u^* = -(u-U_2)/U_2$. Observe that the boundary conditions (2.41) are unchanged.

If $C \to \infty$, the equations for the Rayleigh problem are obtained with unchanged boundary conditions. This corresponds to the case when $U_w/U_2 \to 1$, i.e., such as obtained by a weak shock. We then have $u^* = u/U_w$.

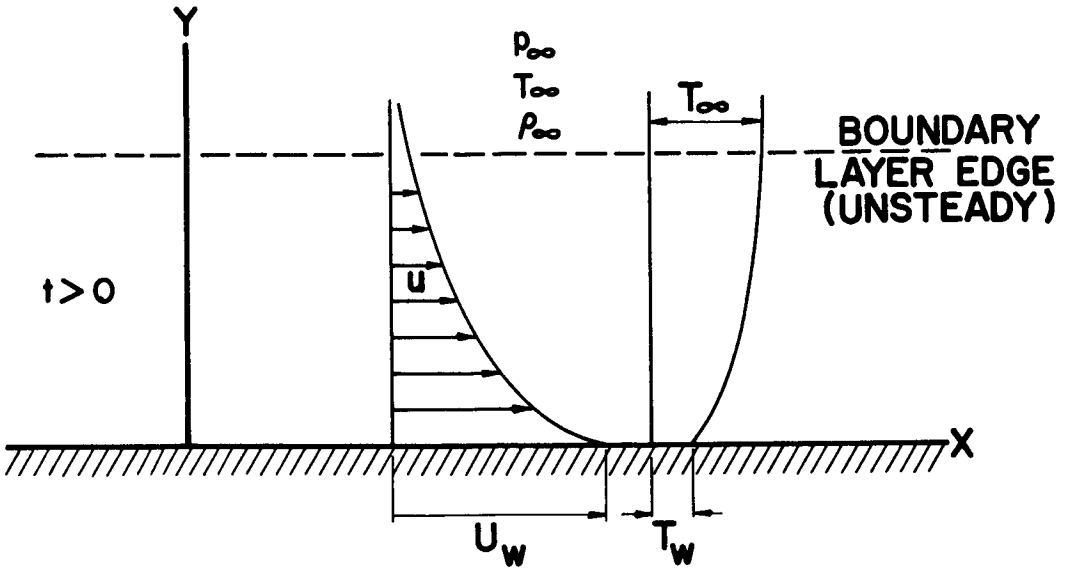


Fig. 1. Rayleigh's boundary layer. Definition of coordinate system and significant variables.

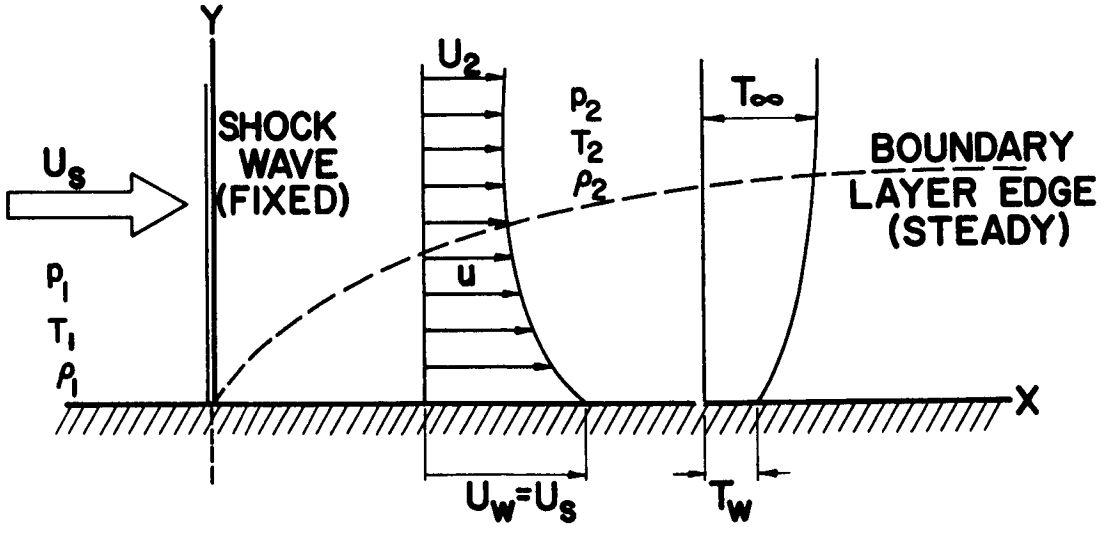


Fig. 2. Shock tube side-wall boundary layer. Definition of shock wave fixed coordinate system and significant variables.

## 3. ELECTRICAL CHARACTERISTICS OF A PARTIALLY IONIZED BOUNDARY LAYER

### a. The Induced Electric Field

In a partially ionized gas containing regions with gradients in composition, temperature, etc. which cause diffusion, the electrons, due to their larger thermal speed, tend to diffuse at a faster rate than the heavier ions. In such a region, there will therefore, in general, be a tendency toward an excess of ions if there are no applied electromagnetic fields. An induced electric field will then be present. This field will slow down the faster diffusing electrons and accelerate the diffusion of the ions. For the case of a weakly ionized gas and simple, ideal gas properties it is well known (e.g., Allis [26]), that in the limit of strong coupling of the electron and ion motion, i.e., the ambipolar diffusion limit, the effective common diffusion-coefficient is twice the free diffusion-coefficient for the ions alone. In this limit the ratio of number density electrons and ions is close to unity. Ambipolar diffusion has been studied in simple limits of constant gas properties by, for example, Allis and Rose [27], and Frost [28].

Strong coupling between the diffusive motion of the electrons and the ions, ambipolar diffusion, is possible only when the Debye length is much smaller than a characteristic length for the diffusion region. The Debye length is defined in MKSA units as

$$\ell_D = \left[\frac{\epsilon_o kT}{n_e q_e^2}\right]^{1/2} = 69.0 \left[\frac{T}{n_e}\right]^{1/2} \quad \text{(meters)} \qquad (3.1)$$

Here, $\epsilon_o$ is the permittivity of vacuum, $k$ the Boltzmann constant, $n_e$

the electron number density, and $q_e$ the charge of the electron. In the present plasma boundary layer problem, the Debye length of the unperturbed, shock heated plasma is considerably smaller than the thickness of the thermal boundary layer, which is the characteristic length for the associated diffusion problem in the boundary layer. Therefore, the conditions will be close to ambipolar at least in the outer part of the boundary layers. However, closer to the wall, which we assume is "cold", the number density of free electrons $n_e$, will decrease rapidly, if we assume a boundary layer in thermo-chemical equilibrium. Then the Debye length will increase. Specifically, at some distance $y$ from this wall, the value of the local Debye length will be equal to $y$. Still closer to the wall, the Debye length will increase further and be larger than the corresponding distance to the wall. Ambipolar conditions presumably will not be present. Here the diffusive motion of the electron and the ion fluids are weakly coupled. The total number fluxes of electrons and ions, however, are largely determined by the conditions in the ambipolar region, if the reaction rates are slow. We may speak here of a sheath of considerable relative charge separation. The diffusion is almost of the type "free". The sheath contains an excess of ions, for the case that the net current to the wall is zero.

In what follows we shall derive some diffusional properties, including the strength of the induced electric field in the ambipolar, transition, and sheath regions of the ionized boundary layer. The net current to the wall is assumed to be zero which is a relevant condition, e.g., in a shock tube experiment. The diffusive flow is steady, and quasi-one dimensional, i.e., perpendicular to the wall, and the convection negligible.

From the continuity equation (2.3) for the electron and ion fluids, we find, upon elimination of the collision-term, the following simple relation

$$\nabla_{\vec{r}} \cdot (n_e \vec{V}_e) = \nabla_{\vec{r}} \cdot (n_i \vec{V}_i) \tag{3.2}$$

Here, $\vec{V}_e$ and $\vec{V}_i$ are the electron and ion diffusional velocities. This relation holds for nonequilibrium situations as well. Assuming that the total current density is zero, we find the following simple expression:

$$\vec{\Gamma}_e = \vec{\Gamma}_i \tag{3.3}$$

Here, $\vec{\Gamma}_e = \vec{V}_e n_e$ is the electron diffusive flux vector and $\vec{\Gamma}_i$ the ion flux vector.

When the gas pressure p is constant, as in our plasma boundary layer, and thermal diffusion can be neglected, the following expressions can easily be obtained for the diffusion velocities of the components in the partially ionized gas

$$\vec{V}_s = \frac{n^2}{n_s \rho} \sum_j^3 m_j D_{sj} \vec{d}_j \; ; \quad (s = a,e,i) \tag{3.4}$$

$$\left.\begin{aligned} \vec{d}_a &= \frac{\partial}{\partial \vec{r}} (n_a/n) + \frac{n_a m_a}{p\rho} \vec{E}\, q_i (n_i - n_e) \\ \vec{d}_i &= \frac{\partial}{\partial \vec{r}} (n_i/n) - \frac{n_i m_a}{p\rho} \vec{E}\, q_i (n - n_i) \\ \vec{d}_e &= \frac{\partial}{\partial \vec{r}} (n_e/n) + \frac{n_e m_a}{p\rho} \vec{E}\, q_i (n - n_e) \end{aligned}\right\} \tag{3.5}$$

Here the usual notation in kinetic theory (e.g., [17]) is used. Hence, $\vec{d}_s$ is a driving force for diffusion, $D_{sj}$ the multicomponent diffusion coefficient, $n$ the total number density ($n = n_a + n_e + n_i$), $m_a$ the atom mass, and $\vec{E}$ the strength of the electric field.

The electric field strength can be calculated if we substitute the expressions (3.5) for the driving forces into equations (3.3, 3.4). The somewhat complicated result is

$$\frac{n_e q_i \vec{E}}{nkT} = \frac{(D_{ea}-D_{ia}-D_{ei}) \frac{\partial}{\partial \vec{r}} (\frac{n_i}{n}) + (D_{ea}-D_{ia}+\frac{m_e}{m_a} D_{ie}) \frac{\partial}{\partial \vec{r}} (\frac{n_e}{n})}{\frac{n_i}{n_e}\frac{n-n_i}{n-n_e}(D_{ea}-D_{ia}-D_{ei}) - (D_{ea}-D_{ia}+\frac{m_e}{m_a} D_{ie})} \tag{3.6}$$

If, in the ambipolar limit, which means $n_i/n_e \simeq 1$, we observe the relations between multicomponent diffusion coefficients and the binary diffusion coefficients applied to a three-component gas mixture, our plasma, and also make use of the fact that the electron mass $m_e$ is very small compared to the ion and atom mass $m_a$, the expression for the electric field strength becomes extremely simple:

$$\frac{q_i \vec{E}}{kT} \doteq - \frac{n}{n_e} \frac{\partial}{\partial \vec{r}} (\frac{n_e}{n}) \tag{3.7}$$

With this expression we have an estimate of the electric field necessary to maintain ambipolar diffusion. However, nothing can be concluded from this about the extent of the ambipolar region.

The ambipolar diffusion velocities may next be evaluated. By introducing the calculated ambipolar electric field strength into equation (3.4) we find

$$\left.\begin{aligned} \vec{V}_e &\doteq -2\,\frac{n/n_e}{1-n_e/n}\,D_{ia}\,\frac{\partial}{\partial\vec{r}}\left(\frac{n_e}{n}\right) \\ \vec{V}_i &\doteq \vec{V}_e \\ \vec{V}_a &\doteq -\frac{n_i}{n_a}\,\vec{V}_i \end{aligned}\right\} \qquad (3.8)$$

At this point it should be recalled that the multicomponent diffusion coefficient is $D_{ia} \doteq \mathcal{D}_{ia}$, where $\mathcal{D}_{ia}$ is the binary ion-atom diffusion coefficient. In accordance with simple kinetic theory, we have

$$\mathcal{D}_{ia} = \frac{1}{n}\,\frac{3}{8}\left(\frac{\pi}{2}\,\frac{m_i+m_a}{m_i m_a}\,kT\right)^{1/2}\frac{1}{Q_{ia}} \qquad (3.9)$$

Here, $Q_{ia}$ is an effective hard-sphere ion-atom collision cross-section.

From the expression (3.8) can be recognized the familiar result, that it is the ion-atom diffusion coefficient which determines the ambipolar diffusive flux of charged particles, and that the electron and ion diffusion velocities are equal.

A very simple, but useful expression for the electric potential difference between two arbitrary points (1) and (2) in the ambipolar region of a partially ionized gas is derived next. Introducing the degree of ionization $\alpha$, which is still a useful concept for a quasi-neutral gas, the potential difference upon integration of equation (3.7) becomes

$$V_2 - V_1 = -\int_1^2 \vec{E}\cdot d\vec{r} = \int_1^2 \frac{kT}{q_i}\,\frac{1}{\alpha(1+\alpha)}\,d\alpha \qquad (3.10)$$

This integral can be evaluated easily in practice, since there exists for an equilibrium ionized gas at constant pressure, a unique relation

between the temperature and the degree of ionization $\alpha$. The results of such integrations are shown in Fig. 3 for argon in thermal equilibrium. We note that the potential differences across the ambipolar region of the boundary layers can be of the order 10 volts, when the average plasma kinetic energy is of the order of only 1 eV. The fact that there is a large potential difference associated with the ambipolar diffusion region has not been sufficiently anticipated in the literature. The unexplained large potential difference across the boundary layer in [5], could be attributed to the voltage difference across the ambipolar region, which was not considered. In the plasma boundary layers considered here, the sheath potential may typically amount only to 0.5 volt, and is hence small compared to the ambipolar potential difference.

### b. Charge Separation and the Sheath

In the previous analysis of the ambipolar region we assumed quasi-neutrality, i.e., the ratio of the ion and electron densities is close to unity, $n_e/n_i \simeq 1$. We shall study this assumption in some more detail and determine the charge separation exactly. Furthermore, it will be shown how the ambipolar conditions break down in a transition region to the sheath, in which more or less free collision-dominated diffusion prevails.

Consider now the space charge distribution. It may be determined with the aid of the Poisson equation,

$$\nabla_{\vec{r}} \cdot \vec{E} = \frac{\omega}{\epsilon_o} \tag{3.11}$$

Inserting the results for the induced electric field, equation (3.7), we may describe the charge separation in the ambipolar region by the relation

$$\frac{q_i(n_i-n_e)}{\epsilon_o} \doteq -\frac{\partial}{\partial\vec{r}}\left(\frac{kT}{q_i}\frac{n}{n_e}\frac{\partial}{\partial\vec{r}}\left(\frac{n_e}{n}\right)\right) \tag{3.12}$$

Alternatively, introduction of a Debye-length, $\ell_D$, from equation (3.1) yields the expression

$$\frac{n_i}{n_e} - 1 \doteq -\ell_D^2 \frac{1}{T}\frac{\partial}{\partial\vec{r}}\left(T\frac{\partial}{\partial\vec{r}}\left(\ell n\, n_e/n\right)\right) \tag{3.13}$$

From this relation it can be seen, that the relative charge separation $(n_i/n_e - 1)$ is largely determined by the ratio of the Debye length and y, $\ell_D/y$, where y is the distance from the wall. Ambipolar conditions, i.e., $n_i/n_e - 1 \ll 1$, then prevail approximately only where the Debye length is larger than y, i.e., where $n_e$ is very small. Adjacent to the wall itself, the Debye length $\ell_D$ is considerably larger than the distance y to the wall, and the ambipolar conditions are no longer valid. Figure 4 shows the Debye length for equilibrium ionized argon as a function of temperature and pressure. At thermodynamic conditions corresponding to the boundary layer free stream plasma, the Debye length is typically of the order $10^{-8} < \ell_D < 10^{-7}$ meter. It rapidly increases with decreasing temperature. At 3000°K, for example, $\ell_D$ is as large as 2 mm. Presently, our interest is mainly with boundary layer thicknesses of the order 1 mm. Therefore, we may conclude that for the equilibrium argon plasma, the ambipolar region will roughly exist above 4000°K. At lower

temperatures a transition to the sheath with nearly "free" diffusion takes place rapidly. If the gas was not in chemical equilibrium, the number density of charged particles should be higher near the wall. Therefore, the sheath becomes considerably thinner than for the equilibrium case. As will be shown later for the argon plasma boundary layer, the equilibrium assumption is not at all valid at the temperatures and number densities typical for the sheath, i.e., $T < 4000°K$. Further analysis of an equilibrium argon sheath is therefore not of practical interest.

In the sheath and the transition region the gas will be only weakly ionized. If, instead of equilibrium, we consider a case with very slow electron-ion reaction rates (frozen flow), and equal temperatures of the electron, ion, and atom fluids, the following set of flux equations govern the collision-dominated, steady, diffusive motion of the electron and ion fluids:

$$\Gamma_i = \Gamma_e = \text{constant} = \Gamma \tag{3.14}$$

$$\frac{\Gamma}{n_e D_{ea}} = -\frac{1}{n_e/n}\frac{d}{dy}(n_e/n) - \frac{Eq_i}{kT} \tag{3.15}$$

$$\frac{\Gamma}{n_i D_{ia}} = -\frac{1}{n_i/n}\frac{d}{dy}(n_i/n) + \frac{Eq_i}{kT} \tag{3.16}$$

Here, $D_{ea}$ and $D_{ia}$ are the electron-atom and ion-atom multicomponent diffusion coefficients, $y$ the coordinate perpendicular to the (plane) wall, and $E$ the electric field strength in the y-direction. The electron and ion fluxes in the y-direction are equal since there is neither any net current nor electron-ion reactions. Before proceeding, it should be mentioned that the assumption of equal temperatures is

unrealistic, at least for an argon high density plasma. At typical shock tube conditions the elastic collisional energy transfer rate between the electrons and the heavy particles is too small to maintain thermal equilibrium. In part, this is due to the Ramsauer effect, which makes the elastic electron-atom collision cross-section very small. The Ramsauer minimum occurs at an energy of about 0.3 eV.

For reference, we shall develop the general diffusion equations (3.15, 3.16) one step further. It is found convenient to normalize them with appropriate parameters somewhere in the ambipolar region, at a distance $y_s$ from the wall, where is valid $|n_i/n_e - 1| \ll 1$. With new non-dimensionalized variables defined as

$$\left.\begin{aligned} \tilde{n}_e &= n_e/n_{es} \;; \qquad \tilde{n}_i = n_i/n_{es} \\ \tilde{y} &= y/y_s \end{aligned}\right\} \tag{3.17}$$

the equations (3.15, 3.16) governing the diffusive flow outside and inside the sheath, take the dimensionless form

$$\text{electrons:} \quad \frac{d}{d\tilde{y}}\left(\ell n\, \tilde{n}_e/n\right) = -\frac{\Gamma y_s}{n_e D_{ea}} - \frac{y_s^2}{\ell_D^2}\frac{1}{\tilde{n}_e}\left[\frac{E_s \epsilon_o}{q_i y_s n_{e_s}} - \int_{\tilde{y}}^{\tilde{y}_s}(\tilde{n}_i - \tilde{n}_e)d\tilde{y}\right] \tag{3.18}$$

$$\text{ions:} \quad \frac{d}{d\tilde{y}}\left(\ell n\, \tilde{n}_i/n\right) = -\frac{\Gamma y_s}{n_i D_{ia}} + \frac{y_s^2}{\ell_D^2}\frac{1}{\tilde{n}_e}\left[\frac{E_s \epsilon_o}{q_i y_s n_{e_s}} - \int_{\tilde{y}}^{\tilde{y}_s}(\tilde{n}_i - \tilde{n}_e)d\tilde{y}\right] \tag{3.19}$$

The electric field strength $E$ has been eliminated with the help of the Poisson equation (3.11). The parameter $E_s$ is the electric field strength at the reference point in the ambipolar region. It cannot

be neglected, but is essential to the sheath solution. In fact, for the partially ionized boundary layers considered here, $E_s$ will be quite large and possibly even larger than the electric field strength inside the sheath.

The boundary conditions for equations (3.18, 3.19) are the following:

$$\left.\begin{aligned} \tilde{n}_e(\tilde{y} = 1) &= 1 \qquad & \tilde{n}_e(\tilde{y} = 0) &\doteq 0 \\ \tilde{n}_i(\tilde{y} = 1) &= 1 \qquad & \tilde{n}_i(\tilde{y} = 0) &\doteq 0 \end{aligned}\right\} \tag{3.20}$$

It is clearly seen from the diffusion equations again how strong coupling in the diffusive motion of the electron and ion fluids comes about when the Debye length $l_D$ becomes small in comparison to $y_s$; conversely, there is weak coupling and "free" diffusion when $\ell_D$ is larger than $y_s$.

It should be pointed out, that although the gas is weakly ionized the electron-ion collisions are still important for the sheath structure, e.g., for ionized noble gases with low Ramsauer minima in the elastic electron-atom cross-section. The multicomponent diffusion-coefficient, $D_{ea}$ in equation (3.18), should in this case, not be replaced by the binary electron-atom diffusion-coefficient, $\mathcal{D}_{ea}$, but rather by the expression

$$D_{ea} \doteq \frac{n_i + n_a}{\frac{Q_{ei}}{Q_{ea}} n_i + n_a} \mathcal{D}_{ea} \tag{3.21}$$

or, in the weakly ionized limit, by

$$D_{ea} \doteq \frac{1}{1 + \frac{Q_{ei}}{Q_{ea}} \frac{n_i}{n}} \mathcal{D}_{ea} \; ; \qquad \mathcal{D}_{ea} \doteq \frac{1}{n} \frac{3}{8} \left(\frac{\pi}{2} \frac{kT}{m_e}\right)^{1/2} \frac{1}{Q_{ea}} \tag{3.22}$$

Here, the quantity $\left(\frac{Q_{ei}}{Q_{ea}} \frac{n_i}{n}\right)$ is not small compared to unity even though $n_i/n \ll 1$. At this point, we shall not go further and solve these faily complex diffusive flux equations. Such a calculation and further discussion of the sheath structure is left to a forthcoming report. It should then be interesting to allow for different temperatures of the electron and ion-atom fluids.

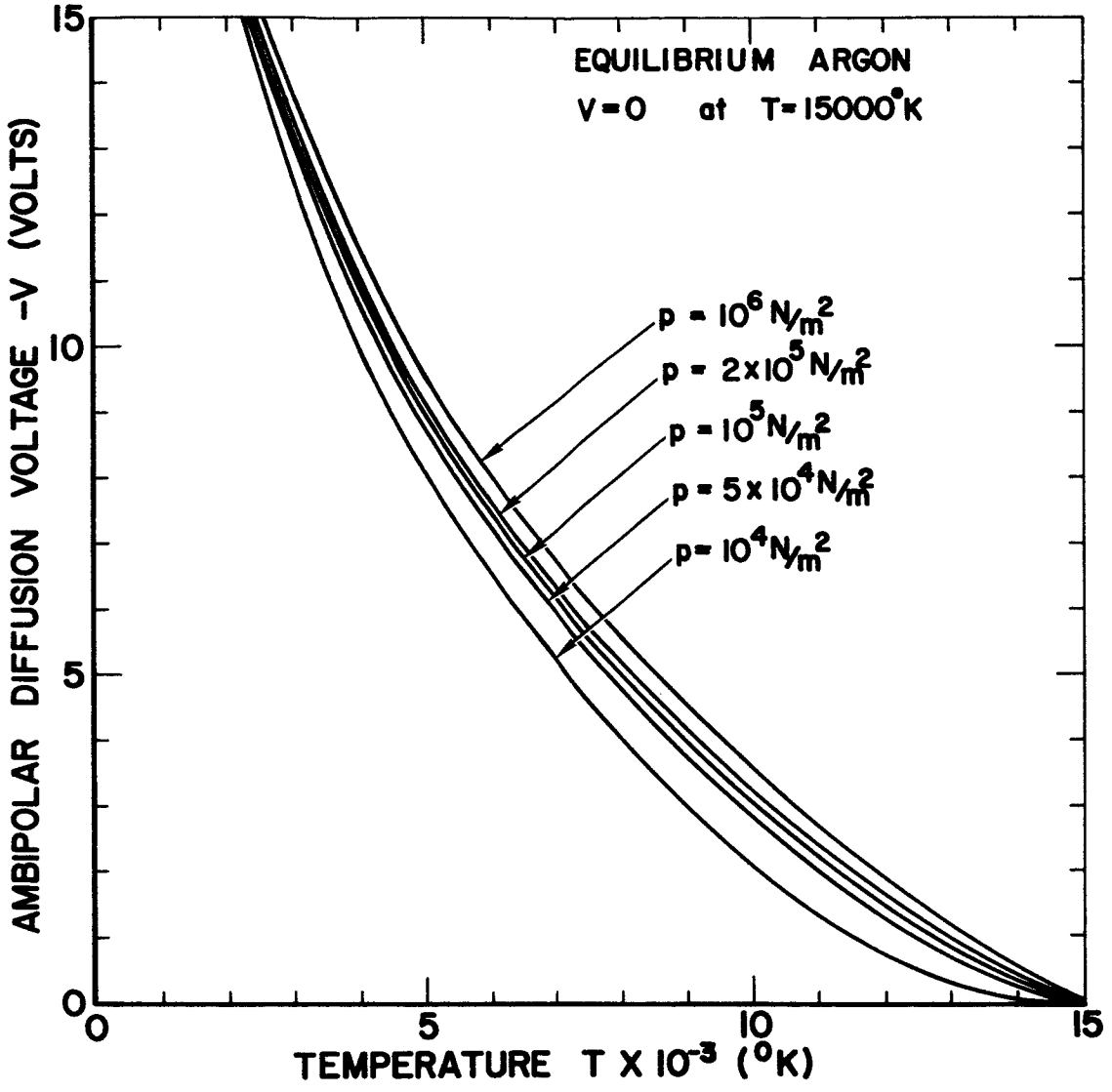


Fig. 3. Electric potential in ambipolar diffusion region for equilibrium partially ionized argon.

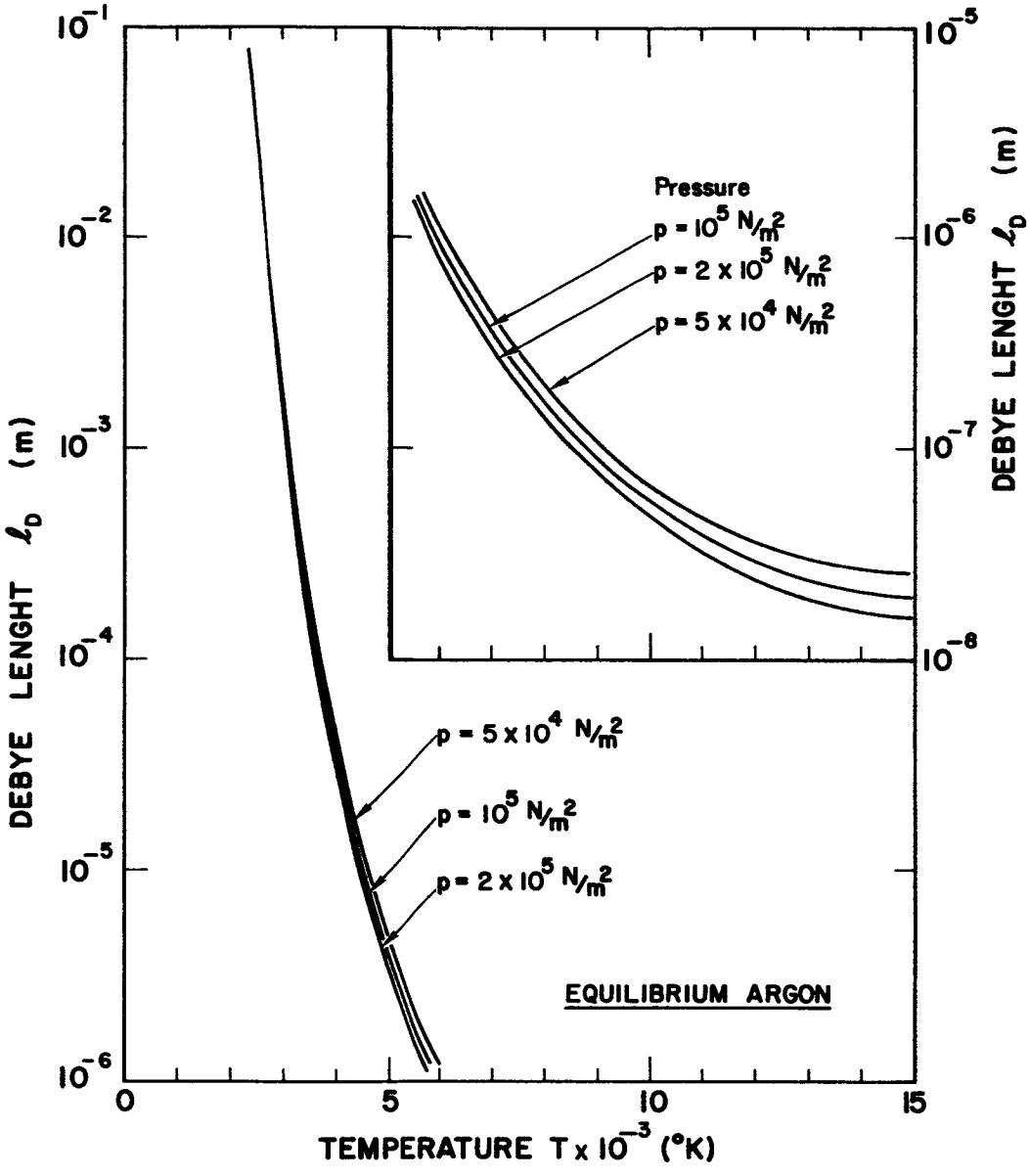


Fig. 4. Debye length for equilibrium, partially ionized argon.

## 4. THERMOGASDYNAMIC PROPERTIES OF SHOCK-HEATED, PARTIALLY IONIZED ARGON

### a. Equilibrium Thermodynamics

The boundary layer equations are to be solved for an equilibrium argon plasma. Therefore we review briefly the appropriate thermogasdynamic properties in this section. Firstly, the simple thermodynamic properties will be discussed, and thereafter the thermogasdynamic properties behind a normal, ionizing shock wave will be displayed.

The partition functions and related thermodynamic properties of argon plasmas have been analyzed by several authors, e.g., Drellishak, Knopp, and Cambel [29], and reviewed by Cambel, Duclos, and Anderson [30]. The previous authors calculated the partition functions for an argon plasma including the first four ions, using both observed and predicted energy levels of the atoms and ions. The usually divergent set of partition functions was terminated by use of a Debye cut-off. The lowering of the ionization potential due to energy perturbations arising from electrostatic interactions with other charged particles was considered as well.

For present purposes we are interested mainly in plasma temperatures below 15,000-20,000°K at pressures of the order of magnitude of $0.1 < p < 10$ atm. The argon plasma is then essentially only singly ionized. If we also neglect the lowering of the ionization potential, which typically will amount only to a fraction of one electron volt for argon, the equilibrium composition and thermodynamic properties are particularly simple to evaluate. The equilibrium composition neglecting

the induced electric field, is given by the relation

$$\frac{n_e n_i}{n_a} = \left(\frac{2\pi\, m_e kT}{h^2}\right)^{3/2} \frac{2\, Z_i^{elec.}}{Z_a^{elec.}} \exp\left(-\frac{I_1}{kT}\right) \tag{4.1}$$

Here $Z_i^{elec.}$ is the electronic partition function for the singly-charged ion, $Z_a^{elec.}$ the electronic partition function for the atom, $I_1$ the first ionization potential, and $h$ the Planck's constant. The factor 2 in front of the ion electronic partition function stands for the two possible orientations of spin of the free electron, and represents its statistical weight. For argon the ratio of the ion-atom electronic partition functions is approximately

$$\frac{Z_i^{elec.}}{Z_a^{elec.}} \doteq \frac{4 + 2\exp(-2062/T)}{1} \tag{4.2}$$

Assuming that the gas is quasi-neutral, which is true, e.g., in the ambipolar region of the plasma boundary layer, it is meaningful to use the degree of ionization $\alpha$, defined as

$$\alpha = \frac{n_e}{n_a + n_e} \tag{4.3}$$

With the aid of the perfect gas law for each component, i.e., $p_e = n_e kT$ for the electrons, etc., the equilibrium relation (4.1) reduces to the familiar Saha type equation

$$\frac{\alpha^2}{1-\alpha^2} = \left(\frac{2\pi\, m_e}{h^2}\right)^{3/2} \frac{(kT)^{5/2}}{p} \frac{8 + 4\exp(-2062/T)}{1} \exp(-182900/T) \tag{4.4}$$

The first ionization potential for argon , $I_1 = 15.7$ eV, has been inserted, i.e., $I_1/k = 182{,}900°K$.

The thermodynamic properties are determined easily from the partition functions. If we neglect the contribution of electronic excited states to the enthalpy $h$ of the plasma, we have

$$h \doteq \frac{k}{m_a} \left[\frac{5}{2} (1+\alpha)T + \alpha I_1/k\right] \tag{4.5}$$

The electronic excited states would affect this value at most 1-2% when the temperature is below 15,000°K. For our purposes, expression (4.5) could possibly be used even up to temperatures of 20,000°K. The equilibrium specific heat $c_p$, which, e.g., is of interest in the evaluation of the Prandtl number in a subsequent section, then becomes

$$c_p = \left(\frac{\partial h}{\partial T}\right)_p \doteq \frac{k}{m_a} \left[\frac{5}{2} (1+\alpha) + \left(\frac{5}{2} T + \frac{I_1}{k}\right)\left(\frac{\partial \alpha}{\partial T}\right)_p\right] \tag{4.6}$$

The derivative $(\partial\alpha/\partial T)_p$ could be calculated with the help of equation (4.4).

### b. Thermogasdynamic Properties

The equilibrium conditions behind a strong, ionizing, plane shock wave could be calculated from the usual shock relations neglecting radiation. Thermodynamic data for shock heated plasmas have not been reported extensively in the literature, although the calculations are quite simple to perform with the help of a digital computer. Limited data for the noble gases have however been reported by, for example,

Niblett and Kenny [31]. Therefore, for reference we shall briefly give here calculated thermogasdynamic properties of a shock heated argon plasma as a function of shock speed. The primary interest is for initial pressures of $1 < p_1 < 20$ mm Hg, and shock velocities of $3000 < U_s < 7000$ m/sec, since these conditions partly are within a possible experimental range.

The shock relations relate the conditions in front of and behind the shock wave. They are

$$\left.\begin{aligned} \rho_1 U_s &= \rho_2 U_2 \\ p_1 + \rho_1 U_s^2 &= p_2 + \rho_2 U_2^2 \\ h_1 + \tfrac{1}{2} U_s^2 &= h_2 + \tfrac{1}{2} U_2^2 \end{aligned}\right\} \qquad (4.7)$$

where subscript "1" refers to the conditions in front of the shock wave, and subscript "2" to conditions behind the shock wave in a coordinate system moving with the shock wave. These equations were solved simultaneously with the help of a digital computer. The plasma considered was an equilibrium argon plasma. Initially, the gas was non-ionized with a temperature of $T_1 = 298°K$. The numerical method of solution used was an iterative technique in the density behind the shock wave, $\rho_2$, which is the least sensitive to a variation in shock velocity of the thermodynamic variables behind the shock wave. Typically, a relative accuracy of $10^{-4}$ in the density $\rho_2$ was obtained after only four iterations from a roughly guessed value.

The results of the numerical calculations are shown in Figures 5-8. Typically, number density of free electrons behind the shock wave

is in the range $10^{22} < n_e < 10^{24}$ $m^{-3}$. The ranges of other variables are the degree of ionization $0.1 < \alpha < 0.3$, the temperature $12{,}000 < T < 14{,}000°K$, the density ratio $6 < \rho_2/\rho_1 < 10$.

Similar results can be easily obtained for the properties behind the reflected shock wave at the end-wall of a shock tube. Such data are of interest to the end-wall boundary layer problem. We shall, however, not report the results of such calculations here.

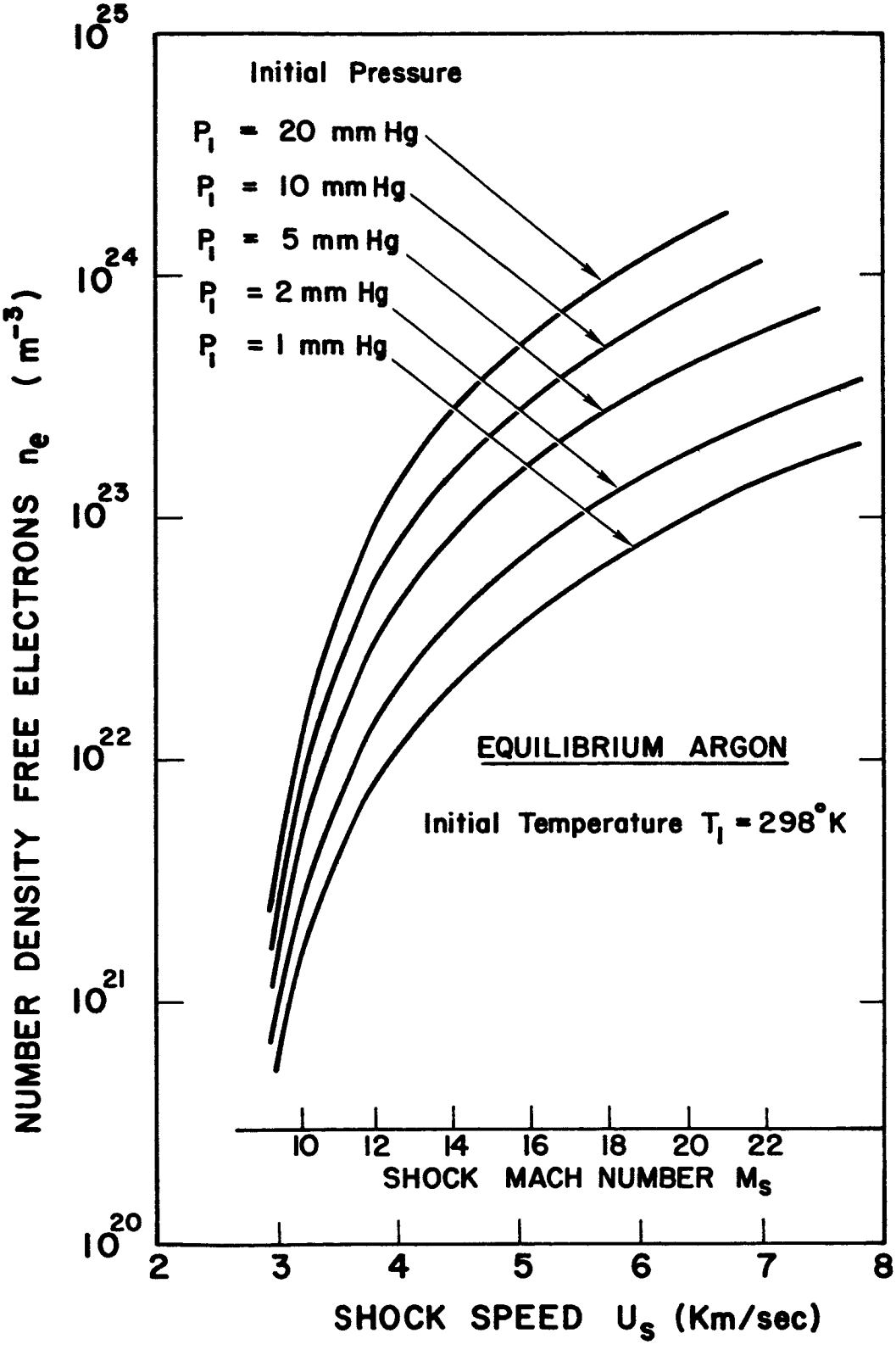


Fig. 5. Number density of free electrons at equilibrium behind a normal shock wave in argon.

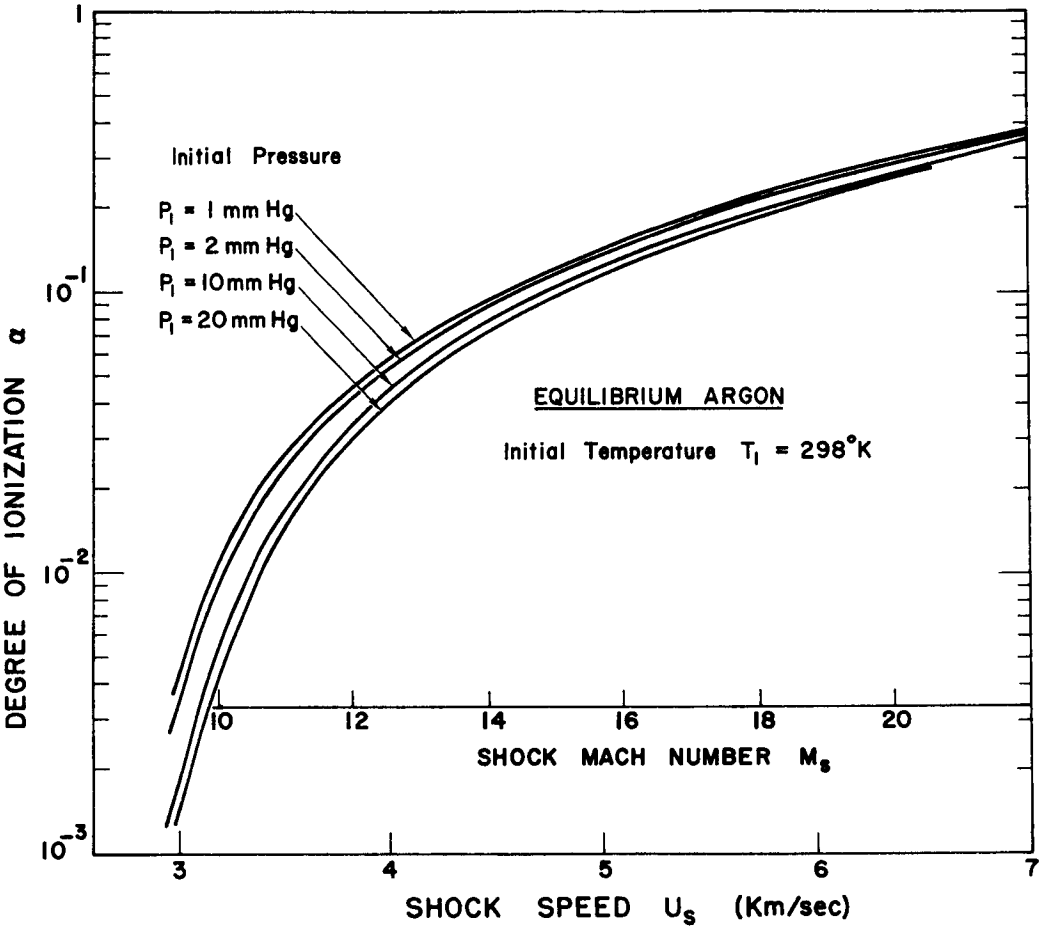


Fig. 6. Degree of ionization at equilibrium behind a normal shock wave in argon.

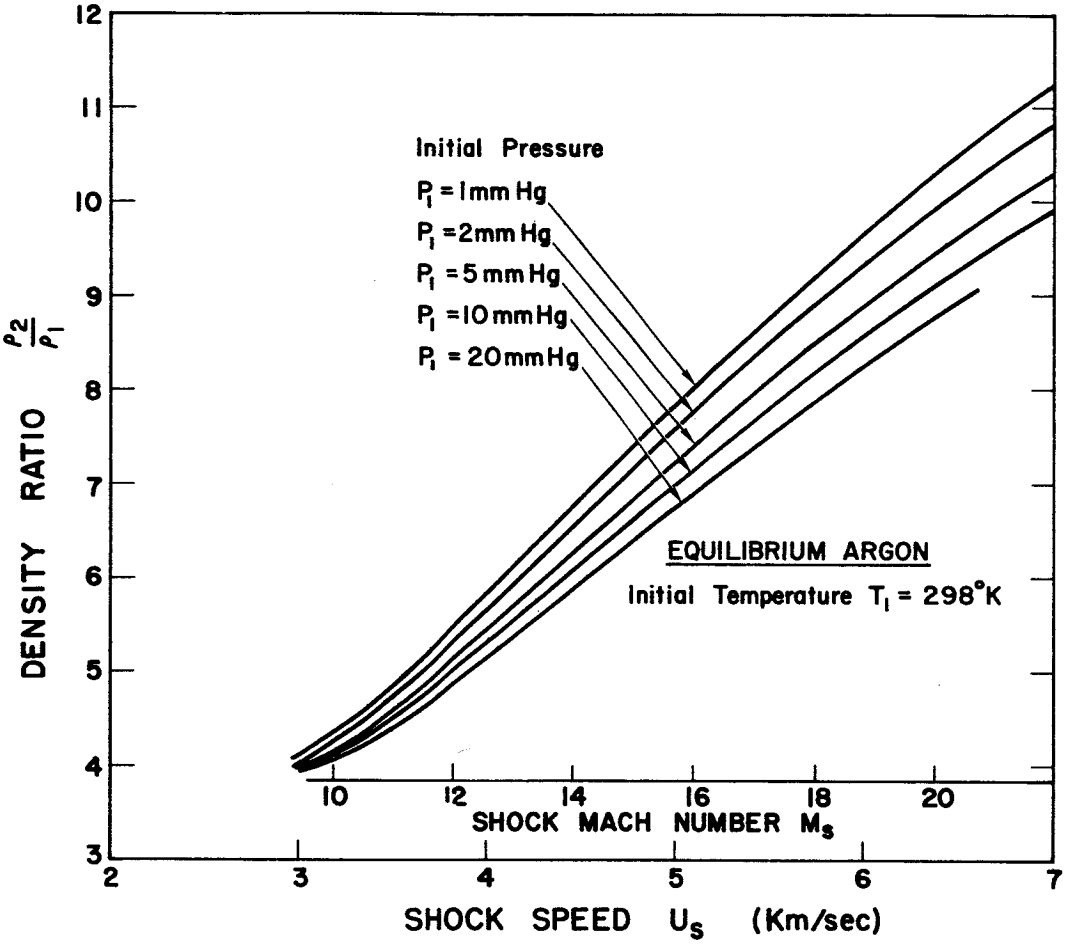


Fig. 7. Temperature at equilibrium behind a normal shock wave in argon.

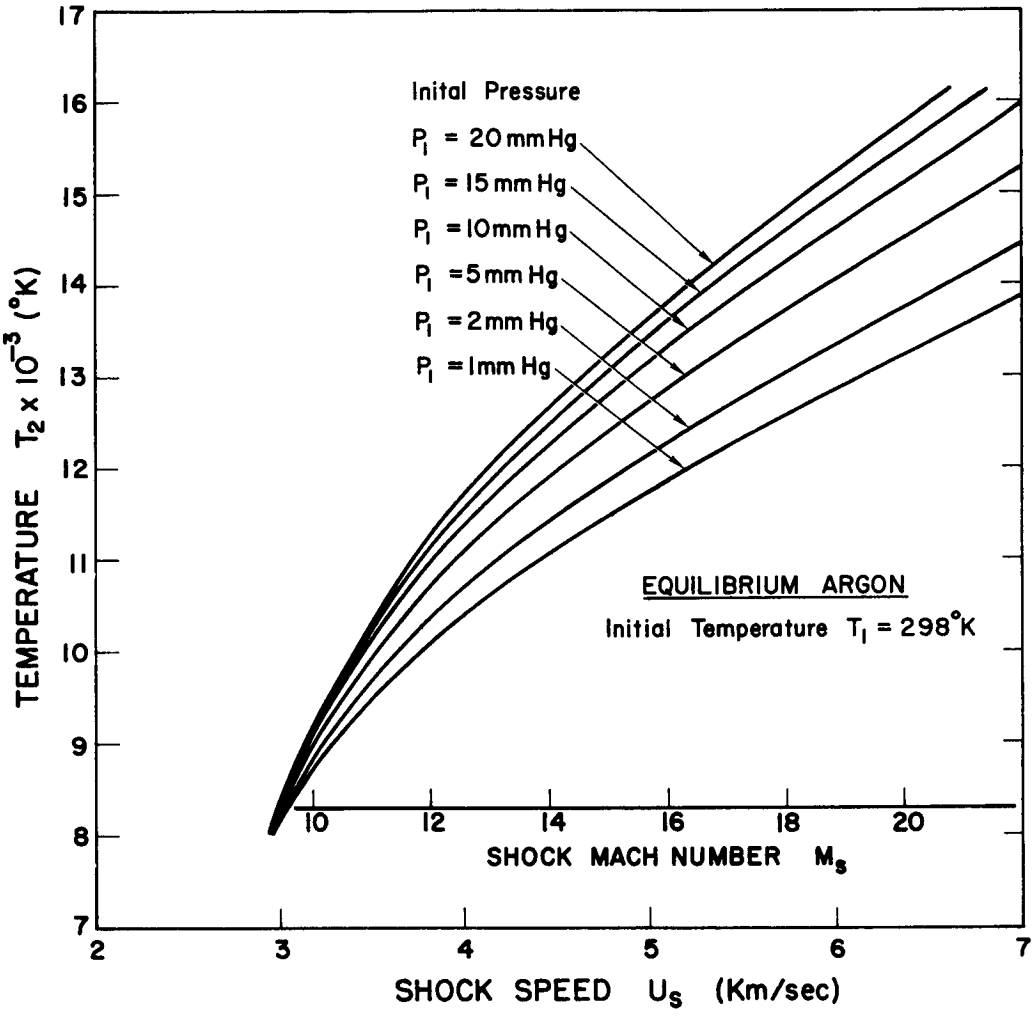


Fig. 8. Density-ratio at equilibrium across a normal shock wave in argon.

# 5. ARGON TRANSPORT PROPERTIES

## a. General

In order to solve the plasma boundary layer equations, we require the transport properties for argon in the complete range from an unionized to a strongly or completely ionized state. In particular, we are interested in ambipolar diffusion coefficients, the viscosity, and the total thermal conductivity. It would, in principle, be desirable to know the transport properties for a reacting gas, including cases where the electron temperature is different from the temperature of the ions and atoms. Such information is not available at the present state of the art. However, here it is quite feasible to neglect the contribution from inelastic and reacting collisions on the overall transport properties. This is possible because elastic collisions are much more frequent than inelastic ones. Indeed, the possibility of energy nonequipartition, i.e., different species temperatures, does not seem to pose an insoluble problem. For our range of thermogasdynamic conditions, energy nonequipartition seems to occur mainly in regions close to the wall, where the degree of ionization is low. Atom transport properties could then be used, e.g., for the thermal conductivity and viscosity, to calculate the boundary layer, overall structure. Only the diffusion coefficients are affected significantly by such a nonequilibrium effect, and the electrical characteristics of the boundary layer hereby changed.

The transport properties for a quasi-equilibrium plasma with particle velocity distribution functions close to Maxwellian, could in principle be calculated with the usual Chapman-Enskog procedure [32].

Such calculations have recently been made for partially ionized gases, e.g., by Sherman [33] and De Voto [34] in various degrees of approximations. The limited amount of information carried in these and other references renders application to the present boundary layer problem somewhat difficult. We shall, therefore, estimate the necessary transport properties of partially ionized argon by use of simple kinetic theory. By doing so we will obtain simplicity and perhaps a clearer understanding of the relative importance of the various type of collisions in the gas. In this approach the transport coefficients are calculated from effective hard-sphere collision cross-sections $Q_{ij}$ for collisions between type $i$ particles and type $j$ particles. The total transport coefficients are constructed as the sum of individual contributions from the electrons, ions and atoms, e.g., with mean free paths estimated by considering all type of collisions.

### b. Diffusion

The diffusion properties were briefly discussed in Section 3 in connection with the electrical properties of the plasma boundary layer. It was then found that, neglecting the current and the thermal diffusion, the common ambipolar diffusion velocity of the electron and ion fluids was given by

$$\vec{V}_e \doteq \vec{V}_i \doteq -2 \mathcal{D}_{ia} \frac{1}{1-n_e/n} \frac{\partial}{\partial \vec{r}} (\ell n\, n_e/n) \tag{5.1}$$

Here $\mathcal{D}_{ia}$ is the ion-atom binary diffusion coefficient. The effect of electron-ion collisions is negligible due to the small electron mass

and inertia. The binary ion-atom diffusion coefficient can therefore, from simple kinetic theory, be expressed as

$$\mathcal{D}_{ia} = \frac{1}{n} \frac{3}{8} \left(\pi \frac{kT}{m_a}\right)^{1/2} \frac{1}{Q_{ia}} \tag{5.2}$$

where $Q_{ia}$ is an effective, average hard-sphere collision cross-section for ion-atom collisions. It will depend upon the temperature of the ion and atom fluids. The contribution to $Q_{ia}$ from elastic collisions is quite small compared to that from charge transfer collisions. Typically, the elastic contribution only amounts to 30 $\text{Å}^2$, and is quite insensitive to temperature (relative speed). For simplicity we shall here use a constant value, $Q_{ia} = 30\ \text{Å}^2$, for this average elastic hard-sphere collision cross-section.

The contribution to the effective hard-sphere cross-section $Q_{ia}$ from the symmetric resonant charge transfer collisions is the dominant contribution. It amounts to about 100 $\text{Å}^2$ at 15,000°K, and becomes even larger at lower temperatures. Much theoretical work has been published, e.g., Dalgarno [35], on symmetric resonant charge transfer processes. However, for low relative velocities, which are of interest for our 1 eV plasma, the available amount of information is very limited. In this energy regime the problem of charge exchange is theoretically more difficult to treat, since only a rigorous wave-mechanical treatment may be used. Few experiments have been performed at low energies. Here we will employ a charge exchange cross-section having the form

$$(Q_{tr}^{tot})^{1/2} = -k_1 \ln g + k_2 \tag{5.3}$$

where $g$ is the relative speed and $k_1$ and $k_2$ constants. For argon we assign values to these constants as in [34]. Integration over Maxwellian atom and ion velocity distribution functions yields the appropriate contribution from the symmetric resonant charge transfer to $Q_{ia}$. The results are shown in Fig. 9. For reference this figure also shows other important effective hard sphere cross-sections used in the present analysis.

In terms of the degree of ionization $\alpha$, equation (5.1) for the ambipolar diffusion velocity reduces to the simple form

$$\vec{V}_e \doteq - 2 \mathfrak{D}_{ia} \frac{\partial}{\partial \vec{r}} (\ell n\, \alpha) \tag{5.4}$$

It is therefore convenient to define the ambipolar diffusion coefficient as $D_{amb} = 2 \mathfrak{D}_{ia}$. This coefficient has been calculated at various pressures and temperatures for the equilibrium argon plasma, using the previously described collisional cross-section data. Figure 10 shows the results of the calculation.

### c. Viscosity

The viscosity of partially ionized argon, in analogy with the results from simple kinetic theory for a pure gas, is here calculated as

$$\mu = \frac{5\pi}{32} \sum_j^3 \rho_j \ell_j U_j \tag{5.5}$$

where $\rho_j$ is the density of component "j," $U_j$ the mean thermal speed $U_j = (8\ kT/(\pi\ m_j)^{1/2}$, and $l_j$ an appropriate mean free path. Specifically, by the mean free path we mean here the average distance travelled between

successive collisions by a particle of kind "j," in which the momentum vector is changed by a considerable amount. Due to the small mass and momentum of the electrons, we will make the assumption that electrons make no contribution to the viscosity, although the collision frequency with heavy particles is large. The mean free paths for the atoms and the ions, neglecting collisions with the electrons, become

$$\ell_a = \frac{1}{\sqrt{2}(n_a Q_{aa} + n_i Q_{ai})} \tag{5.6}$$

$$\ell_i = \frac{1}{\sqrt{2}(n_i Q_{ii} + n_a Q_{ai})} \tag{5.7}$$

Here $Q_{ai}$ is an effective hard-sphere collision momentum exchange cross-section for the atom-ion collisions, and $Q_{ii}$ an effective hard-sphere cross-section for the ion-ion (Coulomb-) collisions. The viscosity of the ionized gas is then

$$\mu = \frac{5\pi}{32}\frac{m_a U_a}{Q_{aa}} \frac{1 + \frac{\alpha}{1-\alpha}\frac{Q_{ai}}{Q_{aa}}}{\frac{\frac{Q_{ai}}{Q_{aa}} + \frac{\alpha}{1-\alpha}\frac{Q_{ii}}{Q_{aa}}}{1 + \frac{\alpha}{1-\alpha}\frac{Q_{ai}}{Q_{aa}}}} \tag{5.8}$$

Note that in deriving this expression we have assumed that the temperatures of the atoms and ions are equal, i.e., their mean thermal speeds are equal. It should be pointed out, that the pure atom viscosity is

$$\mu_{atoms} = \frac{5\pi}{32}\frac{m_a U_a}{Q_{aa}} \tag{5.9}$$

Amdur and Mason [36] have made a theoretical study of the viscosity of pure argon, neglecting excitation, with force laws calculated from beam experiments. Using their data, the appropriate hard-sphere collision cross-section for the atom-atom collisions $Q_{aa}$ can be calculated. The result is

$$Q_{aa} \doteq 17\left(\frac{T}{10^4}\right)^{-0.26} \qquad (\text{Å}^2) \tag{5.10}$$

Hence, the value of cross-section is about 15 $\text{Å}^2$ for temperatures of interest here. Note, with the help of equation (5.9), that the pure atom viscosity depends upon temperature as $\mu_{atoms} \sim T^{0.76}$.

The effective hard-sphere ion-ion collision cross-section $Q_{ii}$ to be used for calculation of the viscosity in equation (5.8) is a Coulomb scattering cross-section. We apply a cut-off in the force-law at the Debye length from the nucleus (Rose and Clark [37]). The result is

$$Q_{ii} \doteq \frac{q_e^2 \ln \Lambda}{4\pi \epsilon_o^2 (3kT)^2} \simeq \frac{387 \ln \Lambda}{(T/10^4)^2} \qquad (\text{Å}^2) \tag{5.11}$$

where, if $\Lambda \gg 1$

$$\Lambda = \frac{12\pi (\epsilon_o kT/q_e^2)^{3/2}}{n_e^{1/2}} \simeq 1.24 \times 10^7 \frac{T^{3/2}}{n_e^{1/2}} \tag{5.12}$$

This cross-section is quite large, of the order $10^3$-$10^4$ $\text{Å}^2$ as is shown in Fig. 9.

With the above cross-section data, the viscosity of partially ionized

argon was calculated from equation (5.8). The results are shown in Fig. 11. It is very interesting that the viscosity shows a maximum at temperatures around $T = 10{,}000°K$ for constant pressure. The degree of ionization is then quite small, in fact, of the order $\alpha = 10^{-2}$. The maximum is attributed to the large charge exchange cross-section which becomes increasingly important to the viscosity when the ion number density increases. The viscosity decreases rapidly with temperature above $10{,}000°K$ and approaches above $15{,}000°K$ the small ion viscosity, as calculated, e.g., by Braginskii [38].

We demonstrate in part the above statements in the limit of small degree of ionization, $\alpha \ll 1$, by linearizing equation (5.8). One then finds the following viscosity formula

$$\alpha \ll 1: \qquad \mu \doteq \mu_{atoms} \left(1 - \alpha \frac{Q_{ai}}{Q_{aa}} + \cdots \right) \tag{5.13}$$

Hence, the charge exchange collision cross-section causes the viscosity maximum.

Of particular interest to the plasma boundary layer problem is the variation of the density-viscosity factor $\rho\mu$ at constant pressure. This parameter appeared in boundary layer equations (2.39, 2.40). In classical treatments of boundary layers [21], the parameter $\rho\mu$ is often assumed to be constant across the boundary layer, i.e., the viscosity is proportional to temperature $\mu \sim T$, which makes the boundary layer equations particularly simple to solve. For the present boundary layer analysis, this assumption is not possible. Typically the variation in the density-viscosity product $\rho\mu$ will for the argon plasma span one

or two orders of magnitude. Partly, the reason for this is the small plasma viscosity. As an example, Fig. 12 shows the variation in the density-viscosity factor $\rho\mu$ with temperature and pressure for our ionized gas.

### d. Thermal Conductivity

The total convective energy flux vector $\vec{q}$ consists of species flux vectors $\vec{q}_s$, which are defined by equation (2.6). In the case of thermal equilibrium among the fluids, the energy flux $\vec{q}$ can be written

$$\vec{q} = \sum \rho_j h_j \vec{V}_j - \lambda \frac{\partial T}{\partial \vec{r}} \tag{5.14}$$

Here $\lambda$ is the usual thermal conductivity, $h_j$ the species enthalpy per unit mass, and $\vec{V}_j$ the diffusion velocity of fluid "j". We make the assumptions of ambipolar diffusion and negligible thermal diffusion, which in fact is quite a good assumption here ([34]). The total convective heat flux vector then becomes

$$\vec{q} = -\lambda \frac{\partial T}{\partial \vec{r}} - \left(\frac{5}{2} kT + I_1\right) \frac{2n D_{ia}}{1-n_e/n} \frac{\partial}{\partial \vec{r}} n_e/n \tag{5.15}$$

We have, as in Section 4, neglected a small contribution to the enthalpy from electronically excited states of the atoms and ions.

When the pressure is constant, as for the boundary layers, and the flow is in thermo-chemical equilibrium, there exists a unique relation between the gradient $\frac{\partial}{\partial \vec{r}} \frac{n_e}{n}$, appearing in equation (5.15), and the temperature gradient $\frac{\partial T}{\partial \vec{r}}$. If we neglect the slow variation with

temperature of the ratio of the electronic partition functions (4.2) is found

$$\left(\frac{\partial}{\partial \vec{r}} \frac{n_e}{n}\right)_{\substack{p=\text{const} \\ \text{equilibrium}}} \doteq \frac{\alpha}{2} \frac{1-\alpha}{1+\alpha} \frac{1}{T} \left\{\frac{5}{2} + \frac{I_1}{kT}\right\} \frac{\partial T}{\partial \vec{r}} \tag{5.16}$$

With the help of this relation, the total convective heat flux vector could be written

$$\vec{q} = - \lambda_{tot} \frac{\partial T}{\partial \vec{r}} \tag{5.17}$$

where

$$\lambda_{tot} \doteq \lambda + \frac{\alpha(1-\alpha)}{2} D_{amb} \frac{p}{T} \left[\frac{5}{2} + \frac{I_1}{kT}\right]^2 \tag{5.18}$$

Hence, the total energy flux vector is related to a temperature gradient, thermodynamic variables and transport properties. The second term in equation (3.18) will be referred to as the "reactive conductivity". The terminology is somewhat misleading, but is commonly used for non-ionized gases. The reactive conductivity is of extreme importance when the gas is partially ionized.

Next, the thermal conductivity $\lambda$ will be calculated. Here we will use a simple mixture rule first suggested by Fay [39] for a partially ionized gas. The thermal conductivity then reads

$$\lambda = \sum_i^3 \frac{x_j \lambda_j}{\sum_i^3 x_i G_{ji}} \tag{5.19}$$

where

$$\underline{G} = G_{ji} = \left(\frac{2m_i}{m_j+m_i}\right)^{1/2} \frac{Q_{ji}}{Q_{jj}} \tag{5.20}$$

Here $\lambda_j$ is the thermal conductivity of the component "j", $x_j$ the number density fraction, $m_i$ the particle mass, and $Q_{ji}$ an effective hard-sphere cross-section for collisional energy transfer. The tensor $\underline{G}$ has been introduced to modify the collisional mean free paths of the pure components, and to allow for different persistence ratios in the collisions between particles with different masses. When the equations (5.19, 5.20) are applied to the mixture of electrons, atoms and singly ionized ions, the expressions can be somewhat simplified by the fact that the electron mass is small compared to the atom and ion masses. In terms of $\alpha$, the degree of ionization, and self-explanatory cross-sections, the conductivity then becomes

$$\lambda \doteq \frac{\lambda_a}{1 + \frac{\alpha}{1-\alpha}\frac{Q_{ai}}{Q_{aa}}} + \frac{\lambda_i}{1 + \frac{1-\alpha}{\alpha}\frac{Q_{ai}}{Q_{ii}}} + \frac{\lambda_e}{1 + \sqrt{2} + \sqrt{2}\frac{1-\alpha}{\alpha}\frac{Q_{ea}}{Q_{ee}}} \tag{5.21}$$

Following Fay [39], we adjust the values of the ion thermal conductivity and the electron thermal conductivity to agree with the values calculated by Spitzer [40] and others for a fully ionized plasma. These are

$$\alpha = 1: \quad \begin{cases} \lambda_s = 1.84 \times 10^{-10}\, T^{5/2}/\ell n\, \Lambda \quad \left(\frac{Nm}{m\text{-}sec\text{-}^\circ K}\right) & (5.22) \\ \frac{\lambda_i}{\lambda_e} = \left(\frac{m_e}{m_i}\right)^{1/2} & (5.23) \end{cases}$$

The thermal conductivity of the ions can be neglected. The final result is therefore

$$\lambda \doteq \frac{\lambda_a}{1 + \frac{\alpha}{1-\alpha}\frac{Q_{ai}}{Q_{aa}}} + \frac{\lambda_s}{1 + \frac{1-\alpha}{\alpha}\frac{\sqrt{2}}{1+\sqrt{2}}\frac{Q_{ea}}{Q_{ii}}} \tag{5.24}$$

The pure argon atom thermal conductivity $\lambda_a$ is for our case

$$\lambda_a = \frac{75\pi}{128} k \frac{U_a}{\sqrt{2}\, Q_{aa}} \doteq 2.43 \times 10^{-4}\, T^{3/4} \left(\frac{Nm}{m\text{-}sec\text{-}^\circ K}\right) \tag{5.25}$$

To calculate the total thermal conductivity, one requires the elastic electron-atom effective hard-sphere cross-section $Q_{ea}$, which appears in equation (5.24). This cross-section will exhibit unusual features due to the previously mentioned Ramsauer effect, which is of purely quantum-mechanical nature and appears only at low relative velocities of the colliding electron and atom. In nature, it is a resonance between the electron cloud in the atom and the incident electronic wave, i.e., the electron. The electron-atom cross-section then becomes very small, less than $1\ \text{Å}^2$ for most noble gases, for energies in the neighborhood of one electronvolt. We shall here assume Maxwellian distribution for the fast-moving electrons and use an effective hard-sphere cross-section $Q_{ea}$, which is calculated from recent experimental data for argon by Frost and Phelps [41]. The results are shown in Fig. 13.

The total convective thermal conductivity for partially ionized argon was finally calculated from equation (5.18). The numerical results are presented in Fig. 14. We see, that for the thermal conductivity, the effects of ionization seem to play in at temperatures above 6000°K. However, the total thermal conductivity is quite insensitive to pressure

up to 12,000°K. Thereafter, a higher pressure level gives a larger total thermal conductivity. Figure 15 shows the relative importance of the electron thermal conductivity and the reactive conductivity term. It is worth noting that the electron contribution starts at about 6000°K, when the degree of ionization is still very small, and rapidly becomes most important at temperatures above 10,000°K. The reactive conductivity contributes to the total thermal conductivity at temperatures above 8000°K. Its maximum importance occurs at temperatures about 13,000 - 14,000°K for pressures of the order magnitude 1 atm. Typically it here amounts to 30% of the total thermal conductivity. The reactive conductivity makes the total conductivity rise with temperature, level off, and even causes a weak maximum around 14,000°K for low pressures. This is demonstrated in Fig. 14. The contribution from pure atoms is very small above 13,000°K, and can definitely be neglected above 15,000°K.

Finally, we will calculate and discuss the Prandtl number. As the boundary layer equations indicated, this dimensionless parameter is very important to the problem. The Prandtl number is essentially a dimensionless measure of the ratio of the diffusivity of energy and the diffusivity of momentum or vorticity. It has been pointed out, e.g., by Fay [42], that for a fully ionized gas, the Prandtl number will be very small. The reason for this is that the plasma thermal conductivity will then be caused by fast moving, light electrons and the viscosity by the heavier ions. From simple kinetic theory it is seen that the Prandtl number is then approximately $Pr = (m_e/m_i)^{1/2}$, and hence much smaller than unity. Thermal boundary layers will therefore develop in plasmas considerably faster than viscous boundary layers.

Partially ionized gases behave similarly. The Prandtl number will be smaller than unity, but not as small as for the fully ionized gas. The appropriate Prandtl number to use here (thermo-chemical equilibrium) is the following

$$Pr = \frac{c_p^{eq.} \mu}{\lambda_{tot}} \tag{5.26}$$

where $c_p^{eq.}$ is the equilibrium specific heat, $\mu$ the viscosity, and $\lambda_{tot}$ the total thermal conductivity. The equilibrium specific heat $c_p^{eq.}$ may take very large values in the regime of partial ionization. In fact, when the pressure is of the order one atmosphere, the equilibrium specific heat is one order of magnitude larger than the frozen specific heat at $T = 14{,}000°K$ (Fig. 16). Therefore, the Prandtl number for an equilibrium partially ionized gas will be much larger than if the composition were frozen and $c_p$ were depending only upon translational modes. The calculated values for equilibrium argon Pr are shown in Fig. 17. The Prandtl number is approximately $Pr = 0.65$ at low temperatures, but starts to decrease at temperatures above $6000°K$ due to the increasingly important electron thermal conductivity. The decrease is also attributed to the charge exchange collision between the ions and atoms, giving a low viscosity. Above $9000°K$ the gas is no longer weakly ionized, and the equilibrium specific heat $c_p$ takes large values. The Prandtl number therefore exhibits first a weak minimum at $8500°K$, and thereafter a pronounced maximum at $11{,}000°K$. The Prandtl number maximum could be larger than unity, if the pressure level is low. At temperatures above $12{,}000°K$ the viscosity of the plasma decreases and the total thermal

conductivity is large. Hence, the Prandtl number then again decreases to very low values with increasing temperature. At temperatures above $T = 15{,}000°K$ the Prandtl number may be as low as $Pr \sim 10^{-2}$ as was earlier pointed out to be the case for a strongly ionized gas.

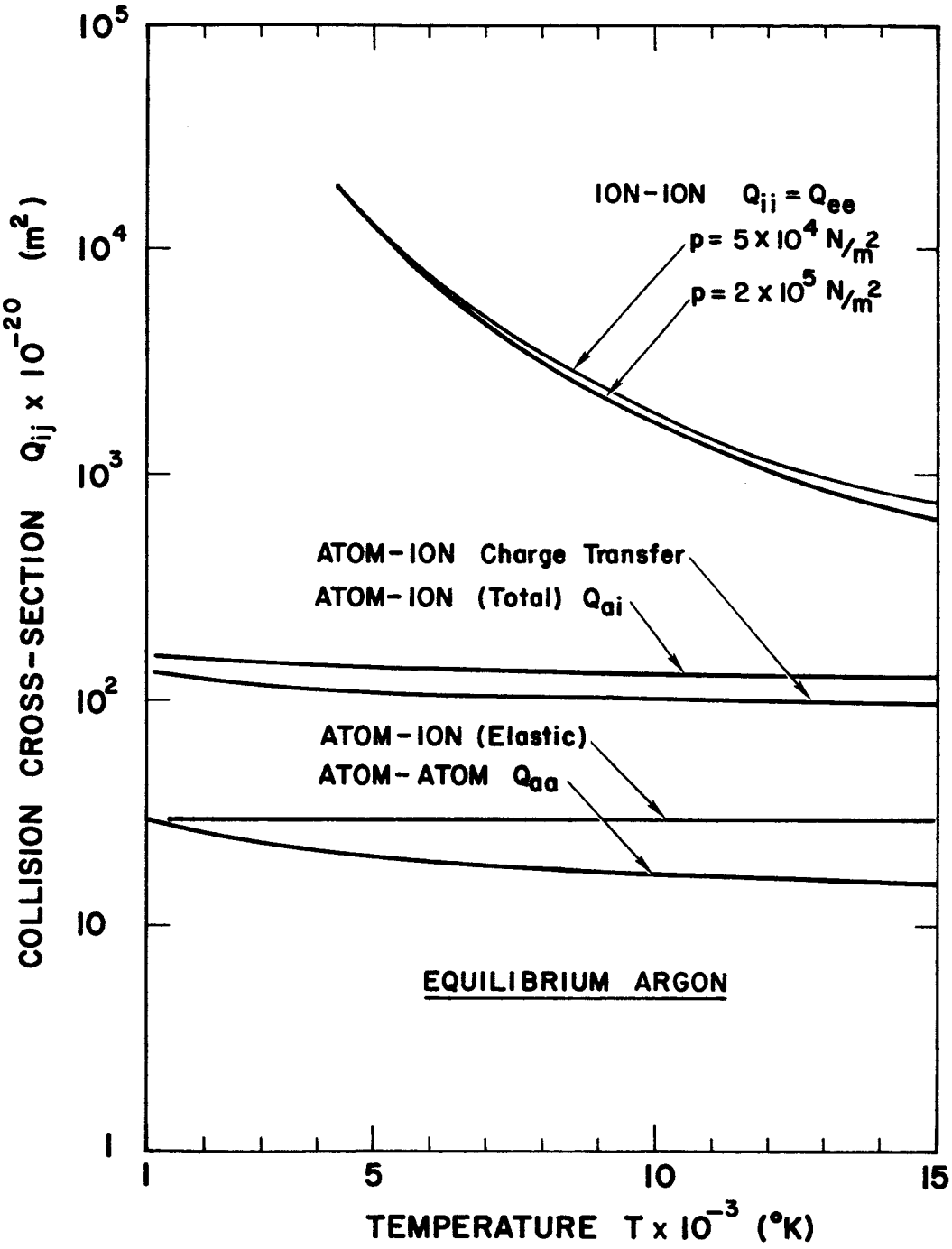


Fig. 9. Effective hard-sphere collision cross-sections used in calculations of transport properties of equilibrium partially ionized argon.

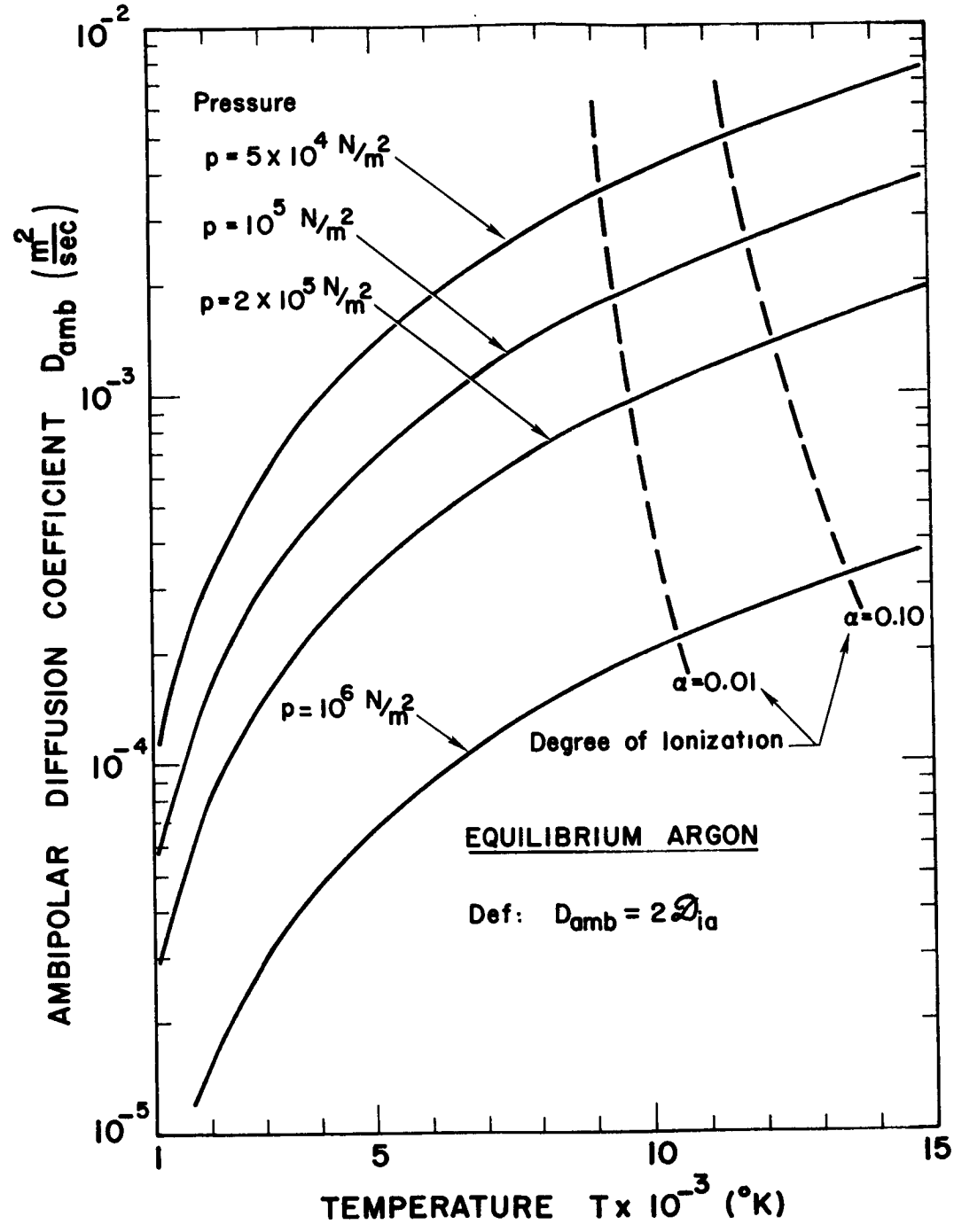


Fig. 10. The ambipolar diffusion coefficient for equilibrium partially ionized argon.

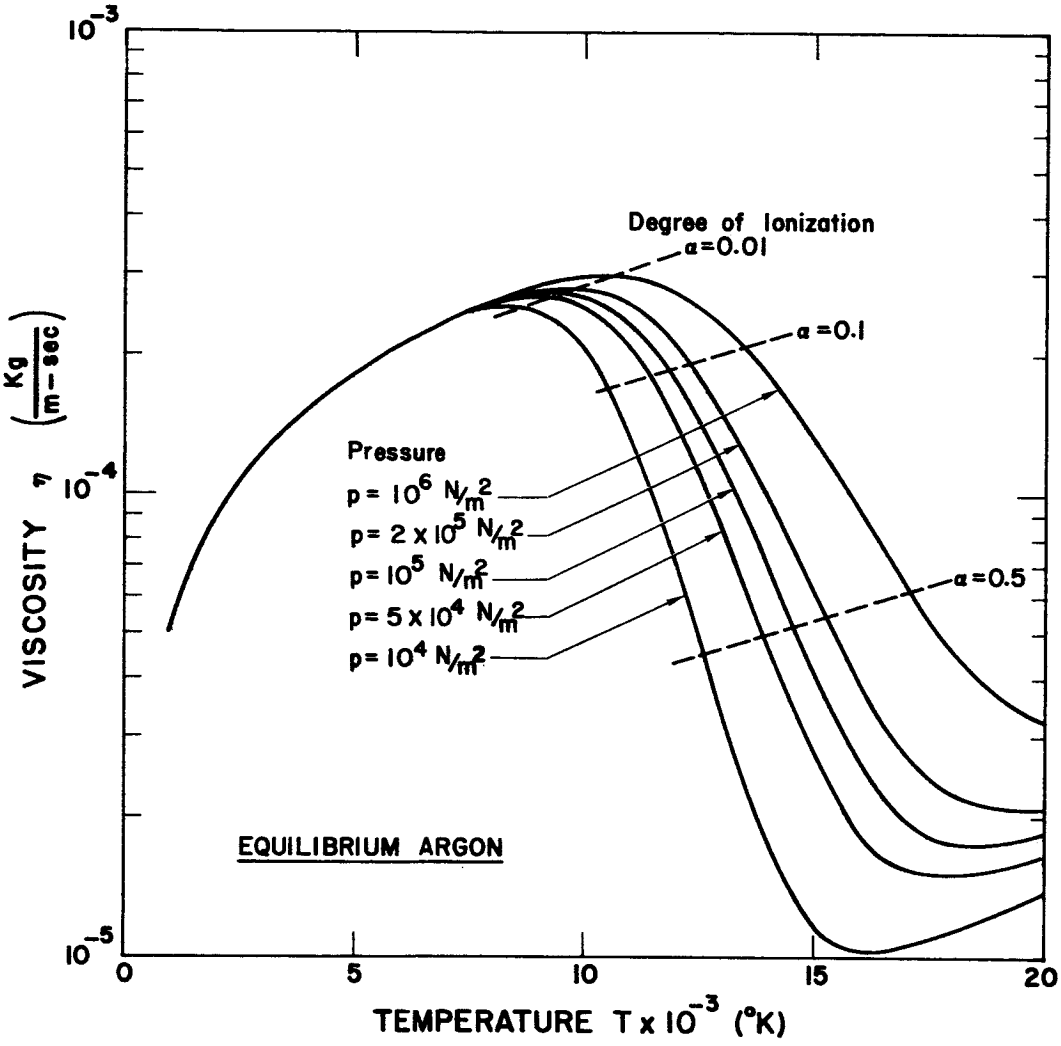


Fig. 11. The viscosity of equilibrium partially ionized argon.

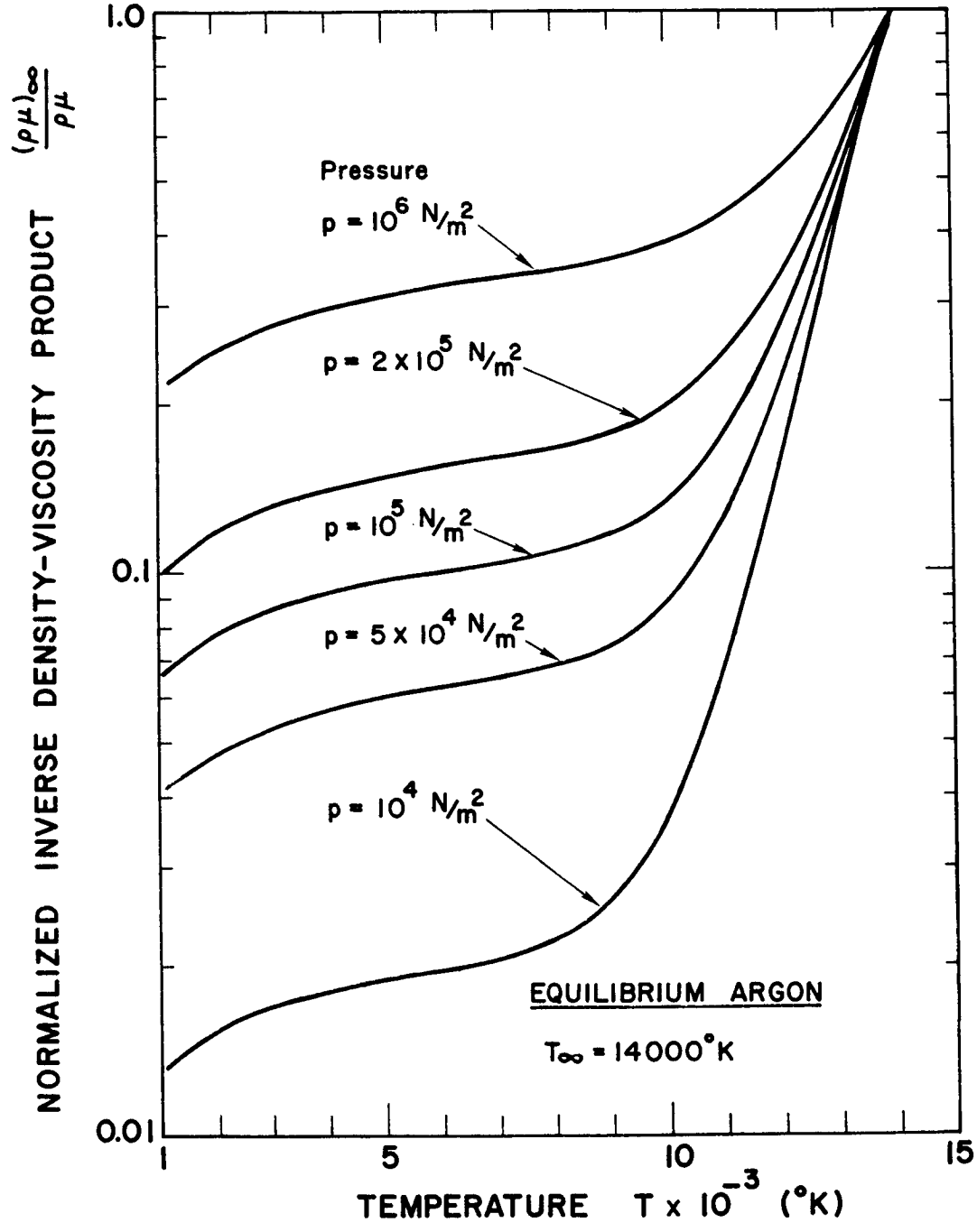


Fig. 12. The inverse density-viscosity product for equilibrium partially ionized argon.

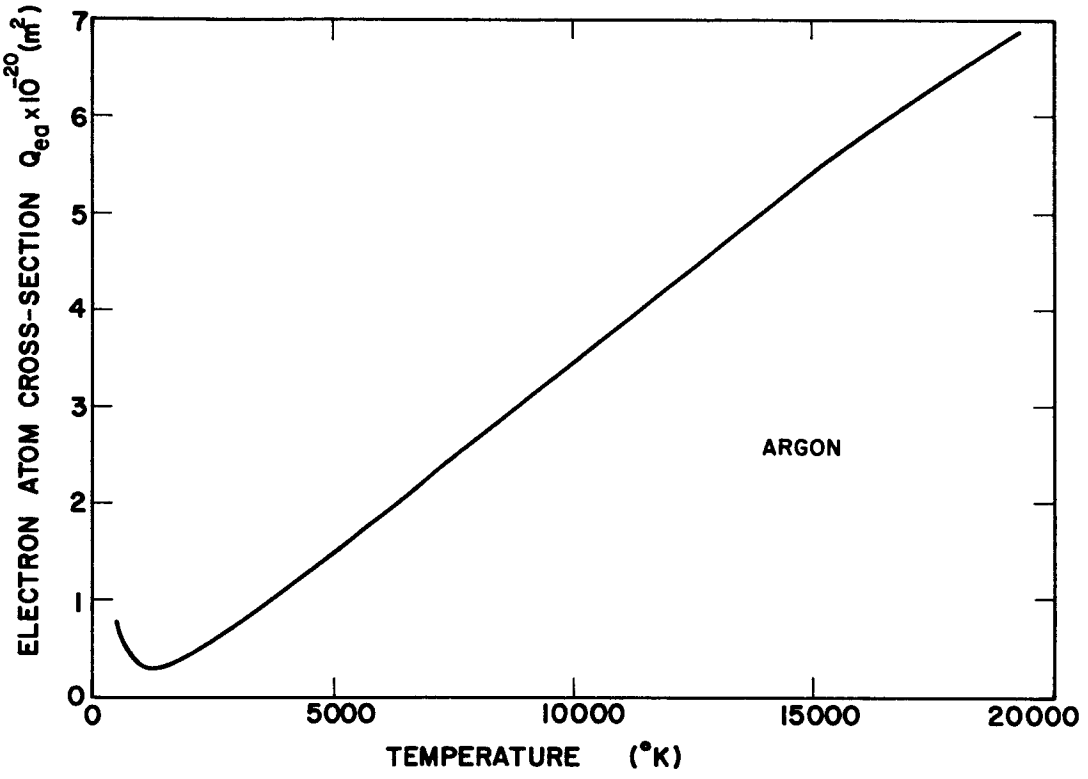


Fig. 13. Effective hard-sphere electron-atom collision cross-section $Q_{ea}$ used for calculation of thermal conductivity of partially ionized argon.

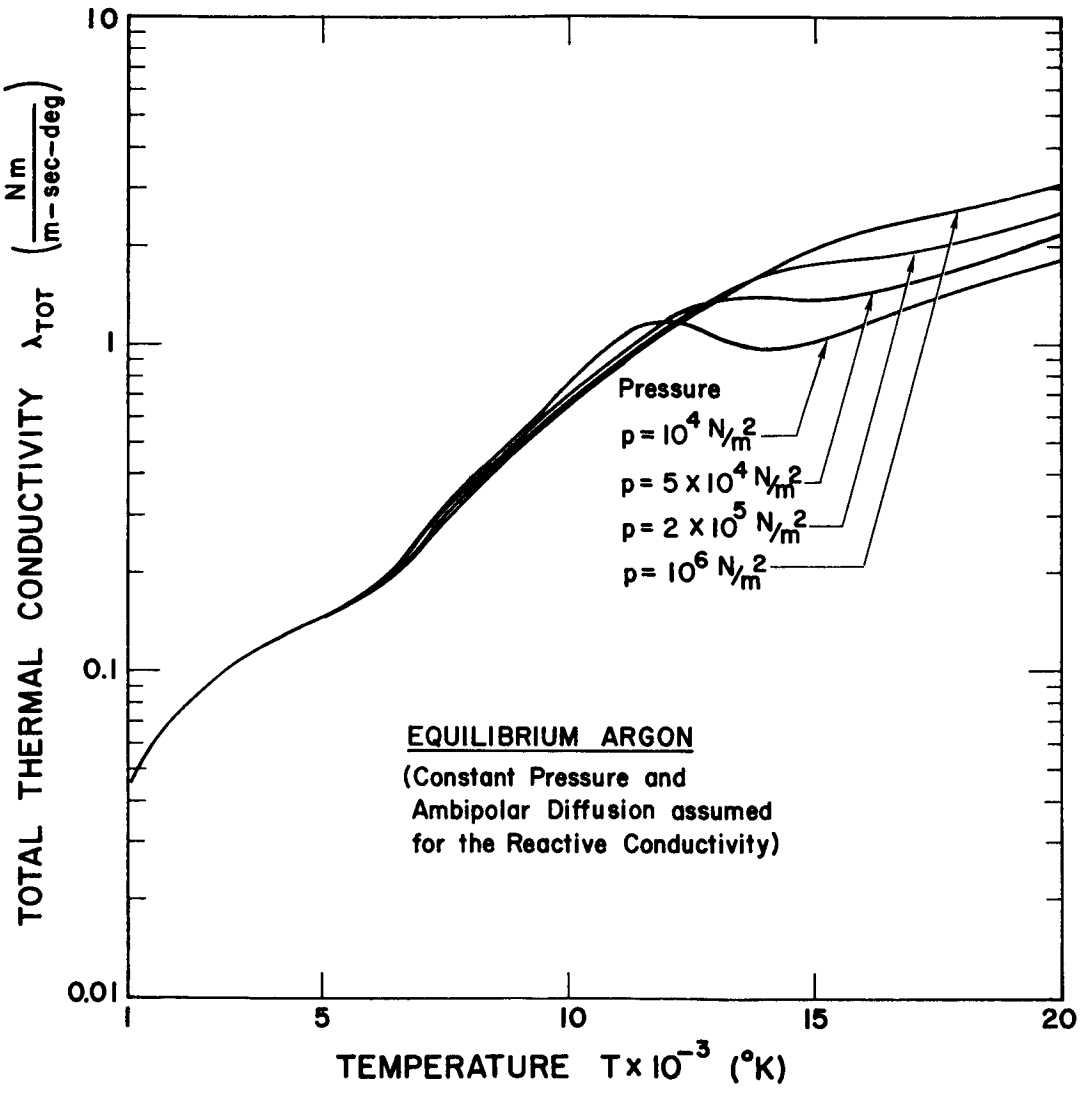


Fig. 14. Total thermal conductivity for equilibrium partially ionized argon.

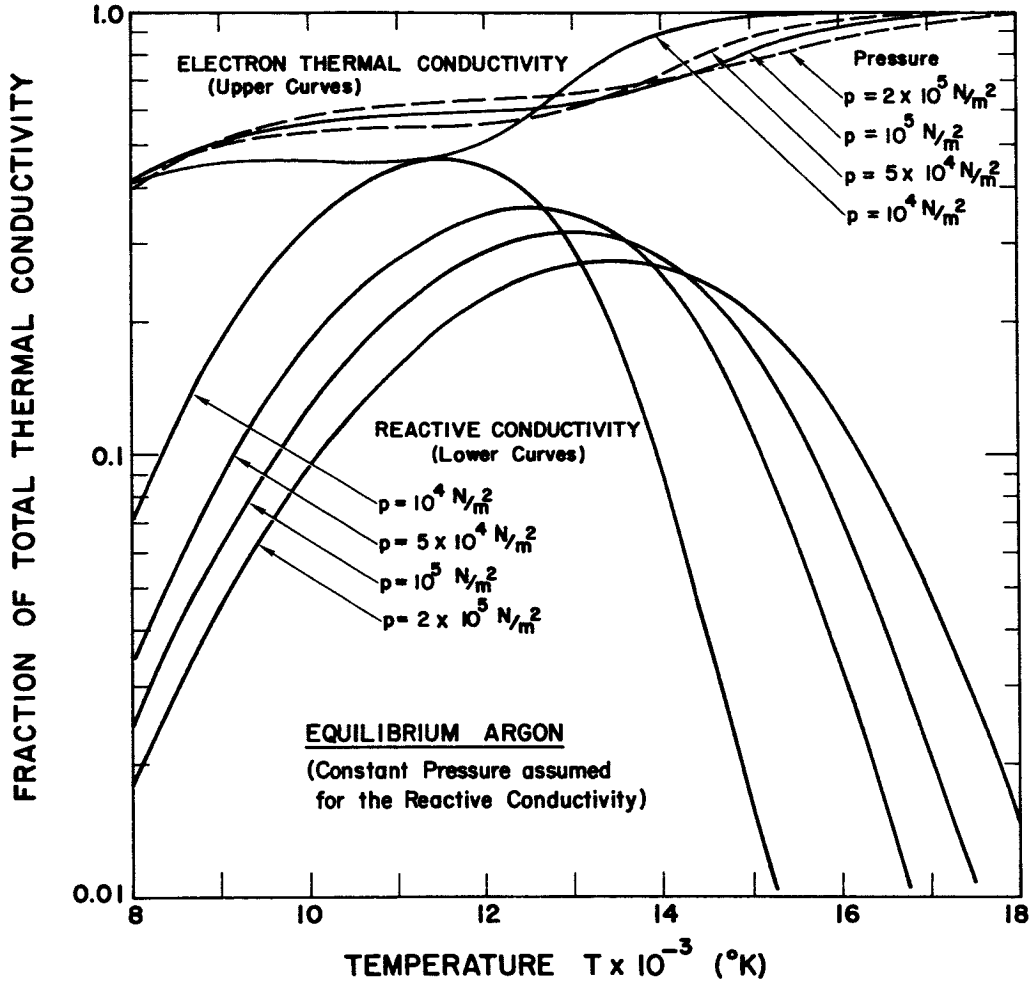


Fig. 15. Relative importance of the reactive conductivity and the electron thermal conductivity.

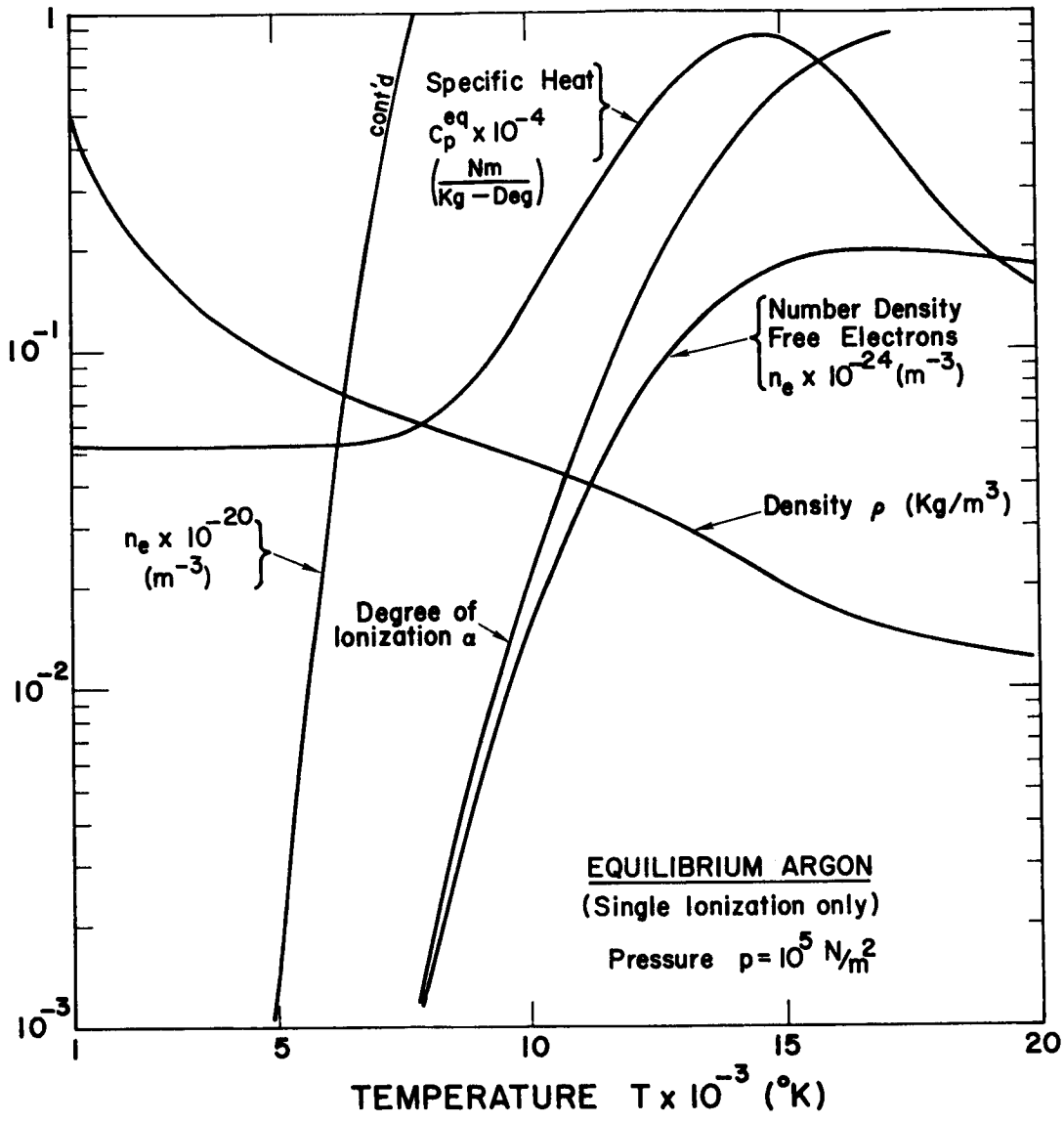


Fig. 16. Thermodynamic quantities for equilibrium partially ionized argon at p = 1 atm.

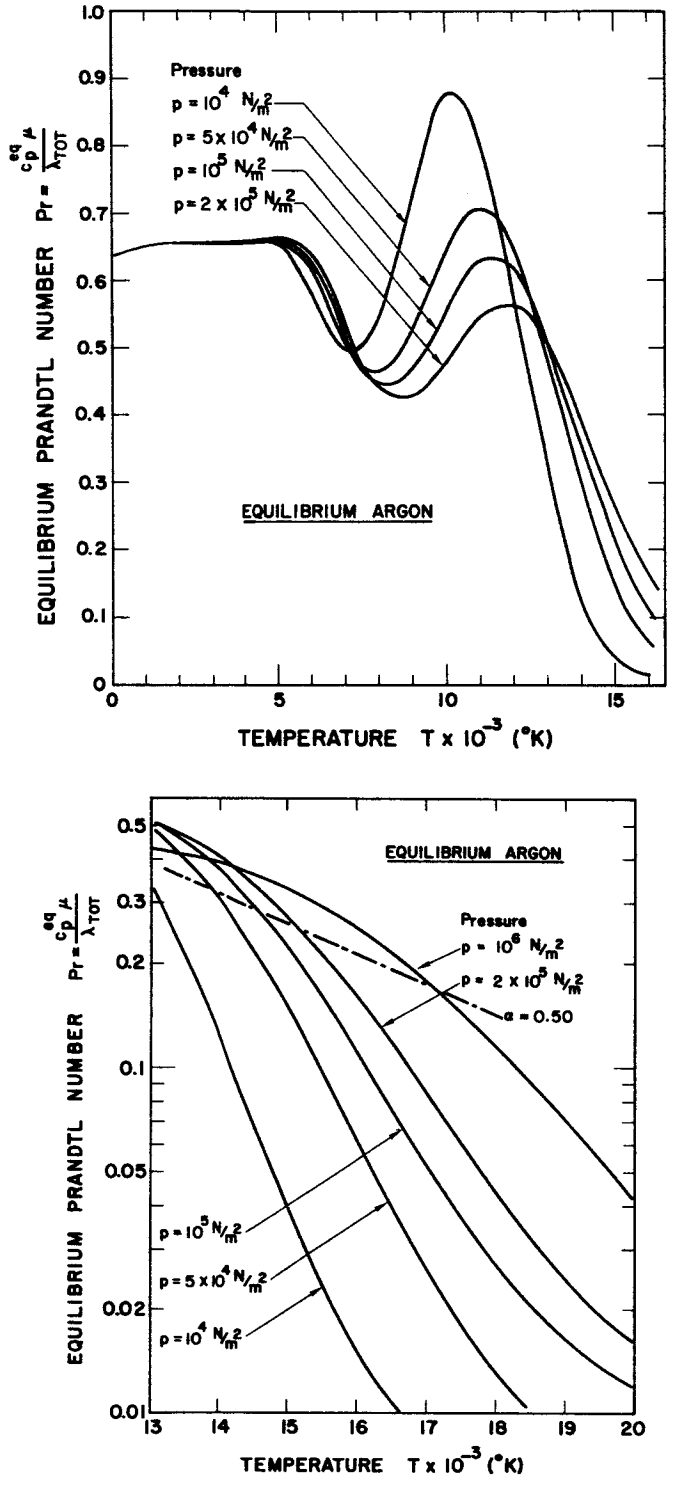


Fig. 17. Prandtl number Pr for equilibrium partially ionized argon.

## 6. METHOD OF SOLUTION AND RESULTS

### a. Integration of the Boundary Layer Equations

The mathematical problem to be solved is a two-point boundary value problem. The two governing ordinary differential equations are, for the case of a plasma, strongly coupled and of non-linear, parabolic type. In the present analysis the equations will be solved numerically with a predictor-corrector finite difference technique, (see e.g., Fox [43]).

The differential equations will first be transferred into a more convenient form for numerical integration. In the case of the Rayleigh boundary layer problem, we note that for large values of the similarily variable $\eta$, i.e., in the outer region of the boundary layer, the solution is the following

$$\left.\begin{aligned} \eta \to \infty: \qquad \frac{du^*}{d\eta} &\sim \exp(-\eta^2/Pr_\infty) \\ \frac{dh^*}{d\eta} &\sim \exp(-\eta^2) \end{aligned}\right\} \tag{6.1}$$

Guided hereby, we introduce two new functions $F(\eta)$ and $G(\eta)$, defined by the relations

$$\left.\begin{aligned} \text{Rayleigh's b.l.} \qquad \frac{du^*}{d\eta} &= -A^* F(\eta) \exp(-\eta^2/Pr_\infty) \\ \frac{dh^*}{d\eta} &= B^* G(\eta) \exp(-\eta^2) \end{aligned}\right\} \tag{6.2}$$

For convenience we require that $F(0) = 1$ and $G(0) = 1$. The constants $A^*$ and $B^*$, which are to be determined from the boundary conditions

$u^*(\infty) = 0$ and $h^*(\infty) = 1$, then simple are the magnitudes of the velocity and enthalpy derivatives at the wall. At infinity, $F(\eta)$ and $G(\eta)$ should be constant according to equation (6.1). In terms of the new functions the values of the dimensionless velocity and enthalpy are

$$\left.\begin{aligned} u^* &= 1 - A^* \int_0^\eta F(\eta)\, \exp(-\eta^2/Pr_\infty)d\eta \\ h^* &= B^* \int_0^\eta G(\eta)\, \exp(-\eta^2)d\eta \end{aligned}\right\} \tag{6.3}$$

We claim, that if the density-viscosity product $\rho\mu$ and the Prandtl number $Pr$ do not vary too drastically across the boundary layer, the functions $F(\eta)$ and $G(\eta)$ should be of the order magnitude unity and well behaved functions of $\eta$. They are determined from the boundary layer overall momentum and energy relations (2.26, 2.27). Integrated once, these equations become

$$F(\eta) = \frac{(\rho\mu)_\infty}{\rho\mu} \exp(\eta^2/Pr_\infty)\left[\frac{(\rho\mu)_w}{(\rho\mu)_\infty} - \frac{2}{Pr_\infty}\int_0^\eta \eta\, F(\eta)\, \exp(-\eta^2(Pr_\infty)d\eta\right] \tag{6.4}$$

$$G(\eta) = \frac{(\rho\mu)_\infty}{\rho\mu}\frac{Pr}{Pr_\infty} \exp(\eta^2)\left[\frac{(\rho\mu)_w}{(\rho\mu)_\infty}\frac{Pr_\infty}{Pr} - 2\int_0^\eta \eta\, G(\eta)\, \exp(-\eta^2)d\eta - \right.$$

$$\left. - \frac{A^{*2}}{B^*}\frac{U_w^2}{h_\infty - h_w} Pr_\infty \int_0^\eta \frac{\rho\mu}{(\rho\mu)_\infty} F^2(\eta)\, \exp(-2\eta^2/Pr_\infty)d\eta\right] \tag{6.5}$$

These equations are here written in a convenient form for numerical integration.

For reference, we shall mention that $F = 1$ is the solution to the momentum equation when the density-viscosity product $\rho\mu$ is constant.

From the boundary condition $u^*(\infty) = 0$, the parameter $A^*$ is found to be $A^* = 2\sqrt{\pi\, Pr_\infty}$. If, in addition, the Prandtl number is constant, the energy equation becomes

$$G(\eta) = \exp(\eta^2)\left[1 - 2\int_0^\eta \eta\, G(\eta)\exp(-\eta^2)d\eta - \right.$$

$$\left. - \frac{A^{*2}}{B^*}\frac{U_w^2}{h_\infty - h_w} Pr_\infty \int_0^\eta \exp(-2\eta^2/Pr_\infty)d\eta\right] \qquad (6.6)$$

The integration of $G(\eta)$ could easily be performed numerically. The parameter $B^*$ is given by the boundary condition at infinity, $h^*(\infty) = 1$. We note that if the factor $U_w^2/(h_\infty - h_w)$ in the viscous dissipation term is sufficiently large, there will be a local enthalpy maximum in the boundary layer, provided that the wall enthalpy gradient is positive, i.e., if $B^* > 0$. This is also true for the full problem (equations (6.4, 6.5)).

In the shock tube side-wall plasma boundary layer problem it is not convenient to use the transformations (6.2). The reason for this lies in the additional terms $(u^*+C)/C$ in the boundary layer momentum and energy equations which add to the non-linearity of the problem. Even for constant density-viscosity product $\rho\mu$ and Prandtly number $Pr$ the functions $F(\eta)$ and $G(\eta)$ would be irregular. We simply choose to solve the side-wall boundary layer equations directly in terms of normalized velocity and enthalpy gradients. For this purpose, we introduce the two functions $H(\eta)$ and $K(\eta)$ defined as

$$\left.\begin{aligned} \frac{du^*}{d\eta} &= -A^* K(\eta) \\ \frac{dh^*}{d\eta} &= B^* H(\eta) \end{aligned}\right\} \qquad (6.7)$$

We require that $K(0) = 1$ and $H(0) = 1$. Both functions must vanish at infinity. In terms of $K(\eta)$ and $H(\eta)$ the dimensionless velocity $u^*$ and enthalpy $h^*$ become

$$\left.\begin{aligned} u^* &= 1 - A^* \int_0^\eta K(\eta)d\eta \\ h^* &= B^* \int_C^\eta H(\eta)d\eta \end{aligned}\right\} \tag{6.8}$$

The governing equations for $K(\eta)$ and $H(\eta)$, namely the momentum and energy equations are

$$K(\eta) = \frac{(\rho\mu)_\infty}{\rho\mu} \frac{C}{u^*+C} \left( \frac{(\rho\mu)_w}{(\rho\mu)_\infty} \frac{1+C}{C} - \frac{2}{Pr_\infty} \int_0^\eta \eta\, K(\eta)d\eta \right) \tag{6.9}$$

$$H(\eta) = \frac{(\rho\mu)_\infty}{\rho\mu} \frac{C}{u^*+C} \frac{Pr}{Pr_\infty} \left( \frac{(\rho\mu)_w}{(\rho\mu)_\infty} \frac{Pr_\infty}{Pr} \frac{1+C}{C} - 2\int_0^\eta \eta\, H(\eta)d\eta - \frac{A^{*2}}{B^*} \frac{(U_w-U_2)^2}{h_\infty-h_w} Pr_\infty \int_0^\eta \frac{\rho\mu}{(\rho\mu)_\infty} \frac{u^*+C}{C} K^2(\eta)d\eta \right) \tag{6.10}$$

In the shock tube side-wall problem, the four equations (6.8-6.10) uniquely determine $K(\eta)$ and $H(\eta)$ as well as $u^*(\eta)$ and $h^*(\eta)$, provided that the constants of the integration $A^*$ and $B^*$ are known. In the present method, the values of $A^*$ and $B^*$ had to be guessed initially. These values were improved successively by iteration. A finite difference technique was applied in performing calculations from the wall to $\eta = 5$ (in some examples), which is well outside the essential boundary layer. The calculated values for velocity and enthalpy at "infinity", i.e., $\eta = 5$, were compared with the required boundary

conditions, namely $u^* = 1$ and $h^* = 1$. New values of $A^*$ and $B^*$ were then estimated on the basis of this comparison. Since the boundary layer equations (6.8, 6.9) are highly non-linear in nature, the convergence to the correct values of $A^*$ and $B^*$ presented difficulties. Several convergence techniques were tried, but not many of them were both stable and rapid. In fact, stable convergence was obtained only if the initial guesses for $A^*$ and $B^*$ was sufficiently close to the correct values. Typically 8-15 iterations had to be performed for a certain set of free stream conditions layer until the boundary conditions were satisfied. The required accuracy was normally $u^*(5) = 0 \pm 10^{-4}$ and $h^*(5) = 1 \pm 10^{-4}$. The Rayleigh boundary layer equations were integrated in a similar fashion.

The finite difference technique used was in principle a predictor-corrector method, and the same for both the Rayleigh and the side-wall boundary layers. We shall not go into much detail, but illustrate the method used only by showing how, e.g., the boundary layer momentum equation (6.8) for the side-wall problem was treated. Assume therefore that the solution to boundary layer equations is known in the region $0 \leq \eta \leq \eta_i$, where $i$ denotes the i-th step. In the integration the constant step-size is $\Delta\eta$, and by assumption much smaller than unity. The predictor formula used to calculate the function $K$ at the point $\eta_i + \Delta\eta$, $K_{i+1}$, was the following

Predictor:

$$K_{i+1} = \left[2\left(\frac{(\rho\mu)_\infty}{\rho\mu}\frac{C}{u^*+C}\right)_i - \left(\frac{(\rho\mu)_\infty}{\rho\mu}\frac{C}{u^*+C}\right)_{i+1}\right]\times \qquad (6.11)$$

$$\times\left[\frac{(\rho\mu)_w}{(\rho\mu)_\infty}\frac{1+C}{C} - \frac{2}{Pr_\infty}\left(\int_0^\eta \eta\, K(\eta)d\eta + \frac{\Delta\eta}{12}\left(23\eta_i K_i - 16\eta_{i-1}K_{i-1} + 5\eta_{i-2}K_{i-2}\right)\right)\right]$$

This formula predicts a value for $K_{i+1}$, which in fact may be fairly inaccurate. A similar predictor formula was derived from the energy equation and used to determine $H_{i+1}$. With the aid of equation (6.8) the associated values of velocity $u^*_{i+1}$ and enthalpy $h^*_{i+1}$ could also be predicted. Hence, the thermodynamic state of the gas at the point $\eta_{i+1}$ was then known approximately from $h^*_{i+1}$, and the related transport properties could be calculated. The following deferred correction formula was used thereafter to improve the accuracy of the predicted value $K_{i+1}$

Corrector:

$$K_{i+1} = \left(\frac{(\rho\mu)_\infty}{\rho\mu}\frac{C}{u^*+C}\right)_i \left[\left(\frac{(\rho\mu)_w}{(\rho\mu)_\infty}\frac{1+C}{C} - \right.\right.$$

$$\left.\left. - \frac{2}{Pr_\infty}\left(\int_0^{\eta_i} \eta\, K(\eta)d\eta + \frac{\Delta\eta}{12}\left(5\eta_{i+1}K_{i+1}+8\eta_i K_i-\eta_{i-1}K_{i-1}\right)\right)\right)\right] \qquad (6.12)$$

This corrector and corresponding corrector formulas for $H_{i+1}$, $u^*_{i+1}$, and $h^*_{i+1}$ were used repeatedly until the iteration error became acceptably small. In general, the corrector formulas were used only once or twice to obtain desired accuracy when the step size was smaller than $\Delta\eta = 0.01$.

The numerical calculations were performed on a digital computer (Burrough's B5500).* Typically, the necessary computing time for one

---

* The author gratefully will be willing to supply any interested person with copies of the computer programs developed. These are written in a Stanford University version of the computer language ALGOL.

boundary layer was 1-2 minutes if the boundary conditions, $u^*$ and $h^*$ at $\eta = 5$, were to be within $10^{-4}$ of the desired values. The mentioned computing time also includes calculations of the thermodynamic and transport properties of the argon plasma at the particular pressure. After that integration of the plasma boundary layer equations was performed, certain optical properties, such as fringe shifts and deflection angles of monochromatic light through the plasma boundary layer, were calculated on the basis of the boundary layer density solutions.

b. Solutions to the Rayleigh Boundary Layer

In this section we will present a few of the significant results of the numerical calculations of the equilibrium Rayleigh argon plasma boundary layer. We include the results for the shock tube end-wall boundary layer calculations as a special case of the Rayleigh boundary layer, namely for $U_w = 0$. The range of plasma free stream conditions considered are such as can be obtained experimentally behind normal shock waves in argon. These properties were reported in Section 4. Hence, we shall consider cases when the plasma temperature is of the order $T = 14{,}000°K$, the number density free electrons $n_e \sim 10^{23}$ $m^{-3}$ and the pressure $p = 1$ atm ($10^5$ Newtons/$m^2$). The wall temperature is in all cases assumed to be $T_w = 300°K$. The temperature jump for a metallic wall will be calculated subsequently and is shown to be small. The above assumption for the wall temperature is therefore quite realistic.

Results for the dimensionless velocity and enthalpy profiles are shown in Figures 18-21. It is clear from these figures that these profiles are quite different from the usual error function curves. The

latter are solutions to the simple Rayleigh problem with no dissipation and constant fluid transport properties. In all cases studied numerically, the velocity boundary layer is thinner than the enthalpy boundary layer. The transition to free stream conditions is smooth only for the enthalpy profile. Typically $h^*$ is larger than 0.99 when $\eta > 2.5$. Approaching the wall, the velocity increases rapidly from zero to large values between $\eta = 2$ and $\eta = 1$. The derivative $\frac{d^2u^*}{d\eta^2}$ is very large at the outer edge of the velocity boundary layer. The reason for this is the small value of the plasma density-viscosity product $\rho\mu$ in this region.

The velocity and enthalpy profiles are quite sensitive to change of the pressure level. As is demonstrated in Fig. 18, a higher pressure tends to make the boundary layer thinner along the $\eta$-coordinate. However, in the true physical plane, this is not certainly a true statement. Furthermore, the enthalpy profiles are quite different when the wall velocity $U_w$ is varied. As may be seen from Fig. 19, the enthalpy for a given value of $\eta$ becomes larger with increasing wall velocity. The reason herefore is the viscous dissipation. That the effect of changing the wall velocity on the enthalpy profile is drastic, is also shown in Fig. 20. For a wall velocity of 8000 m/sec and a free stream temperature of $T = 14{,}000°K$ and pressure $p = 10^5$ N/m$^2$ (1 atm.), there is still no local temperature maximum in the boundary layer due to the viscous dissipation. If the wall velocity were raised above 10,000 m/sec such a maximum will, however occur. For small values of the similarity parameter $\eta$, the dimensionless velocity profiles do not change much with a varying wall velocity $U_w$. From Fig. 20 it is found that for $\eta < 0.5$ there is no noticeable difference in $u^*$, when the wall velocity is varied from $U_w = 4000$ m/sec to $U_w = 8000$ m/sec.

The enthalpy profiles presented exhibit a change of sign in $\frac{d^2h^*}{d\eta^2}$ at positions corresponding to temperatures at which the electron thermal conductivity and the reactive conductivity start to become important. It corresponds to the "hump" in the total thermal conductivity at $T \sim 7000°K$ (Fig. 14) and an increasing value of the specific heat $c_p$ (Fig. 16). Any similar effect is not noticeable for the boundary layer temperature profiles.

The integrations of the boundary layer equations is performed with the similarity parameter $\eta$ as independent variable. After the solution $h^* = h^*(\eta)$ is known, a translation back to the physical plane $(y,t)$ is possible. From the original transformations we find immediately the following relation

$$\frac{y}{\sqrt{t}} = 2\sqrt{\frac{\lambda_\infty}{c_{p_\infty}\rho_\infty}}\, y^* \tag{6.13}$$

where, by definition

$$y^* = \int_0^\eta \frac{\rho_\infty}{\rho}\, d\eta \tag{6.14}$$

The relation between $y^*$ and $\eta$ is highly non-linear due to the large variation in density across the boundary layer. In Fig. 23 such a relation between $y^*$ and $\eta$ is shown for the case $T = 14{,}000°K$ and $T_w = 300°K$. In the following figure, the distance from the wall per unit of $y^*$, i.e., $y/y^*$, is given as a function of time $t$ for a few selected argon plasma free stream conditions. Naturally, this relation is independent of wall velocity $U_w$.

Various boundary layer thicknesses were obtained by use of the above relations. In Fig. 25 is shown the enthalpy boundary layer thickness defined as $y(h^* = 0.99)$. Its variation with wall velocity $U_w$ is shown. It is interesting to note that the enthalpy boundary layer thickness slightly decreases with velocity in the velocity range considered. The velocity boundary layer thickness, $y(u^* = 0.01)$, stays more constant when the wall velocity is changed. The latter occupies 68% of the enthalpy boundary layer thickness in this example ($T = 14{,}000°K$, $p = 1$ atm) roughly. Classical boundary layer theory for constant properties says that the velocity boundary layer should fill a fraction $\sqrt{Pr}$ of the enthalpy layer. Using the calculated value $Pr_\infty = 0.374$ for the free stream plasma, classical theory underestimates slightly the ratio of these layers to 61%, as compared with the above-mentioned value of 68%.

The induced velocity $v$ in the y-direction (Fig. 1) is calculated easily from the continuity equation (2.15) if $\rho = \rho(\eta)$ is known. The result is

$$v = \frac{\rho_\infty}{\rho} \frac{\partial}{\partial t} \int_0^y \frac{\rho}{\rho_\infty} \, dy = \left(\frac{\partial y}{\partial \tau}\right)_Y \tag{6.15}$$

After some simple algebraic work one finds

$$v\sqrt{t} = -\sqrt{\frac{\lambda_\infty}{c_{p_\infty} \rho_\infty}} \left[\frac{\rho_\infty}{\rho} \eta - y^*\right] \tag{6.16}$$

Hence, the velocity $v$ depends upon time as $t^{-1/2}$. If the density in the boundary layer is everywhere decreasing with $\eta$, as is the typical case here, the induced motion is directed towards the wall. If the density was increasing, i.e., a decreasing temperature profile, the

induced motion is everywhere directed away from the wall (i.e., in the positive y-direction. This is the case for a thermally insulated wall. The same effect could also be present when the wall velocity $U_w$ is sufficiently large. The viscous dissipation then leads to a very low average gas density in the boundary layer. Here we shall only consider moderate wall velocities and dissipation with the motion directed towards the wall. The velocity $v(\eta)$ is shown in Fig. 26 for a typical set of free stream conditions. We note, that the magnitude of the velocity $v$ rapidly decreases to zero when $\eta$ approaches $\eta = 0$. It should also be noted that the induced velocity decreases in magnitude with increasing wall velocity for large values of $\eta$. The reason for this is that the viscous dissipation causes a decrease in the average density in the boundary layer, and hence reduces the magnitude of the induced velocity $v_\infty$.

The boundary layer displacement thickness $\delta^{displ.}$ could be calculated from the fundamental relation (e.g., [20])

$$\delta^{displ.} = \int_0^t v_\infty dt \tag{6.17}$$

with the help of equation (6.16) for the perpendicular velocity, the following useful expression for the Rayleigh boundary layer displacement thickness could be derived

$$\delta^{displ.} = 2v_\infty t = -2\sqrt{\frac{\lambda_\infty t}{c_{p_\infty}\rho_\infty}}\left[\frac{\rho_\infty}{\rho}\eta - y^*\right]_{\eta\to\infty} \tag{6.18}$$

Hence, the displacement thickness varies with time as $t^{1/2}$, as do also the

velocity and enthalpy boundary layer thicknesses. As shown in Fig. 25, the displacement thickness typically amount to 50% of the enthalpy boundary layer thickness. This is quite a large value from a classical boundary layer stand-point. However, the effect is quite obvious, when considering that in the particular example shown, the wall density is very high, namely, $\rho_w = 65\ \rho_\infty$.

The total convective energy transfer flux at the wall is calculated from the relation

$$q_w = -\left(\lambda_{tot} \frac{\partial T}{\partial y}\right)_w = -\lambda_w \frac{\rho_w}{\rho_\infty} \sqrt{\frac{c_{p_\infty} \rho_\infty}{4\lambda_\infty t}} \left(\frac{dT}{d\eta}\right)_w \tag{6.19}$$

The temperature gradient is here evaluated from the numerical boundary layer solutions. Naturally $q_w$ changes with time $t$ as $t^{-1/2}$. When the wall temperature is small, and the flow is in equilibrium, as in the present calculations, the total thermal conductivity in expression (6.19) takes the pure atom value. The fact that the gas is in the ionized state does therefore not introduce additional modes of convective energy transfer over the non-ionized boundary layers. However, the temperature gradient at the wall is strongly dependent upon the plasma outer conditions with a resultant effect on the energy flux. The total energy transfer rate at the wall, $q_w$, may be written in the following appropriate dimensionless form

$$\frac{q_w\, t^{1/2}\, c_{p_w}}{(h_\infty - h_w)\sqrt{c_{p_\infty} \rho_\infty \lambda_{tot_\infty}}} = -\frac{1}{2} \frac{(\lambda\rho)_w}{(\lambda_{tot}\rho)_\infty} \left(\frac{dh^*}{d\eta}\right)_w \tag{6.20}$$

Heat transfer rates have been evaluated according to this formula for

the plasma Rayleigh boundary layers. In Fig. 27 are shown a few results. The heat transfer rate is seen to increase with wall velocity $U_w$ and increasing pressure, for a given free stream equilibrium plasma temperature.

At this point it is appropriate to calculate the wall temperature jump $\Delta T_w$ at time $t = 0$ for a homogeneous metallic wall. It is a well known fact that the wall temperature will take a constant value for times $t > 0$, if the heat transfer rate to the wall is of the form $q_w \sim t^{-1/2}$, as it is in present cases. If $\lambda$, $\rho$ and $c$ are the (constant) thermal conductivity, density, and specific heat for the wall material, the temperature jump $\Delta T_w$ becomes

$$\Delta T_w = -q_w \, t^{1/2} \left(\frac{\pi}{\lambda \rho c}\right)^{1/2} \tag{6.21}$$

Here $q_w$ is the heat transfer rate in the gas at the wall, as calculated e.g., from equation (6.19). For the case of aluminum material, the theoretical results for wall temperature jump $\Delta T_w$ are shown in Fig. 28 as a function of pressure for a typical set of free stream conditions. From this figure it is concluded that the wall temperature jump is only between 2.5 and 15°K when the pressure is $0.1 < p < 100$ atm, for a free stream temperature of 14,000°K. Hence, in an experimental situation the wall temperature may easily be kept at $T_w \sim 300$°K, which was one of the initial assumptions in the present plasma boundary layer analysis.

Furthermore, the shear stress at the wall $\tau_w$, could be determined from the following expression

$$\tau_w = \left(\mu \frac{\partial u}{\partial y}\right)_w = \frac{(\rho\mu)_w}{(\rho\mu)_\infty} \frac{\sqrt{Pr_\infty}}{2\sqrt{t}} \sqrt{(\rho\mu)_\infty} \; U_w \left(\frac{du^*}{d\eta}\right)_w \tag{6.22}$$

In terms of the non-dimensional skin friction coefficient, this could also be written

$$c_f = \frac{-\tau_w}{\rho_\infty U_w^2/2} = \frac{(\rho\mu)_w}{(\rho\mu)_\infty} \sqrt{Pr_\infty} \frac{1}{\sqrt{R}} \left(-\frac{du^*}{d\eta}\right)_w \tag{6.23}$$

Here $R$ is a Reynolds number defined as

$$R = \frac{t\, U_w^2}{\mu_\infty/\rho_\infty} \tag{6.24}$$

Naturally, in order for the boundary layer calculations to be valid, we require that this Reynolds number is much larger than unity, $R \gg 1$. For times $t$ larger than one microsecond and pressures larger than 0.01 atm, which has mainly been considered here, this condition is certainly satisfied. If $R$ is larger than, e.g., $10^6$, turbulence is likely to occur. We leave the question of transition to turbulent plasma boundary layer open.

Finally, it is of interest to mention, under which conditions the convective net energy flux from the gas is positive or negative. The motion of the wall naturally introduces energy to the gas through the shear stress, in the present frame of reference. Part of this energy is given to the gas directly as kinetic energy, and part as thermal energy through the dissipation mechanism. The net energy flux from the gas per unit time and unit wall surface area is $(-q_w - U_w\tau_w)$. With the help of equations (6.20, 6.22) it is easy to show that this quantity is positive, i.e., the gas is losing energy, when the following non-equality is satisfied

$$Pr_w \frac{U_w^2}{h_\infty - h_w} \frac{\left(-\frac{du^*}{d\eta}\right)_w}{\left(\frac{dh^*}{d\eta}\right)_w} < 1 \qquad (6.25)$$

Most Rayleigh plasma boundary layers which are analysed here satisfy this relation, i.e., the plasma boundary layer is giving away energy to the wall.

Finally shall be given results for the ambipolar electrical characteristics of the Rayleigh boundary layers. The strength of the induced ambipolar electric field $E_y$ in the y-direction is calculated from equation (3.7). After some algebraic reduction the following result is obtained

$$E_y \sqrt{t} = -\frac{1}{2} \sqrt{\frac{c_{p_\infty} \rho_\infty}{\lambda_\infty}} \frac{kT}{q_i} \frac{\rho}{\rho_\infty} \frac{1}{(1+\alpha)} \frac{d}{d\eta} (\ell n\, \alpha) \qquad (6.26)$$

Hence, the induced electric field is directed in the negative y-direction since the degree of ionization $\alpha$ increases with $\eta$. Furthermore, the electric field varies with time as $E \sim t^{-1/2}$. The same dependence upon time is true also for the diffusion velocity, the boundary layer thickness, etc. In Fig. (29) is shown a numerical evaluation of the electric field strength. We see that the value of $E_y$ monotomically increases with decreasing value of the wall distance parameter $\eta$ and decreasing temperature T. For example, after t = 10 microsec at a position in the boundary layer corresponding to a temperature of 13,000°K, the strength of the electric field is 2.1 Volts/mm. At the temperature 6000°K the corresponding field strength is as much as 110 Volts/mm.

The ambipolar electric field solution breaks down when the local Debye length, $l_D$ is of the same order magnitude or larger than the distance to the wall y. This occurs at temperatures of the order 4000°K or lower for times t on the microsecond level. The results in Fig. 29 should then only be used at temperatures above 4000°K ($\eta > 0.3$).

With the electric field associated electric ambipolar potential difference V can be calculated by integration of the electric field strength $E_y$ in the y-direction. Results of such an integration are already given in Section 3, and grafically shown in Fig. 3 for the equilibrium argon plasma. The potential difference across the ambipolar region between two given temperatures was shown to be independent of time.

The electron current density $j_e$ is obtained from the expression

$$j_e = n_e V_e q_e \tag{6.27}$$

Here $V_e$ is the ambipolar electron diffusion velocity, which is given by equation (3.8). Since the ambipolar diffusion velocity here is in the negative y-direction, the electron current is positive and directed in the positive y-direction. The ion current is in the negative y-direction and equal to the electron current in magnitude, since by assumption, the total current density is zero. Using the expression (3.8) for the ambipolar diffusion velocity, the electron current density becomes

$$j_e\sqrt{t} = \frac{1}{2}\sqrt{\frac{c_{p_\infty}\rho_\infty}{\lambda_\infty}}\, q_i\, D_{amb}\, n_e\, \frac{\rho}{\rho_\infty}\, \frac{d}{d\eta}\,(\ell n\, \alpha) \tag{6.28}$$

Hence, the electron current density varies with time as $j_e \sim t^{-1/2}$ (as the electric field strength). Due to the rapid decrease in number density of free electrons $n_e$ with decreasing temperature for the equilibrium argon plasma, the electron current becomes small at temperatures below 8000°K. As could be seen in Fig. 29, the electron current density $j_e$ has a maximum at a temperature 11,500°K in the particular example where the free stream temperature is 14,000°K. At time $t$ = 10 microsec, the maximum electron current density is $j_e$ = 24 Ampéres/cm$^2$.

For reference is also given the ambipolar diffusion velocity and the average mass velocity $v$ in the y-direction in Fig. 29. In the example shown, the ambipolar diffusion velocity is larger in magnitude than the mass velocity when the temperature is lower than 12,000°K. At the temperature 7000°K, the diffusion velocity is two orders of magnitude larger than the mass velocity $v$, and of the order 100 m/sec for $t$ = 10 microsec.

### c. Solutions to the Shock Tube Side-Wall Boundary Layer

Solutions to the shock tube side-wall boundary layer problem were obtained in a fashion similar to that for the Rayleigh boundary layer. The results are qualitatively the same.

Due to the appearance of the term $(u^*+C)/C$ in the boundary layer equations, the behavior of the solutions $u^*(\eta)$ and $h^*(\eta)$ are, however, quite different from the Rayleigh solutions. Only when $u^*$ is small, $u^* < C$, i.e., the factor $(u^*+C)/C$ is close to unity, the solutions are similar in shape. The side-wall boundary layer solutions

$u^*(\eta)$ and $h^*(\eta)$ approach the free stream values $u^*(\infty) = 0$ and $h^*(\infty) = 1$ at larger values of $\eta$ than the Rayleigh solutions. Typically the boundary layer edge $\eta(h^* = 0.99)$ now corresponds to $\eta \simeq 3.5$, instead of the previous $\eta \simeq 2.5$ for the Rayleigh boundary layer. This is shown in Fig. 30 for the case of a shock wave with speed $U_s = 6000$ m/sec in argon of initial temperature $T = 298°K$ and pressure $p_1 = 5$ mm Hg. In the same figure is also shown the derivative functions $K(\eta)$ and $H(\eta)$, defined by equation (6.7), and in terms of which the numerical integration were carried out. It is interesting to note that both functions $K(\eta)$ and $H(\eta)$ have pronounced maxima at $\eta = 2.6$ and $\eta = 2.8$ respectively, close to the outer edge of the boundary layer. In particular the maximum for the velocity derivative function $K(\eta)$ is sharp, $K_{max} \sim 6.5$. The function $K(\eta)$ very rapidly decrease to zero behind the maximum. Hence, the velocity $u^*(\eta)$ very rapidly approach the free stream value $u^*(\infty) = 0$, and with a large value of the second derivative $\frac{d^2u^*}{d\eta^2}$. Furthermore, the function $H(\eta)$ has a local maximum at $\eta \simeq 0.7$, corresponding to $T = 5000°K$ in the particular example shown. This feature is common with the Rayleigh boundary layer in equilibrium argon plasmas. The reason for this local maximum in $H(\eta)$ is the rapidly increasing total thermal conductivity and a thereby associated lowering of the Prandtl number in this temperature region of the argon gas.

Figure 31 shows the temperature and velocity profiles for the same side-wall boundary layer. For reference is also plotted the degree of ionization $\alpha$, the Prandtl number Pr, and the inverse density-viscosity product $(\rho\mu)_\infty/(\rho\mu)$. The variation in the density-viscosity product

across the boundary layer is large, and here as much as one order of magnitude. The variation in the Prandtl number is moderate, $0.65 < Pr < 0.4$. The gas is strongly ionized above 10,000°K, and the free stream value of the ionization is $\alpha_\infty = 0.242$. Further results are shown in the Appendix.

The transformation back to the physical plane $(x,y)$ is done by the relation

$$\frac{y}{\sqrt{x}} = 2\sqrt{\frac{\lambda_\infty}{c_{p_\infty}\rho_\infty}\frac{1}{U_2}}\; y^* \tag{6.29}$$

where the dimensionless quantity $y^*$ is defined as

$$y^* = \int_0^\eta \frac{\rho_\infty}{\rho}\frac{C}{u^*+C}\,d\eta \tag{6.30}$$

These relations are analogous to the Rayleigh boundary layer relations (6.13, 6.14). The results of a transformation of this kind are demonstrated in Fig. 32 and also in the Appendix. We note that the enthalpy boundary layer edge, $\eta \simeq 3.5$ roughly corresponds to the value $y^* \simeq 1$. The enthalpy boundary layer thickness in the particular example could therefore approximately be written

$$y^* = 1: \qquad \delta^{\text{enthalpy}} \simeq 2\sqrt{\frac{\lambda_\infty}{c_{p_\infty}\rho_\infty}\frac{x}{U_2}} \tag{6.31}$$

For a given value of $x$, the distance from the wall, $y$, is directly proportional to the dimensionless quantity $y^*$. From Fig. 32 we may then conclude that the physical wall distance $y$ is very much smaller than the enthalpy boundary layer thickness when $\eta < 0.5$. For reference we shall give the following table which relates the distance from the

wall, y (millimeters), to the temperature, T, in the boundary layer for the previously discussed side-wall boundary layer.

Distance from wall y(mm):

| x meter | T=6000°K | T=8000°K | T=10,000°K | T=12,000°K | T=14,070°K |
|---|---|---|---|---|---|
| 0.01 | 0.0069 | 0.0132 | 0.0275 | 0.0618 | 0.343 |
| 0.05 | 0.0152 | 0.0294 | 0.0615 | 0.138 | 0.768 |
| 0.20 | 0.0308 | 0.0588 | 0.123 | 0.277 | 1.535 |

$U_s$ = 6000 m/sec

$U_2$ = 675 m/sec

$p$ = $3.4 \times 10^5$ N/m$^2$; ($p_1$ = 5 mm Hg.)

$T_\infty$ = 14,100°K

$T_w$ = 300°K

Notice: Last column corresponds to enthalpy boundary layer edge since $T(h^* = 0.990) = 14{,}070°K$.

Hence at a distance x = 0.05 meter behind the shock wave the enthalpy boundary layer thickness is $\delta^{\text{enthalpy}} = 0.768$ mm. At a distance 0.0615 mm from the wall the temperature is 10,000°K. This wall distance corresponds only to 8% of the enthalpy boundary layer thickness.

The induced velocity v in the y-direction (perpendicular to the wall, y = 0) is calculated from the continuity equation (2.30). We find that

$$v = u\left(\frac{\partial y}{\partial x}\right)_\psi \tag{6.32}$$

and therefore

$$v\sqrt{x} = -\sqrt{\frac{\lambda_\infty U_2}{c_{p_\infty}\rho_\infty}}\left[\eta\,\frac{\rho_\infty}{\rho} - \frac{u^*+C}{C}\,y^*\right] \tag{6.33}$$

As was found for some of the Rayleigh boundary layers, the induced velocity $v$ is negative everywhere in the boundary layer and hence directed towards the wall. A calculation of the induced velocity $v$ is demonstrated in Fig. 32. At a distance $x = 0.01$ from the shock wave the magnitude of the induced velocity $v$ is of the order $v_\infty = 5$ m/sec at the boundary layer edge. It rapidly decreases to zero when $\eta < 1$.

The boundary layer displacement thickness $\delta^{\text{displ.}}$ becomes

$$\delta^{\text{displ.}} = \frac{1}{U_2}\int_0^x v_\infty(x)dx = \frac{2xv_\infty(x)}{U_2} = -2\sqrt{\frac{\lambda_\infty}{c_{p_\infty}\rho_\infty}\,\frac{x}{U_2}}\,[\eta - y^*]_{\eta\to\infty} \tag{6.34}$$

The expression inside the bracket should be evaluated at free stream conditions. Since $v_\infty$ is negative, the displacement thickness also becomes negative. The magnitude of the displacement thickness is quite large in the particular example studied and amounts to 43% of the thermal boundary layer thickness.

The total energy flux at the wall, the wall shear stress, etc. can be calculated from the boundary layer solutions $u^*(\eta)$ and $h^*(\eta)$, as was done for the Rayleigh boundary layers. We shall here not give the results of such straightforward calculations.

d. Criterion for Chemical Equilibrium in the Boundary Layer Flow

Most calculations presented herein assume chemical equilibrium in the boundary layer. This is an ideal assumption and will not be correct throughout the boundary layer for the argon plasma for example. We shall determine where the equilibrium assumption is valid, and where it breaks down. In this connection, we must examine the electron continuity equation (2.3) which in the physical plane $(y,t)$ reads, for the case of the Rayleigh problem,

$$\frac{\partial n_e}{\partial t} + \frac{\partial}{\partial y}\left(n_e(v+V_e)\right) = \left(\frac{\partial n_e}{\partial t}\right)_{coll} \tag{6.35}$$

Here again, $v$ is the mean mass velocity in the y-direction, and $V_e$ the electron diffusion velocity in the same direction. In the original treatment of the plasma boundary layer we did not have to solve this equation when the gas was in local equilibrium. It was then replaced by a relation of the Saha type for the composition. However, the continuity equation is still very important in the equilibrium case. It provides information about the magnitude of the collision term $\left(\frac{\partial n_e}{\partial t}\right)_{coll}$, which now expresses the equilibrium change of number density electrons per unit time due to reacting collisions (ionizing collisions and recombinations).

We evaluate the collision-term from the equilibrium solution and make use of the facts that $v \sim t^{-1/2}$ and $V_e \sim t^{-1/2}$. We shall here only be concerned with the ambipolar region, i.e., $V_e$ is the ambipolar diffusion velocity. In terms of the similarity parameter $\eta$, the collision-term then takes the form

Rayleigh's b.l:

$$\frac{t}{n_e}\left(\frac{\partial n_e}{\partial t}\right)_{coll} = -\frac{1}{2}\eta\frac{1}{n_e}\frac{dn_e}{d\eta} + \frac{\rho}{\rho_\infty}\frac{1}{2\sqrt{\frac{\lambda_\infty}{c_{p_\infty}\rho_\infty}}}\frac{d}{d\eta}\left(v\sqrt{t}\right) +$$

$$+\frac{\rho}{\rho_\infty}\frac{1}{2\sqrt{\frac{\lambda_\infty}{c_{p_\infty}\rho_\infty}}}\frac{1}{n_e}\frac{d}{d\eta}\left(n_e V_e\sqrt{t}\right) \qquad (6.36)$$

Here we find from equation (6.16)

$$\frac{d}{d\eta}\left(v\sqrt{t}\right) = -\sqrt{\frac{\lambda_\infty}{c_{p_\infty}\rho_\infty}}\,\eta\frac{d}{d\eta}\left(\frac{\rho_\infty}{\rho}\right) \qquad (6.37)$$

The following expression is deduced from the ambipolar relations

$$n_e V_e\sqrt{t} = -D_{amb}\frac{1}{\alpha}\frac{\rho}{\rho_\infty}n_e\frac{1}{2\sqrt{\frac{\lambda_\infty}{c_{p_\infty}\rho_\infty}}}\frac{d\alpha}{d\eta} \qquad (6.38)$$

Therefore, the collision-term for equilibrium flow becomes

$$\underline{\text{equilibrium:}}\quad \frac{t}{n_e}\left(\frac{\partial n_e}{\partial t}\right)_{coll} = -\left(Q^{conv.} + Q^{diff.}\right) \qquad (6.39)$$

where

$$Q^{conv.} = \frac{1}{2}\eta\left[\frac{1}{n_e}\frac{dn_e}{d\eta} + \frac{\rho}{\rho_\infty}\frac{d}{d\eta}\left(\frac{\rho_\infty}{\rho}\right)\right] = \frac{1}{2}\eta\frac{d}{d\eta}\left(\ell n\,\frac{n_e}{\rho}\right) \qquad (6.40)$$

$$Q^{diff.} = \frac{c_{p_\infty}\rho_\infty}{4\lambda_\infty}\frac{\rho}{\rho_\infty}\frac{1}{n_e}\frac{d}{d\eta}\left(D_{amb}\frac{n_e}{\alpha}\frac{\rho}{\rho_\infty}\frac{d\alpha}{d\eta}\right) \qquad (6.41)$$

Here $Q^{conv.}$ is a dimensionless measure of the collisional loss of electrons necessary for equilibrium and due to the change of density of the gas with time (the convective cooling). The quantity $Q^{diff.}$ is a measure of the required loss of electrons due to the diffusion. The quantity $Q^{diff.}$ will naturally be most important close to the wall in the boundary layer, where the diffusion is large. This is clearly demonstrated in Fig. 33. For the particular example shown here, the convective term $Q^{conv.}$ is less than two orders of magnitude smaller than $Q^{diff.}$ when the temperature is below 6000°K. At $T = 12{,}000°K$ the diffusive term is zero. For temperatures higher than this, it is interesting to note that $Q^{diff.}$ is negative. As we approach free stream conditions, the ratio $Q^{diff.}/Q^{conv.}$ is almost constant, and approaches the value $-0.44$ in this example. Since there is no temperature overshoot in the particular examples shown, it is not surprising that the collision-term is everywhere negative. This means that for equilibrium, the number of de-ionizing collisions uniformly must exceed the number of ionizing collisions in the boundary layer.

Figure 34 shows the available number of de-ionizing collisions for the argon plasma. The relevant argon recombination process in the temperature range of interest is the usual three-body recombination

$$e + e + A^{+} \rightarrow e + A^{*} + h\nu$$

where $A^{+}$ is the argon ion, $e$ the electron, and $A^{*}$ an exited atom. In order to calculate the available number of recombinations, $Q^{avail.}$, per unit time per electron, results from classical electron impact theory were used below $T_e = 4000°K$, and results from [12] for high

temperatures. Hence, the data used are the following

$$Q^{\text{avail.}} = -\frac{1}{n_e}\left(\frac{\partial n_e}{\partial t}\right)_{\text{rec}} = -k_{\text{rec}}\, n_e^2 \tag{6.42}$$

where

$$\left.\begin{aligned} k_{\text{rec}} &= 2.3 \times 10^{-20} \times T_e^{-4.5} \quad (m^6/\text{sec}) \quad (T_e < 4000°K) \\ k_{\text{rec}} &= 1.3 \times 10^{-44} \left(2 + \frac{134000}{T_e}\right) \exp(49000/T_e) \quad (m^6/\text{sec}) \\ &\qquad\qquad (T_e \geq 4000°K) \end{aligned}\right\} \tag{6.43}$$

Here $Q^{\text{avail.}}$ is the available number of recombinations per electron per unit time. Thus, this quantity has the dimension $t^{-1}$.

Obviously the gas in the boundary layer will be in near chemical equilibrium when the number of recombinations per unit time exceeds the necessary net number of recombinations for equilibrium, as calculated from equation (6.39). We state, therefore, that the gas composition will be locally in equilibrium in the Rayleigh boundary layer when the following non-equality is satisfied locally:

$$\text{Equilibrium Criterion:} \qquad \frac{Q^{\text{avail.}}}{-\frac{1}{n_e}\left(\frac{\partial n_e}{\partial t}\right)} = \frac{t\, Q^{\text{avail.}}}{Q^{\text{conv.}} + Q^{\text{diff.}}} \gg 1 \tag{6.44}$$

We conclude, e.g., from Figs. 33, 34 for the argon Rayleigh boundary layers that for the pressure $p = 10^5$ N/m$^2$ ($\sim$ 1 atm), the gas will be in near equilibrium only at temperatures above 13,000°K at times $t > 10^{-5}$ sec, above 10,500°K for $t > 10^{-3}$ sec, and above 8500°K for $t > 10^{-1}$ sec. At lower pressures corresponding times are longer. For

time scales of experimental interest, and time scales smaller or of the same order of magnitude as those characteristic of radiation cooling, i.e., times of the order $t \tilde{>} 10^{-4}$ sec, we conclude that the Rayleigh boundary layers in argon will be in equilibrium only above, say 11,000°K, and close to frozen in the region below 8000°K.

A similar analysis could be carried out for the shock tube side-wall boundary layer. Here, we shall give only the formula for the determination of the net collisional change of electron number density necessary for the flow to be in chemical equilibrium. The relation is

$$\frac{x/U_2}{n_e}\left(\frac{\partial n_e}{\partial t}\right)_{coll} = -\left(Q^{conv.} + Q^{diff.}\right) \tag{6.45}$$

where

$$Q^{conv.} = \frac{1}{2}\,\eta\,\frac{u^*+C}{C}\left[\frac{1}{n_e}\frac{dn_e}{d\eta} + \frac{\rho}{\rho_\infty}\frac{d}{d\eta}\left(\frac{\rho}{\rho_\infty}\right)\right] = \frac{1}{2}\,\eta\,\frac{u^*+C}{C}\frac{d}{d\eta}\left(\ell n\,\frac{n_e}{\rho}\right) \tag{6.46}$$

$$Q^{diff.} = \frac{c_{p_\infty}\rho_\infty}{4\,\lambda_\infty}\frac{u^*+C}{C}\frac{\rho}{\rho_\infty}\frac{1}{n_e}\frac{d}{d\eta}\left(D_{amb}\,\frac{u^*+C}{C}\,\frac{n_e}{\alpha}\,\frac{\rho}{\rho_\infty}\,\frac{d\alpha}{d\eta}\right) \tag{6.47}$$

These expressions also degenerate to the expressions for the Rayleigh boundary layer, if we let $C \to \infty$. As was the case for the Rayleigh boundary layer, the diffusive term is most important close to the wall, and the convective term most important close to free stream conditions. The qualitative results for the extent of the equilibrium region, determined from a similar criterion resemble the previous results for the Rayleigh problem, and will not be reported here.

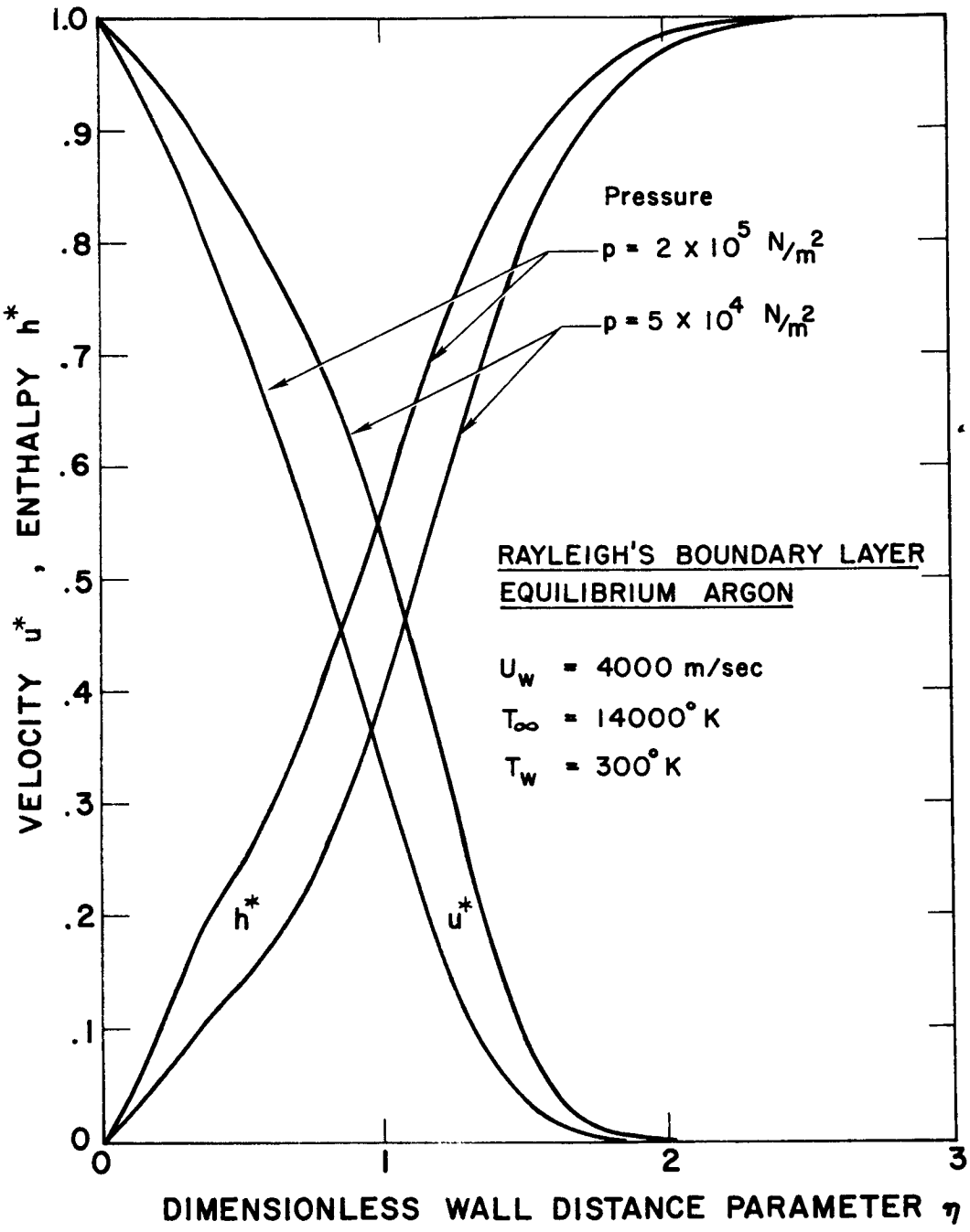


Fig. 18. Equilibrium argon velocity and enthalpy profiles for Rayleigh's boundary layer as a function of pressure.

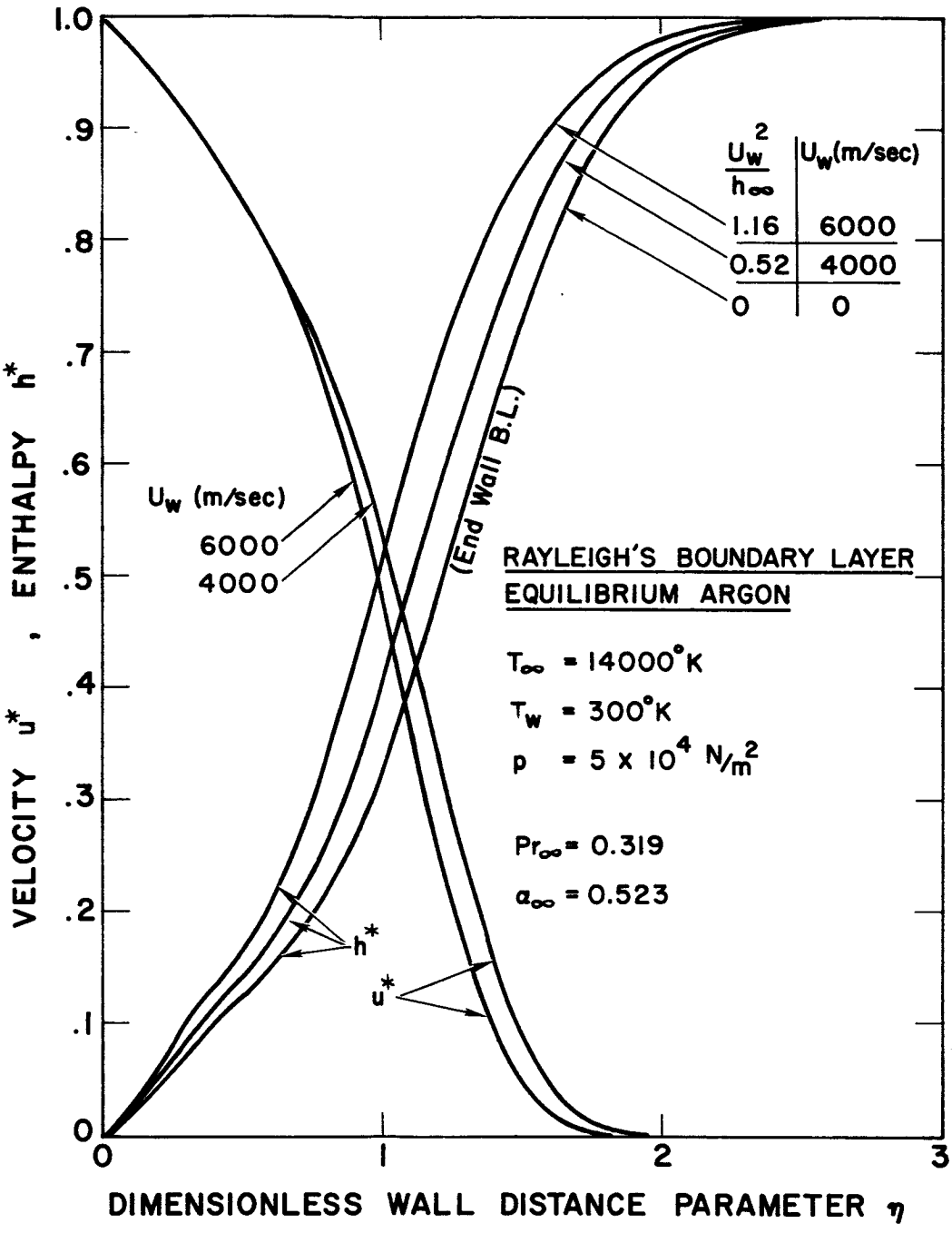


Fig. 19. Equilibrium argon velocity and enthalpy profiles for Rayleigh's boundary layer as a function of wall velocity.

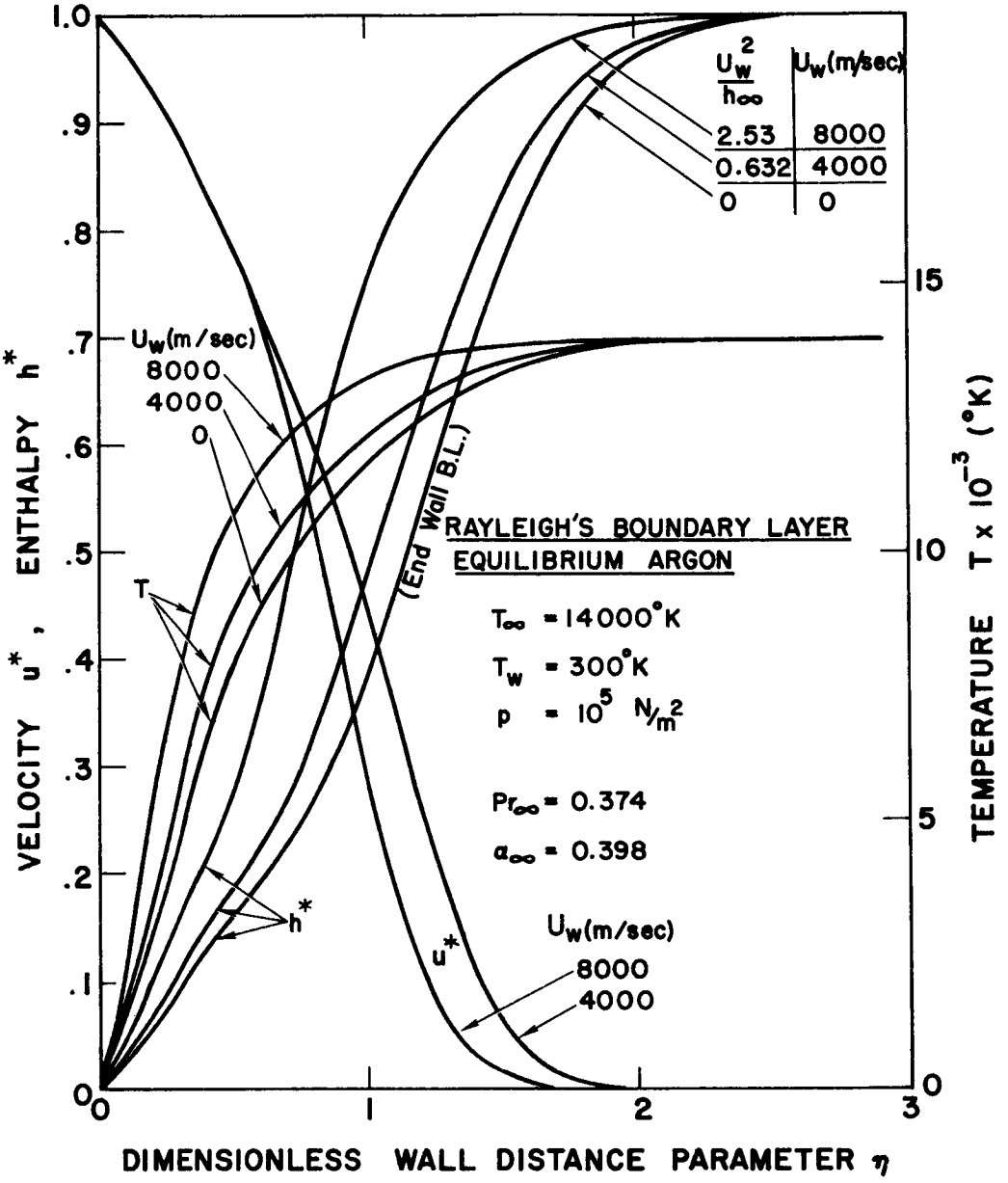


Fig. 20. Equilibrium argon velocity, enthalpy and temperature profiles for Rayleigh's boundary layer as a function of wall velocity.

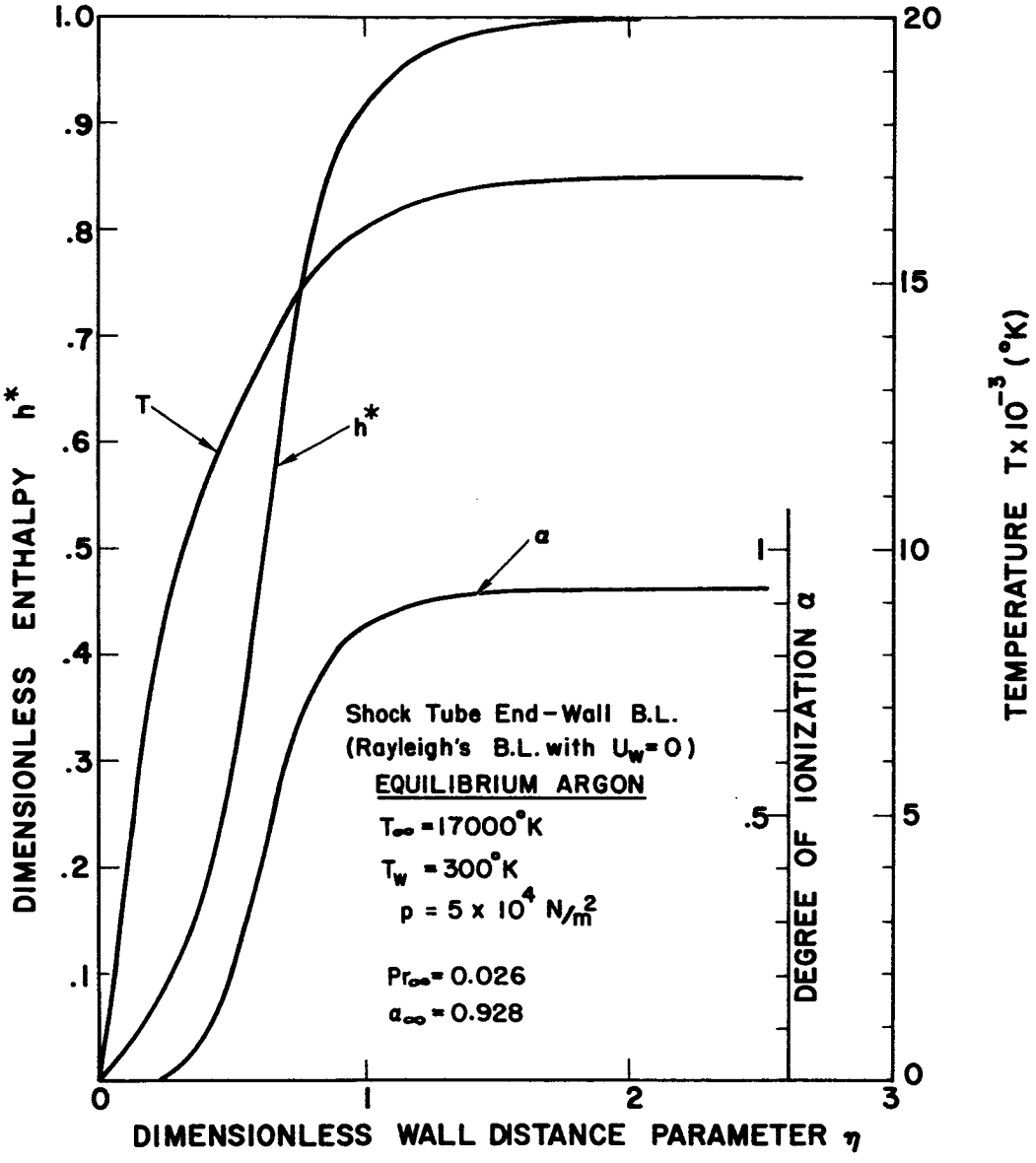


Fig. 21. Equilibrium argon enthalpy, temperature and degree of ionization profiles for end-wall boundary layer.

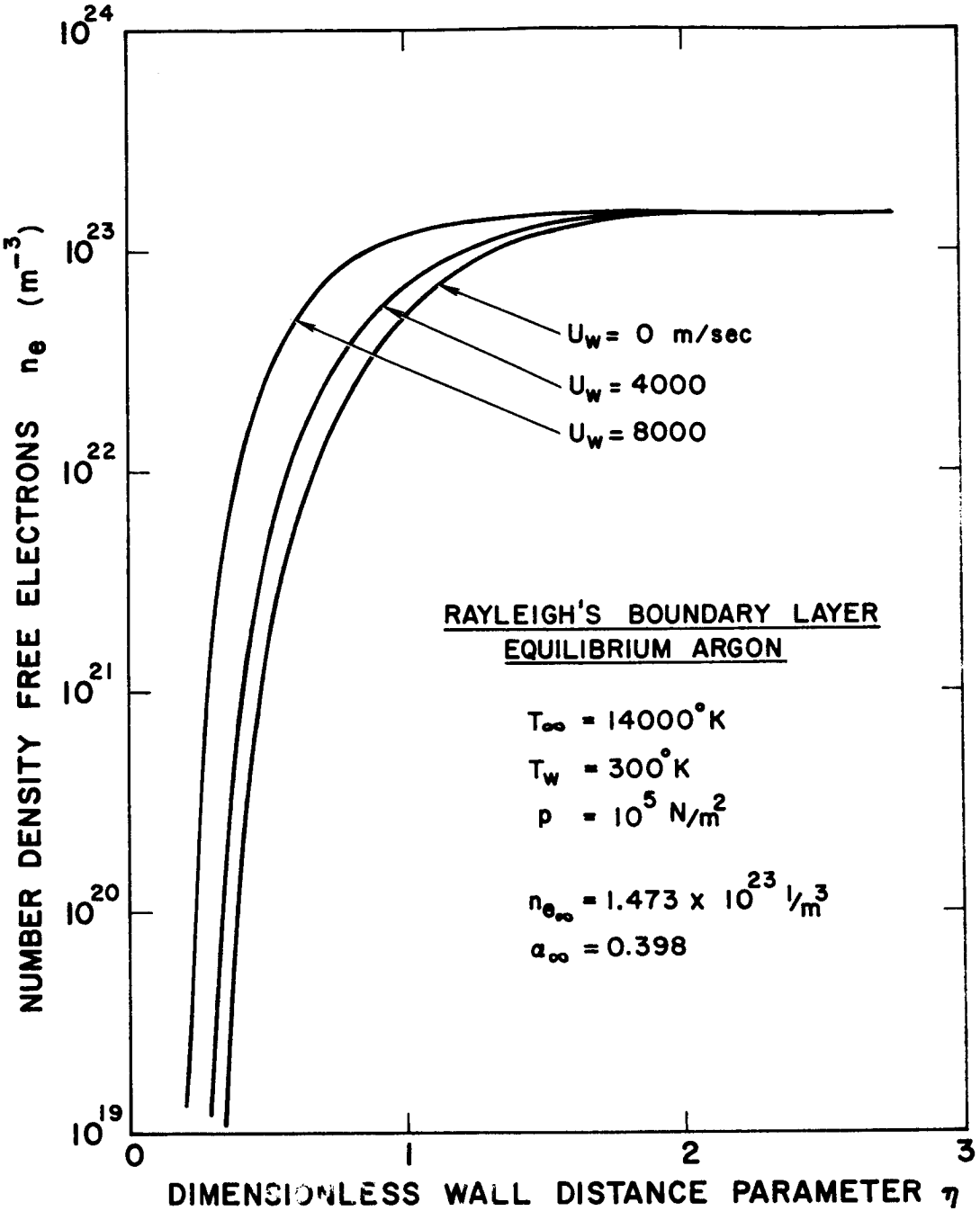


Fig. 22. Electron density profiles in equilibrium argon for Rayleigh's boundary layer as a function of wall velocity.

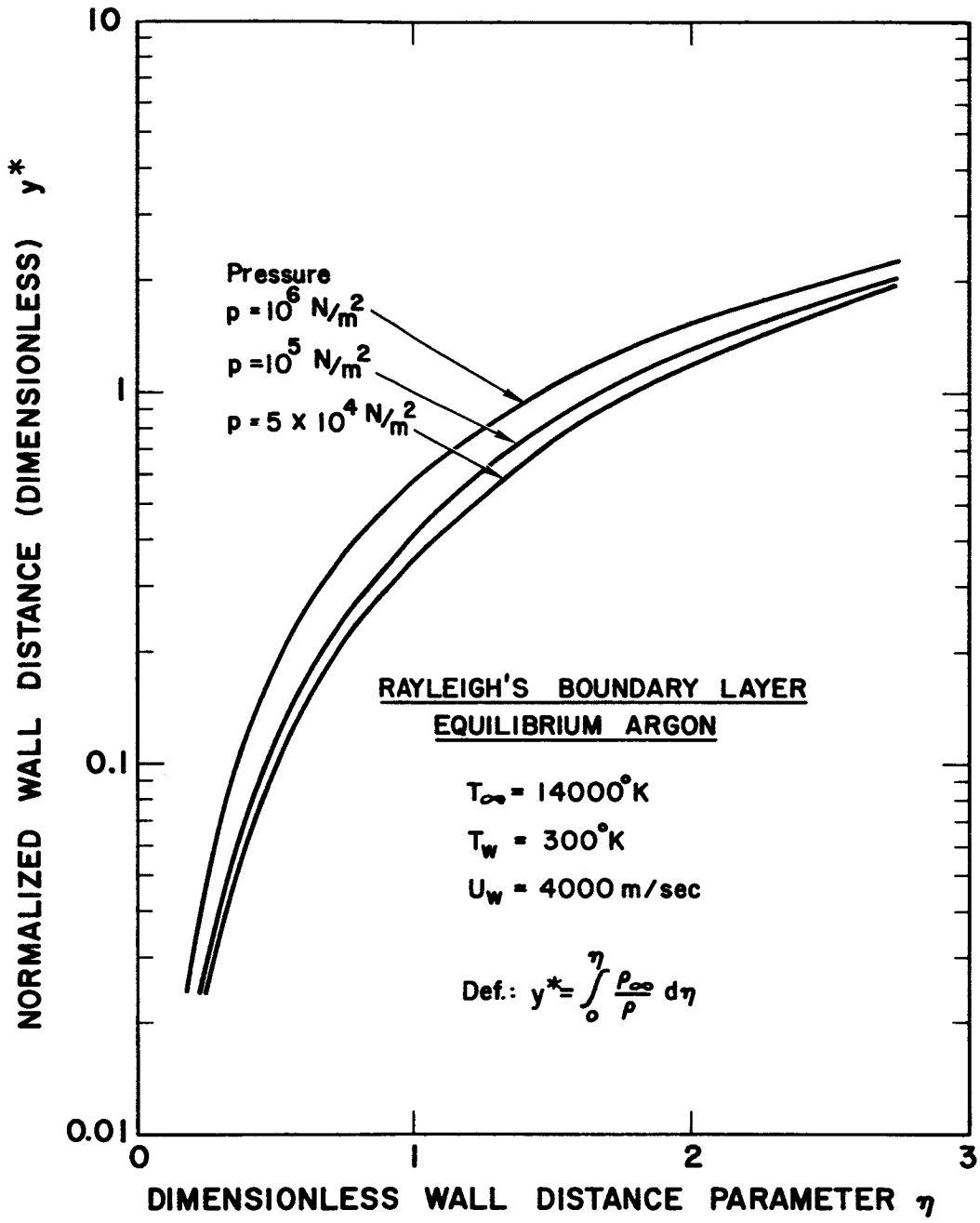


Fig. 23. Normalized wall distance $y^*$ as a function of the similarity variable $\eta$ for equilibrium argon plasma Rayleigh boundary layers.

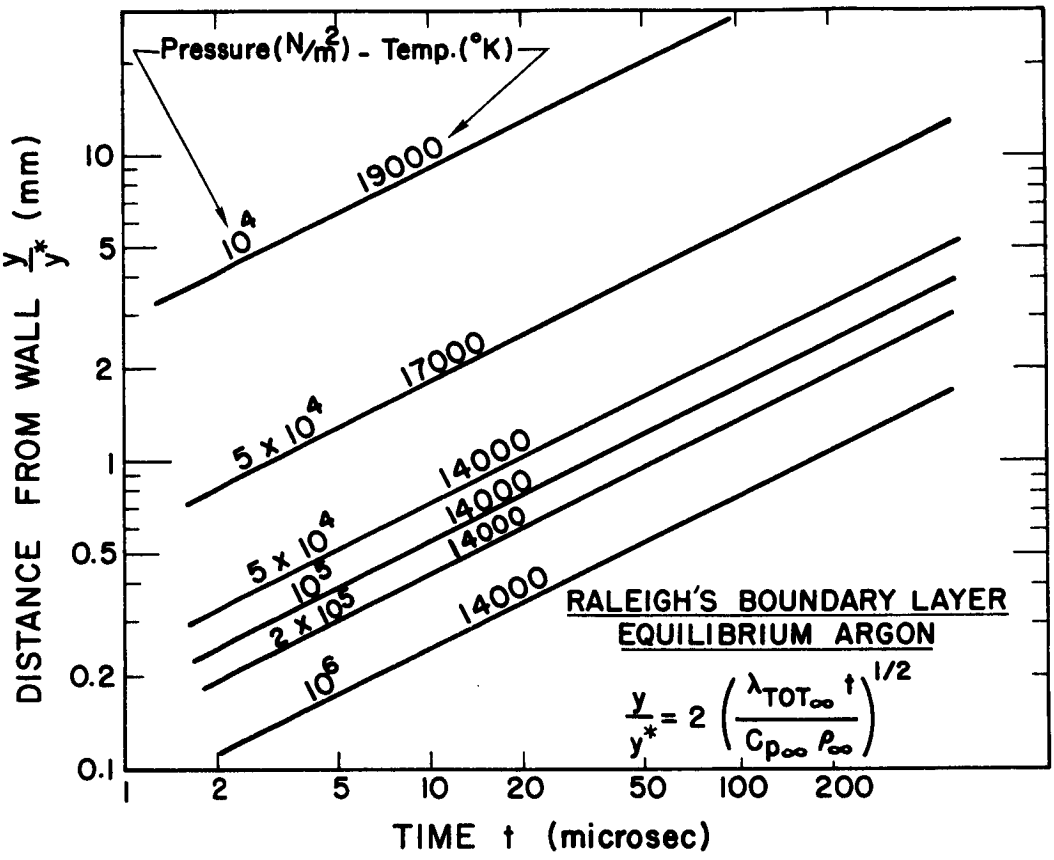


Fig. 24. The ratio $y/y^*$ as a function of time $t$ for some equilibrium argon plasma Rayleigh boundary layers.

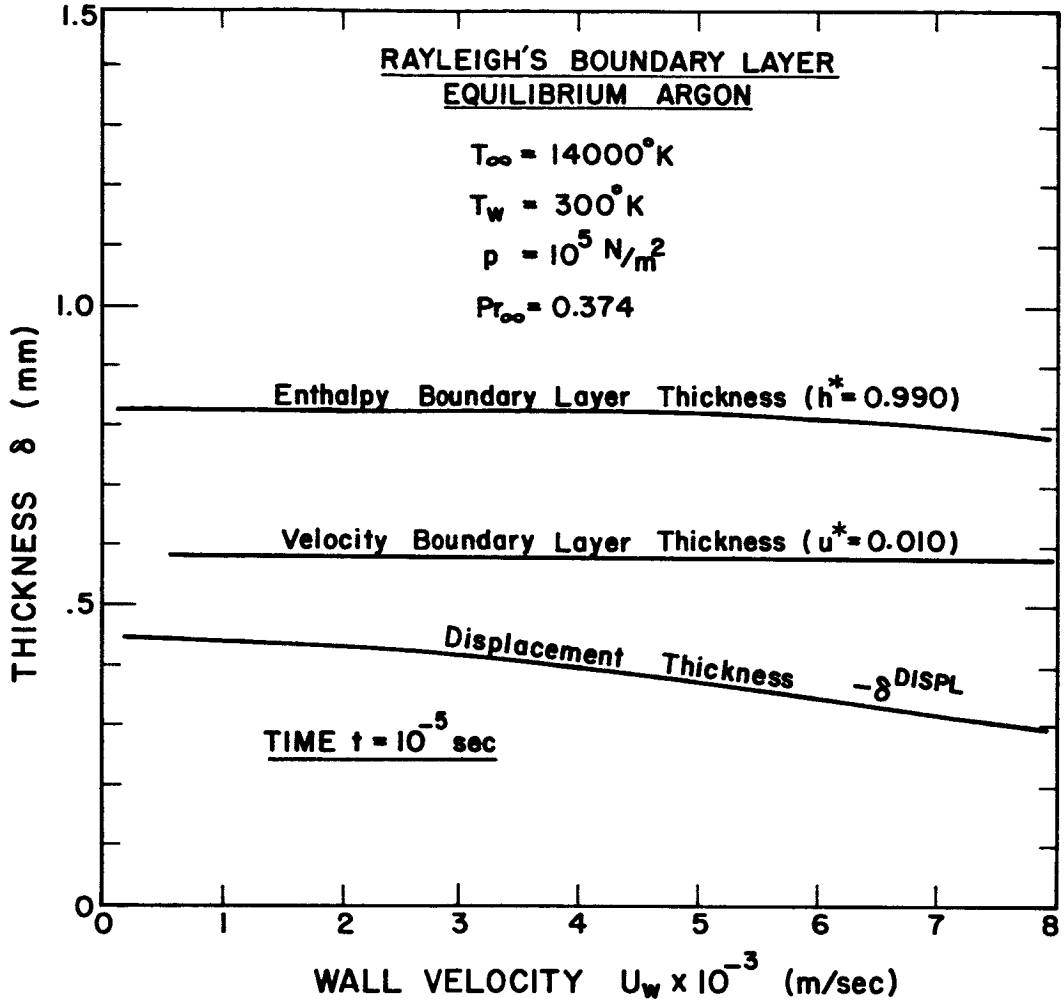


Fig. 25. Boundary layer thicknesses as a function of wall velocity for an equilibrium argon plasma Rayleigh boundary layer.

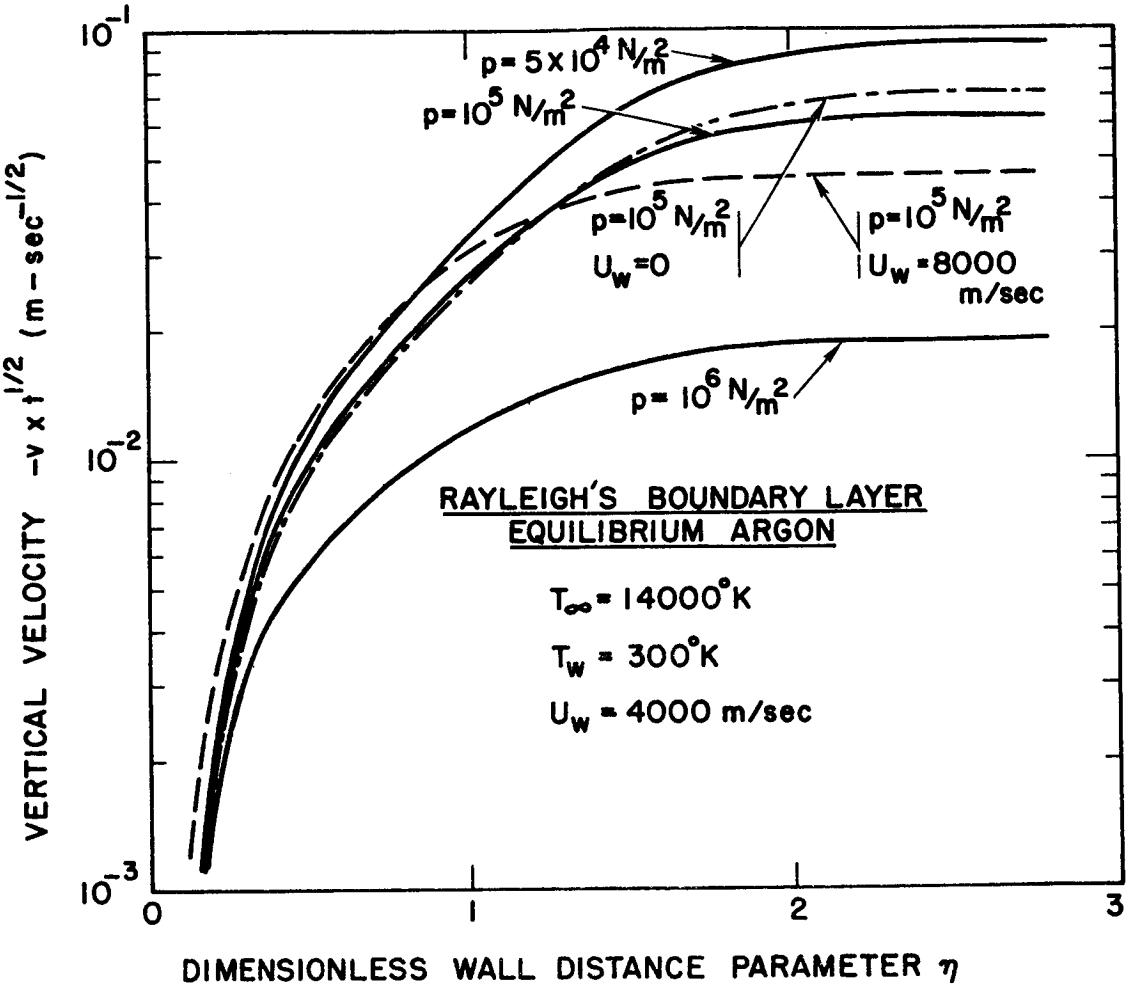


Fig. 26. The induced vertical velocity v in equilibrium argon plasma Rayleigh boundary layers.

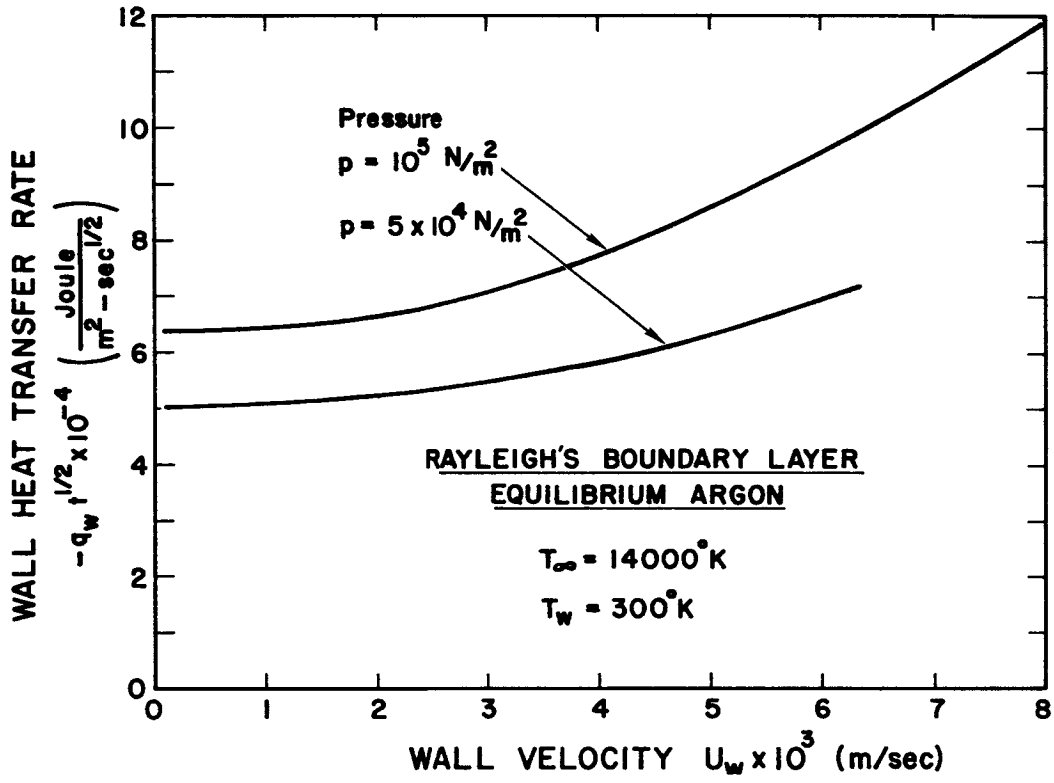


Fig. 27. Wall heat transfer rate as a function of wall velocity for equilibrium argon plasma Rayleigh boundary layers.

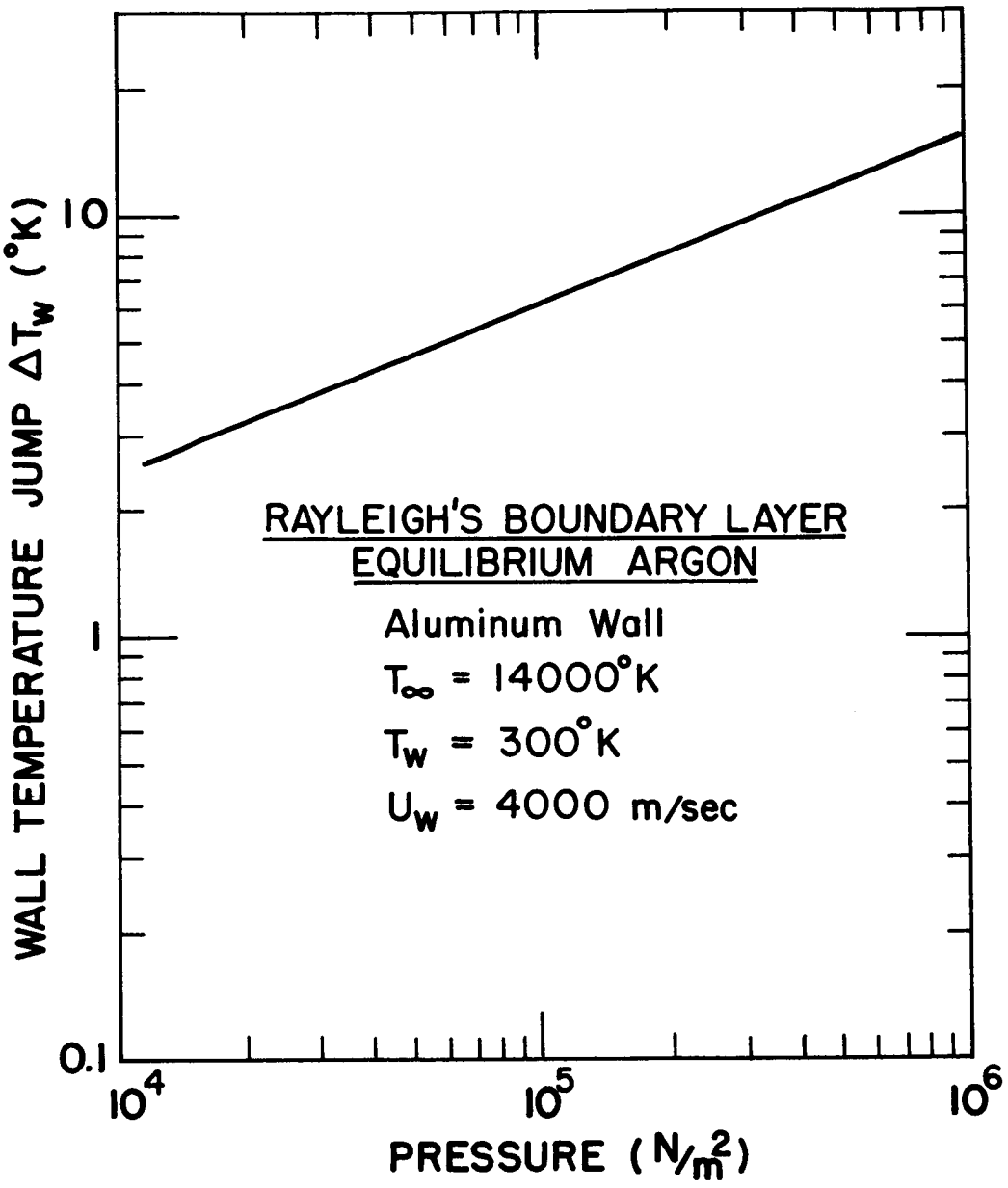


Fig. 28. Aluminum wall temperature jump at time $t = 0$ as a function of pressure for an equilibrium argon plasma Rayleigh boundary layer.

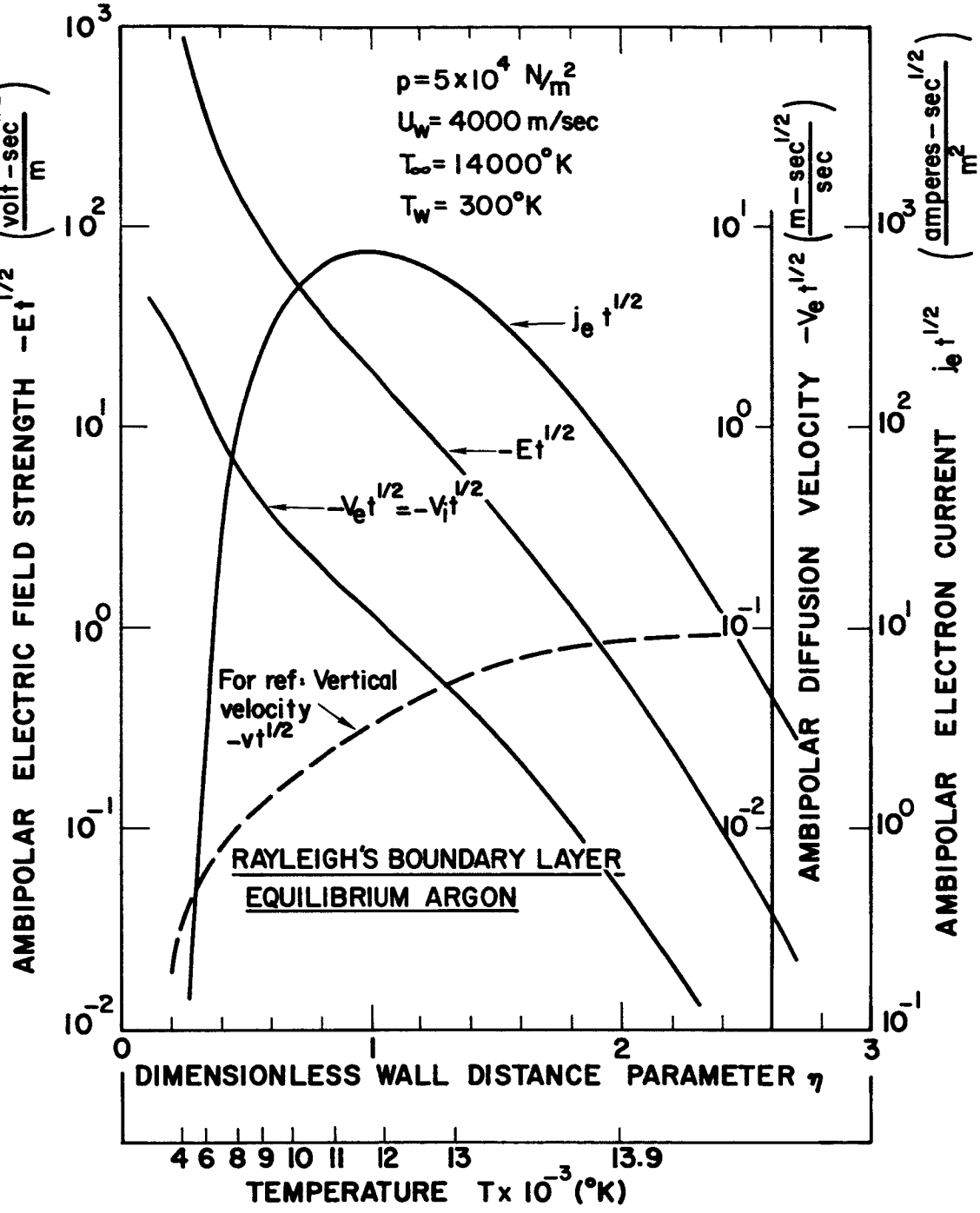


Fig. 29. Induced ambipolar electric field, electron current density, and ambipolar diffusion velocity in an equilibrium argon plasma Rayleigh boundary layer.

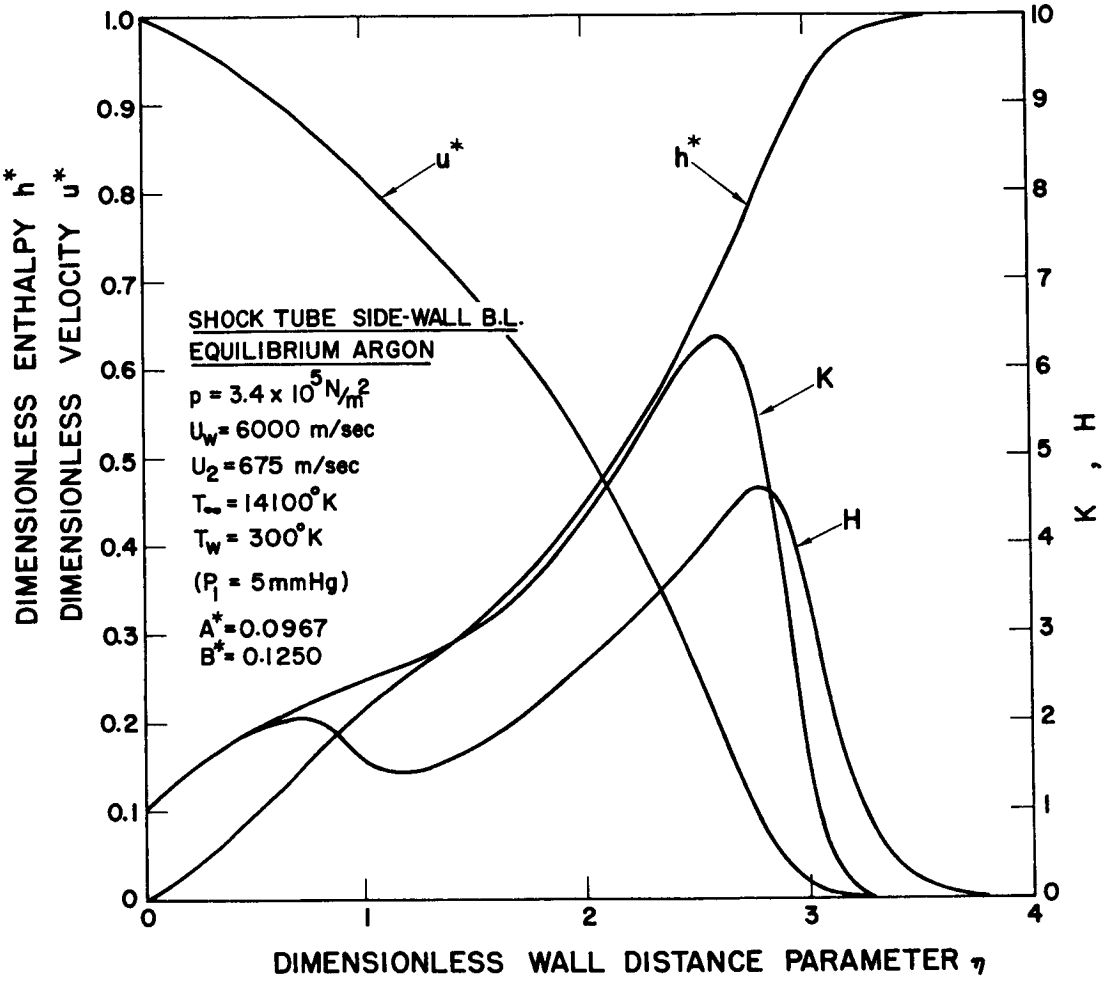


Fig. 30. Dimensionless velocity and enthalpy profiles for an equilibrium argon plasma shock tube side-wall boundary layer. The functions K and H are the normalized velocity and enthalpy derivatives with respect to $\eta$.

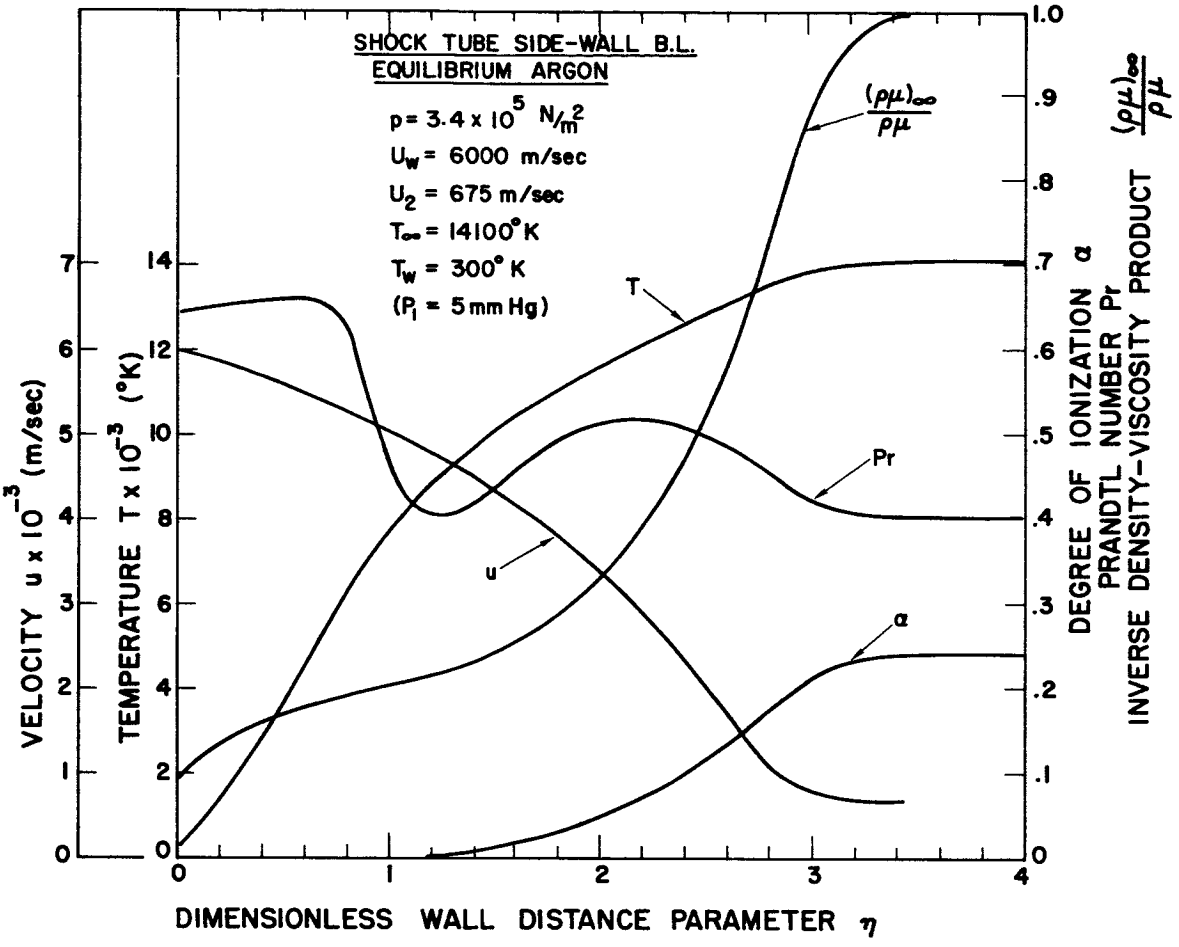


Fig. 31. Velocity, temperature, and degree of ionization profiles for an equilibrium argon plasma shock tube side-wall boundary layer.

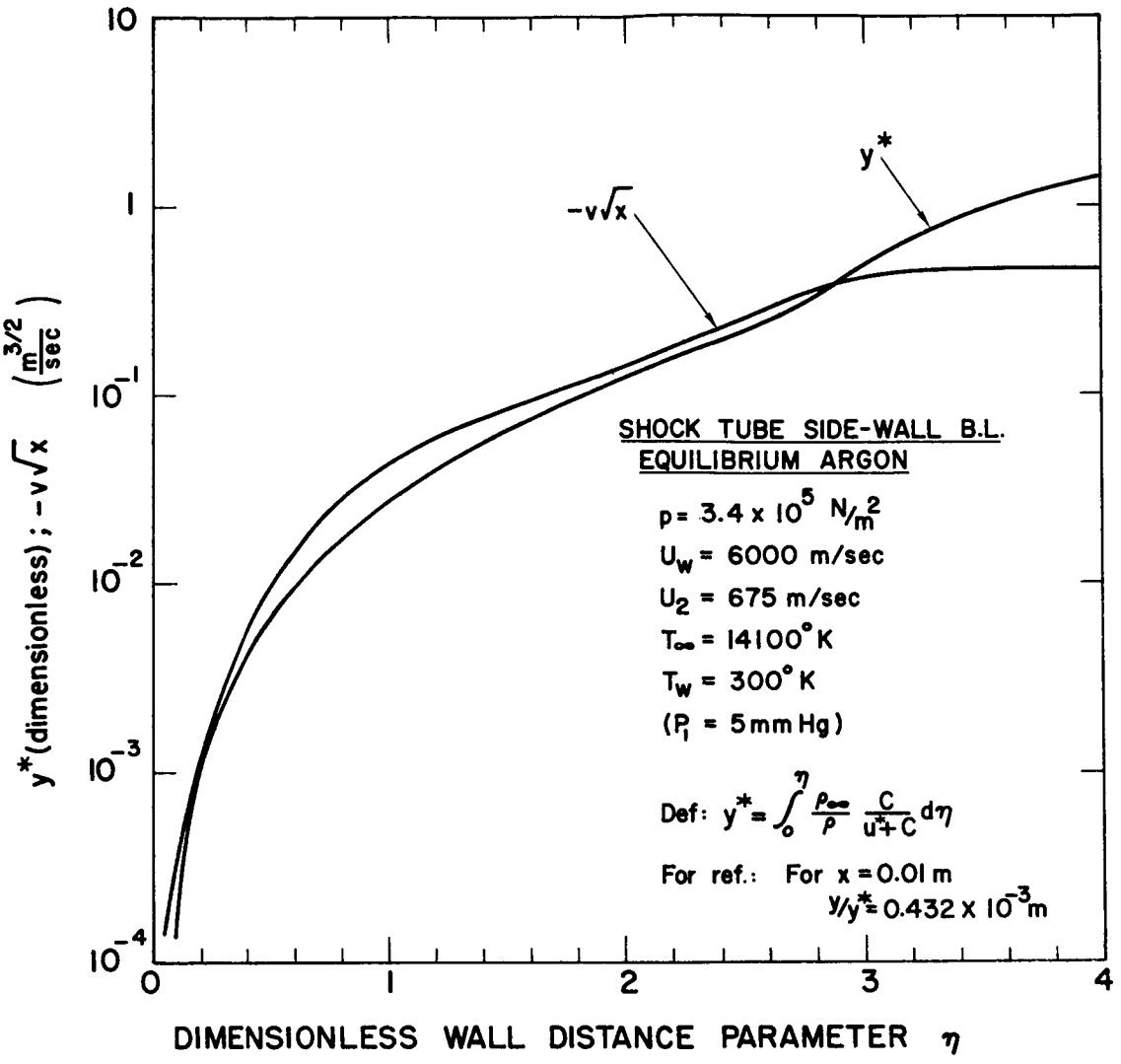


Fig. 32. Normalized wall distance $y^*$ and vertical velocity $v$ as a function of the wall distance similarily parameter $\eta$ for an equilibrium argon plasma shock tube side-wall boundary la[illegible].

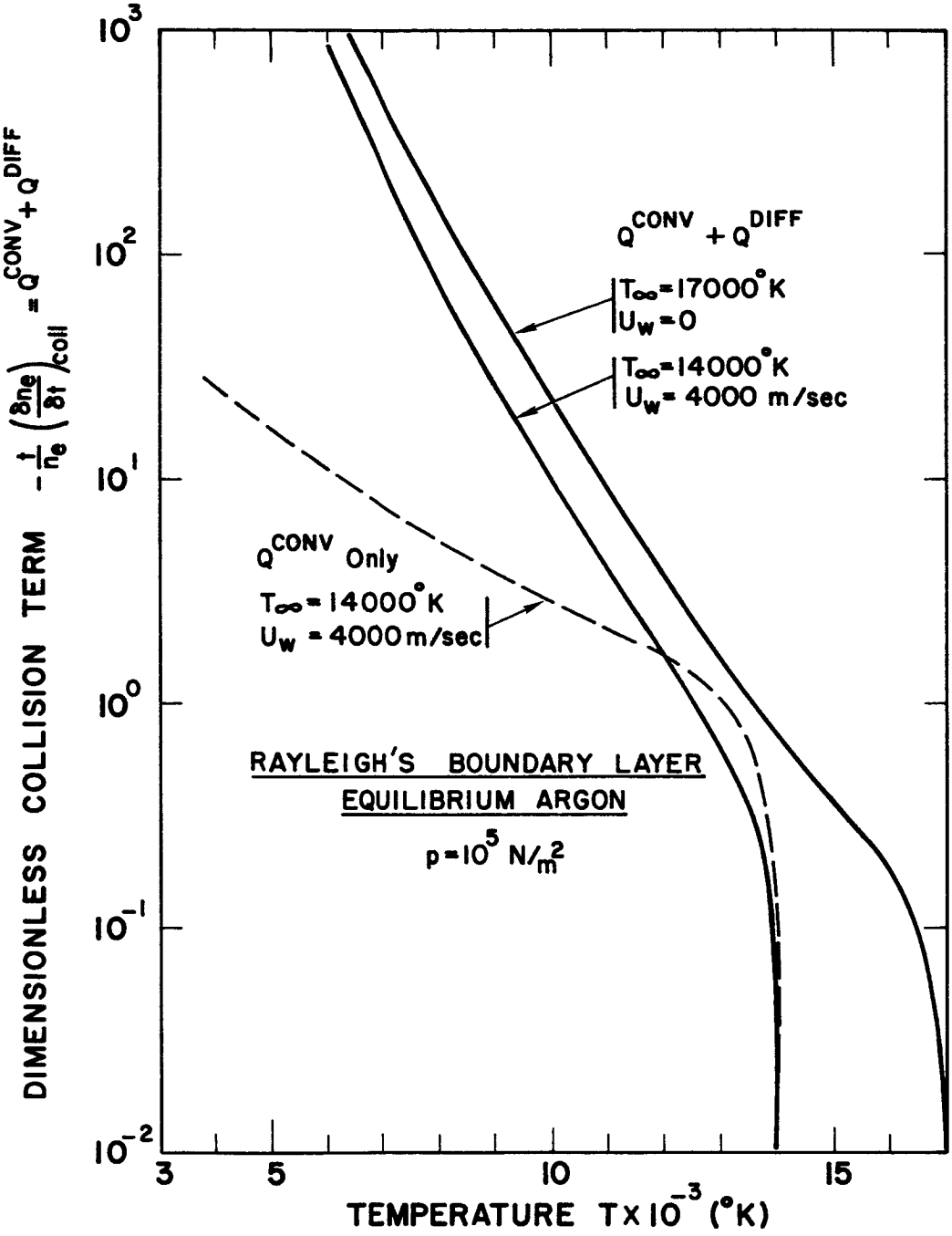


Fig. 33. Required collisional loss rate of free electrons for maintaining equilibrium composition in an argon plasma Rayleigh boundary layer.

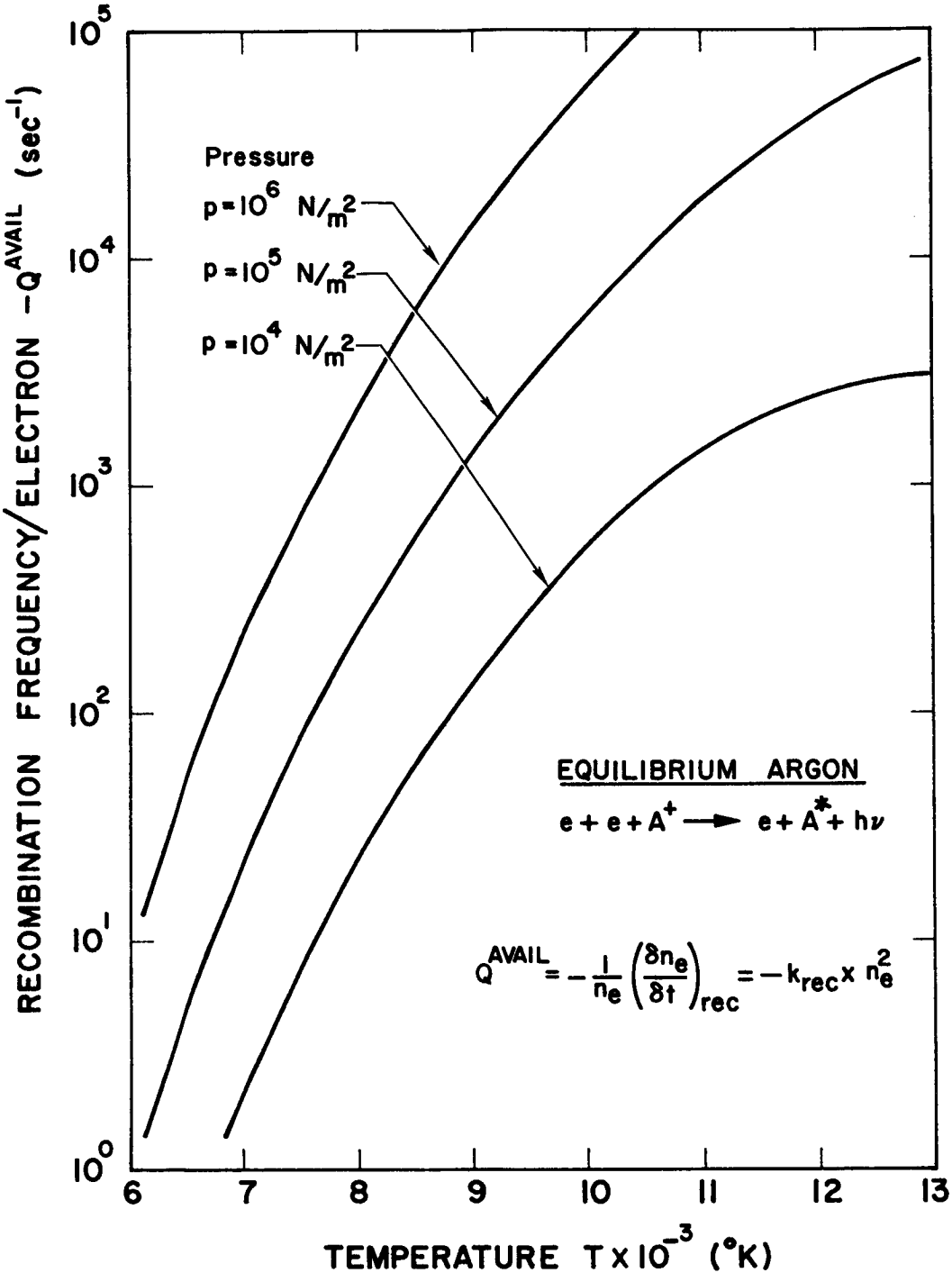


Fig. 34. Kinetic theory result for the available electron-ion recombination collision frequency as a function of temperature for an equilibrium argon plasma.

## 7. TWO-TEMPERATURE BOUNDARY LAYER: A LINEARIZED MODEL

### a. General

In the previous analysis we have assumed that the temperature of the electron, ion, and atom fluids are equal. This assumption will now be studied in some detail. Due to the ineffective energy transfer rate between electrons and heavy particles, the electron temperature may deviate substantially from the heavy particle temperature. In particular, this is true in the cold region of the boundary layer, close to the wall.

The collisional energy transfer rate between the heavy particles and the electrons necessary to maintain temperature equilibrium between the electron and heavy particle fluids may be calculated from the electron energy equation (2.10). The approach is similar in nature to the one used to determine the extent of chemical equilibrium. We shall, for simplicity, assume here that the flow is in chemical equilibrium. Restricting ourselves to the Rayleigh boundary layer, we note first that the collision-term in the electron energy equation takes the form

$$\frac{\partial}{\partial t}(\rho_e e_e)_{coll} = \frac{\partial}{\partial t}(\rho_e e_e) + \frac{\partial}{\partial y}(\rho_e e_e v) + \frac{\partial}{\partial y} q_e - j_{e_y} \cdot E_y + p_e \frac{\partial v}{\partial y} \qquad (7.1)$$

With the similarity parameter $\eta$ as the independent variable, we find for the equilibrium case

$$t \frac{\partial}{\partial t}(\rho_e e_e)_{coll} = -\frac{1}{2}\eta \frac{d}{d\eta}(\rho_e e_e) + \rho_e e_e \frac{\rho}{\rho_\infty}\frac{1}{2}\sqrt{\frac{c_{p_\infty}\rho_\infty}{\lambda_\infty}}\frac{d}{d\eta}(v\sqrt{t}) +$$

$$+ \frac{\rho}{\rho_\infty}\frac{1}{2}\sqrt{\frac{c_{p_\infty}\rho_\infty}{\lambda_\infty}}\frac{d}{d\eta}(q_e\sqrt{t}) - t\, j_{e_y} \cdot E_y + p_e \frac{\rho}{\rho_\infty}\frac{1}{2}\sqrt{\frac{c_{p_\infty}\rho_\infty}{\lambda_\infty}}\frac{d}{d\eta}(v\sqrt{t}) \qquad (7.2)$$

An alternative expression is obtained if we subtract herefrom the total energy equation (2.13), which has no collision-term. The result is

$$t\frac{\partial}{\partial t}(\rho_e e_e)_{coll} = -\frac{1}{2}\eta\frac{d}{d\eta}(\rho_e e_e - \rho e) + (\rho_e e_e - \rho e)\frac{\rho}{\rho_\infty}\frac{1}{2}\sqrt{\frac{c_{p_\infty}\rho_\infty}{\lambda_\infty}}\frac{d}{d\eta}(v\sqrt{t}) +$$

$$+\frac{\rho}{\rho_\infty}\frac{1}{2}\sqrt{\frac{c_{p_\infty}\rho_\infty}{\lambda_\infty}}\frac{d}{d\eta}[(q_e - q)\sqrt{t}] - t\, j_{e_y} E_y + (p_e - p)\frac{\rho}{\rho_\infty}\frac{1}{2}\sqrt{\frac{c_{p_\infty}\rho_\infty}{\lambda_\infty}}\frac{d}{d\eta}(v\sqrt{t}) +$$

$$+\frac{1}{4}\frac{c_{p_\infty}\rho_\infty}{\lambda_\infty}\mu\left(\frac{\rho}{\rho_\infty}\right)^2\left(\frac{du}{d\eta}\right)^2 \quad ; \tag{7.3}$$

The last term here represents the viscous dissipation. As previously, it has been assumed that the total current $j$ is zero. The expression on the right hand side of these equations is independent of time $t$ in the ambipolar region. In particular this is true for the Joule heating term since $j_{e_y} \sim t^{-1/2}$ and $E_y \sim t^{-1/2}$. In the ambipolar region we have

$$j_{e_y} = 2 D_{ia} q_i \frac{n}{1 - n_e/n}\frac{\partial}{\partial y}\left(\frac{n_e}{n}\right) \tag{7.4}$$

$$E_y = -\frac{kT}{q_i}\frac{n}{n_e}\frac{\partial}{\partial y}\left(\frac{n_e}{n}\right) \tag{7.5}$$

One may arrive at the following expression for the electron Joule heating associated with the ambipolar diffusion:

$$j_{e_y} E_y = -\frac{1}{t}\frac{D_{amb} p}{4}\frac{c_{p_\infty}\rho_\infty}{\lambda_\infty}\frac{1}{\alpha(1+\alpha)^2}\left(\frac{\rho}{\rho_\infty}\right)^2\left(\frac{d\alpha}{d\eta}\right)^2 \tag{7.6}$$

Furthermore, the electron heat transfer term becomes

$$\frac{d}{d\eta}\left(q_e\sqrt{t}\right) = \frac{1}{2}\sqrt{\frac{c_{p_\infty}\rho_\infty}{\lambda_\infty}}\,\frac{d}{d\eta}\left(\lambda_e\,\frac{\rho}{\rho_\infty}\,\frac{dT}{d\eta}\right) \tag{7.7}$$

Here we have made the assumption that $q_e = \lambda_e \frac{\partial T}{\partial y}$, where $\lambda_e$ is the electron thermal conductivity.

With the above calculated Joule heating and heat transfer terms, the dimensionless collisional energy transfer rate necessary for maintaining temperature equilibrium becomes

$$\tilde{S}^{equil.} \equiv \frac{t}{\rho_e e_e}\frac{\partial}{\partial t}\left(\rho_e e_e\right)_{coll} = -\frac{1}{2}\,\eta\,\frac{d}{d\eta}\,\ell n\left(\frac{p_e}{\rho^{5/2}}\right) +$$

$$+\frac{1}{6}\,\frac{c_{p_\infty}\rho_\infty}{\lambda_\infty}\left(\frac{\rho}{\rho_\infty}\right)^2\left[\frac{D_{amb}}{1+\alpha}\left(\frac{d\ \ell n\ \alpha}{d\eta}\right)^2 - \frac{1}{n_e kT}\,\frac{\rho_\infty}{\rho}\,\frac{d}{d\eta}\left(\lambda_e\,\frac{\rho}{\rho_\infty}\,\frac{dT}{d\eta}\right)\right] \tag{7.8}$$

Here $p_e$ is the electron pressure. An alternative expression is the following:

$$\tilde{S}^{equil.} \equiv \frac{t}{\rho_e e_e}\frac{\partial}{\partial t}\left(\rho_e e_e\right)_{coll} = -\frac{1}{2}\,\eta\,\frac{d}{d\eta}\,\ell n\ p_e +$$

$$+\frac{1}{6}\,\frac{c_{p_\infty}\rho_\infty}{\lambda_\infty}\left(\frac{\rho}{\rho_\infty}\right)^2\left[\frac{D_{amb}}{1+\alpha}\left(\frac{d\ \ell n\ \alpha}{d\eta}\right)^2 - \frac{1}{n_e kT}\,\frac{\rho_\infty}{\rho}\,\frac{d}{d\eta}\left(\left(\lambda_e-\lambda\right)\frac{\rho}{\rho_\infty}\,\frac{dT}{d\eta}\right) +\right.$$

$$\left.+\frac{\mu}{n_e kT}\left(\frac{du}{d\eta}\right)^2\right] \tag{7.9}$$

We have here made use of the fact that the plasma pressure $p$ is constant throughout the boundary layer. The first term on the right hand side of equation (7.8) represents the required collisional energy transfer

rate due to convection. We note that when the electron pressure increases with $\eta$, as is the case for the present boundary layers, the associated contribution to the collision term is negative. The first term inside the bracket in the same equation represents the effect of the induced electric field and ambipolar diffusion in the direction thereof, i.e., the Joule heating term. Hence, there is obviously a loss of electron energy when the electron fluid diffuses in the direction of the electric field, i.e., in the negative y-direction. Finally, the last term in equation (7.8) represents the effect of heat transfer in the electron fluid itself. This effect is very important and may in fact be the dominant when the gas is partially ionized. The contribution to $\tilde{S}^{equil.}$ from the electron heat transfer term may take both positive and negative values in the presently investigated boundary layers. Close to the wall it is in general negative, i.e., the electron fluid has to transfer energy to the ion-atom fluids if the temperatures should be equal. In the ambipolar region, which is the only one considered here, the heat transfer term is much larger than the term arising from the Joule heating. We mention that a corresponding analysis of the energy balance in the charge separation sheath should show that the Joule heating term is important here. In fact, in the sheath region the electron energy equation would express only the coupling between the Joule heating and the electron thermal flux, since the convective terms are small and can be neglected.

The main energy transfer mechanism between the electron fluid and the ion and atom fluids is the elastic two-body collision between either an electron and an ion, or between an electron and an atom. The

contribution from inelastic collisions is assumed to be small since the number density of particles, which have kinetic energies comparable to the excitation energies in argon are small.

We assume that the electron fluid has a Maxwellian velocity distribution function at temperature $T_e$, and that the ion and atom fluids have similar distributions at their common temperature $T_a = T_i$. In a Lorentzian model, in which the ions and atoms are stationary and only the electrons are moving, the elastic energy transfer rate $\epsilon_{ae}$ to the electrons from the atoms becomes (e.g., [12])

$$\epsilon_{ae} \doteq \frac{m_e^2}{m_a} \left[\frac{T_a}{T_e} - 1\right] n_a n_e \langle Q_{ae}(w_e) w_e^3 \rangle \tag{7.10}$$

and from the ions to the electrons

$$\epsilon_{ie} \doteq \frac{m_e^2}{m_i} \left[\frac{T_i}{T_e} - 1\right] n_i n_e \langle Q_{ie}(w_e) w_e^3 \rangle \tag{7.11}$$

Here $Q_{ae}(w_e)$ is an effective hard sphere elastic collision cross-section for the electron-atom collisions, and $Q_{ie}(w_e)$ the corresponding cross-section for electron-ion collisions. The brackets indicate a mean value taken over the Maxwellian electron distribution function. For simplicity we shall give here a simplified treatment, and assume that the cross-sections do not vary much with electron speed. We may then use the following expressions for the mean values

$$\left.\begin{aligned} \langle Q_{ae}(w_e) w_e^3 \rangle &\doteq \left(\frac{3kT_e}{m_e}\right)^{3/2} Q_{ae}(T_e) \\ \langle Q_{ie}(w_e) w_e^3 \rangle &\doteq \left(\frac{3kT_e}{m_e}\right)^{3/2} Q_{ie}(T_e) \end{aligned}\right\} \tag{7.12}$$

Here $Q_{ae}(T_e)$ and $Q_{ie}(T_e)$ are effective average cross-sections at the electron temperature $T_e$, e.g., those previously discussed in Section 5. With this assumption the elastic energy transfer rate to the electron fluid simply becomes

$$\epsilon = \epsilon_{ae} + \epsilon_{ie} = \frac{m_e^{1/2}}{m_a} (3kT_e)^{3/2} n_e^2 \left[\frac{T_a}{T_e} - 1\right]\left[Q_{ie}(T_e) + \frac{1+\alpha}{\alpha} Q_{ae}(T_e)\right] \tag{7.13}$$

We have assumed here that the gas is quasi-neutral, i.e., $n_i/n_e \simeq 1$; and hence introduced $\alpha$, the degree of ionization. The energy transfer rate $S^{avail.}$ per unit energy of the electron fluid and unit relative temperature difference $(T_a/T_e - 1)$ is then

$$S^{avail.} \equiv \frac{\epsilon}{\rho_e e_e (T_a/T_e - 1)} = 2 \frac{m_e}{m_a} \left(\frac{3kT_e}{m_e}\right)^{1/2} n_e \left[Q_{ie}(T_e) + \frac{1+\alpha}{\alpha} Q_{ae}(T_e)\right] \tag{7.14}$$

This quantity has the dimension $t^{-1}$. The electron and the heavy particle fluids obviously have temperatures which are close to equal when this rate is much larger than the required rate to maintain temperature equilibrium, as calculated, e.g., for the Rayleigh boundary layer in equation (7.9). The criterion for local temperature equilibrium in the boundary layer is then

$$\begin{matrix}\text{Temperature} \\ \text{Equilibrium} \\ \text{Criterion:}\end{matrix} = \frac{t\, S^{avail.}}{\tilde{S}^{equil.}} \gg 1 \tag{7.15}$$

Notice that at large times $t$, this inequality will be satisfied, since $S^{avail.}$ and $\tilde{S}^{equil.}$ are time-independent.

b. The Electron Temperature in a Linearized Model

The extent of the temperature equilibrium region in the Rayleigh argon plasma boundary layer can be determined by help of the criterion (7.15). A similar criterion can be developed and used for the shock-tube side-wall boundary layer. We shall here go one step further and actually calculate the difference in electron and ion-atom temperatures, when it is small. Hence, the electron temperature distribution in the boundary layer calculated in the following is valid for large times, when the entire boundary layer flow approaches both temperature and chemical equilibrium.

It is convenient to introduce a dimensionless electron temperature perturbation parameter $\varphi$, defined as

$$T_e = T_a(1+\varphi) \tag{7.16}$$

where $T_a$ is the heavy particle temperature. Assuming that $\varphi \ll 1$, the following relation is found from equations (7.8, 7.14)

$$\frac{\varphi}{1+\varphi} \doteq -\frac{1}{t}\frac{\tilde{S}^{equil.}(T_a)}{S^{avail.}(T_a)} \tag{7.17}$$

By help of equations (7.9, 7.14) the temperature perturbation $\varphi$ may therefore by written

$\varphi \ll 1$:

$$\frac{\varphi}{1+\varphi}\, t = \frac{C_1 + C_2 + C_3 + C_4}{2\,\frac{m_e}{m_a}\left(\frac{3kT}{m_a}\right)^{1/2} n_e\left[Q_{ie}(T) + \frac{1+\alpha}{\alpha} Q_{ae}(T)\right]} \tag{7.18}$$

where

$$C_1 = \frac{1}{2}\,\eta\,\frac{d}{d\eta}\,(\ell n\ p_e)$$

$$C_2 = -\frac{1}{6}\,\frac{c_{p_\infty}\rho_\infty}{\lambda_\infty}\,\left(\frac{\rho}{\rho_\infty}\right)^2\,\frac{D_{amb}}{1+\alpha}\,\left(\frac{d\ \ell n\ \alpha}{d\eta}\right)^2 \qquad (7.19)$$

$$C_3 = \frac{1}{6}\,\frac{c_{p_\infty}\rho_\infty}{\lambda_\infty}\,\left(\frac{\rho}{\rho_\infty}\right)\,\frac{1}{n_e kT}\,\frac{d}{d\eta}\,\left[(\lambda_e-\lambda_{tot})\,\frac{\rho}{\rho_\infty}\,\frac{dT}{d\eta}\right]$$

$$C_4 = -\frac{1}{6}\,\frac{c_{p_\infty}\rho_\infty}{\lambda_\infty}\,\left(\frac{\rho}{\rho_\infty}\right)^2\,\frac{\mu}{n_e kT}\,\left(\frac{du}{d\eta}\right)^2$$

Here $C_1$ is a dimensionless contribution to the temperature perturbation due to the convective cooling of the plasma, at which the total pressure is constant but not the electron fluid pressure $p_e$. The dimensionless (in general negative) term $C_2$ expresses the cooling of the electron fluid when it diffuses in the direction of the electric field, i.e., towards the wall. The also dimensionless term $C_3$, which is the most important, is a contribution from the fact that the electron fluid itself and the plasma have different thermal conductivities. Finally, the negative term $C_2$ comes from the heating of the heavy fluids through the viscous dissipation.

The temperature perturbation function $\varphi$ has been calculated for some Rayleigh boundary layers. The results are shown in Fig. 35. For the pressure levels of interest, the perturbation function $\varphi t$ is less than $10^{-6}$ sec, at temperatures above 12,000°K. Therefore, at times $t$ larger than $t$ = 1 microsec, the temperature perturbation is small, i.e., $\varphi \ll 1$, and we state with confidence that temperature equilibrium is present in the boundary layer. At temperatures lower than 10,000°K the perturbation

function $\varphi t$ becomes larger than $10^{-5}$ sec. Hence, if $t$ is of the order microseconds, we here expect temperature non-equilibrium. In the particular example shown, the electron temperature is larger than the heavy particle temperature. At temperatures lower than 8000°K the perturbation function $\varphi t$ becomes larger than $10^{-2}$ (sec) and increases very rapidly with decreasing temperature. The electron temperature is here not in equilibrium with the heavy particle temperature. It is here practically meaningless to calculate the actual deviation in electron temperature by equation (7.18) without considering simultaneously the effect of chemical non-equilibrium, which (in the previous section) was also shown to exist in this temperature region.

It is very interesting to calculate the relative importance of the four different terms $C_i$ which compose the temperature perturbation $\varphi$. The result of a numerical calculation is shown in Fig. 36. The individual contributions are here normalized with the convective contribution $C_1$, which is positive. The ratio between the electron heat transfer term and the convective term, $C_3/C_1$, is the largest throughout the ambipolar region. Even close to free stream conditions this ratio is large. The effect of viscous dissipation in the atom and ion fluids (term $C_4$) becomes increasingly important with decreasing value of the similarity parameter $\eta$, i.e., with smaller distance to the wall. At 13,000°K in the example given, $C_4$ is of equal importance as the convective term $C_1$, but it is still about 5 times smaller than $C_3$. However at 11,000°K $C_4$ amounts to as much as 50% of the electron thermal conduction term $C_3$. For still lower temperatures the electron thermal conduction is by far the most important term. At 7000°K the absolute value of the ratio $C_4/C_3$

if of the order 20. The effect on the electron temperature from the diffusion of the electron fluid in the direction of the electric field, described by the term $C_2$, is quite small everywhere in the ambipolar diffusion region. For temperatures below 11,000°K it is shown in Fig. 36 to be more important than the convection. At 8000°K we have $C_2/C_1=-10$, but the absolute value of $C_2$ is here still two orders of magnitude smaller than $C_3$.

For large values of the wall velocity $U_w$ and $U_w^2/(h_\infty-h_w)$, the effect of dissipation through the term $C_4$ may become major. The electron temperature will then be lower than the heavy particle temperature. In the outer region of the boundary layer the term $C_3$ will still be the most important since the viscous dissipation here is small. Then the boundary layer may contain regions both where the electron temperature is higher than the heavy particle temperature (close to the free stream) and where the electron temperature is lower (close to the wall).

In the case of shock tube side-wall boundary layers a similar analysis could be performed. The viscous dissipation is here only moderate due to the coupling in shock velocity and enthalpy $h_\infty$. An electron conductive term, analogous to $C_3$, is then again the most important to the electron temperature perturbation. The electron temperature for a quasi-equilibrium argon shock tube side-wall boundary layer as before becomes larger than the heavy particle temperature.

It is not clear at all that in any argon plasma flow situation with shear and heat conduction the effect of thermal conduction in the electron fluid itself (through a term such as $C_3$ in the Rayleigh boundary layer) gives an elevated electron temperature. In fact, there has been

theoretically found situations where the effect of thermal conduction in the electron fluid causes a low electron temperature. For temperatures $T < 8000°K$ this phenomenon is not likely to occur for equilibrium argon, since its electron thermal conductivity rapidly increases with temperature, as is shown in Fig. 37. Hence, terms similar to $C_3$ for the Rayleigh boundary layer becomes positive.

It is evident from an analysis like the present, that the argon plasma boundary layers will be in temperature equilibrium far away from the wall, say for $T > 10,000°K$. This region may typically amount to 90% of the total boundary layer thickness. The non-equilibrium region may still be of extreme importance to the wall energy flux, shear stress and electrical characteristics. For present purposes, the effects of temperature non-equilibrium as well as chemical non-equilibrium should not be drastic for the equilibrium velocity and enthalpy profiles since the degree of ionization is small in the non-equilibrium region. We therefore believe that the calculated equilibrium velocity and enthalpy profiles closely resemble the true profiles. For lower pressure levels say, $p < 0.1$ atm., the temperature non-equilibrium region will extend further out to higher temperature and a large degree of ionization $\alpha$, may then cause non-negligible discrepancies.

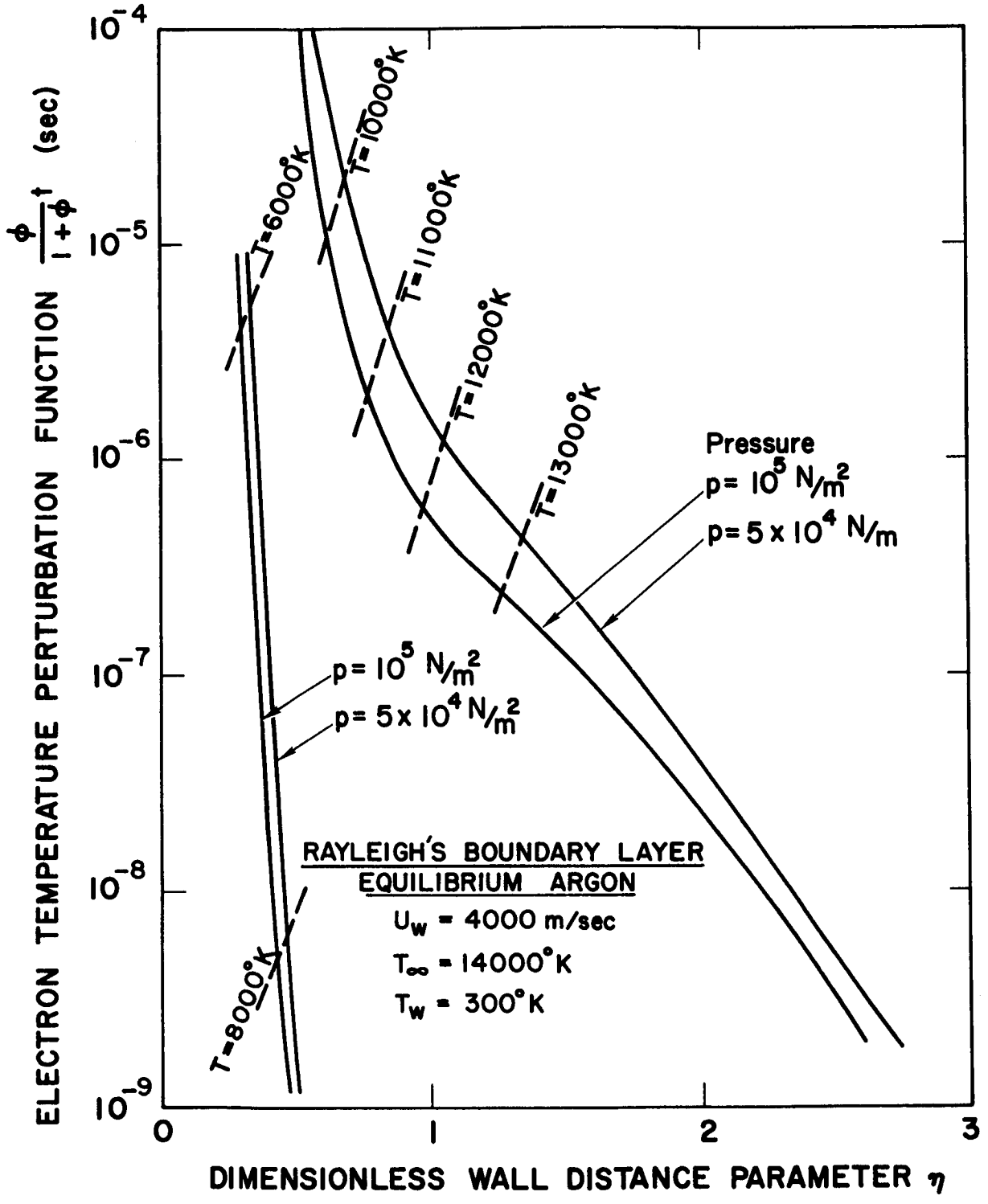


Fig. 35. The electron temperature perturbation function for the Rayleigh boundary layer in a quasi-equilibrium argon plasma.

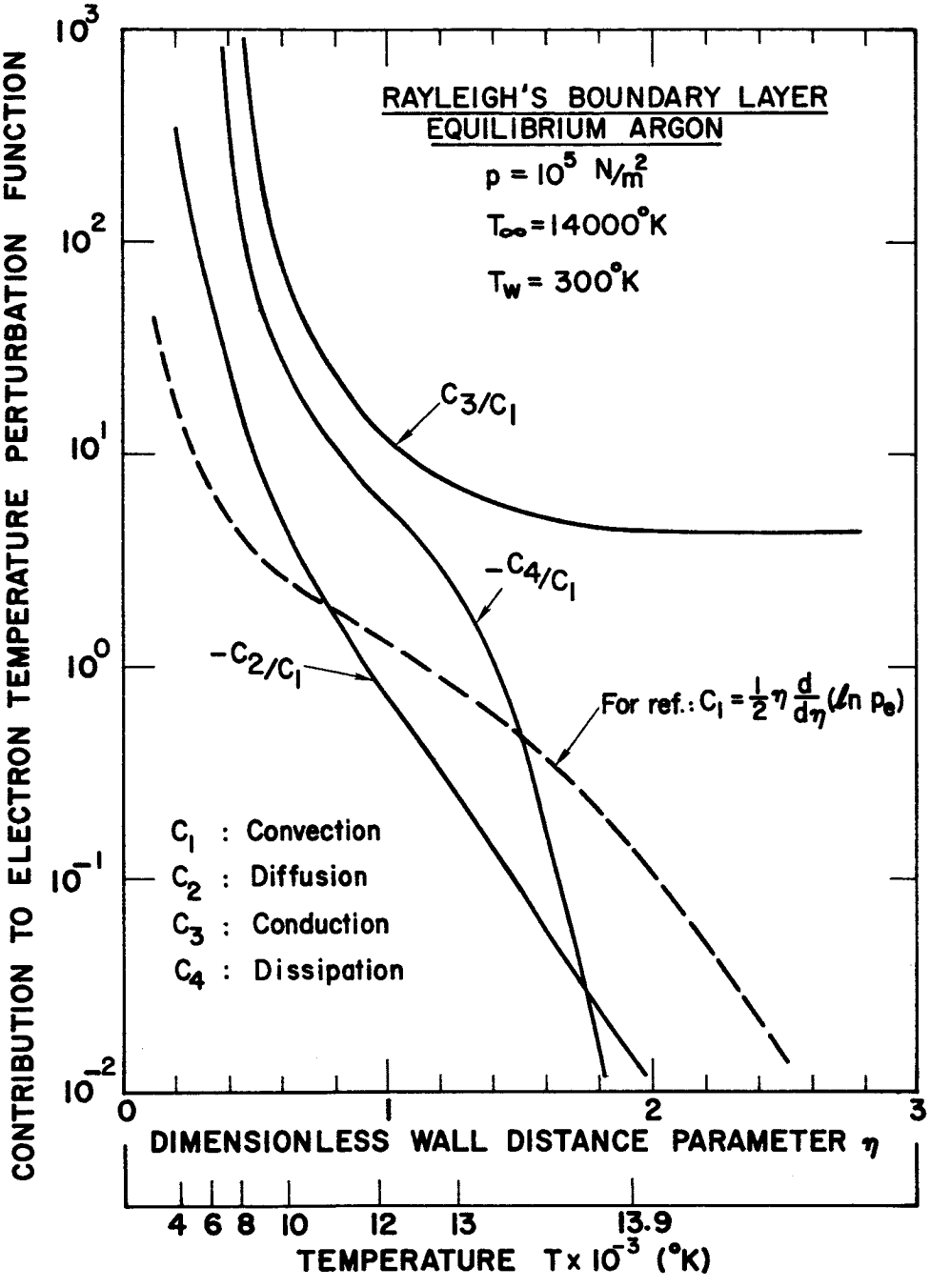


Fig. 36. The relative contribution to the electron temperature perturbation function from convection ($C_1$), diffusion ($C_2$), electron thermal conduction ($C_3$), and viscous dissipation ($C_4$).

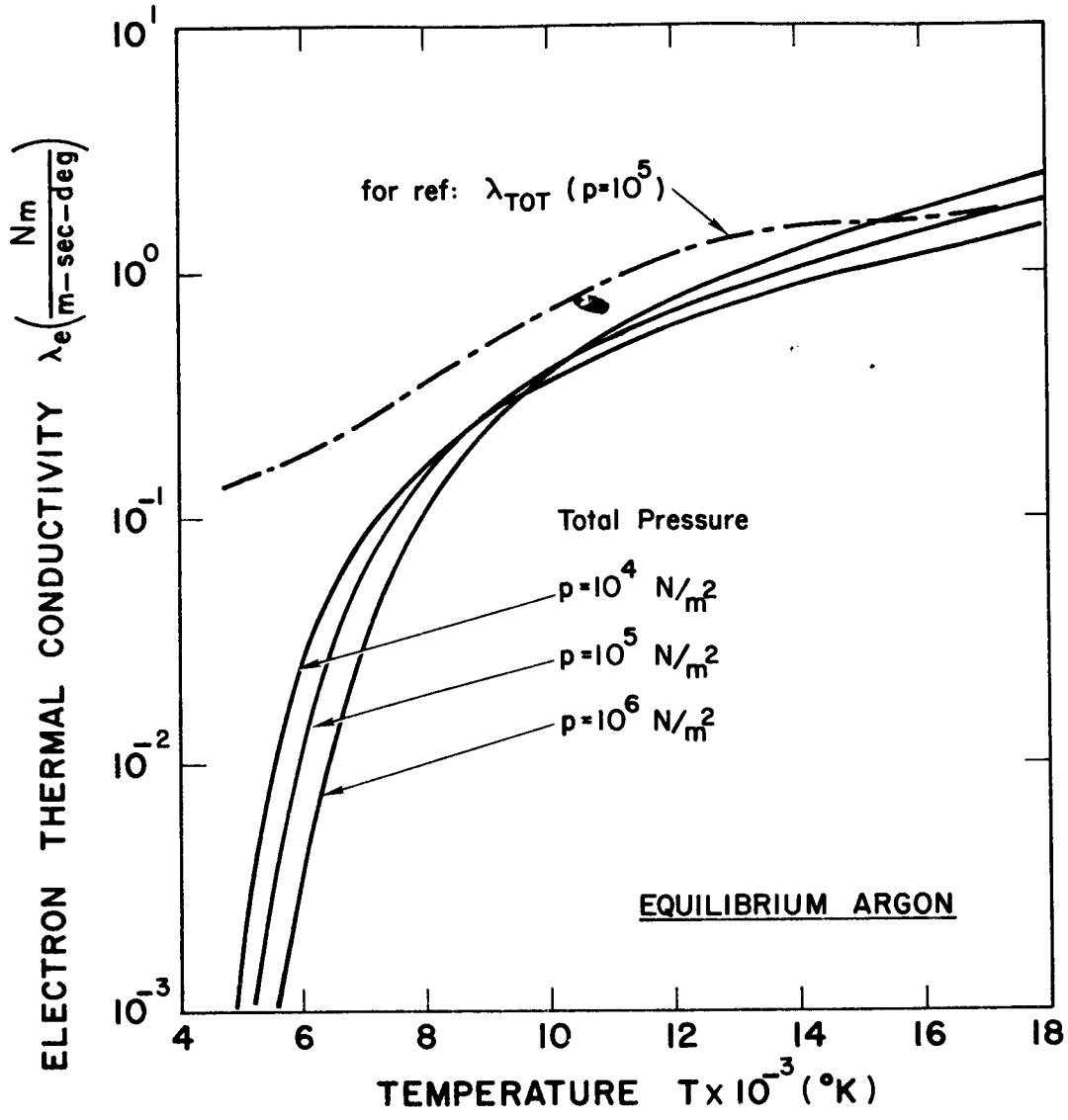


Fig. 37. The electron thermal conductivity in an equilibrium argon plasma.

# 8. SUMMARY AND CONCLUDING REMARKS

The structure of convective laminar boundary layers in high density plasma flows has been analyzed. The boundary layers studied are the Rayleigh's boundary layer with both momentum and energy exchange between the plasma and the cold wall, the shock tube end-wall, and the shock tube side-wall boundary layer. The analysis was intended to apply especially to conditions in which the free stream plasma energy is typically 1 eV and the number density of free electrons $n_e \sim 10^{23}$ $m^{-3}$, e.g., as obtained in argon behind a strong normal shock wave, for shock Mach numbers larger than $M_s = 15$ and initial pressures of the order $p_1 = 1$ mm Hg. The temperature of the wall over which the boundary layer develops is assumed to be $T = 300°K$.

The governing boundary layer equations were derived in a multi-fluid, continuum model for the electrons, ions and atoms. Chemical and temperature equilibrium were assumed initially and radiation neglected. No applied electromagnetic fields were considered, but it was shown that the induced electric field is important. The diffusive motion of the electron and ion fluids are strongly coupled by this electric field throughout most of the boundary layer. These ambipolar conditions were shown not to hold only in a thin sheath adjacent to the body, in the temperature range typically below 3000°K.

The appropriate transport properties were calculated for an equilibrium argon plasma under the assumption of ambipolar conditions. For this purpose, simple kinetic theory was used, which proved to be fruitful. Pertinent results for the viscosity, thermal conductivity,

and Prandtl number were presented up to temperatures T = 20,000°K. The viscosity was found to decrease strongly with increasing temperature in the region corresponding to partial ionization. The reason for this is the charge exchange and ion-ion Coulomb collisions, which then become increasingly important over the atom-atom collisions, which has a small cross-section. Furthermore, it was demonstrated that the ambipolar "reactive" conductivity, i.e., the energy flux associated with the diffusive motion of the species, plays an important role when the gas is in a partially ionized state. Typically this conductivity amounts to 20-40% of the total thermal conductivity at temperatures around 12,000°K for the argon plasma. The Prandtl number, for the same plasma, which was calculated with the equilibrium value of the specific heat $c_p$, had a local minimum at 9000°K, and then rapidly decreased to a low value of the order of $10^{-2}$, when the temperature was larger than 14,000°K (strongly ionized gas). Due to the low plasma viscosity, it was interesting to note that the density-viscosity product at constant pressure typically was two orders of magnitude larger at the wall temperature than at, e.g., T = 14,000°K. Hence, neither the Prandtl number and the density-viscosity product could be assumed to be constant across the present type of boundary layers.

The governing boundary layer equations were solved for the case of equilibrium composition and equal temperatures of the electron, ion and atom fluids. The correct variation with temperature of the transport properties was included. The method of solution was a finite difference predictor-corrector technique. Several interesting solutions were obtained and discussed. Due to the small plasma viscosity and therefore

also small Prandtl number, the velocity boundary layer was found to be always embedded in the thermal boundary layer. However, once the velocity boundary layer started to develop, the velocity gradient was steep. Wall heat transfer rates were calculated as was the associated small wall temperature jump of a metallic wall, when suddenly brought into contact with the plasma at time $t = 0$.

The assumption of equilibrium composition was checked in a rigorous way. This was done with the help of the mass conservation equation for the electron fluid together with argon recombination rate data. It was found that the assumption of an equilibrium plasma composition breaks down typically below temperatures of 10,000°K. Equilibrium was established with large certainty above 11,000°K. Below 8000°K the recombinations are so rare that they could almost be neglected, i.e., the flow is frozen here. The fact that the gas is not in equilibrium below 10,000°K should not drastically change the velocity and enthalpy profiles much from those calculated for equilibrium. This statement should also hold, e.g., for the wall heat transfer. The degree of ionization in the non-equilibrium region will be small, and the boundary layer structure therefore mainly determined by the atom fluid. The electrical characteristics calculated for equilibrium composition, however, will change drastically by the lack of equilibrium.

The assumption of equal temperatures of the electron, atom and ion fluids was analysed similarly as the assumption of chemical equilibrium. Since the collisional elastic energy transfer rate between the electron fluid and the ion and atom fluids is very ineffective due to the discrepancy in mass of the particles, the electron fluid was expected possibly to have a different temperature than the ion-atom fluids. This effect

was found true, and in fact very pronounced at low temperatures. The electron temperature for an argon plasma was determined thereafter in a linearized model, in which the deviation from the heavy fluid temperature was assumed to be small. It was found that the deviation in temperature was caused by the facts that the electron pressure is not constant across the boundary layer (as is the case for the total pressure), that the electron thermal conductivity has a different behavior with temperature than the total thermal conductivity, that the electron current is oriented in the opposite direction from the ion current and therefore the Joule heating is different for the electron and ion fluids, and finally that the viscous dissipation heats only the ion and atom fluids. When the heavy particle temperature is lower than about 9000°K and the thermal boundary layer thickness is of the order 1mm, the argon boundary layer will not be in temperature equilibrium. The electron temperature will be higher than the atom-ion temperature, at least when the viscous dissipation is small and the diffusion ambipolar. At temperatures above 11,000°K the temperature difference between the fluids is small for the same boundary layer thickness, but the tendency is that the electron temperature is the higher. It is concluded that a more rigorous analysis of the present plasma boundary layers should certainly include the possibility of simultaneous non-equilibrium in temperature and composition. It would be quite unrealistic to treat the non-equilibrium effects separately, since they are strongly coupled.

## REFERENCES


1. J. A. Fay and N. H. Kemp, AIAA Journal 1, 2741 (1963).
2. P. H. Rose and J. O. Stankevics, AIAA Journal 1, 2752 (1963).
3. M. Camac, J. A. Fay, R. M. Feinberg, and N. H. Kemp, Proceedings of the 1963 Heat Transfer and Fluid Mechanics Institute, Stanford Univ. Press (1963), p. 58.
4. I. Pollin, Phys. Fluids, 7, 1433 (1964).
5. D. L. Turcotte and J. Gillespie, ARS Preprint 2634-62 (1962).
6. C. Su and S. H. Lam, Phys. Fluids 6, 1479 (1963).
7. S. H. Lam, AIAA Journal 1, 256 (1964).
8. C. H. Su, MIT Fluid Mech. Lab. No. 64-3 (1964).
9. P. M. Chung, Phys. Fluids 7, 110 (1964).
10. P. M. Chung, Aerospace Corp. TDR-269 (1964).
11. L. Landau, Physik. Z. Sowjetunion 10, 154 (1936).
12. H. Petschek and S. R. Byron, Ann. Physics 1, 270 (1957).
13. T. F. Morse, Phys. Fluids 6, 1420 (1963).
14. D. M. Dix, AIAA Journal 2, 2081 (1964).
15. M. Camac and N. H. Kemp, AIAA Preprint 63-460 (1963).
16. M. Jaffrin, Phys. Fluids 8, 606 (1965).
17. S. Chapman and T. G. Cowling, The Mathematical Theory of Non-Uniform Gases, Cambridge Univ. Press (1961).

18. Lord Rayleigh, Phil Mag. 21, (6), 697 (1911).

19. L. Howarth, Proc. Cambridge Phil. Soc. 46, 400 (1951).

20. M. D. Van Dyke, Z.A.M.P. 3, 343 (1952).

21. P. A. Lagerström, Theory of laminar flows, Princeton Univ. Press (1964), editor F. K. Moore.

22. R. N. Hollyer, Univ. Michigan Rept., (1953).

23. H. Mirels, Grenzschichtforschung, Springer (1958), edited by H. Görtler, p. 283.

24. D. Bershader and J. Allport, Princeton Univ., Physics Rept. II-22, (1956).

25. E. Becker, Progress in Aeronautical Sciences Vol. 1., Pergamon Press (1961), p. 104.

26. W. P. Allis, Handbuch der Physik, Band XXI, Springer (1956), p. 383.

27. W. P. Allis and D. J. Rose, Phys. Rev. 93, 84 (1954).

28. L. S. Frost, Phys. Rev. 105, 354 (1957).

29. K. S. Drellishak, C. F. Knopp, and A. B. Cambel, Phys. Fluids 6, 1280 (1963).

30. A. B. Cambel, D. P. Duclos, and T. P. Anderson, Real Gases, Academic Press (1963).

31. G. B. F. Niblett and A. Kenny, Princeton Univ., Dept. of Physics Rept. TR-II-24 (1957).

32. J. O. Hirschfelder, C. F. Curtiss, and R. B. Bird, Molecular Theory of Gases and Liquids, Wiley (1954).

33. M. P. Sherman, Princeton Univ., Dept. Aero. Eng. Report 673 (1963).

34. R. S. Devoto, to be published (also, Dept. Aeronautics and Astronatics, Stanford Univ., SUDAER 217 (1965).

35. A. Dalgarno, Phil. Trans. Roy. Soc. A250, 426 (1958).

36. I. Amdur and E. A. Mason, Phys. Fluids 1, 370 (1958).

37. D. J. Rose and M. Clark, Plasmas and Controlled Fusion, M.I.T. Press (1961).

38. S. I. Braginskii, Soviet Physics JETP 6, 358 (1958).

39. J. A. Fay, Avco-Everett Research Lab. AMP 71 (1962).

40. L. Spitzer and R. Härm, Phys. Rev., 89, 977 (1953).

41. L. S. Frost and A. V. Phelps, Phys. Rev. 136, 1538 (1964).

42. J. A. Fay, in Combustion and Propulsion, AGARD (1963).

43. L. Fox, Numerical solution of ordinary and partial differential equations, Pergamon Press (1962).

## APPENDIX I

## THERMODYNAMIC AND TRANSPORT PROPERTIES OF EQUILIBRIUM ARGON

Numerical results for equilibrium argon thermodynamic and transport properties are presented for the pressures $p = 10^4$, $p = 10^5$, and $p = 10^5$ $N/m^2$.

The symbols used are the following

| | |
|---|---|
| T | Temperature T |
| H | Enthalpy h |
| ALFA | Degree of ionization $\alpha$ |
| NE | Number density of free electrons $n_e$ |
| RO | Density $\rho$ |
| CP | Specific heat $c_p$ |
| QMINUS | $-Q^{avail.}$ (defined in equation (6.42)) |
| TEMP | Temperature T |
| VISCOSITY | Viscosity $\mu$ |
| AMBIDIFF | Ambipolar diffusion coefficient $D_{amb}$ |
| TOTCOND | Total conductivity $\lambda_{tot}$ |
| REACT | Reactive conductivity fraction in $\lambda_{tot}$ |
| ELECTR | Electron thermal conductivity fraction in $\lambda_{tot}$ |
| PRANDTL | Prandtl number $Pr = \frac{c_p^{eg.}\,\mu}{\lambda_{tot}}$ |
| QAA | Atom-atom elastic cross-section |
| QAI | Total atom-ion cross-section |
| QII | Ion-ion cross-section |

---

MKSA - units are used throughout the calculation.

THERMODYNAMIC DATA FOR EQUILIBRIUM ARGON  LOG(PRESSURE)= 4  (NEWTON/M2)

| T KELVIN | H NM/KG | ALFA | NE 1/M3 | RO KG/M3 | CP NM/(KG DEG) | OMINUS REC/SEC-ELECTRON |
|---|---|---|---|---|---|---|
| 100 | 5.20477E+04 | 0.00000 | | 4.8033E-01 | 5.2048E+02 | |
| 200 | 1.04095E+05 | 0.00000 | | 2.4016E-01 | 5.2048E+02 | |
| 300 | 1.56143E+05 | 0.00000 | | 1.6011E-01 | 5.2048E+02 | |
| 400 | 2.08191E+05 | 0.00000 | | 1.2008E-01 | 5.2048E+02 | |
| 500 | 2.60239E+05 | 0.00000 | | 9.6066E-02 | 5.2048E+02 | |
| 600 | 3.12286E+05 | 0.00000 | | 8.0055E-02 | 5.2048E+02 | |
| 700 | 3.64334E+05 | 0.00000 | | 6.8618E-02 | 5.2048E+02 | |
| 800 | 4.16382E+05 | 0.00000 | | 6.0041E-02 | 5.2048E+02 | |
| 900 | 4.68429E+05 | 0.00000 | | 5.3370E-02 | 5.2048E+02 | |
| 1000 | 5.20477E+05 | 0.00000 | | 4.8033E-02 | 5.2048E+02 | |
| 1200 | 6.24572E+05 | 0.00000 | | 4.0027E-02 | 5.2048E+02 | |
| 1400 | 7.28668E+05 | 0.00000 | | 3.4309E-02 | 5.2048E+02 | |
| 1600 | 8.32763E+05 | 0.00000 | | 3.0021E-02 | 5.2048E+02 | |
| 1800 | 9.36859E+05 | 0.00000 | | 2.6685E-02 | 5.2048E+02 | |
| 2000 | 1.04095E+06 | 0.00000 | | 2.4016E-02 | 5.2048E+02 | |
| 2200 | 1.14505E+06 | 0.00000 | 2.4840E+07 | 2.1833E-02 | 5.2048E+02 | -1.2916E-20 |
| 2400 | 1.24914E+06 | 0.00000 | 8.1633E+08 | 2.0014E-02 | 5.2048E+02 | -9.4300E-18 |
| 2600 | 1.35324E+06 | 0.00000 | 1.5707E+10 | 1.8474E-02 | 5.2048E+02 | -2.4352E-15 |
| 2800 | 1.45734E+06 | 0.00000 | 1.9841E+11 | 1.7155E-02 | 5.2048E+02 | -2.7838E-13 |
| 3000 | 1.56143E+06 | 0.00000 | 1.7897E+12 | 1.6011E-02 | 5.2048E+02 | -1.6605E-11 |
| 3200 | 1.66553E+06 | 0.00000 | 1.2278E+13 | 1.5010E-02 | 5.2048E+02 | -3.8417E-10 |
| 3400 | 1.76962E+06 | 0.00000 | 6.7222E+13 | 1.4127E-02 | 5.2048E+02 | -4.4161E-09 |
| 3600 | 1.87372E+06 | 0.00000 | 3.0498E+14 | 1.3342E-02 | 5.2048E+02 | -3.8658E-08 |
| 3800 | 1.97781E+06 | 0.00000 | 1.1810E+15 | 1.2640E-02 | 5.2048E+02 | -2.6004E-07 |
| 4000 | 2.08191E+06 | 0.00000 | 3.9970E+15 | 1.2008E-02 | 5.2048E+02 | -1.5408E-06 |
| 4200 | 2.18601E+06 | 0.00000 | 1.2052E+16 | 1.1436E-02 | 5.2049E+02 | -7.4667E-06 |
| 4400 | 2.29011E+06 | 0.00000 | 3.2893E+16 | 1.0917E-02 | 5.2052E+02 | -3.1325E-05 |
| 4600 | 2.39422E+06 | 0.00000 | 8.2308E+16 | 1.0442E-02 | 5.2057E+02 | -1.1593E-04 |
| 4800 | 2.49834E+06 | 0.00000 | 1.9090E+17 | 1.0007E-02 | 5.2069E+02 | -3.8449E-04 |
| 5000 | 2.60250E+06 | 0.00000 | 4.1412E+17 | 9.6065E-03 | 5.2091E+02 | -1.1579E-03 |
| 5200 | 2.70673E+06 | 0.00001 | 8.4674E+17 | 9.2370E-03 | 5.2134E+02 | -3.2019E-03 |
| 5400 | 2.81108E+06 | 0.00001 | 1.6426E+18 | 8.8949E-03 | 5.2209E+02 | -8.2074E-03 |
| 5600 | 2.91563E+06 | 0.00002 | 3.0402E+18 | 8.5771E-03 | 5.2337E+02 | -1.9661E-02 |
| 5800 | 3.02054E+06 | 0.00004 | 5.3948E+18 | 8.2812E-03 | 5.2546E+02 | -4.4328E-02 |
| 6000 | 3.12601E+06 | 0.00008 | 9.2166E+18 | 8.0049E-03 | 5.2873E+02 | -9.4629E-02 |
| 6200 | 3.23234E+06 | 0.00013 | 1.5215E+19 | 7.7462E-03 | 5.3371E+02 | -1.9229E-01 |
| 6400 | 3.33996E+06 | 0.00022 | 2.4348E+19 | 7.5035E-03 | 5.4106E+02 | -3.7366E-01 |
| 6600 | 3.44948E+06 | 0.00035 | 3.7876E+19 | 7.2752E-03 | 5.5165E+02 | -6.9716E-01 |
| 6800 | 3.56169E+06 | 0.00054 | 5.7417E+19 | 7.0598E-03 | 5.6651E+02 | -1.2534E+00 |
| 7000 | 3.67764E+06 | 0.00082 | 8.5006E+19 | 6.8562E-03 | 5.8694E+02 | -2.1780E+00 |
| 7200 | 3.79869E+06 | 0.00123 | 1.2315E+20 | 6.6631E-03 | 6.1445E+02 | -3.6686E+00 |
| 7400 | 3.92656E+06 | 0.00179 | 1.7486E+20 | 6.4793E-03 | 6.5085E+02 | -6.0040E+00 |
| 7600 | 4.06339E+06 | 0.00256 | 2.4374E+20 | 6.3040E-03 | 6.9818E+02 | -9.5679E+00 |
| 7800 | 4.21179E+06 | 0.00361 | 3.3397E+20 | 6.1359E-03 | 7.5880E+02 | -1.4875E+01 |
| 8000 | 4.37495E+06 | 0.00500 | 4.5035E+20 | 5.9742E-03 | 8.3535E+02 | -2.2600E+01 |
| 8200 | 4.55664E+06 | 0.00682 | 5.9829E+20 | 5.8180E-03 | 9.3075E+02 | -3.3602E+01 |
| 8400 | 4.76134E+06 | 0.00917 | 7.8377E+20 | 5.6662E-03 | 1.0482E+03 | -4.8958E+01 |
| 8600 | 4.99424E+06 | 0.01218 | 1.0133E+21 | 5.5180E-03 | 1.1912E+03 | -6.9977E+01 |
| 8800 | 5.26137E+06 | 0.01597 | 1.2939E+21 | 5.3725E-03 | 1.3634E+03 | -9.8211E+01 |
| 9000 | 5.56960E+06 | 0.02070 | 1.6326E+21 | 5.2287E-03 | 1.5687E+03 | -1.3546E+02 |
| 9200 | 5.92670E+06 | 0.02655 | 2.0369E+21 | 5.0859E-03 | 1.8113E+03 | -1.8372E+02 |
| 9400 | 6.34140E+06 | 0.03372 | 2.5138E+21 | 4.9432E-03 | 2.0953E+03 | -2.4518E+02 |
| 9600 | 6.82336E+06 | 0.04241 | 3.0701E+21 | 4.7999E-03 | 2.4249E+03 | -3.2206E+02 |
| 9800 | 7.38320E+06 | 0.05286 | 3.7114E+21 | 4.6552E-03 | 2.8040E+03 | -4.1655E+02 |
| 10000 | 8.03242E+06 | 0.06533 | 4.4424E+21 | 4.5087E-03 | 3.2361E+03 | -5.3058E+02 |
| 10200 | 8.78327E+06 | 0.08008 | 5.2657E+21 | 4.3600E-03 | 3.7241E+03 | -6.6562E+02 |
| 10400 | 9.64856E+06 | 0.09739 | 6.1816E+21 | 4.2087E-03 | 4.2694E+03 | -8.2245E+02 |
| 10600 | 1.06413E+07 | 0.11754 | 7.1882E+21 | 4.0548E-03 | 4.8719E+03 | -1.0008E+03 |
| 10800 | 1.17744E+07 | 0.14081 | 8.2792E+21 | 3.8985E-03 | 5.5284E+03 | -1.1993E+03 |
| 11000 | 1.30595E+07 | 0.16744 | 9.4453E+21 | 3.7404E-03 | 6.2322E+03 | -1.4148E+03 |
| 11200 | 1.45065E+07 | 0.19762 | 1.0673E+22 | 3.5810E-03 | 6.9716E+03 | -1.6428E+03 |
| 11400 | 1.61222E+07 | 0.23150 | 1.1946E+22 | 3.4214E-03 | 7.7288E+03 | -1.8772E+03 |
| 11600 | 1.79088E+07 | 0.26909 | 1.3242E+22 | 3.2628E-03 | 8.4789E+03 | -2.1103E+03 |
| 11800 | 1.98619E+07 | 0.31028 | 1.4538E+22 | 3.1067E-03 | 9.1896E+03 | -2.3337E+03 |
| 12000 | 2.19699E+07 | 0.35476 | 1.5808E+22 | 2.9546E-03 | 9.8224E+03 | -2.5384E+03 |
| 12200 | 2.42115E+07 | 0.40204 | 1.7027E+22 | 2.8081E-03 | 1.0335E+04 | -2.7159E+03 |
| 12400 | 2.65564E+07 | 0.45142 | 1.8170E+22 | 2.6689E-03 | 1.0686E+04 | -2.8592E+03 |
| 12600 | 2.89654E+07 | 0.50200 | 1.9216E+22 | 2.5380E-03 | 1.0840E+04 | -2.9632E+03 |
| 12800 | 3.13930E+07 | 0.55277 | 2.0147E+22 | 2.4167E-03 | 1.0777E+04 | -3.0251E+03 |
| 13000 | 3.37907E+07 | 0.60263 | 2.0954E+22 | 2.3055E-03 | 1.0495E+04 | -3.0452E+03 |
| 13200 | 3.61113E+07 | 0.65055 | 2.1631E+22 | 2.2046E-03 | 1.0011E+04 | -3.0260E+03 |
| 13400 | 3.83135E+07 | 0.69561 | 2.2178E+22 | 2.1140E-03 | 9.3619E+03 | -2.9722E+03 |
| 13600 | 4.03652E+07 | 0.73714 | 2.2603E+22 | 2.0331E-03 | 8.5944E+03 | -2.8897E+03 |
| 13800 | 4.22451E+07 | 0.77468 | 2.2915E+22 | 1.9613E-03 | 7.7612E+03 | -2.7848E+03 |
| 14000 | 4.39433E+07 | 0.80804 | 2.3126E+22 | 1.8976E-03 | 6.9109E+03 | -2.6641E+03 |
| 14200 | 4.54598E+07 | 0.83725 | 2.3248E+22 | 1.8411E-03 | 6.0838E+03 | -2.5331E+03 |
| 14400 | 4.68022E+07 | 0.86251 | 2.3297E+22 | 1.7909E-03 | 5.3090E+03 | -2.3969E+03 |
| 14600 | 4.79837E+07 | 0.88414 | 2.3284E+22 | 1.7461E-03 | 4.6047E+03 | -2.2593E+03 |
| 14800 | 4.90202E+07 | 0.90249 | 2.3220E+22 | 1.7059E-03 | 3.9795E+03 | -2.1234E+03 |
| 15000 | 4.99289E+07 | 0.91798 | 2.3115E+22 | 1.6696E-03 | 3.4346E+03 | -1.9915E+03 |
| 15200 | 5.07269E+07 | 0.93099 | 2.2978E+22 | 1.6365E-03 | 2.9665E+03 | -1.8649E+03 |
| 15400 | 5.14301E+07 | 0.94189 | 2.2816E+22 | 1.6062E-03 | 2.5688E+03 | -1.7447E+03 |
| 15600 | 5.20530E+07 | 0.95099 | 2.2636E+22 | 1.5782E-03 | 2.2336E+03 | -1.6313E+03 |
| 15800 | 5.26084E+07 | 0.95860 | 2.2440E+22 | 1.5522E-03 | 1.9527E+03 | -1.5250E+03 |
| 16000 | 5.31072E+07 | 0.96496 | 2.2235E+22 | 1.5278E-03 | 1.7183E+03 | -1.4257E+03 |
| 16200 | 5.35588E+07 | 0.97027 | 2.2021E+22 | 1.5049E-03 | 1.5232E+03 | -1.3332E+03 |
| 16400 | 5.39711E+07 | 0.97472 | 2.1803E+22 | 1.4832E-03 | 1.3610E+03 | -1.2472E+03 |
| 16600 | 5.43507E+07 | 0.97844 | 2.1582E+22 | 1.4625E-03 | 1.2263E+03 | -1.1674E+03 |
| 16800 | 5.47031E+07 | 0.98157 | 2.1360E+22 | 1.4428E-03 | 1.1143E+03 | -1.0934E+03 |
| 17000 | 5.50329E+07 | 0.98420 | 2.1137E+22 | 1.4240E-03 | 1.0212E+03 | -1.0249E+03 |
| 17200 | 5.53438E+07 | 0.98642 | 2.0915E+22 | 1.4058E-03 | 9.4370E+02 | -9.6140E+02 |
| 17400 | 5.56391E+07 | 0.98830 | 2.0694E+22 | 1.3884E-03 | 8.7905E+02 | -9.0258E+02 |
| 17600 | 5.59211E+07 | 0.98989 | 2.0476E+22 | 1.3715E-03 | 8.2504E+02 | -8.4806E+02 |
| 17800 | 5.61922E+07 | 0.99124 | 2.0260E+22 | 1.3552E-03 | 7.7982E+02 | -7.9751E+02 |
| 18000 | 5.64541E+07 | 0.99239 | 2.0046E+22 | 1.3393E-03 | 7.4188E+02 | -7.5063E+02 |

THERMODYNAMIC DATA FOR EQUILIBRIUM ARGON  LOG(PRESSURE)= 5  (NEWTON/M2)

| T KELVIN | H NM/KG | ALFA | NE 1/M3 | RO KG/M3 | CP NM/(KG DEG) | OMINUS REC/SEC-ELECTRON |
|---|---|---|---|---|---|---|
| 100 | 5.20477E+04 | 0.00000 | | 4.8033E+00 | 5.2048E+02 | |
| 200 | 1.04095E+05 | 0.00000 | | 2.4016E+00 | 5.2048E+02 | |
| 300 | 1.56143E+05 | 0.00000 | | 1.6011E+00 | 5.2048E+02 | |
| 400 | 2.08191E+05 | 0.00000 | | 1.2008E+00 | 5.2048E+02 | |
| 500 | 2.60239E+05 | 0.00000 | | 9.6066E-01 | 5.2048E+02 | |
| 600 | 3.12286E+05 | 0.00000 | | 8.0055E-01 | 5.2048E+02 | |
| 700 | 3.64334E+05 | 0.00000 | | 6.8618E-01 | 5.2048E+02 | |
| 800 | 4.16382E+05 | 0.00000 | | 6.0041E-01 | 5.2048E+02 | |
| 900 | 4.68429E+05 | 0.00000 | | 5.3370E-01 | 5.2048E+02 | |
| 1000 | 5.20477E+05 | 0.00000 | | 4.8033E-01 | 5.2048E+02 | |
| 1200 | 6.24572E+05 | 0.00000 | | 4.0027E-01 | 5.2048E+02 | |
| 1400 | 7.28668E+05 | 0.00000 | | 3.4309E-01 | 5.2048E+02 | |
| 1600 | 8.32763E+05 | 0.00000 | | 3.0021E-01 | 5.2048E+02 | |
| 1800 | 9.36859E+05 | 0.00000 | | 2.6685E-01 | 5.2048E+02 | |
| 2000 | 1.04095E+06 | 0.00000 | | 2.4016E-01 | 5.2048E+02 | |
| 2200 | 1.14505E+06 | 0.00000 | 7.8550E+07 | 2.1833E-01 | 5.2048E+02 | -1.2916E-19 |
| 2400 | 1.24914E+06 | 0.00000 | 2.5815E+09 | 2.0014E-01 | 5.2048E+02 | -9.4300E-17 |
| 2600 | 1.35324E+06 | 0.00000 | 4.9670E+10 | 1.8474E-01 | 5.2048E+02 | -2.4352E-14 |
| 2800 | 1.45734E+06 | 0.00000 | 6.2743E+11 | 1.7155E-01 | 5.2048E+02 | -2.7838E-12 |
| 3000 | 1.56143E+06 | 0.00000 | 5.6595E+12 | 1.6011E-01 | 5.2048E+02 | -1.6605E-10 |
| 3200 | 1.66553E+06 | 0.00000 | 3.8825E+13 | 1.5010E-01 | 5.2048E+02 | -3.8417E-09 |
| 3400 | 1.76962E+06 | 0.00000 | 2.1258E+14 | 1.4127E-01 | 5.2048E+02 | -4.4161E-08 |
| 3600 | 1.87372E+06 | 0.00000 | 9.6442E+14 | 1.3342E-01 | 5.2048E+02 | -3.8658E-07 |
| 3800 | 1.97781E+06 | 0.00000 | 3.7346E+15 | 1.2640E-01 | 5.2048E+02 | -2.6904E-06 |
| 4000 | 2.08191E+06 | 0.00000 | 1.2640E+16 | 1.2008E-01 | 5.2048E+02 | -1.5408E-05 |
| 4200 | 2.18600E+06 | 0.00000 | 3.8113E+16 | 1.1436E-01 | 5.2048E+02 | -7.4667E-05 |
| 4400 | 2.29010E+06 | 0.00000 | 1.0402E+17 | 1.0917E-01 | 5.2049E+02 | -3.1325E-04 |
| 4600 | 2.39420E+06 | 0.00000 | 2.6028E+17 | 1.0442E-01 | 5.2051E+02 | -1.1593E-03 |
| 4800 | 2.49831E+06 | 0.00000 | 6.0367E+17 | 1.0007E-01 | 5.2054E+02 | -3.8449E-03 |
| 5000 | 2.60242E+06 | 0.00000 | 1.3096E+18 | 9.6066E-02 | 5.2062E+02 | -1.1579E-02 |
| 5200 | 2.70656E+06 | 0.00000 | 2.6777E+18 | 9.2371E-02 | 5.2075E+02 | -3.2019E-02 |
| 5400 | 2.81073E+06 | 0.00000 | 5.1944E+18 | 8.8949E-02 | 5.2099E+02 | -8.2075E-02 |
| 5600 | 2.91498E+06 | 0.00001 | 9.6142E+18 | 8.5772E-02 | 5.2140E+02 | -1.9662E-01 |
| 5800 | 3.01933E+06 | 0.00001 | 1.7061E+19 | 8.2814E-02 | 5.2206E+02 | -4.4330E-01 |
| 6000 | 3.12386E+06 | 0.00002 | 2.9147E+19 | 8.0053E-02 | 5.2310E+02 | -9.4639E-01 |
| 6200 | 3.22866E+06 | 0.00004 | 4.8118E+19 | 7.7469E-02 | 5.2468E+02 | -1.9232E+00 |
| 6400 | 3.33387E+06 | 0.00007 | 7.7006E+19 | 7.5046E-02 | 5.2702E+02 | -3.7377E+00 |
| 6600 | 3.43968E+06 | 0.00011 | 1.1980E+20 | 7.2769E-02 | 5.3039E+02 | -6.9749E+00 |
| 6800 | 3.54634E+06 | 0.00017 | 1.8164E+20 | 7.0625E-02 | 5.3512E+02 | -1.2543E+01 |
| 7000 | 3.65419E+06 | 0.00026 | 2.6896E+20 | 6.8601E-02 | 5.4163E+02 | -2.1805E+01 |
| 7200 | 3.76364E+06 | 0.00039 | 3.8975E+20 | 6.6686E-02 | 5.5040E+02 | -3.6748E+01 |
| 7400 | 3.87526E+06 | 0.00057 | 5.5364E+20 | 6.4873E-02 | 5.6200E+02 | -6.0187E+01 |
| 7600 | 3.98970E+06 | 0.00081 | 7.7213E+20 | 6.3150E-02 | 5.7709E+02 | -9.6015E+01 |
| 7800 | 4.10781E+06 | 0.00114 | 1.0587E+21 | 6.1510E-02 | 5.9644E+02 | -1.4949E+02 |
| 8000 | 4.23058E+06 | 0.00158 | 1.4290E+21 | 5.9946E-02 | 6.2088E+02 | -2.2755E+02 |
| 8200 | 4.35922E+06 | 0.00216 | 1.9008E+21 | 5.8451E-02 | 6.5135E+02 | -3.3917E+02 |
| 8400 | 4.49513E+06 | 0.00290 | 2.4941E+21 | 5.7017E-02 | 6.8889E+02 | -4.9576E+02 |
| 8600 | 4.63996E+06 | 0.00385 | 3.2312E+21 | 5.5638E-02 | 7.3462E+02 | -7.1152E+02 |
| 8800 | 4.79563E+06 | 0.00505 | 4.1364E+21 | 5.4309E-02 | 7.8974E+02 | -1.0038E+03 |
| 9000 | 4.96430E+06 | 0.00655 | 5.2364E+21 | 5.3023E-02 | 8.5556E+02 | -1.3935E+03 |
| 9200 | 5.14847E+06 | 0.00840 | 6.5593E+21 | 5.1775E-02 | 9.3344E+02 | -1.9052E+03 |
| 9400 | 5.35091E+06 | 0.01067 | 8.1349E+21 | 5.0559E-02 | 1.0248E+03 | -2.5675E+03 |
| 9600 | 5.57473E+06 | 0.01342 | 9.9942E+21 | 4.9372E-02 | 1.1312E+03 | -3.4130E+03 |
| 9800 | 5.82338E+06 | 0.01674 | 1.2169E+22 | 4.8206E-02 | 1.2540E+03 | -4.4780E+03 |
| 10000 | 6.10067E+06 | 0.02070 | 1.4691E+22 | 4.7059E-02 | 1.3950E+03 | -5.8022E+03 |
| 10200 | 6.41075E+06 | 0.02540 | 1.7591E+22 | 4.5925E-02 | 1.5556E+03 | -7.4279E+03 |
| 10400 | 6.75813E+06 | 0.03093 | 2.0898E+22 | 4.4800E-02 | 1.7374E+03 | -9.3993E+03 |
| 10600 | 7.14767E+06 | 0.03740 | 2.4641E+22 | 4.3680E-02 | 1.9421E+03 | -1.1760E+04 |
| 10800 | 7.58457E+06 | 0.04493 | 2.8842E+22 | 4.2563E-02 | 2.1709E+03 | -1.4554E+04 |
| 11000 | 8.07435E+06 | 0.05363 | 3.3520E+22 | 4.1444E-02 | 2.4252E+03 | -1.7819E+04 |
| 11200 | 8.62284E+06 | 0.06362 | 3.8690E+22 | 4.0321E-02 | 2.7061E+03 | -2.1587E+04 |
| 11400 | 9.23605E+06 | 0.07504 | 4.4356E+22 | 3.9193E-02 | 3.0145E+03 | -2.5882E+04 |
| 11600 | 9.92019E+06 | 0.08801 | 5.0517E+22 | 3.8058E-02 | 3.3506E+03 | -3.0714E+04 |
| 11800 | 1.06815E+07 | 0.10267 | 5.7161E+22 | 3.6916E-02 | 3.7145E+03 | -3.6078E+04 |
| 12000 | 1.15262E+07 | 0.11913 | 6.4264E+22 | 3.5766E-02 | 4.1052E+03 | -4.1949E+04 |
| 12200 | 1.24601E+07 | 0.13753 | 7.1792E+22 | 3.4611E-02 | 4.5210E+03 | -4.8282E+04 |
| 12400 | 1.34886E+07 | 0.15797 | 7.9698E+22 | 3.3452E-02 | 4.9588E+03 | -5.5009E+04 |
| 12600 | 1.46164E+07 | 0.18053 | 8.7924E+22 | 3.2292E-02 | 5.4143E+03 | -6.2037E+04 |
| 12800 | 1.58469E+07 | 0.20529 | 9.6397E+22 | 3.1134E-02 | 5.8816E+03 | -6.9251E+04 |
| 13000 | 1.71822E+07 | 0.23227 | 1.0504E+23 | 2.9984E-02 | 6.3526E+03 | -7.6516E+04 |
| 13200 | 1.86222E+07 | 0.26145 | 1.1375E+23 | 2.8847E-02 | 6.8176E+03 | -8.3679E+04 |
| 13400 | 2.01646E+07 | 0.29277 | 1.2243E+23 | 2.7728E-02 | 7.2648E+03 | -9.0577E+04 |
| 13600 | 2.18042E+07 | 0.32610 | 1.3099E+23 | 2.6633E-02 | 7.6806E+03 | -9.7045E+04 |
| 13800 | 2.35326E+07 | 0.36124 | 1.3931E+23 | 2.5570E-02 | 8.0504E+03 | -1.0293E+05 |
| 14000 | 2.53382E+07 | 0.39792 | 1.4729E+23 | 2.4543E-02 | 8.3591E+03 | -1.0807E+05 |
| 14200 | 2.72059E+07 | 0.43580 | 1.5484E+23 | 2.3559E-02 | 8.5925E+03 | -1.1237E+05 |
| 14400 | 2.91178E+07 | 0.47447 | 1.6188E+23 | 2.2623E-02 | 8.7356E+03 | -1.1573E+05 |
| 14600 | 3.10533E+07 | 0.51348 | 1.6834E+23 | 2.1737E-02 | 8.7885E+03 | -1.1810E+05 |
| 14800 | 3.29907E+07 | 0.55236 | 1.7417E+23 | 2.0907E-02 | 8.7382E+03 | -1.1947E+05 |
| 15000 | 3.49074E+07 | 0.59061 | 1.7932E+23 | 2.0132E-02 | 8.5887E+03 | -1.1986E+05 |
| 15200 | 3.67820E+07 | 0.62777 | 1.8381E+23 | 1.9413E-02 | 8.3447E+03 | -1.1933E+05 |
| 15400 | 3.85947E+07 | 0.66342 | 1.8761E+23 | 1.8751E-02 | 8.0234E+03 | -1.1796E+05 |
| 15600 | 4.03289E+07 | 0.69721 | 1.9077E+23 | 1.8142E-02 | 7.6339E+03 | -1.1587E+05 |
| 15800 | 4.19714E+07 | 0.72887 | 1.9330E+23 | 1.7584E-02 | 7.1955E+03 | -1.1315E+05 |
| 16000 | 4.35130E+07 | 0.75821 | 1.9525E+23 | 1.7074E-02 | 6.7259E+03 | -1.0990E+05 |
| 16200 | 4.49484E+07 | 0.78514 | 1.9668E+23 | 1.6609E-02 | 6.2420E+03 | -1.0634E+05 |
| 16400 | 4.62759E+07 | 0.80963 | 1.9763E+23 | 1.6185E-02 | 5.7589E+03 | -1.0247E+05 |
| 16600 | 4.74968E+07 | 0.83173 | 1.9816E+23 | 1.5797E-02 | 5.2888E+03 | -9.8411E+04 |
| 16800 | 4.86149E+07 | 0.85154 | 1.9832E+23 | 1.5442E-02 | 4.8410E+03 | -9.4258E+04 |
| 17000 | 4.96359E+07 | 0.86919 | 1.9816E+23 | 1.5116E-02 | 4.4220E+03 | -9.0076E+04 |
| 17200 | 5.05665E+07 | 0.88484 | 1.9772E+23 | 1.4816E-02 | 4.0358E+03 | -8.5922E+04 |
| 17400 | 5.14142E+07 | 0.89866 | 1.9706E+23 | 1.4539E-02 | 3.6841E+03 | -8.1841E+04 |
| 17600 | 5.21867E+07 | 0.91083 | 1.9620E+23 | 1.4282E-02 | 3.3672E+03 | -7.7865E+04 |
| 17800 | 5.28915E+07 | 0.92152 | 1.9518E+23 | 1.4043E-02 | 3.0839E+03 | -7.4020E+04 |
| 18000 | 5.35361E+07 | 0.93089 | 1.9403E+23 | 1.3820E-02 | 2.8323E+03 | -7.0322E+04 |

THERMODYNAMIC DATA FOR EQUILIBRIUM ARGON  LOG(PRESSURE)= 6  (NEWTON/M2)

| T KELVIN | H NM/KG | ALFA | NE 1/M3 | RO KG/M3 | CP NM/(KG DEG) | OMINUS REC/SEC-ELECTRON |
|---|---|---|---|---|---|---|
| 100 | 5.20477E+04 | 0.00000 | | 4.8033E+01 | 5.2048E+02 | |
| 200 | 1.04095E+05 | 0.00000 | | 2.4016E+01 | 5.2048E+02 | |
| 300 | 1.56143E+05 | 0.00000 | | 1.6011E+01 | 5.2048E+02 | |
| 400 | 2.08191E+05 | 0.00000 | | 1.2008E+01 | 5.2048E+02 | |
| 500 | 2.60239E+05 | 0.00000 | | 9.6066E+00 | 5.2048E+02 | |
| 600 | 3.12286E+05 | 0.00000 | | 8.0055E+00 | 5.2048E+02 | |
| 700 | 3.64334E+05 | 0.00000 | | 6.8618E+00 | 5.2048E+02 | |
| 800 | 4.16382E+05 | 0.00000 | | 6.0041E+00 | 5.2048E+02 | |
| 900 | 4.68429E+05 | 0.00000 | | 5.3370E+00 | 5.2048E+02 | |
| 1000 | 5.20477E+05 | 0.00000 | | 4.8033E+00 | 5.2048E+02 | |
| 1200 | 6.24572E+05 | 0.00000 | | 4.0027E+00 | 5.2048E+02 | |
| 1400 | 7.28668E+05 | 0.00000 | | 3.4309E+00 | 5.2048E+02 | |
| 1600 | 8.32763E+05 | 0.00000 | | 3.0021E+00 | 5.2048E+02 | |
| 1800 | 9.36859E+05 | 0.00000 | | 2.6685E+00 | 5.2048E+02 | |
| 2000 | 1.04095E+06 | 0.00000 | | 2.4016E+00 | 5.2048E+02 | |
| 2200 | 1.14505E+06 | 0.00000 | 2.4840E+08 | 2.1833E+00 | 5.2048E+02 | -1.2916E-18 |
| 2400 | 1.24914E+06 | 0.00000 | 8.1633E+09 | 2.0014E+00 | 5.2048E+02 | -9.4300E-16 |
| 2600 | 1.35324E+06 | 0.00000 | 1.5707E+11 | 1.8474E+00 | 5.2048E+02 | -2.4352E-13 |
| 2800 | 1.45734E+06 | 0.00000 | 1.9841E+12 | 1.7155E+00 | 5.2048E+02 | -2.7838E-11 |
| 3000 | 1.56143E+06 | 0.00000 | 1.7897E+13 | 1.6011E+00 | 5.2048E+02 | -1.6605E-09 |
| 3200 | 1.66553E+06 | 0.00000 | 1.2278E+14 | 1.5010E+00 | 5.2048E+02 | -3.8417E-08 |
| 3400 | 1.76962E+06 | 0.00000 | 6.7222E+14 | 1.4127E+00 | 5.2048E+02 | -4.4161E-07 |
| 3600 | 1.87372E+06 | 0.00000 | 3.0498E+15 | 1.3342E+00 | 5.2048E+02 | -3.8658E-06 |
| 3800 | 1.97781E+06 | 0.00000 | 1.1810E+16 | 1.2640E+00 | 5.2048E+02 | -2.6904E-05 |
| 4000 | 2.08191E+06 | 0.00000 | 3.9970E+16 | 1.2008E+00 | 5.2048E+02 | -1.5408E-04 |
| 4200 | 2.18600E+06 | 0.00000 | 1.2052E+17 | 1.1436E+00 | 5.2048E+02 | -7.4667E-04 |
| 4400 | 2.29010E+06 | 0.00000 | 3.2893E+17 | 1.0917E+00 | 5.2048E+02 | -3.1325E-03 |
| 4600 | 2.39420E+06 | 0.00000 | 8.2308E+17 | 1.0442E+00 | 5.2049E+02 | -1.1593E-02 |
| 4800 | 2.49829E+06 | 0.00000 | 1.9090E+18 | 1.0007E+00 | 5.2050E+02 | -3.8449E-02 |
| 5000 | 2.60240E+06 | 0.00000 | 4.1412E+18 | 9.6066E-01 | 5.2052E+02 | -1.1579E-01 |
| 5200 | 2.70651E+06 | 0.00000 | 8.4675E+18 | 9.2371E-01 | 5.2056E+02 | -3.2019E-01 |
| 5400 | 2.81063E+06 | 0.00000 | 1.6426E+19 | 8.8950E-01 | 5.2064E+02 | -8.2076E-01 |
| 5600 | 2.91477E+06 | 0.00000 | 3.0403E+19 | 8.5773E-01 | 5.2077E+02 | -1.9662E+00 |
| 5800 | 3.01894E+06 | 0.00000 | 5.3951E+19 | 8.2815E-01 | 5.2098E+02 | -4.4331E+00 |
| 6000 | 3.12318E+06 | 0.00001 | 9.2172E+19 | 8.0054E-01 | 5.2131E+02 | -9.4642E+00 |
| 6200 | 3.22750E+06 | 0.00001 | 1.5217E+20 | 7.7471E-01 | 5.2181E+02 | -1.9233E+01 |
| 6400 | 3.33194E+06 | 0.00002 | 2.4352E+20 | 7.5050E-01 | 5.2255E+02 | -3.7380E+01 |
| 6600 | 3.43658E+06 | 0.00003 | 3.7887E+20 | 7.2775E-01 | 5.2361E+02 | -6.9760E+01 |
| 6800 | 3.54149E+06 | 0.00005 | 5.7445E+20 | 7.0633E-01 | 5.2511E+02 | -1.2546E+02 |
| 7000 | 3.64677E+06 | 0.00008 | 8.5069E+20 | 6.8613E-01 | 5.2717E+02 | -2.1813E+02 |
| 7200 | 3.75256E+06 | 0.00012 | 1.2328E+21 | 6.6704E-01 | 5.2994E+02 | -3.6767E+02 |
| 7400 | 3.85903E+06 | 0.00018 | 1.7514E+21 | 6.4898E-01 | 5.3361E+02 | -6.0234E+02 |
| 7600 | 3.96640E+06 | 0.00026 | 2.4431E+21 | 6.3185E-01 | 5.3838E+02 | -9.6122E+02 |
| 7800 | 4.07493E+06 | 0.00036 | 3.3506E+21 | 6.1558E-01 | 5.4450E+02 | -1.4972E+03 |
| 8000 | 4.18493E+06 | 0.00050 | 4.5234E+21 | 6.0011E-01 | 5.5223E+02 | -2.2804E+03 |
| 8200 | 4.29679E+06 | 0.00068 | 6.0197E+21 | 5.8537E-01 | 5.6186E+02 | -3.4017E+03 |
| 8400 | 4.41094E+06 | 0.00092 | 7.9027E+21 | 5.7130E-01 | 5.7373E+02 | -4.9773E+03 |
| 8600 | 4.52792E+06 | 0.00122 | 1.0245E+22 | 5.5784E-01 | 5.8819E+02 | -7.1527E+03 |
| 8800 | 4.64832E+06 | 0.00160 | 1.3126E+22 | 5.4496E-01 | 6.0563E+02 | -1.0108E+04 |
| 9000 | 4.77284E+06 | 0.00207 | 1.6633E+22 | 5.3260E-01 | 6.2645E+02 | -1.4060E+04 |
| 9200 | 4.90226E+06 | 0.00266 | 2.0862E+22 | 5.2071E-01 | 6.5108E+02 | -1.9272E+04 |
| 9400 | 5.03746E+06 | 0.00337 | 2.5913E+22 | 5.0927E-01 | 6.7999E+02 | -2.6053E+04 |
| 9600 | 5.17942E+06 | 0.00424 | 3.1896E+22 | 4.9823E-01 | 7.1364E+02 | -3.4763E+04 |
| 9800 | 5.32924E+06 | 0.00529 | 3.8925E+22 | 4.8755E-01 | 7.5253E+02 | -4.5817E+04 |
| 10000 | 5.48813E+06 | 0.00655 | 4.7118E+22 | 4.7720E-01 | 7.9718E+02 | -5.9688E+04 |
| 10200 | 5.65741E+06 | 0.00803 | 5.6601E+22 | 4.6716E-01 | 8.4809E+02 | -7.6905E+04 |
| 10400 | 5.83852E+06 | 0.00979 | 6.7499E+22 | 4.5738E-01 | 9.0581E+02 | -9.8055E+04 |
| 10600 | 6.03303E+06 | 0.01184 | 7.9940E+22 | 4.4784E-01 | 9.7086E+02 | -1.2378E+05 |
| 10800 | 6.24260E+06 | 0.01422 | 9.4053E+22 | 4.3851E-01 | 1.0438E+03 | -1.5477E+05 |
| 11000 | 6.46926E+06 | 0.01698 | 1.0996E+23 | 4.2937E-01 | 1.1251E+03 | -1.9176E+05 |
| 11200 | 6.71434E+06 | 0.02016 | 1.2779E+23 | 4.2039E-01 | 1.2154E+03 | -2.3552E+05 |
| 11400 | 6.98047E+06 | 0.02379 | 1.4766E+23 | 4.1155E-01 | 1.3151E+03 | -2.8684E+05 |
| 11600 | 7.26964E+06 | 0.02793 | 1.6968E+23 | 4.0283E-01 | 1.4248E+03 | -3.4651E+05 |
| 11800 | 7.58412E+06 | 0.03262 | 1.9394E+23 | 3.9420E-01 | 1.5449E+03 | -4.1532E+05 |
| 12000 | 7.92631E+06 | 0.03792 | 2.2053E+23 | 3.8565E-01 | 1.6759E+03 | -4.9401E+05 |
| 12200 | 8.29871E+06 | 0.04387 | 2.4953E+23 | 3.7717E-01 | 1.8182E+03 | -5.8328E+05 |
| 12400 | 8.70388E+06 | 0.05052 | 2.8098E+23 | 3.6873E-01 | 1.9720E+03 | -6.8372E+05 |
| 12600 | 9.14450E+06 | 0.05795 | 3.1491E+23 | 3.6033E-01 | 2.1378E+03 | -7.9581E+05 |
| 12800 | 9.62330E+06 | 0.06619 | 3.5133E+23 | 3.5196E-01 | 2.3157E+03 | -9.1990E+05 |
| 13000 | 1.01430E+07 | 0.07530 | 3.9023E+23 | 3.4361E-01 | 2.5057E+03 | -1.0561E+06 |
| 13200 | 1.07064E+07 | 0.08535 | 4.3156E+23 | 3.3527E-01 | 2.7079E+03 | -1.2045E+06 |
| 13400 | 1.13163E+07 | 0.09638 | 4.7522E+23 | 3.2694E-01 | 2.9220E+03 | -1.3646E+06 |
| 13600 | 1.19754E+07 | 0.10844 | 5.2113E+23 | 3.1863E-01 | 3.1475E+03 | -1.5360E+06 |
| 13800 | 1.26862E+07 | 0.12160 | 5.6912E+23 | 3.1033E-01 | 3.3840E+03 | -1.7178E+06 |
| 14000 | 1.34512E+07 | 0.13589 | 6.1903E+23 | 3.0205E-01 | 3.6304E+03 | -1.9089E+06 |
| 14200 | 1.42725E+07 | 0.15135 | 6.7063E+23 | 2.9379E-01 | 3.8856E+03 | -2.1078E+06 |
| 14400 | 1.51522E+07 | 0.16802 | 7.2369E+23 | 2.8558E-01 | 4.1480E+03 | -2.3128E+06 |
| 14600 | 1.60917E+07 | 0.18593 | 7.7791E+23 | 2.7741E-01 | 4.4156E+03 | -2.5220E+06 |
| 14800 | 1.70920E+07 | 0.20508 | 8.3300E+23 | 2.6931E-01 | 4.6861E+03 | -2.7329E+06 |
| 15000 | 1.81536E+07 | 0.22549 | 8.8862E+23 | 2.6130E-01 | 4.9566E+03 | -2.9432E+06 |
| 15200 | 1.92763E+07 | 0.24712 | 9.4440E+23 | 2.5339E-01 | 5.2239E+03 | -3.1502E+06 |
| 15400 | 2.04591E+07 | 0.26997 | 9.9999E+23 | 2.4560E-01 | 5.4842E+03 | -3.3513E+06 |
| 15600 | 2.17001E+07 | 0.29397 | 1.0550E+24 | 2.3795E-01 | 5.7335E+03 | -3.5437E+06 |
| 15800 | 2.29964E+07 | 0.31906 | 1.1090E+24 | 2.3047E-01 | 5.9672E+03 | -3.7247E+06 |
| 16000 | 2.43441E+07 | 0.34514 | 1.1617E+24 | 2.2318E-01 | 6.1810E+03 | -3.8919E+06 |
| 16200 | 2.57384E+07 | 0.37211 | 1.2127E+24 | 2.1609E-01 | 6.3700E+03 | -4.0431E+06 |
| 16400 | 2.71732E+07 | 0.39982 | 1.2617E+24 | 2.0923E-01 | 6.5299E+03 | -4.1762E+06 |
| 16600 | 2.86417E+07 | 0.42814 | 1.3083E+24 | 2.0261E-01 | 6.6566E+03 | -4.2897E+06 |
| 16800 | 3.01358E+07 | 0.45687 | 1.3523E+24 | 1.9625E-01 | 6.7465E+03 | -4.3825E+06 |
| 17000 | 3.16471E+07 | 0.48585 | 1.3934E+24 | 1.9016E-01 | 6.7971E+03 | -4.4539E+06 |
| 17200 | 3.31666E+07 | 0.51487 | 1.4315E+24 | 1.8435E-01 | 6.8067E+03 | -4.5037E+06 |
| 17400 | 3.46847E+07 | 0.54373 | 1.4664E+24 | 1.7882E-01 | 6.7747E+03 | -4.5321E+06 |
| 17600 | 3.61922E+07 | 0.57224 | 1.4981E+24 | 1.7358E-01 | 6.7020E+03 | -4.5397E+06 |
| 17800 | 3.76799E+07 | 0.60021 | 1.5265E+24 | 1.6863E-01 | 6.5905E+03 | -4.5277E+06 |
| 18000 | 3.91393E+07 | 0.62746 | 1.5517E+24 | 1.6397E-01 | 6.4431E+03 | -4.4974E+06 |

PRESSURE (N/M2) IS
10000

TRANSPORT DATA EQUILIBRIUM AIR

LOG(PRESSURE)= 4

| TEMP KELVIN | VISCOSITY KG/M-SEC | AMBIDIFF M2/SEC | TOTCOND NM/M-SEC-DEG | REACT | ELECTR FRACTIONS | PRANDTL | QAA M2 | QAI M2 | QII M2 |
|---|---|---|---|---|---|---|---|---|---|
| 100 | 9.362E-06 | 1.364E-05 | 7.684E-03 | 0.0000 | 0.0000 | 0.6341 | 5.63E-19 | 1.94E-18 | |
| 200 | 1.585E-05 | 4.078E-05 | 1.292E-02 | 0.0000 | 0.0000 | 0.6385 | 4.70E-19 | 1.83E-18 | |
| 300 | 2.158E-05 | 7.744E-05 | 1.752E-02 | 0.0000 | 0.0000 | 0.6411 | 4.23E-19 | 1.77E-18 | |
| 400 | 2.685E-05 | 1.221E-04 | 2.173E-02 | 0.0000 | 0.0000 | 0.6430 | 3.93E-19 | 1.73E-18 | |
| 500 | 3.181E-05 | 1.738E-04 | 2.569E-02 | 0.0000 | 0.0000 | 0.6444 | 3.70E-19 | 1.70E-18 | |
| 600 | 3.654E-05 | 2.320E-04 | 2.946E-02 | 0.0000 | 0.0000 | 0.6456 | 3.53E-19 | 1.67E-18 | |
| 700 | 4.108E-05 | 2.961E-04 | 3.307E-02 | 0.0000 | 0.0000 | 0.6466 | 3.39E-19 | 1.65E-18 | |
| 800 | 4.547E-05 | 3.659E-04 | 3.655E-02 | 0.0000 | 0.0000 | 0.6474 | 3.28E-19 | 1.63E-18 | |
| 900 | 4.973E-05 | 4.410E-04 | 3.993E-02 | 0.0000 | 0.0000 | 0.6482 | 3.18E-19 | 1.62E-18 | |
| 1000 | 5.387E-05 | 5.211E-04 | 4.321E-02 | 0.0000 | 0.0000 | 0.6489 | 3.09E-19 | 1.60E-18 | |
| 1200 | 6.188E-05 | 6.957E-04 | 4.954E-02 | 0.0000 | 0.0000 | 0.6501 | 2.95E-19 | 1.58E-18 | |
| 1400 | 6.957E-05 | 8.884E-04 | 5.562E-02 | 0.0000 | 0.0000 | 0.6511 | 2.83E-19 | 1.56E-18 | |
| 1600 | 7.700E-05 | 1.098E-03 | 6.147E-02 | 0.0000 | 0.0000 | 0.6519 | 2.74E-19 | 1.54E-18 | |
| 1800 | 8.421E-05 | 1.324E-03 | 6.715E-02 | 0.0000 | 0.0000 | 0.6527 | 2.66E-19 | 1.52E-18 | |
| 2000 | 9.123E-05 | 1.565E-03 | 7.267E-02 | 0.0000 | 0.0000 | 0.6534 | 2.58E-19 | 1.51E-18 | |
| 2200 | 9.809E-05 | 1.820E-03 | 7.806E-02 | 0.0000 | 0.0000 | 0.6540 | 2.52E-19 | 1.50E-18 | |
| 2400 | 1.048E-04 | 2.090E-03 | 8.332E-02 | 0.0000 | 0.0000 | 0.6546 | 2.46E-19 | 1.49E-18 | |
| 2600 | 1.114E-04 | 2.373E-03 | 8.848E-02 | 0.0000 | 0.0006 | 0.6551 | 2.41E-19 | 1.48E-18 | 9.38E-16 |
| 2800 | 1.178E-04 | 2.669E-03 | 9.354E-02 | 0.0000 | 0.0008 | 0.6556 | 2.37E-19 | 1.47E-18 | 7.52E-16 |
| 3000 | 1.242E-04 | 2.978E-03 | 9.850E-02 | 0.0000 | 0.0010 | 0.6560 | 2.32E-19 | 1.46E-18 | 6.12E-16 |
| 3200 | 1.304E-04 | 3.300E-03 | 1.034E-01 | 0.0000 | 0.0013 | 0.6565 | 2.29E-19 | 1.45E-18 | 5.05E-16 |
| 3400 | 1.365E-04 | 3.633E-03 | 1.082E-01 | 0.0000 | 0.0016 | 0.6569 | 2.25E-19 | 1.44E-18 | 4.22E-16 |
| 3600 | 1.426E-04 | 3.979E-03 | 1.129E-01 | 0.0000 | 0.0020 | 0.6572 | 2.22E-19 | 1.43E-18 | 3.57E-16 |
| 3800 | 1.486E-04 | 4.336E-03 | 1.176E-01 | 0.0000 | 0.0024 | 0.6576 | 2.19E-19 | 1.43E-18 | 3.04E-16 |
| 4000 | 1.545E-04 | 4.704E-03 | 1.222E-01 | 0.0000 | 0.0029 | 0.6579 | 2.16E-19 | 1.42E-18 | 2.62E-16 |
| 4200 | 1.603E-04 | 5.083E-03 | 1.268E-01 | 0.0000 | 0.0035 | 0.6583 | 2.13E-19 | 1.41E-18 | 2.27E-16 |
| 4400 | 1.661E-04 | 5.473E-03 | 1.313E-01 | 0.0000 | 0.0041 | 0.6586 | 2.10E-19 | 1.41E-18 | 1.98E-16 |
| 4600 | 1.718E-04 | 5.874E-03 | 1.357E-01 | 0.0000 | 0.0048 | 0.6589 | 2.08E-19 | 1.40E-18 | 1.74E-16 |
| 4800 | 1.775E-04 | 6.285E-03 | 1.400E-01 | 0.0001 | 0.0053 | 0.6558 | 2.06E-19 | 1.40E-18 | 1.54E-16 |
| 5000 | 1.831E-04 | 6.706E-03 | 1.461E-01 | 0.0002 | 0.0109 | 0.6526 | 2.04E-19 | 1.39E-18 | 1.37E-16 |
| 5200 | 1.886E-04 | 7.136E-03 | 1.520E-01 | 0.0004 | 0.0209 | 0.6467 | 2.02E-19 | 1.39E-18 | 1.22E-16 |
| 5400 | 1.941E-04 | 7.579E-03 | 1.591E-01 | 0.0007 | 0.0370 | 0.6370 | 2.00E-19 | 1.38E-18 | 1.10E-16 |
| 5600 | 1.995E-04 | 8.030E-03 | 1.677E-01 | 0.0012 | 0.0607 | 0.6227 | 1.98E-19 | 1.38E-18 | 9.87E-17 |
| 5800 | 2.049E-04 | 8.491E-03 | 1.782E-01 | 0.0021 | 0.0919 | 0.6040 | 1.96E-19 | 1.37E-18 | 8.93E-17 |
| 6000 | 2.101E-04 | 8.961E-03 | 1.908E-01 | 0.0032 | 0.1291 | 0.5823 | 1.94E-19 | 1.37E-18 | 8.11E-17 |
| 6200 | 2.154E-04 | 9.441E-03 | 2.054E-01 | 0.0049 | 0.1693 | 0.5595 | 1.92E-19 | 1.37E-18 | 7.40E-17 |
| 6400 | 2.205E-04 | 9.930E-03 | 2.217E-01 | 0.0073 | 0.2096 | 0.5382 | 1.91E-19 | 1.36E-18 | 6.76E-17 |
| 6600 | 2.255E-04 | 1.043E-02 | 2.392E-01 | 0.0104 | 0.2477 | 0.5200 | 1.89E-19 | 1.36E-18 | 6.21E-17 |
| 6800 | 2.304E-04 | 1.094E-02 | 2.577E-01 | 0.0145 | 0.2822 | 0.5063 | 1.88E-19 | 1.35E-18 | 5.71E-17 |
| 7000 | 2.350E-04 | 1.145E-02 | 2.770E-01 | 0.0199 | 0.3129 | 0.4979 | 1.87E-19 | 1.35E-18 | 5.27E-17 |
| 7200 | 2.394E-04 | 1.198E-02 | 2.971E-01 | 0.0266 | 0.3397 | 0.4952 | 1.85E-19 | 1.35E-18 | 4.87E-17 |
| 7400 | 2.435E-04 | 1.251E-02 | 3.180E-01 | 0.0351 | 0.3630 | 0.4983 | 1.84E-19 | 1.34E-18 | 4.52E-17 |
| 7600 | 2.471E-04 | 1.305E-02 | 3.398E-01 | 0.0455 | 0.3832 | 0.5076 | 1.83E-19 | 1.34E-18 | 4.20E-17 |
| 7800 | 2.501E-04 | 1.360E-02 | 3.628E-01 | 0.0580 | 0.4006 | 0.5230 | 1.81E-19 | 1.34E-18 | 3.91E-17 |
| 8000 | 2.524E-04 | 1.416E-02 | 3.872E-01 | 0.0728 | 0.4154 | 0.5446 | 1.80E-19 | 1.33E-18 | 3.65E-17 |
| 8200 | 2.539E-04 | 1.473E-02 | 4.132E-01 | 0.0899 | 0.4279 | 0.5718 | 1.79E-19 | 1.33E-18 | 3.41E-17 |
| 8400 | 2.543E-04 | 1.530E-02 | 4.410E-01 | 0.1096 | 0.4382 | 0.6043 | 1.78E-19 | 1.33E-18 | 3.20E-17 |
| 8600 | 2.534E-04 | 1.589E-02 | 4.709E-01 | 0.1317 | 0.4465 | 0.6410 | 1.77E-19 | 1.33E-18 | 3.00E-17 |
| 8800 | 2.511E-04 | 1.648E-02 | 5.031E-01 | 0.1560 | 0.4529 | 0.6805 | 1.76E-19 | 1.32E-18 | 2.82E-17 |
| 9000 | 2.473E-04 | 1.708E-02 | 5.378E-01 | 0.1825 | 0.4575 | 0.7213 | 1.75E-19 | 1.32E-18 | 2.66E-17 |
| 9200 | 2.418E-04 | 1.769E-02 | 5.753E-01 | 0.2106 | 0.4606 | 0.7613 | 1.74E-19 | 1.32E-18 | 2.51E-17 |
| 9400 | 2.345E-04 | 1.830E-02 | 6.156E-01 | 0.2401 | 0.4621 | 0.7984 | 1.73E-19 | 1.31E-18 | 2.37E-17 |
| 9600 | 2.256E-04 | 1.893E-02 | 6.589E-01 | 0.2703 | 0.4624 | 0.8302 | 1.72E-19 | 1.31E-18 | 2.25E-17 |
| 9800 | 2.150E-04 | 1.956E-02 | 7.052E-01 | 0.3006 | 0.4617 | 0.8549 | 1.71E-19 | 1.31E-18 | 2.13E-17 |
| 10000 | 2.030E-04 | 2.020E-02 | 7.543E-01 | 0.3303 | 0.4602 | 0.8709 | 1.70E-19 | 1.31E-18 | 2.02E-17 |
| 10200 | 1.898E-04 | 2.085E-02 | 8.060E-01 | 0.3587 | 0.4583 | 0.8771 | 1.69E-19 | 1.30E-18 | 1.92E-17 |
| 10400 | 1.758E-04 | 2.150E-02 | 8.595E-01 | 0.3850 | 0.4563 | 0.8733 | 1.68E-19 | 1.30E-18 | 1.83E-17 |
| 10600 | 1.613E-04 | 2.216E-02 | 9.140E-01 | 0.4086 | 0.4549 | 0.8598 | 1.67E-19 | 1.30E-18 | 1.75E-17 |
| 10800 | 1.466E-04 | 2.283E-02 | 9.686E-01 | 0.4288 | 0.4544 | 0.8373 | 1.67E-19 | 1.30E-18 | 1.67E-17 |
| 11000 | 1.321E-04 | 2.351E-02 | 1.020E+00 | 0.4449 | 0.4555 | 0.8073 | 1.66E-19 | 1.30E-18 | 1.60E-17 |
| 11200 | 1.180E-04 | 2.419E-02 | 1.067E+00 | 0.4566 | 0.4588 | 0.7710 | 1.65E-19 | 1.29E-18 | 1.53E-17 |
| 11400 | 1.047E-04 | 2.488E-02 | 1.108E+00 | 0.4631 | 0.4651 | 0.7300 | 1.64E-19 | 1.29E-18 | 1.47E-17 |
| 11600 | 9.216E-05 | 2.558E-02 | 1.140E+00 | 0.4640 | 0.4749 | 0.6854 | 1.64E-19 | 1.29E-18 | 1.41E-17 |
| 11800 | 8.065E-05 | 2.629E-02 | 1.161E+00 | 0.4589 | 0.4891 | 0.6384 | 1.63E-19 | 1.29E-18 | 1.36E-17 |
| 12000 | 7.020E-05 | 2.700E-02 | 1.170E+00 | 0.4472 | 0.5083 | 0.5895 | 1.62E-19 | 1.29E-18 | 1.31E-17 |
| 12200 | 6.084E-05 | 2.772E-02 | 1.166E+00 | 0.4287 | 0.5332 | 0.5394 | 1.61E-19 | 1.28E-18 | 1.26E-17 |
| 12400 | 5.256E-05 | 2.845E-02 | 1.150E+00 | 0.4032 | 0.5640 | 0.4883 | 1.61E-19 | 1.28E-18 | 1.22E-17 |
| 12600 | 4.533E-05 | 2.918E-02 | 1.125E+00 | 0.3710 | 0.6007 | 0.4367 | 1.60E-19 | 1.28E-18 | 1.18E-17 |
| 12800 | 3.908E-05 | 2.992E-02 | 1.094E+00 | 0.3329 | 0.6426 | 0.3848 | 1.59E-19 | 1.28E-18 | 1.14E-17 |
| 13000 | 3.374E-05 | 3.067E-02 | 1.061E+00 | 0.2904 | 0.6885 | 0.3336 | 1.59E-19 | 1.28E-18 | 1.11E-17 |
| 13200 | 2.922E-05 | 3.143E-02 | 1.030E+00 | 0.2456 | 0.7362 | 0.2840 | 1.58E-19 | 1.27E-18 | 1.08E-17 |
| 13400 | 2.543E-05 | 3.219E-02 | 1.003E+00 | 0.2012 | 0.7833 | 0.2373 | 1.58E-19 | 1.27E-18 | 1.05E-17 |
| 13600 | 2.229E-05 | 3.296E-02 | 9.834E-01 | 0.1596 | 0.8272 | 0.1948 | 1.57E-19 | 1.27E-18 | 1.02E-17 |
| 13800 | 1.971E-05 | 3.373E-02 | 9.713E-01 | 0.1228 | 0.8662 | 0.1575 | 1.56E-19 | 1.27E-18 | 9.93E-18 |
| 14000 | 1.760E-05 | 3.452E-02 | 9.670E-01 | 0.0919 | 0.8989 | 0.1258 | 1.56E-19 | 1.27E-18 | 9.69E-18 |
| 14200 | 1.590E-05 | 3.530E-02 | 9.698E-01 | 0.0672 | 0.9252 | 0.0997 | 1.55E-19 | 1.27E-18 | 9.45E-18 |
| 14400 | 1.453E-05 | 3.610E-02 | 9.788E-01 | 0.0482 | 0.9455 | 0.0788 | 1.55E-19 | 1.26E-18 | 9.23E-18 |
| 14600 | 1.344E-05 | 3.690E-02 | 9.930E-01 | 0.0341 | 0.9608 | 0.0623 | 1.54E-19 | 1.26E-18 | 9.01E-18 |
| 14800 | 1.259E-05 | 3.771E-02 | 1.011E+00 | 0.0239 | 0.9719 | 0.0495 | 1.54E-19 | 1.26E-18 | 8.81E-18 |
| 15000 | 1.193E-05 | 3.852E-02 | 1.032E+00 | 0.0166 | 0.9800 | 0.0397 | 1.53E-19 | 1.26E-18 | 8.62E-18 |
| 15200 | 1.142E-05 | 3.935E-02 | 1.056E+00 | 0.0115 | 0.9857 | 0.0321 | 1.52E-19 | 1.26E-18 | 8.43E-18 |
| 15400 | 1.104E-05 | 4.017E-02 | 1.082E+00 | 0.0079 | 0.9898 | 0.0262 | 1.52E-19 | 1.26E-18 | 8.25E-18 |
| 15600 | 1.077E-05 | 4.101E-02 | 1.109E+00 | 0.0055 | 0.9926 | 0.0217 | 1.51E-19 | 1.25E-18 | 8.08E-18 |
| 15800 | 1.059E-05 | 4.185E-02 | 1.137E+00 | 0.0038 | 0.9947 | 0.0182 | 1.51E-19 | 1.25E-18 | 7.91E-18 |
| 16000 | 1.048E-05 | 4.270E-02 | 1.167E+00 | 0.0026 | 0.9961 | 0.0154 | 1.50E-19 | 1.25E-18 | 7.75E-18 |
| 16200 | 1.043E-05 | 4.355E-02 | 1.197E+00 | 0.0018 | 0.9971 | 0.0133 | 1.50E-19 | 1.25E-18 | 7.59E-18 |
| 16400 | 1.043E-05 | 4.441E-02 | 1.228E+00 | 0.0013 | 0.9978 | 0.0116 | 1.49E-19 | 1.25E-18 | 7.44E-18 |
| 16600 | 1.047E-05 | 4.528E-02 | 1.259E+00 | 0.0009 | 0.9984 | 0.0102 | 1.49E-19 | 1.25E-18 | 7.30E-18 |
| 16800 | 1.054E-05 | 4.615E-02 | 1.291E+00 | 0.0006 | 0.9987 | 0.0091 | 1.49E-19 | 1.25E-18 | 7.16E-18 |
| 17000 | 1.065E-05 | 4.703E-02 | 1.324E+00 | 0.0005 | 0.9990 | 0.0082 | 1.48E-19 | 1.24E-18 | 7.02E-18 |
| 17200 | 1.077E-05 | 4.791E-02 | 1.357E+00 | 0.0003 | 0.9992 | 0.0075 | 1.48E-19 | 1.24E-18 | 6.89E-18 |
| 17400 | 1.093E-05 | 4.880E-02 | 1.391E+00 | 0.0002 | 0.9994 | 0.0069 | 1.47E-19 | 1.24E-18 | 6.76E-18 |
| 17600 | 1.109E-05 | 4.970E-02 | 1.425E+00 | 0.0002 | 0.9995 | 0.0064 | 1.47E-19 | 1.24E-18 | 6.63E-18 |
| 17800 | 1.128E-05 | 5.060E-02 | 1.459E+00 | 0.0001 | 0.9996 | 0.0060 | 1.46E-19 | 1.24E-18 | 6.51E-18 |
| 18000 | 1.148E-05 | 5.151E-02 | 1.494E+00 | 0.0001 | 0.9997 | 0.0057 | 1.46E-19 | 1.24E-18 | 6.40E-18 |

PRESSURE (N/M2) IS
100000

TRANSPORT DATA EQUILIBRIUM ARGON

LOG(PRESSURE)= 5

| TEMP KELVIN | VISCOSITY KG/M-SEC | AMBIDIFF M2/SEC | TOTCOND NM/M-SEC-DEG | REACT | ELECTR FRACTIONS | PRANDTL | QAA M2 | QAI M2 | QII M2 |
|---|---|---|---|---|---|---|---|---|---|
| 100 | 9.362E-06 | 1.364E-06 | 7.684E-03 | 0.0000 | 0.0000 | 0.6341 | 5.63E-19 | 1.04E-18 | |
| 200 | 1.585E-05 | 4.078E-06 | 1.292E-02 | 0.0000 | 0.0000 | 0.6385 | 4.70E-19 | 1.83E-18 | |
| 300 | 2.154E-05 | 7.744E-06 | 1.752E-02 | 0.0000 | 0.0000 | 0.6411 | 4.23E-19 | 1.77E-18 | |
| 400 | 2.685E-05 | 1.221E-05 | 2.173E-02 | 0.0000 | 0.0000 | 0.6430 | 3.93E-19 | 1.73E-18 | |
| 500 | 3.181E-05 | 1.738E-05 | 2.569E-02 | 0.0000 | 0.0000 | 0.6444 | 3.70E-19 | 1.70E-18 | |
| 600 | 3.654E-05 | 2.320E-05 | 2.946E-02 | 0.0000 | 0.0000 | 0.6456 | 3.53E-19 | 1.67E-18 | |
| 700 | 4.108E-05 | 2.961E-05 | 3.307E-02 | 0.0000 | 0.0000 | 0.6466 | 3.39E-19 | 1.65E-18 | |
| 800 | 4.547E-05 | 3.659E-05 | 3.655E-02 | 0.0000 | 0.0000 | 0.6474 | 3.28E-19 | 1.63E-18 | |
| 900 | 4.973E-05 | 4.410E-05 | 3.993E-02 | 0.0000 | 0.0000 | 0.6482 | 3.18E-19 | 1.62E-18 | |
| 1000 | 5.387E-05 | 5.211E-05 | 4.321E-02 | 0.0000 | 0.0000 | 0.6489 | 3.09E-19 | 1.60E-18 | |
| 1200 | 6.188E-05 | 6.957E-05 | 4.954E-02 | 0.0000 | 0.0000 | 0.6501 | 2.95E-19 | 1.58E-18 | |
| 1400 | 6.957E-05 | 8.888E-05 | 5.562E-02 | 0.0000 | 0.0000 | 0.6511 | 2.83E-19 | 1.56E-18 | |
| 1600 | 7.700E-05 | 1.098E-04 | 6.147E-02 | 0.0000 | 0.0000 | 0.6519 | 2.74E-19 | 1.54E-18 | |
| 1800 | 8.421E-05 | 1.324E-04 | 6.715E-02 | 0.0000 | 0.0000 | 0.6527 | 2.66E-19 | 1.52E-18 | |
| 2000 | 9.123E-05 | 1.565E-04 | 7.267E-02 | 0.0000 | 0.0000 | 0.6534 | 2.58E-19 | 1.51E-18 | |
| 2200 | 9.809E-05 | 1.820E-04 | 7.806E-02 | 0.0000 | 0.0000 | 0.6540 | 2.52E-19 | 1.50E-18 | |
| 2400 | 1.048E-04 | 2.090E-04 | 8.332E-02 | 0.0000 | 0.0000 | 0.6546 | 2.46E-19 | 1.49E-18 | |
| 2600 | 1.114E-04 | 2.373E-04 | 8.848E-02 | 0.0000 | 0.0006 | 0.6551 | 2.41E-19 | 1.48E-18 | 9.05E-16 |
| 2800 | 1.178E-04 | 2.669E-04 | 9.354E-02 | 0.0000 | 0.0008 | 0.6556 | 2.37E-19 | 1.47E-18 | 7.23E-16 |
| 3000 | 1.242E-04 | 2.978E-04 | 9.850E-02 | 0.0000 | 0.0011 | 0.6560 | 2.32E-19 | 1.46E-18 | 5.87E-16 |
| 3200 | 1.304E-04 | 3.300E-04 | 1.034E-01 | 0.0000 | 0.0014 | 0.6565 | 2.29E-19 | 1.45E-18 | 4.84E-16 |
| 3400 | 1.365E-04 | 3.633E-04 | 1.082E-01 | 0.0000 | 0.0017 | 0.6569 | 2.25E-19 | 1.44E-18 | 4.03E-16 |
| 3600 | 1.426E-04 | 3.979E-04 | 1.129E-01 | 0.0000 | 0.0021 | 0.6572 | 2.22E-19 | 1.43E-18 | 3.39E-16 |
| 3800 | 1.486E-04 | 4.336E-04 | 1.176E-01 | 0.0000 | 0.0026 | 0.6574 | 2.19E-19 | 1.43E-18 | 2.89E-16 |
| 4000 | 1.545E-04 | 4.704E-04 | 1.222E-01 | 0.0000 | 0.0031 | 0.6579 | 2.16E-19 | 1.42E-18 | 2.48E-16 |
| 4200 | 1.603E-04 | 5.083E-04 | 1.268E-01 | 0.0000 | 0.0037 | 0.6583 | 2.13E-19 | 1.41E-18 | 2.14E-16 |
| 4400 | 1.661E-04 | 5.473E-04 | 1.313E-01 | 0.0000 | 0.0044 | 0.6586 | 2.10E-19 | 1.41E-18 | 1.86E-16 |
| 4600 | 1.718E-04 | 5.874E-04 | 1.357E-01 | 0.0000 | 0.0052 | 0.6589 | 2.08E-19 | 1.40E-18 | 1.63E-16 |
| 4800 | 1.775E-04 | 6.285E-04 | 1.401E-01 | 0.0000 | 0.0060 | 0.6592 | 2.06E-19 | 1.40E-18 | 1.44E-16 |
| 5000 | 1.831E-04 | 6.706E-04 | 1.445E-01 | 0.0001 | 0.0070 | 0.6595 | 2.04E-19 | 1.39E-18 | 1.28E-16 |
| 5200 | 1.886E-04 | 7.138E-04 | 1.489E-01 | 0.0001 | 0.0081 | 0.6552 | 2.02E-19 | 1.39E-18 | 1.14E-16 |
| 5400 | 1.941E-04 | 7.579E-04 | 1.551E-01 | 0.0002 | 0.0132 | 0.6517 | 2.00E-19 | 1.38E-18 | 1.02E-16 |
| 5600 | 1.995E-04 | 8.030E-04 | 1.611E-01 | 0.0004 | 0.0230 | 0.6458 | 1.98E-19 | 1.38E-18 | 9.16E-17 |
| 5800 | 2.049E-04 | 8.491E-04 | 1.680E-01 | 0.0007 | 0.0381 | 0.6367 | 1.96E-19 | 1.37E-18 | 8.27E-17 |
| 6000 | 2.102E-04 | 8.961E-04 | 1.763E-01 | 0.0011 | 0.0594 | 0.6237 | 1.94E-19 | 1.37E-18 | 7.50E-17 |
| 6200 | 2.155E-04 | 9.441E-04 | 1.864E-01 | 0.0017 | 0.0875 | 0.6068 | 1.92E-19 | 1.37E-18 | 6.82E-17 |
| 6400 | 2.207E-04 | 9.930E-04 | 1.984E-01 | 0.0026 | 0.1216 | 0.5862 | 1.91E-19 | 1.36E-18 | 6.22E-17 |
| 6600 | 2.259E-04 | 1.043E-03 | 2.127E-01 | 0.0037 | 0.1605 | 0.5632 | 1.89E-19 | 1.36E-18 | 5.69E-17 |
| 6800 | 2.310E-04 | 1.094E-03 | 2.291E-01 | 0.0052 | 0.2017 | 0.5394 | 1.88E-19 | 1.35E-18 | 5.23E-17 |
| 7000 | 2.360E-04 | 1.145E-03 | 2.476E-01 | 0.0070 | 0.2432 | 0.5162 | 1.87E-19 | 1.35E-18 | 4.81E-17 |
| 7200 | 2.408E-04 | 1.198E-03 | 2.677E-01 | 0.0094 | 0.2832 | 0.4952 | 1.85E-19 | 1.35E-18 | 4.44E-17 |
| 7400 | 2.456E-04 | 1.251E-03 | 2.893E-01 | 0.0122 | 0.3204 | 0.4771 | 1.84E-19 | 1.34E-18 | 4.11E-17 |
| 7600 | 2.502E-04 | 1.305E-03 | 3.121E-01 | 0.0157 | 0.3543 | 0.4626 | 1.83E-19 | 1.34E-18 | 3.81E-17 |
| 7800 | 2.546E-04 | 1.360E-03 | 3.360E-01 | 0.0199 | 0.3848 | 0.4519 | 1.81E-19 | 1.34E-18 | 3.54E-17 |
| 8000 | 2.587E-04 | 1.416E-03 | 3.608E-01 | 0.0249 | 0.4121 | 0.4451 | 1.80E-19 | 1.33E-18 | 3.30E-17 |
| 8200 | 2.625E-04 | 1.473E-03 | 3.866E-01 | 0.0307 | 0.4363 | 0.4422 | 1.79E-19 | 1.33E-18 | 3.08E-17 |
| 8400 | 2.659E-04 | 1.530E-03 | 4.134E-01 | 0.0374 | 0.4578 | 0.4430 | 1.78E-19 | 1.33E-18 | 2.88E-17 |
| 8600 | 2.688E-04 | 1.589E-03 | 4.413E-01 | 0.0452 | 0.4769 | 0.4475 | 1.77E-19 | 1.33E-18 | 2.70E-17 |
| 8800 | 2.711E-04 | 1.648E-03 | 4.702E-01 | 0.0540 | 0.4938 | 0.4554 | 1.76E-19 | 1.32E-18 | 2.53E-17 |
| 9000 | 2.728E-04 | 1.708E-03 | 5.004E-01 | 0.0638 | 0.5087 | 0.4664 | 1.75E-19 | 1.32E-18 | 2.38E-17 |
| 9200 | 2.737E-04 | 1.769E-03 | 5.319E-01 | 0.0748 | 0.5220 | 0.4803 | 1.74E-19 | 1.32E-18 | 2.24E-17 |
| 9400 | 2.737E-04 | 1.830E-03 | 5.648E-01 | 0.0868 | 0.5336 | 0.4966 | 1.73E-19 | 1.31E-18 | 2.12E-17 |
| 9600 | 2.727E-04 | 1.893E-03 | 5.993E-01 | 0.0998 | 0.5439 | 0.5147 | 1.72E-19 | 1.31E-18 | 2.00E-17 |
| 9800 | 2.706E-04 | 1.956E-03 | 6.353E-01 | 0.1138 | 0.5529 | 0.5341 | 1.71E-19 | 1.31E-18 | 1.89E-17 |
| 10000 | 2.673E-04 | 2.020E-03 | 6.731E-01 | 0.1287 | 0.5607 | 0.5541 | 1.70E-19 | 1.31E-18 | 1.79E-17 |
| 10200 | 2.628E-04 | 2.085E-03 | 7.126E-01 | 0.1444 | 0.5674 | 0.5737 | 1.69E-19 | 1.30E-18 | 1.70E-17 |
| 10400 | 2.571E-04 | 2.150E-03 | 7.540E-01 | 0.1607 | 0.5732 | 0.5924 | 1.68E-19 | 1.30E-18 | 1.61E-17 |
| 10600 | 2.500E-04 | 2.216E-03 | 7.973E-01 | 0.1773 | 0.5780 | 0.6091 | 1.67E-19 | 1.30E-18 | 1.54E-17 |
| 10800 | 2.418E-04 | 2.283E-03 | 8.425E-01 | 0.1942 | 0.5821 | 0.6232 | 1.67E-19 | 1.30E-18 | 1.46E-17 |
| 11000 | 2.325E-04 | 2.351E-03 | 8.895E-01 | 0.2111 | 0.5855 | 0.6339 | 1.66E-19 | 1.30E-18 | 1.39E-17 |
| 11200 | 2.222E-04 | 2.419E-03 | 9.384E-01 | 0.2277 | 0.5884 | 0.6408 | 1.65E-19 | 1.29E-18 | 1.33E-17 |
| 11400 | 2.111E-04 | 2.488E-03 | 9.890E-01 | 0.2436 | 0.5908 | 0.6434 | 1.64E-19 | 1.29E-18 | 1.27E-17 |
| 11600 | 1.993E-04 | 2.558E-03 | 1.041E+00 | 0.2588 | 0.5930 | 0.6416 | 1.64E-19 | 1.29E-18 | 1.22E-17 |
| 11800 | 1.871E-04 | 2.629E-03 | 1.094E+00 | 0.2727 | 0.5952 | 0.6353 | 1.63E-19 | 1.29E-18 | 1.17E-17 |
| 12000 | 1.746E-04 | 2.700E-03 | 1.148E+00 | 0.2853 | 0.5976 | 0.6247 | 1.62E-19 | 1.29E-18 | 1.12E-17 |
| 12200 | 1.621E-04 | 2.772E-03 | 1.201E+00 | 0.2961 | 0.6004 | 0.6101 | 1.61E-19 | 1.28E-18 | 1.07E-17 |
| 12400 | 1.497E-04 | 2.845E-03 | 1.254E+00 | 0.3049 | 0.6039 | 0.5920 | 1.61E-19 | 1.28E-18 | 1.03E-17 |
| 12600 | 1.376E-04 | 2.918E-03 | 1.305E+00 | 0.3114 | 0.6084 | 0.5708 | 1.60E-19 | 1.28E-18 | 9.95E-18 |
| 12800 | 1.259E-04 | 2.992E-03 | 1.354E+00 | 0.3155 | 0.6141 | 0.5470 | 1.59E-19 | 1.28E-18 | 9.58E-18 |
| 13000 | 1.148E-04 | 3.067E-03 | 1.399E+00 | 0.3169 | 0.6215 | 0.5211 | 1.59E-19 | 1.28E-18 | 9.25E-18 |
| 13200 | 1.042E-04 | 3.143E-03 | 1.440E+00 | 0.3154 | 0.6306 | 0.4935 | 1.58E-19 | 1.27E-18 | 8.93E-18 |
| 13400 | 9.437E-05 | 3.219E-03 | 1.475E+00 | 0.3109 | 0.6419 | 0.4647 | 1.58E-19 | 1.27E-18 | 8.64E-18 |
| 13600 | 8.523E-05 | 3.296E-03 | 1.505E+00 | 0.3033 | 0.6554 | 0.4350 | 1.57E-19 | 1.27E-18 | 8.36E-18 |
| 13800 | 7.683E-05 | 3.373E-03 | 1.529E+00 | 0.2925 | 0.6713 | 0.4047 | 1.56E-19 | 1.27E-18 | 8.10E-18 |
| 14000 | 6.916E-05 | 3.452E-03 | 1.546E+00 | 0.2786 | 0.6896 | 0.3740 | 1.56E-19 | 1.27E-18 | 7.86E-18 |
| 14200 | 6.222E-05 | 3.530E-03 | 1.557E+00 | 0.2619 | 0.7103 | 0.3433 | 1.55E-19 | 1.27E-18 | 7.63E-18 |
| 14400 | 5.598E-05 | 3.610E-03 | 1.564E+00 | 0.2426 | 0.7330 | 0.3128 | 1.55E-19 | 1.26E-18 | 7.42E-18 |
| 14600 | 5.042E-05 | 3.690E-03 | 1.567E+00 | 0.2213 | 0.7573 | 0.2827 | 1.54E-19 | 1.26E-18 | 7.22E-18 |
| 14800 | 4.548E-05 | 3.771E-03 | 1.568E+00 | 0.1985 | 0.7828 | 0.2534 | 1.54E-19 | 1.26E-18 | 7.03E-18 |
| 15000 | 4.113E-05 | 3.852E-03 | 1.568E+00 | 0.1750 | 0.8087 | 0.2253 | 1.53E-19 | 1.26E-18 | 6.85E-18 |
| 15200 | 3.732E-05 | 3.935E-03 | 1.569E+00 | 0.1515 | 0.8342 | 0.1986 | 1.52E-19 | 1.26E-18 | 6.69E-18 |
| 15400 | 3.402E-05 | 4.017E-03 | 1.572E+00 | 0.1289 | 0.8587 | 0.1736 | 1.52E-19 | 1.26E-18 | 6.53E-18 |
| 15600 | 3.116E-05 | 4.101E-03 | 1.577E+00 | 0.1078 | 0.8815 | 0.1508 | 1.51E-19 | 1.25E-18 | 6.38E-18 |
| 15800 | 2.870E-05 | 4.185E-03 | 1.587E+00 | 0.0886 | 0.9021 | 0.1302 | 1.51E-19 | 1.25E-18 | 6.24E-18 |
| 16000 | 2.661E-05 | 4.270E-03 | 1.600E+00 | 0.0717 | 0.9203 | 0.1119 | 1.50E-19 | 1.25E-18 | 6.11E-18 |
| 16200 | 2.483E-05 | 4.355E-03 | 1.617E+00 | 0.0573 | 0.9359 | 0.0958 | 1.50E-19 | 1.25E-18 | 5.98E-18 |
| 16400 | 2.333E-05 | 4.441E-03 | 1.638E+00 | 0.0452 | 0.9489 | 0.0820 | 1.49E-19 | 1.25E-18 | 5.86E-18 |
| 16600 | 2.209E-05 | 4.528E-03 | 1.663E+00 | 0.0353 | 0.9597 | 0.0702 | 1.49E-19 | 1.25E-18 | 5.74E-18 |
| 16800 | 2.105E-05 | 4.615E-03 | 1.691E+00 | 0.0273 | 0.9684 | 0.0602 | 1.49E-19 | 1.25E-18 | 5.63E-18 |
| 17000 | 2.020E-05 | 4.703E-03 | 1.722E+00 | 0.0210 | 0.9753 | 0.0519 | 1.48E-19 | 1.24E-18 | 5.52E-18 |
| 17200 | 1.951E-05 | 4.791E-03 | 1.756E+00 | 0.0161 | 0.9808 | 0.0448 | 1.48E-19 | 1.24E-18 | 5.42E-18 |
| 17400 | 1.897E-05 | 4.880E-03 | 1.792E+00 | 0.0122 | 0.9851 | 0.0390 | 1.47E-19 | 1.24E-18 | 5.32E-18 |
| 17600 | 1.854E-05 | 4.970E-03 | 1.829E+00 | 0.0093 | 0.9884 | 0.0341 | 1.47E-19 | 1.24E-18 | 5.22E-18 |
| 17800 | 1.822E-05 | 5.060E-03 | 1.868E+00 | 0.0070 | 0.9910 | 0.0301 | 1.46E-19 | 1.24E-18 | 5.13E-18 |
| 18000 | 1.798E-05 | 5.151E-03 | 1.908E+00 | 0.0053 | 0.9929 | 0.0267 | 1.46E-19 | 1.24E-18 | 5.04E-18 |

PRESSURE (N/M2) IS
1000000

TRANSPORT DATA EQUILIBRIUM ARGON

LOG(PRESSURE)= 6

| TEMP KELVIN | VISCOSITY KG/M-SEC | AMBIDIFF M2/SEC | THTCOND NM/M-SEC-DEG | REACT FRACTIONS | ELECTR | PRANDTL | QAA M2 | QAI M2 | QII M2 |
|---|---|---|---|---|---|---|---|---|---|
| 100 | 9.362E-06 | 1.364E-07 | 7.684E-03 | 0.0000 | 0.0000 | 0.6341 | 5.63E-19 | 1.94E-18 | |
| 200 | 1.585E-05 | 4.078E-07 | 1.292E-02 | 0.0000 | 0.0000 | 0.6385 | 4.70E-19 | 1.83E-18 | |
| 300 | 2.158E-05 | 7.744E-07 | 1.752E-02 | 0.0000 | 0.0000 | 0.6411 | 4.23E-19 | 1.77E-18 | |
| 400 | 2.685E-05 | 1.221E-06 | 2.173E-02 | 0.0000 | 0.0000 | 0.6430 | 3.93E-19 | 1.73E-18 | |
| 500 | 3.181E-05 | 1.738E-06 | 2.569E-02 | 0.0000 | 0.0000 | 0.6444 | 3.70E-19 | 1.70E-18 | |
| 600 | 3.654E-05 | 2.320E-06 | 2.946E-02 | 0.0000 | 0.0000 | 0.6456 | 3.53E-19 | 1.67E-18 | |
| 700 | 4.108E-05 | 2.961E-06 | 3.307E-02 | 0.0000 | 0.0000 | 0.6466 | 3.39E-19 | 1.65E-18 | |
| 800 | 4.547E-05 | 3.659E-06 | 3.655E-02 | 0.0000 | 0.0000 | 0.6474 | 3.28E-19 | 1.63E-18 | |
| 900 | 4.973E-05 | 4.410E-06 | 3.991E-02 | 0.0000 | 0.0000 | 0.6482 | 3.18E-19 | 1.62E-18 | |
| 1000 | 5.387E-05 | 5.211E-06 | 4.321E-02 | 0.0000 | 0.0000 | 0.6489 | 3.09E-19 | 1.60E-18 | |
| 1200 | 6.188E-05 | 6.957E-06 | 4.954E-02 | 0.0000 | 0.0000 | 0.6501 | 2.95E-19 | 1.58E-18 | |
| 1400 | 6.957E-05 | 8.884E-06 | 5.562E-02 | 0.0000 | 0.0000 | 0.6511 | 2.83E-19 | 1.56E-18 | |
| 1600 | 7.700E-05 | 1.098E-05 | 6.147E-02 | 0.0000 | 0.0000 | 0.6519 | 2.74E-19 | 1.54E-18 | |
| 1800 | 8.421E-05 | 1.324E-05 | 6.715E-02 | 0.0000 | 0.0000 | 0.6527 | 2.66E-19 | 1.52E-18 | |
| 2000 | 9.123E-05 | 1.565E-05 | 7.267E-02 | 0.0000 | 0.0000 | 0.6534 | 2.58E-19 | 1.51E-18 | |
| 2200 | 9.809E-05 | 1.820E-05 | 7.806E-02 | 0.0000 | 0.0000 | 0.6540 | 2.52E-19 | 1.50E-18 | |
| 2400 | 1.048E-04 | 2.090E-05 | 8.332E-02 | 0.0000 | 0.0000 | 0.6546 | 2.46E-19 | 1.49E-18 | |
| 2600 | 1.114E-04 | 2.373E-05 | 8.844E-02 | 0.0000 | 0.0004 | 0.6551 | 2.41E-19 | 1.48E-18 | 8.72E-16 |
| 2800 | 1.178E-04 | 2.669E-05 | 9.344E-02 | 0.0000 | 0.0009 | 0.6556 | 2.37E-19 | 1.47E-18 | 6.95E-16 |
| 3000 | 1.242E-04 | 2.978E-05 | 9.850E-02 | 0.0000 | 0.0011 | 0.6560 | 2.32E-19 | 1.46E-18 | 5.63E-16 |
| 3200 | 1.304E-04 | 3.300E-05 | 1.034E-01 | 0.0000 | 0.0014 | 0.6565 | 2.29E-19 | 1.45E-18 | 4.62E-16 |
| 3400 | 1.365E-04 | 3.633E-05 | 1.082E-01 | 0.0000 | 0.0018 | 0.6569 | 2.25E-19 | 1.44E-18 | 3.84E-16 |
| 3600 | 1.424E-04 | 3.979E-05 | 1.129E-01 | 0.0000 | 0.0022 | 0.6572 | 2.22E-19 | 1.43E-18 | 3.22E-16 |
| 3800 | 1.486E-04 | 4.336E-05 | 1.176E-01 | 0.0000 | 0.0027 | 0.6576 | 2.19E-19 | 1.43E-18 | 2.73E-16 |
| 4000 | 1.545E-04 | 4.704E-05 | 1.222E-01 | 0.0000 | 0.0033 | 0.6579 | 2.16E-19 | 1.42E-18 | 2.34E-16 |
| 4200 | 1.603E-04 | 5.083E-05 | 1.268E-01 | 0.0000 | 0.0039 | 0.6582 | 2.13E-19 | 1.41E-18 | 2.01E-16 |
| 4400 | 1.661E-04 | 5.473E-05 | 1.313E-01 | 0.0000 | 0.0047 | 0.6586 | 2.10E-19 | 1.41E-18 | 1.75E-16 |
| 4600 | 1.718E-04 | 5.874E-05 | 1.357E-01 | 0.0000 | 0.0055 | 0.6589 | 2.08E-19 | 1.40E-18 | 1.53E-16 |
| 4800 | 1.775E-04 | 6.285E-05 | 1.401E-01 | 0.0000 | 0.0065 | 0.6591 | 2.06E-19 | 1.40E-18 | 1.34E-16 |
| 5000 | 1.831E-04 | 6.706E-05 | 1.445E-01 | 0.0000 | 0.0075 | 0.6594 | 2.04E-19 | 1.39E-18 | 1.19E-16 |
| 5200 | 1.886E-04 | 7.138E-05 | 1.488E-01 | 0.0000 | 0.0087 | 0.6597 | 2.02E-19 | 1.39E-18 | 1.06E-16 |
| 5400 | 1.941E-04 | 7.579E-05 | 1.537E-01 | 0.0001 | 0.0043 | 0.6572 | 2.00E-19 | 1.38E-18 | 9.43E-17 |
| 5600 | 1.995E-04 | 8.030E-05 | 1.586E-01 | 0.0001 | 0.0078 | 0.6553 | 1.98E-19 | 1.38E-18 | 8.45E-17 |
| 5800 | 2.049E-04 | 8.491E-05 | 1.637E-01 | 0.0002 | 0.0133 | 0.6521 | 1.96E-19 | 1.37E-18 | 7.61E-17 |
| 6000 | 2.102E-04 | 8.961E-05 | 1.694E-01 | 0.0004 | 0.0218 | 0.6470 | 1.94E-19 | 1.37E-18 | 6.88E-17 |
| 6200 | 2.155E-04 | 9.441E-05 | 1.759E-01 | 0.0006 | 0.0341 | 0.6395 | 1.92E-19 | 1.37E-18 | 6.24E-17 |
| 6400 | 2.208E-04 | 9.930E-05 | 1.834E-01 | 0.0009 | 0.0512 | 0.6291 | 1.91E-19 | 1.36E-18 | 5.68E-17 |
| 6600 | 2.260E-04 | 1.043E-04 | 1.923E-01 | 0.0013 | 0.0738 | 0.6153 | 1.89E-19 | 1.36E-18 | 5.18E-17 |
| 6800 | 2.312E-04 | 1.094E-04 | 2.030E-01 | 0.0018 | 0.1019 | 0.5981 | 1.88E-19 | 1.35E-18 | 4.75E-17 |
| 7000 | 2.363E-04 | 1.145E-04 | 2.156E-01 | 0.0026 | 0.1353 | 0.5778 | 1.87E-19 | 1.35E-18 | 4.36E-17 |
| 7200 | 2.413E-04 | 1.198E-04 | 2.304E-01 | 0.0034 | 0.1728 | 0.5551 | 1.85E-19 | 1.35E-18 | 4.01E-17 |
| 7400 | 2.463E-04 | 1.251E-04 | 2.475E-01 | 0.0045 | 0.2139 | 0.5309 | 1.84E-19 | 1.34E-18 | 3.70E-17 |
| 7600 | 2.512E-04 | 1.305E-04 | 2.670E-01 | 0.0058 | 0.2568 | 0.5065 | 1.83E-19 | 1.34E-18 | 3.43E-17 |
| 7800 | 2.560E-04 | 1.360E-04 | 2.888E-01 | 0.0073 | 0.2961 | 0.4827 | 1.81E-19 | 1.34E-18 | 3.18E-17 |
| 8000 | 2.607E-04 | 1.416E-04 | 3.127E-01 | 0.0091 | 0.3359 | 0.4604 | 1.80E-19 | 1.33E-18 | 2.95E-17 |
| 8200 | 2.653E-04 | 1.473E-04 | 3.386E-01 | 0.0111 | 0.3736 | 0.4402 | 1.79E-19 | 1.33E-18 | 2.75E-17 |
| 8400 | 2.697E-04 | 1.530E-04 | 3.663E-01 | 0.0134 | 0.4085 | 0.4224 | 1.78E-19 | 1.33E-18 | 2.56E-17 |
| 8600 | 2.740E-04 | 1.589E-04 | 3.957E-01 | 0.0160 | 0.4405 | 0.4073 | 1.77E-19 | 1.32E-18 | 2.40E-17 |
| 8800 | 2.780E-04 | 1.648E-04 | 4.265E-01 | 0.0189 | 0.4696 | 0.3948 | 1.76E-19 | 1.32E-18 | 2.25E-17 |
| 9000 | 2.818E-04 | 1.708E-04 | 4.586E-01 | 0.0222 | 0.4959 | 0.3848 | 1.75E-19 | 1.32E-18 | 2.11E-17 |
| 9200 | 2.853E-04 | 1.769E-04 | 4.924E-01 | 0.0258 | 0.5198 | 0.3772 | 1.74E-19 | 1.32E-18 | 1.98E-17 |
| 9400 | 2.885E-04 | 1.830E-04 | 5.273E-01 | 0.0298 | 0.5413 | 0.3720 | 1.73E-19 | 1.31E-18 | 1.86E-17 |
| 9600 | 2.912E-04 | 1.893E-04 | 5.635E-01 | 0.0342 | 0.5607 | 0.3688 | 1.72E-19 | 1.31E-18 | 1.75E-17 |
| 9800 | 2.935E-04 | 1.956E-04 | 6.009E-01 | 0.0390 | 0.5784 | 0.3676 | 1.71E-19 | 1.31E-18 | 1.66E-17 |
| 10000 | 2.953E-04 | 2.020E-04 | 6.397E-01 | 0.0441 | 0.5943 | 0.3680 | 1.70E-19 | 1.31E-18 | 1.57E-17 |
| 10200 | 2.965E-04 | 2.085E-04 | 6.797E-01 | 0.0496 | 0.6088 | 0.3699 | 1.69E-19 | 1.30E-18 | 1.48E-17 |
| 10400 | 2.971E-04 | 2.150E-04 | 7.211E-01 | 0.0555 | 0.6221 | 0.3731 | 1.68E-19 | 1.30E-18 | 1.40E-17 |
| 10600 | 2.969E-04 | 2.216E-04 | 7.639E-01 | 0.0617 | 0.6342 | 0.3774 | 1.67E-19 | 1.30E-18 | 1.33E-17 |
| 10800 | 2.960E-04 | 2.283E-04 | 8.080E-01 | 0.0683 | 0.6453 | 0.3824 | 1.67E-19 | 1.30E-18 | 1.27E-17 |
| 11000 | 2.943E-04 | 2.351E-04 | 8.536E-01 | 0.0752 | 0.6554 | 0.3879 | 1.66E-19 | 1.30E-18 | 1.20E-17 |
| 11200 | 2.917E-04 | 2.419E-04 | 9.006E-01 | 0.0823 | 0.6647 | 0.3937 | 1.65E-19 | 1.29E-18 | 1.15E-17 |
| 11400 | 2.883E-04 | 2.488E-04 | 9.492E-01 | 0.0896 | 0.6733 | 0.3994 | 1.64E-19 | 1.29E-18 | 1.09E-17 |
| 11600 | 2.840E-04 | 2.558E-04 | 9.992E-01 | 0.0972 | 0.6812 | 0.4049 | 1.64E-19 | 1.29E-18 | 1.04E-17 |
| 11800 | 2.788E-04 | 2.629E-04 | 1.051E+00 | 0.1049 | 0.6884 | 0.4098 | 1.63E-19 | 1.29E-18 | 9.97E-18 |
| 12000 | 2.727E-04 | 2.700E-04 | 1.098E+00 | 0.1132 | 0.6934 | 0.4162 | 1.62E-19 | 1.29E-18 | 9.61E-18 |
| 12200 | 2.655E-04 | 2.772E-04 | 1.150E+00 | 0.1213 | 0.6989 | 0.4204 | 1.61E-19 | 1.28E-18 | 9.24E-18 |
| 12400 | 2.581E-04 | 2.845E-04 | 1.202E+00 | 0.1293 | 0.7040 | 0.4233 | 1.61E-19 | 1.28E-18 | 8.88E-18 |
| 12600 | 2.498E-04 | 2.918E-04 | 1.257E+00 | 0.1372 | 0.7086 | 0.4249 | 1.60E-19 | 1.28E-18 | 8.55E-18 |
| 12800 | 2.408E-04 | 2.992E-04 | 1.312E+00 | 0.1449 | 0.7129 | 0.4249 | 1.59E-19 | 1.28E-18 | 8.24E-18 |
| 13000 | 2.313E-04 | 3.067E-04 | 1.369E+00 | 0.1524 | 0.7170 | 0.4234 | 1.59E-19 | 1.28E-18 | 7.94E-18 |
| 13200 | 2.214E-04 | 3.143E-04 | 1.427E+00 | 0.1594 | 0.7208 | 0.4203 | 1.58E-19 | 1.27E-18 | 7.66E-18 |
| 13400 | 2.112E-04 | 3.219E-04 | 1.485E+00 | 0.1660 | 0.7244 | 0.4155 | 1.58E-19 | 1.27E-18 | 7.40E-18 |
| 13600 | 2.008E-04 | 3.296E-04 | 1.545E+00 | 0.1720 | 0.7282 | 0.4091 | 1.57E-19 | 1.27E-18 | 7.15E-18 |
| 13800 | 1.903E-04 | 3.373E-04 | 1.605E+00 | 0.1773 | 0.7319 | 0.4013 | 1.56E-19 | 1.27E-18 | 6.91E-18 |
| 14000 | 1.799E-04 | 3.452E-04 | 1.666E+00 | 0.1819 | 0.7357 | 0.3921 | 1.56E-19 | 1.27E-18 | 6.69E-18 |
| 14200 | 1.695E-04 | 3.530E-04 | 1.726E+00 | 0.1857 | 0.7397 | 0.3815 | 1.55E-19 | 1.27E-18 | 6.48E-18 |
| 14400 | 1.593E-04 | 3.610E-04 | 1.787E+00 | 0.1885 | 0.7440 | 0.3699 | 1.55E-19 | 1.26E-18 | 6.28E-18 |
| 14600 | 1.494E-04 | 3.690E-04 | 1.847E+00 | 0.1904 | 0.7487 | 0.3573 | 1.54E-19 | 1.26E-18 | 6.09E-18 |
| 14800 | 1.399E-04 | 3.771E-04 | 1.906E+00 | 0.1912 | 0.7539 | 0.3439 | 1.54E-19 | 1.26E-18 | 5.91E-18 |
| 15000 | 1.307E-04 | 3.852E-04 | 1.964E+00 | 0.1910 | 0.7594 | 0.3298 | 1.53E-19 | 1.26E-18 | 5.74E-18 |
| 15200 | 1.219E-04 | 3.935E-04 | 2.020E+00 | 0.1896 | 0.7660 | 0.3152 | 1.52E-19 | 1.26E-18 | 5.58E-18 |
| 15400 | 1.135E-04 | 4.017E-04 | 2.074E+00 | 0.1870 | 0.7731 | 0.3001 | 1.52E-19 | 1.26E-18 | 5.42E-18 |
| 15600 | 1.056E-04 | 4.101E-04 | 2.127E+00 | 0.1832 | 0.7809 | 0.2848 | 1.51E-19 | 1.25E-18 | 5.28E-18 |
| 15800 | 9.824E-05 | 4.185E-04 | 2.177E+00 | 0.1783 | 0.7895 | 0.2693 | 1.51E-19 | 1.25E-18 | 5.14E-18 |
| 16000 | 9.133E-05 | 4.270E-04 | 2.224E+00 | 0.1723 | 0.7988 | 0.2538 | 1.50E-19 | 1.25E-18 | 5.01E-18 |
| 16200 | 8.490E-05 | 4.355E-04 | 2.269E+00 | 0.1652 | 0.8088 | 0.2383 | 1.50E-19 | 1.25E-18 | 4.88E-18 |
| 16400 | 7.895E-05 | 4.441E-04 | 2.312E+00 | 0.1572 | 0.8194 | 0.2230 | 1.49E-19 | 1.25E-18 | 4.76E-18 |
| 16600 | 7.347E-05 | 4.528E-04 | 2.353E+00 | 0.1483 | 0.8309 | 0.2079 | 1.49E-19 | 1.25E-18 | 4.65E-18 |
| 16800 | 6.844E-05 | 4.615E-04 | 2.392E+00 | 0.1387 | 0.8427 | 0.1931 | 1.49E-19 | 1.25E-18 | 4.54E-18 |
| 17000 | 6.385E-05 | 4.703E-04 | 2.429E+00 | 0.1286 | 0.8548 | 0.1787 | 1.48E-19 | 1.24E-18 | 4.43E-18 |
| 17200 | 5.967E-05 | 4.791E-04 | 2.465E+00 | 0.1181 | 0.8670 | 0.1648 | 1.48E-19 | 1.24E-18 | 4.33E-18 |
| 17400 | 5.589E-05 | 4.880E-04 | 2.501E+00 | 0.1074 | 0.8792 | 0.1514 | 1.47E-19 | 1.24E-18 | 4.24E-18 |
| 17600 | 5.248E-05 | 4.970E-04 | 2.537E+00 | 0.0968 | 0.8913 | 0.1386 | 1.47E-19 | 1.24E-18 | 4.15E-18 |
| 17800 | 4.942E-05 | 5.060E-04 | 2.574E+00 | 0.0865 | 0.9029 | 0.1266 | 1.46E-19 | 1.24E-18 | 4.06E-18 |
| 18000 | 4.669E-05 | 5.151E-04 | 2.611E+00 | 0.0765 | 0.9140 | 0.1152 | 1.46E-19 | 1.24E-18 | 3.98E-18 |

## APPENDIX II

### SHOCK TUBE SIDE-WALL BOUNDARY LAYER SOLUTIONS FOR

$$U_w = 6000 \text{ m/sec}, \quad p_1 = 5 \text{ mm Hg}$$

Numerical results for an equilibrium argon shock tube side-wall boundary layer is presented for the case

$U_w = 6000$ m/sec

$U_2 = 675$ m/sec

$T_\infty = 14{,}100°K$

$T_w = 300°K$

These conditions are approximately obtained behind an argon shock wave with $U_s = 6000$ m/sec and $T_1 = 298°K$, $p_1 = 5$ mm Hg

The symbols used are the following

| | |
|---|---|
| Z | Similarity parameter $\eta$ |
| F | $K(\eta)$ |
| G | $H(\eta)$ |
| $U^*$ | Dimensionless velocity $u^*$ |
| $H^*$ | Dimensionless enthalpy $h^*$ |
| TEMP | Temperature T |
| VEL | Velocity u |
| ALFA | Degree of ionization $\alpha$ |
| NE | Number density of free electrons |
| PR | Prandtl number Pr |
| ROMY | Inverse density viscosity product $(\rho\mu)_\infty/(\rho\mu)$ |
| YSTAR | Dimensionless wall distance $y^*$ defined by equation (6.30) |

---

MKSA - units are used throughout the calculation.

INPUT DATA AS FOLLOWS

| PRESSURE(N/M2) | UWALL | U2 |
|---|---|---|
| 340000 | 6000.0000000000 | 675.0000000000 |

| T KELVIN | H NM/KG | ALFA | NE 1/M3 | RO KG/M3 | CP NM/(KG DEG) | QMINUS REC/SEC-ELECTRON |
|---|---|---|---|---|---|---|
| 14100 | 1.82967@+07 | 0.24128 | 3.39559@+23 | 9.3310@-02 | 5.7591@+03 | -5.5696@+05 |

| TEMP KELVIN | VISCOSITY KG/M-SEC | AMBIDIFF M2/SEC | TOTCOND NM/M-SEC-DEG | REACT FRACTIONS | ELECTR FRACTIONS | PRANDTL | QAA M2 | QAI M2 | QII M2 |
|---|---|---|---|---|---|---|---|---|---|
| 14100 | 1.1788-04 | 1.0278-03 | 1.6928+00 | 0.2433 | 0.7049 | 0.4011 | 1.558-19 | 1.278-18 | 7.008-18 |

| T | VISCRATIO | DENSRATIO | RU | PR |
|---|---|---|---|---|
| 300 | 0.1831 | 58.340 | 0.0936 | 0.6411 |
| 500 | 0.2700 | 35.004 | 0.1058 | 0.6444 |
| 700 | 0.3487 | 25.003 | 0.1147 | 0.6466 |
| 900 | 0.4220 | 19.447 | 0.1218 | 0.6482 |
| 1100 | 0.4916 | 15.911 | 0.1279 | 0.6495 |
| 1300 | 0.5581 | 13.463 | 0.1331 | 0.6506 |
| 1500 | 0.6222 | 11.668 | 0.1377 | 0.6515 |
| 1700 | 0.6843 | 10.295 | 0.1419 | 0.6523 |
| 1900 | 0.7447 | 9.212 | 0.1458 | 0.6530 |
| 2100 | 0.8036 | 8.334 | 0.1493 | 0.6537 |
| 2300 | 0.8611 | 7.610 | 0.1526 | 0.6543 |
| 2500 | 0.9174 | 7.001 | 0.1557 | 0.6548 |
| 2700 | 0.9727 | 6.482 | 0.1586 | 0.6553 |
| 2900 | 1.0270 | 6.035 | 0.1613 | 0.6558 |
| 3100 | 1.0804 | 5.646 | 0.1639 | 0.6563 |
| 3300 | 1.1329 | 5.304 | 0.1664 | 0.6567 |
| 3500 | 1.1847 | 5.001 | 0.1688 | 0.6570 |
| 3700 | 1.2359 | 4.730 | 0.1711 | 0.6574 |
| 3900 | 1.2863 | 4.488 | 0.1732 | 0.6578 |
| 4100 | 1.3361 | 4.269 | 0.1753 | 0.6581 |
| 4300 | 1.3854 | 4.070 | 0.1773 | 0.6584 |
| 4500 | 1.4341 | 3.889 | 0.1793 | 0.6587 |
| 4700 | 1.4823 | 3.724 | 0.1812 | 0.6590 |
| 4900 | 1.5300 | 3.572 | 0.1830 | 0.6593 |
| 5100 | 1.5772 | 3.432 | 0.1848 | 0.6596 |
| 5300 | 1.6240 | 3.302 | 0.1865 | 0.6564 |
| 5500 | 1.6703 | 3.182 | 0.1881 | 0.6539 |
| 5700 | 1.7163 | 3.071 | 0.1898 | 0.6496 |
| 5900 | 1.7618 | 2.966 | 0.1913 | 0.6429 |
| 6100 | 1.8069 | 2.869 | 0.1929 | 0.6332 |
| 6300 | 1.8516 | 2.778 | 0.1944 | 0.6198 |
| 6500 | 1.8959 | 2.692 | 0.1959 | 0.6028 |
| 6700 | 1.9397 | 2.612 | 0.1974 | 0.5824 |
| 6900 | 1.9829 | 2.536 | 0.1988 | 0.5595 |
| 7100 | 2.0256 | 2.465 | 0.2003 | 0.5354 |
| 7300 | 2.0676 | 2.397 | 0.2018 | 0.5113 |
| 7500 | 2.1088 | 2.333 | 0.2033 | 0.4884 |
| 7700 | 2.1490 | 2.272 | 0.2048 | 0.4677 |
| 7900 | 2.1879 | 2.214 | 0.2065 | 0.4497 |
| 8100 | 2.2254 | 2.159 | 0.2082 | 0.4347 |
| 8300 | 2.2612 | 2.106 | 0.2100 | 0.4229 |
| 8500 | 2.2947 | 2.055 | 0.2120 | 0.4142 |
| 8700 | 2.3256 | 2.007 | 0.2143 | 0.4086 |
| 8900 | 2.3535 | 1.960 | 0.2167 | 0.4058 |
| 9100 | 2.3776 | 1.916 | 0.2196 | 0.4057 |
| 9300 | 2.3974 | 1.872 | 0.2228 | 0.4082 |
| 9500 | 2.4123 | 1.830 | 0.2265 | 0.4129 |
| 9700 | 2.4215 | 1.790 | 0.2307 | 0.4196 |
| 9900 | 2.4244 | 1.750 | 0.2357 | 0.4280 |
| 10100 | 2.4202 | 1.712 | 0.2414 | 0.4378 |
| 10300 | 2.4084 | 1.674 | 0.2481 | 0.4485 |
| 10500 | 2.3884 | 1.637 | 0.2558 | 0.4598 |
| 10700 | 2.3598 | 1.600 | 0.2648 | 0.4713 |
| 10900 | 2.3223 | 1.564 | 0.2753 | 0.4825 |
| 11100 | 2.2759 | 1.528 | 0.2875 | 0.4928 |
| 11300 | 2.2208 | 1.493 | 0.3016 | 0.5020 |
| 11500 | 2.1572 | 1.457 | 0.3181 | 0.5095 |
| 11700 | 2.0859 | 1.422 | 0.3371 | 0.5151 |
| 11900 | 2.0076 | 1.387 | 0.3591 | 0.5184 |
| 12100 | 1.9233 | 1.352 | 0.3846 | 0.5191 |
| 12300 | 1.8341 | 1.317 | 0.4141 | 0.5173 |
| 12500 | 1.7411 | 1.282 | 0.4482 | 0.5129 |
| 12700 | 1.6456 | 1.246 | 0.4876 | 0.5058 |
| 12900 | 1.5489 | 1.211 | 0.5332 | 0.4963 |
| 13100 | 1.4521 | 1.175 | 0.5859 | 0.4845 |
| 13300 | 1.3563 | 1.140 | 0.6468 | 0.4706 |
| 13500 | 1.2624 | 1.105 | 0.7171 | 0.4549 |
| 13700 | 1.1713 | 1.069 | 0.7983 | 0.4376 |
| 13900 | 1.0837 | 1.035 | 0.8919 | 0.4191 |
| 14100 | 1.0000 | 1.000 | 1.0000 | 0.4011 |

SHOCK TUBE BOUNDARY LAYER FOR EQUILIBRIUM ARGON

PRESSURE(N/M2)

WITH TRUE VARIATION IN VISCOSITY AND PRANDTL NUMBER
SIMILARITY BOUNDARY LAYER
AMBIPOLAR DIFFUSION ASSUMED SHEATH NEGLECTED

340000

A**=9.685E-02
B**=1.251E-01

| Z | F | G | U* | H* | TEMP | VEL | ALFA | NE | PR | ROMY | YSTAR |
|---|---|---|---|---|---|---|---|---|---|---|---|
| 0.000 | 1.000 | 1.000 | 1.0000 | 0.0000 | 300 | 6000 | 0.0000 | | 0.641 | 0.094 | 0.00000 |
| 0.050 | 1.154 | 1.156 | 0.9948 | 0.0068 | 535 | 5977 | 0.0000 | | 0.645 | 0.108 | 0.00015 |
| 0.100 | 1.278 | 1.279 | 0.9889 | 0.0144 | 801 | 5941 | 0.0000 | | 0.647 | 0.118 | 0.00039 |
| 0.150 | 1.384 | 1.383 | 0.9824 | 0.0227 | 1092 | 5906 | 0.0000 | | 0.649 | 0.128 | 0.00073 |
| 0.200 | 1.478 | 1.473 | 0.9755 | 0.0317 | 1403 | 5869 | 0.0000 | | 0.651 | 0.136 | 0.00116 |
| 0.250 | 1.564 | 1.554 | 0.9681 | 0.0411 | 1733 | 5830 | 0.0000 | | 0.652 | 0.143 | 0.00171 |
| 0.300 | 1.644 | 1.627 | 0.9603 | 0.0511 | 2080 | 5789 | 0.0000 | | 0.654 | 0.149 | 0.00238 |
| 0.350 | 1.719 | 1.693 | 0.9522 | 0.0615 | 2442 | 5745 | 0.0000 | | 0.655 | 0.155 | 0.00317 |
| 0.400 | 1.790 | 1.755 | 0.9437 | 0.0722 | 2818 | 5700 | 0.0000 | | 0.654 | 0.160 | 0.00409 |
| 0.450 | 1.859 | 1.812 | 0.9349 | 0.0834 | 3207 | 5653 | 0.0000 | 2.827E+13 | 0.656 | 0.165 | 0.00515 |
| 0.500 | 1.924 | 1.866 | 0.9257 | 0.0949 | 3608 | 5604 | 0.0000 | 1.491E+15 | 0.657 | 0.170 | 0.00636 |
| 0.550 | 1.987 | 1.916 | 0.9162 | 0.1067 | 4020 | 5554 | 0.0000 | 2.391E+16 | 0.658 | 0.174 | 0.00772 |
| 0.600 | 2.048 | 1.963 | 0.9065 | 0.1189 | 4442 | 5502 | 0.0000 | 2.273E+17 | 0.659 | 0.179 | 0.00924 |
| 0.650 | 2.108 | 2.008 | 0.8964 | 0.1313 | 4875 | 5448 | 0.0000 | 1.490E+18 | 0.659 | 0.183 | 0.01093 |
| 0.700 | 2.166 | 2.038 | 0.8860 | 0.1439 | 5317 | 5393 | 0.0000 | 7.267E+18 | 0.656 | 0.187 | 0.01279 |
| 0.750 | 2.223 | 2.049 | 0.8754 | 0.1567 | 5762 | 5337 | 0.0000 | 2.809E+19 | 0.648 | 0.190 | 0.01483 |
| 0.800 | 2.277 | 2.015 | 0.8645 | 0.1695 | 6205 | 5279 | 0.0000 | 8.938E+19 | 0.627 | 0.194 | 0.01706 |
| 0.850 | 2.329 | 1.924 | 0.8534 | 0.1818 | 6632 | 5219 | 0.0001 | 2.359E+20 | 0.590 | 0.197 | 0.01946 |
| 0.900 | 2.378 | 1.798 | 0.8420 | 0.1935 | 7031 | 5159 | 0.0001 | 5.252E+20 | 0.544 | 0.200 | 0.02205 |
| 0.950 | 2.425 | 1.674 | 0.8303 | 0.2043 | 7397 | 5097 | 0.0003 | 1.014E+21 | 0.500 | 0.203 | 0.02481 |
| 1.000 | 2.470 | 1.574 | 0.8185 | 0.2145 | 7730 | 5033 | 0.0005 | 1.751E+21 | 0.465 | 0.205 | 0.02774 |
| 1.050 | 2.515 | 1.504 | 0.8064 | 0.2241 | 8036 | 4969 | 0.0009 | 2.777E+21 | 0.439 | 0.208 | 0.03082 |
| 1.100 | 2.561 | 1.462 | 0.7941 | 0.2333 | 8319 | 4904 | 0.0014 | 4.128E+21 | 0.422 | 0.210 | 0.03406 |
| 1.150 | 2.608 | 1.443 | 0.7816 | 0.2424 | 8582 | 4837 | 0.0020 | 5.832E+21 | 0.412 | 0.213 | 0.03745 |
| 1.200 | 2.658 | 1.443 | 0.7689 | 0.2514 | 8829 | 4769 | 0.0028 | 7.919E+21 | 0.406 | 0.216 | 0.04100 |
| 1.250 | 2.712 | 1.460 | 0.7559 | 0.2605 | 9063 | 4700 | 0.0038 | 1.041E+22 | 0.406 | 0.219 | 0.04469 |
| 1.300 | 2.769 | 1.490 | 0.7426 | 0.2697 | 9284 | 4629 | 0.0050 | 1.332E+22 | 0.408 | 0.223 | 0.04854 |
| 1.350 | 2.831 | 1.532 | 0.7290 | 0.2792 | 9495 | 4557 | 0.0065 | 1.666E+22 | 0.413 | 0.226 | 0.05254 |
| 1.400 | 2.898 | 1.585 | 0.7152 | 0.2889 | 9697 | 4483 | 0.0081 | 2.044E+22 | 0.419 | 0.231 | 0.05671 |
| 1.450 | 2.971 | 1.646 | 0.7010 | 0.2990 | 9890 | 4408 | 0.0100 | 2.466E+22 | 0.428 | 0.235 | 0.06104 |
| 1.500 | 3.051 | 1.715 | 0.6864 | 0.3095 | 10076 | 4330 | 0.0121 | 2.933E+22 | 0.437 | 0.241 | 0.06553 |
| 1.550 | 3.137 | 1.791 | 0.6714 | 0.3205 | 10255 | 4250 | 0.0146 | 3.445E+22 | 0.446 | 0.246 | 0.07021 |
| 1.600 | 3.231 | 1.874 | 0.6560 | 0.3319 | 10428 | 4168 | 0.0172 | 4.001E+22 | 0.456 | 0.253 | 0.07507 |
| 1.650 | 3.333 | 1.962 | 0.6401 | 0.3439 | 10595 | 4083 | 0.0202 | 4.601E+22 | 0.465 | 0.260 | 0.08012 |
| 1.700 | 3.444 | 2.054 | 0.6237 | 0.3565 | 10756 | 3996 | 0.0234 | 5.244E+22 | 0.475 | 0.268 | 0.08538 |
| 1.750 | 3.563 | 2.151 | 0.6067 | 0.3696 | 10913 | 3906 | 0.0270 | 5.929E+22 | 0.483 | 0.276 | 0.09085 |
| 1.800 | 3.692 | 2.252 | 0.5892 | 0.3834 | 11066 | 3812 | 0.0308 | 6.655E+22 | 0.491 | 0.285 | 0.09656 |
| 1.850 | 3.830 | 2.356 | 0.5709 | 0.3978 | 11214 | 3715 | 0.0350 | 7.418E+22 | 0.498 | 0.295 | 0.10251 |
| 1.900 | 3.977 | 2.463 | 0.5520 | 0.4128 | 11358 | 3615 | 0.0394 | 8.220E+22 | 0.504 | 0.306 | 0.10873 |
| 1.950 | 4.135 | 2.572 | 0.5324 | 0.4286 | 11499 | 3510 | 0.0442 | 9.060E+22 | 0.509 | 0.318 | 0.11525 |
| 2.000 | 4.302 | 2.683 | 0.5120 | 0.4450 | 11636 | 3401 | 0.0492 | 9.931E+22 | 0.514 | 0.331 | 0.12208 |
| 2.050 | 4.479 | 2.797 | 0.4907 | 0.4621 | 11769 | 3288 | 0.0546 | 1.083E+23 | 0.517 | 0.344 | 0.12926 |
| 2.100 | 4.665 | 2.912 | 0.4686 | 0.4800 | 11900 | 3170 | 0.0603 | 1.177E+23 | 0.518 | 0.359 | 0.13682 |
| 2.150 | 4.858 | 3.028 | 0.4455 | 0.4986 | 12028 | 3047 | 0.0663 | 1.273E+23 | 0.519 | 0.375 | 0.14481 |
| 2.200 | 5.059 | 3.146 | 0.4215 | 0.5179 | 12153 | 2920 | 0.0726 | 1.372E+23 | 0.519 | 0.392 | 0.15328 |
| 2.250 | 5.265 | 3.267 | 0.3965 | 0.5379 | 12276 | 2786 | 0.0793 | 1.474E+23 | 0.518 | 0.410 | 0.16229 |
| 2.300 | 5.472 | 3.388 | 0.3705 | 0.5587 | 12396 | 2648 | 0.0862 | 1.577E+23 | 0.515 | 0.430 | 0.17191 |
| 2.350 | 5.678 | 3.513 | 0.3435 | 0.5803 | 12515 | 2504 | 0.0935 | 1.683E+23 | 0.512 | 0.451 | 0.18224 |
| 2.400 | 5.875 | 3.641 | 0.3155 | 0.6027 | 12631 | 2355 | 0.1011 | 1.791E+23 | 0.509 | 0.473 | 0.19338 |
| 2.450 | 6.056 | 3.772 | 0.2866 | 0.6258 | 12745 | 2201 | 0.1090 | 1.900E+23 | 0.504 | 0.497 | 0.20547 |
| 2.500 | 6.211 | 3.908 | 0.2569 | 0.6499 | 12858 | 2043 | 0.1173 | 2.011E+23 | 0.498 | 0.523 | 0.21867 |
| 2.550 | 6.323 | 4.049 | 0.2266 | 0.6747 | 12969 | 1881 | 0.1259 | 2.124E+23 | 0.492 | 0.550 | 0.23322 |
| 2.600 | 6.372 | 4.195 | 0.1958 | 0.7005 | 13079 | 1718 | 0.1349 | 2.239E+23 | 0.486 | 0.580 | 0.24938 |
| 2.650 | 6.325 | 4.340 | 0.1650 | 0.7272 | 13188 | 1554 | 0.1443 | 2.355E+23 | 0.479 | 0.611 | 0.26749 |
| 2.700 | 6.149 | 4.479 | 0.1347 | 0.7548 | 13296 | 1392 | 0.1540 | 2.472E+23 | 0.471 | 0.645 | 0.28797 |
| 2.750 | 5.795 | 4.592 | 0.1057 | 0.7832 | 13402 | 1238 | 0.1640 | 2.589E+23 | 0.463 | 0.681 | 0.31135 |
| 2.800 | 5.226 | 4.648 | 0.0790 | 0.8121 | 13506 | 1095 | 0.1742 | 2.706E+23 | 0.454 | 0.719 | 0.33818 |
| 2.850 | 4.428 | 4.597 | 0.0555 | 0.8411 | 13606 | 970 | 0.1845 | 2.820E+23 | 0.446 | 0.758 | 0.36898 |
| 2.900 | 3.456 | 4.388 | 0.0364 | 0.8693 | 13700 | 869 | 0.1945 | 2.928E+23 | 0.439 | 0.798 | 0.40407 |
| 2.950 | 2.443 | 3.987 | 0.0221 | 0.8955 | 13785 | 793 | 0.2039 | 3.026E+23 | 0.430 | 0.836 | 0.44331 |
| 3.000 | 1.558 | 3.437 | 0.0125 | 0.9188 | 13858 | 741 | 0.2122 | 3.111E+23 | 0.423 | 0.871 | 0.48610 |
| 3.050 | 0.904 | 2.820 | 0.0066 | 0.9384 | 13918 | 710 | 0.2192 | 3.182E+23 | 0.418 | 0.901 | 0.53155 |
| 3.100 | 0.486 | 2.222 | 0.0033 | 0.9541 | 13965 | 693 | 0.2248 | 3.237E+23 | 0.413 | 0.925 | 0.57878 |
| 3.150 | 0.246 | 1.700 | 0.0016 | 0.9663 | 14002 | 684 | 0.2292 | 3.280E+23 | 0.410 | 0.945 | 0.62710 |
| 3.200 | 0.120 | 1.274 | 0.0008 | 0.9756 | 14029 | 679 | 0.2325 | 3.312E+23 | 0.408 | 0.960 | 0.67608 |
| 3.250 | 0.056 | 0.941 | 0.0004 | 0.9825 | 14049 | 677 | 0.2350 | 3.336E+23 | 0.406 | 0.971 | 0.72543 |
| 3.300 | 0.026 | 0.687 | 0.0002 | 0.9875 | 14064 | 676 | 0.2368 | 3.353E+23 | 0.405 | 0.979 | 0.77501 |
| 3.350 | 0.011 | 0.497 | 0.0001 | 0.9912 | 14075 | 675 | 0.2381 | 3.366E+23 | 0.404 | 0.985 | 0.82473 |
| 3.400 | 0.005 | 0.357 | 0.0001 | 0.9938 | 14082 | 675 | 0.2391 | 3.375E+23 | 0.403 | 0.990 | 0.87454 |
| 3.450 | 0.002 | 0.255 | 0.0000 | 0.9957 | 14088 | 675 | 0.2397 | 3.381E+23 | 0.402 | 0.993 | 0.92441 |
| 3.500 | 0.001 | 0.181 | 0.0000 | 0.9971 | 14092 | 675 | 0.2402 | 3.386E+23 | 0.402 | 0.995 | 0.97432 |
| 3.550 | 0.000 | 0.127 | 0.0000 | 0.9980 | 14094 | 675 | 0.2406 | 3.389E+23 | 0.402 | 0.997 | 1.02426 |
| 3.600 | 0.000 | 0.089 | 0.0000 | 0.9987 | 14096 | 675 | 0.2408 | 3.391E+23 | 0.401 | 0.998 | 1.07421 |
| 3.650 | 0.000 | 0.062 | 0.0000 | 0.9992 | 14098 | 675 | 0.2410 | 3.393E+23 | 0.401 | 0.999 | 1.12418 |
| 3.700 | 0.000 | 0.043 | 0.0000 | 0.9995 | 14099 | 675 | 0.2411 | 3.394E+23 | 0.401 | 0.999 | 1.17416 |
| 3.750 | 0.000 | 0.030 | 0.0000 | 0.9997 | 14099 | 675 | 0.2412 | 3.395E+23 | 0.401 | 1.000 | 1.22414 |
| 3.800 | 0.000 | 0.020 | 0.0000 | 0.9999 | 14100 | 675 | 0.2412 | 3.395E+23 | 0.401 | 1.000 | 1.27412 |
| 3.850 | 0.000 | 0.014 | 0.0000 | 1.0000 | 14100 | 675 | 0.2413 | 3.395E+23 | 0.401 | 1.000 | 1.32411 |
| 3.900 | 0.000 | 0.009 | 0.0000 | 1.0001 | 14100 | 675 | 0.2413 | 3.396E+23 | 0.401 | 1.000 | 1.37411 |
| 3.950 | 0.000 | 0.006 | 0.0000 | 1.0001 | 14100 | 675 | 0.2413 | 3.396E+23 | 0.401 | 1.000 | 1.42410 |
| 4.000 | 0.000 | 0.004 | 0.0000 | 1.0001 | 14100 | 675 | 0.2413 | 3.396E+23 | 0.401 | 1.000 | 1.47409 |
| 4.050 | 0.000 | 0.003 | 0.0000 | 1.0002 | 14100 | 675 | 0.2413 | 3.396E+23 | 0.401 | 1.000 | 1.52409 |
| 4.100 | 0.000 | 0.002 | 0.0000 | 1.0002 | 14101 | 675 | 0.2413 | 3.396E+23 | 0.401 | 1.000 | 1.57408 |
| 4.150 | 0.000 | 0.001 | 0.0000 | 1.0002 | 14101 | 675 | 0.2413 | 3.396E+23 | 0.401 | 1.000 | 1.62408 |
| 4.200 | 0.000 | 0.001 | 0.0000 | 1.0002 | 14101 | 675 | 0.2413 | 3.396E+23 | 0.401 | 1.000 | 1.67407 |
| 4.250 | 0.000 | 0.001 | 0.0000 | 1.0002 | 14101 | 675 | 0.2413 | 3.396E+23 | 0.401 | 1.000 | 1.72407 |
| 4.300 | 0.000 | 0.000 | 0.0000 | 1.0002 | 14101 | 675 | 0.2413 | 3.396E+23 | 0.401 | 1.000 | 1.77406 |
| 4.350 | 0.000 | 0.000 | 0.0000 | 1.0002 | 14101 | 675 | 0.2413 | 3.396E+23 | 0.401 | 1.000 | 1.82406 |
| 4.400 | 0.000 | 0.000 | 0.0000 | 1.0002 | 14101 | 675 | 0.2414 | 3.396E+23 | 0.401 | 1.000 | 1.87405 |
| 4.450 | 0.000 | 0.000 | 0.0000 | 1.0002 | 14101 | 675 | 0.2414 | 3.396E+23 | 0.401 | 1.000 | 1.92405 |

DELTAY AS A FUNCTION OF X (DISTANCE FROM SHOCK)
FOR CASE YSTAR=1;NOTICE Y PROP YSTAR

| Y MM | X(METER) |
|---|---|
| 0.43191 | 0.010 |